# Magneto-Hydrodynamic Activity and Energetic Particles - Application to Beta Alfvén Eigenmodes.

Christine Nguyen

Ecole Doctorale de l'Ecole Polytechnique
Route de Saclay
F-91128 Palaiseau, France.

IRFM, Association Euratom-CEA
Centre de Cadarache
F-13108 Saint Paul-Lez-Durance, France.

# Magneto-HydroDynamic Activity and Energetic Particles
## ∼ Application to Beta Alfvén Eigenmodes ∼

by

**Christine Nguyen**

A dissertation submitted in partial satisfaction
of the requirements for the degree of

**Doctor of Philosophy**
in
**Plasma Physics**
**Ecole Doctorale de l'Ecole Polytechnique**

| | |
|---|---|
| Dr. Xavier Garbet | CEA Research Director - PhD advisor |
| Dr. Pascale Hennequin | CNRS Research Director |
| Dr. Hinrich Lütjens | CNRS Research Scientist |
| Dr. Patrick Mora | CNRS Research Director - Chair of PhD committee |
| Dr. Roland Sabot | CEA Research Director - CEA advisor |
| Dr. Andrei Smolyakov | Professor at the University of Saskatchewan |
| Dr. Laurent Villard | Professor at EPFL - Referee |
| Dr. Fulvio Zonca | Senior Researcher at ENEA - Referee |

Jan 07 - Dec 09

# Résumé

La faisabilité de la fusion magnétique est dépendante de notre capacité à confiner l'énergie des particules supra-thermiques libérées á haute énergie par les réactions de fusion, dans les meilleures conditions de sécurité et d'efficacité. Dans ce but, il est nécessaire de comprendre l'interaction entre les particules énergétiques et le plasma thermo-nucléaire qui constitue l'environnement des réactions de fusion, afin de la contrôler. La thèse que nous présentons ici s'inscrit dans cet effort. Le coeur du travail mené est l'étude d'un type d'instabilité, le Beta Alfvén Eigenmode (BAE), que peuvent exciter les particules énergétiques, et dont on peut craindre qu'il dégrade fortement non seulement le confinement des particules énergétiques mais aussi le confinement du plasma dans sa globalité. Dans un premier temps, nous nous attacherons à décrire les caractéristiques de ce mode et nous dériverons sa relation de dispersion ainsi que sa structure. Dans une seconde partie, nous effectuerons l'étude de la stabilité linéaire de ce mode en présence de particules énergétiques. Cette étude nous a permis de définir un critère analytique rendant compte de la capacité des particules énergétiques à exciter le BAE. Ce critère sera discuté et confronté aux résultats d'expériences menées durant la thèse. Cette étude linéaire présentant cependant quelques limites, il nous est apparu important de nous poser la question de la possibilité d'une modification de la stabilité du BAE liée à l'utilisation d'une description non-linéaire. Nous suggérerons dans cette présentation un processus, vérifié analytiquement et numériquement, dont peut résulter l'existence d'états méta-stables pour le BAE.

# Abstract

The goal of magnetic fusion research is to extract the power released by fusion reactions and carried by the product of these reactions, liberated at energies of the order of a few MeV. The feasibility of fusion energy production relies on our ability to confine these energetic particles, while keeping the thermonuclear plasma in safe operating conditions. For that purpose, it is necessary to understand and find ways to control the interaction between energetic particles and the thermonuclear plasma. Reaching these two goals is the general motivation for the work conducted during the PhD. More specifically, our focus is on one type of instability, the Beta Alfvén Eigenmode (BAE), which can be driven by energetic particles and impact on the confinement of both energetic and thermal particles. In this work, we study the characteristics of BAEs analytically and derive its dispersion relation and structure. Next, we analyze the linear stability of the mode in the presence of energetic particles. First, a purely linear description is used, which makes possible to get an analytical linear criterion for BAE destabilization in the presence of energetic particles. This criterion is compared with experiments conducted in the Tore-Supra tokamak during the PhD. Secondly, because the linear analysis reveals some features of the BAE stability which are subject to a strong nonlinear modification, the question is raised of the possibility of a sub-critical activity of the mode. We propose a simple scenario which makes possible the existence of meta-stable modes, verified analytically and numerically. Such a scenario is found to be relevant to the physics and scales characterizing BAEs.

# Acknowledgements

I am indebted to several people I had the chance to meet during my time as a PhD student, for their advice and for their help, for their knowledge and inexhaustible curiosity, and for their support and chearful presence.

**Starting with English speaking people...**

I want to thank Andrei Smolyakov and Fulvio Zonca for taking part to my PhD committee, for commenting on my work during the whole lengthtime of my PhD, for their continuous support and for their incredibly complete, effective and fast e-mails.

I also want to thank Taik-Soo Hahm, Simon Pinches, Herbert Berk and Boris Breizman, for welcoming me in their respective labs, for taking the time to introduce me into their work and for broadening my overall physical understanding.

**Je poursuivrai en français...**

... pour remercier Alain Becoulet d'avoir accepté ma candidature de thèse et Tuong Hoang d'être toujours disponible, présent et attentif pour nous autres, thésards. Merci également à Valérie Icard et Stéphanie Villechavrolle d'avoir toujours répondu avec le sourire à l'ensemble de mes questions et requêtes, bien que parfois maladroites.

Je souhaite également adresser mes remerciements à l'ensemble des membres francophones du jury, Laurent Villard, Patrick Mora, Hinrich Lütjens et Pascale Hennequin, pour leur lecture attentive de mon manuscrit, pour leurs questions et leurs remarques pertinentes.

J'en arrive maintenant à ces personnes qui ont rythmé le quotidien de ma thèse et sans lesquelles elle n'aurait pu aboutir, en commençant par mon directeur de thèse, Xavier Garbet, que tout simplement je n'aurais pu rêver meilleur. Je lui suis très reconnaissante pour tout ce qu'il m'a appris avec le soucis constant de me me faire comprendre les mécanismes de la fusion au delà des frontières strictes de mon sujet, et en faisant preuve d'une clarté dont je ne peux que faire l'éloge; pour les conseils pertinents et variés et pour les idées toujours nouvelles qu'il a su me donner dans mon travail de thèse; mais aussi pour cette liberté d'action et d'expression dont j'ai toujours eu le sentiment de pouvoir faire usage avec lui, quelque que soit le sujet abordé; et même un peu pour son humour. Je remercie également mon co-directeur de thèse, Roland Sabot, pour m'avoir aidée à faire le lien etre théorie et expérience, ce qui m'a semblé passionnant.

Je salue avec la chaleur toutes les personnes du groupe "MHD+rapides", auquel je souhaite longue vie, et je veux plus particulièrement remercier ces personnes avec lesquelles j'ai pu travailler sur cette thématique: Joan Decker qui, il est vrai, m'a longtemps intimidée mais avec lequel les discussions sont toujours pleines d'intérêt; Patrick Maget dont je ne peux qu'apprécier le calme et l'esprit critique; Guido Huysmans et Lars-Goran Eriksson dont l'aide et les conseils m'ont été extrêmement précieux; Marc Goniche et son enthousiasme toujours présent; Virginie Grandgirard, dont j'ai pu profiter de l'efficacité légendaire.

Merci également aux diverses personnes qui incarnent pour moi l'atmosphère chaleureuse et sympathique du CEA et qui ont été pour moi de très bon conseil en diverses occasions: Marina Becoulet, Chantal Passeron, Clarisse Bourdelle, Gloria Falchetto, Yanick Sarazin, Philippe Ghendrih, Rémi Dumont et Maurizio Ottaviani; ainsi qu'à diverses personnes sans l'aide desquelles réaliser des expériences sur Tore-Supra aurait été impossible, tout particulièrement Philippe Moreau.

Les choses auraient été bien plus moroses sans la présence de cette troupe de "non-permanents" rencontrés durant la thèse: une autre fille (ouf !) vraiment super sympathique, Gaëlle Chevet... dans un milieu assez masculin, mais j'avoue on ne peut plus amical; des

collègues de bureau, qui ont su me supporter, égayer l'*insoutenable* labeur de la thèse, alléger les périodes de stress ou les petites irritations, Guilhem Dif-Pradalier au charme ravageur qui s'est révélé un véritable ami, et Stanislas Pamela, la personne la plus facile à vivre que je connaisse... en particulier, lorsque souffle le vent; des ainés que j'ai très longtemps considérés comme des modèles, l'impétueux Patrick Tamain et l'irréprochable Eric Nardon; un compagnon de route plein d'humour et de détachement Alessandro Casati que j'espère ne pas avoir laissé trop sceptique quant à mes sujets de discussion; des cadets qui ont toute mon affection, Antoine Merle avec lequel j'espère une exploration fructueuse du plus beau sujet de thèse du monde, et David Zarzoso que je remercie pour la relation de confiance qui s'est établie entre nous.

Merci à l'amitié de Kees de Meijeire, à la sagesse de Maxime Lesur, aux remises en question avec Alessandro Macor, aux longues discussions et gentils désaccords avec Frédéric Schwander, aux chambrages de Thomas Gerbaud, au réalisme de Roland Bellessa, à la sérénité de Diego Molina, à la générosité de Daniel Villegas, au caractère accueillant de Nicolas Fedorczak, à la sympathie de Shaodong Song, au sourire et propos souriants de Emile Van-Der-Plas, à l'honnêteté de Özgür Gürcan, à la simplicité et la sincérité immédiate des rapports qui peuvent s'établir avec Zwinglio Guimaraes, à l'à-propos de Jérémie Abiteboul, aux débats avec Francois-Xavier Duthoit.

Merci enfin à celle qui m'a permis d'échapper à ce monde de scientifiques et qui aura été ma confidente au quotidien, Charlotte Largeron. Je regretterai les apéros et les tisanes, et toujours un peu de l'avoir trop souvent réveillée.

Il me reste à remercier ceux qui sont pour moi des soutiens constants depuis bien longtemps. Merci à mes parents et à mon frère de m'avoir appuyée dans mes choix en toutes circonstances, et tout simplement de prendre soin de moi. Merci à Stéphane et à sa fenêtre *gmail* toujours ouverte pour adoucir mon quotidien.

# Contents

# List of Figures

# List of Tables

*To the energy of the future...*

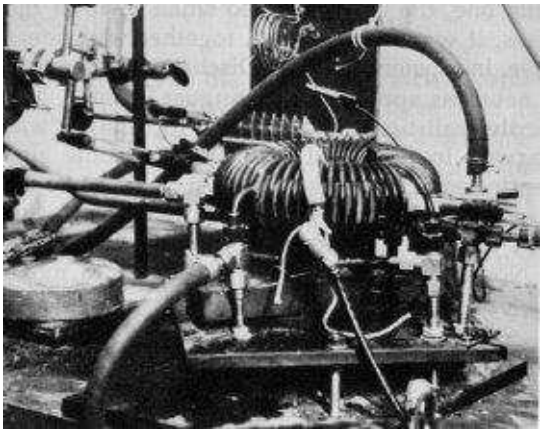

# 1 Introduction

## 1.1 Energy from fusion

The binding energy curve, reproduced in Fig. 1.1, shows that the fusion of two light nuclei can lead to a more strongly bounded state, and consequently release energy. The goal of civilian fusion research is to find ways to produce and extract this energy.

Currently, the most studied fusion reaction is the fusion of two hydrogen isotopes, a **deuterium** nucleus (D) and a **tritium** nucleus (T), leading to the creation of a helium atom (also called **alpha particle**) and a **neutron**, which carry the liberated energy

$$^{2}_{1}\mathrm{D} + ^{3}_{1}\mathrm{T} \longrightarrow ^{4}_{2}\mathrm{He}\ (3.56\ \mathrm{MeV}) + \mathrm{n}\ (14.03\ \mathrm{MeV}). \tag{1.1}$$

Other fusion reactions exist which can liberate energy, but the one described above has the highest cross-section for the energies which can be accessed in laboratories, as illustrated in Fig. 1.2. However, as can be seen in this figure, even for the relatively favorable D-T reac-

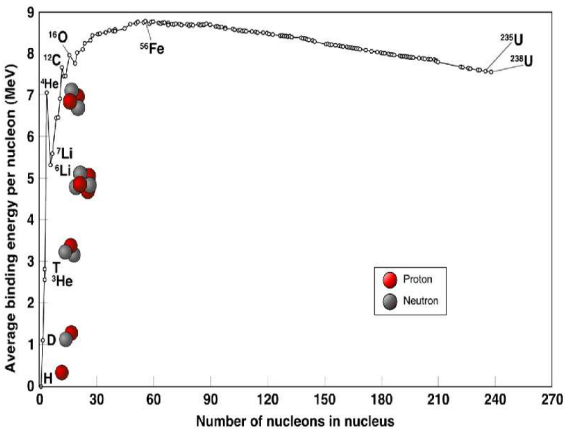


Figure 1.1: The binding energy curve.

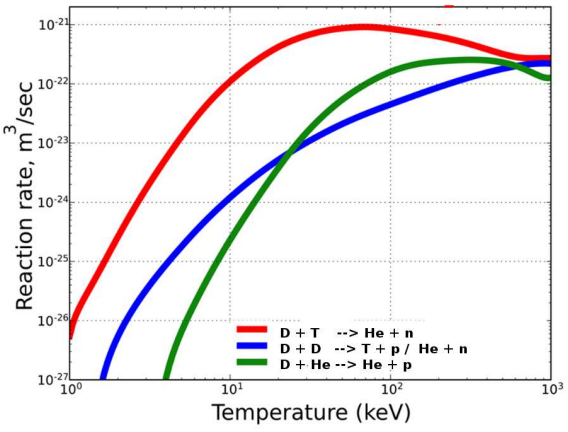


Figure 1.2: Cross-section of the Deuterium-Tritium reaction compared to other fusion reactions.

tion, fusion cross-sections are neglibly small below a few keV because of the necesssity to overcome Coulomb repulsion. For this reason, an efficient production of energy from fusion requires to bring reactants to energies between **10 keV to 30 keV**.

Due to several limitations of non-thermal methods [1], thermal approaches have been preferred to reach these energies, where reactants are kept close to thermal equilibrium and heated to temperatures exceeding several keVs. At these temperatures, equivalent to about $10^8$ K, matter is in the **plasma state**, that is, fully ionized. Consequently, the corresponding

background where fusion reactions can take place is referred to as a **hot thermonuclear plasma**.

Because a hot plasma tends to expand and may eventually get quenched on the surrounding walls, and in order to enhance the probability of fusion reactions, it is necessary to **confine** the plasma to a sufficiently high density. Two techniques have been developed for this purpose.

- **Inertial confinement** is based on the heating and compression of pellets of a solid mixture of deuterium and tritium by large laser beams or accelerated particle beams.

- **Magnetic confinement** relies on the use of large magnetic fields. When charged particles are plunged into a strong magnetic field, their perpendicular motion with respect to this field is a rotational motion around the field lines, or **gyromotion**, which averages out to the lower order. Hence, confinement is achieved because particles are constrained to follow the field lines. Several magnetic devices have been studied, either with closed or open field lines, but it may be shown that a closed system designed to ensure a confinement in all three spacial dimensions is necessarily **topologically equivalent to a torus**. Several torus-like designs, such as spheromaks [2] or stellerators [3] are currently under study, but the configuration assessed to be the most promising at the moment, is the **tokamak** (from the Russian *Toroïdalnaïa kamera s magnitnymi katushkami* or toric magnetic chamber). A schematic of a tokamak is given in Fig. 1.3. As can be seen in this figure, the plasma of a tokamak is confined in an

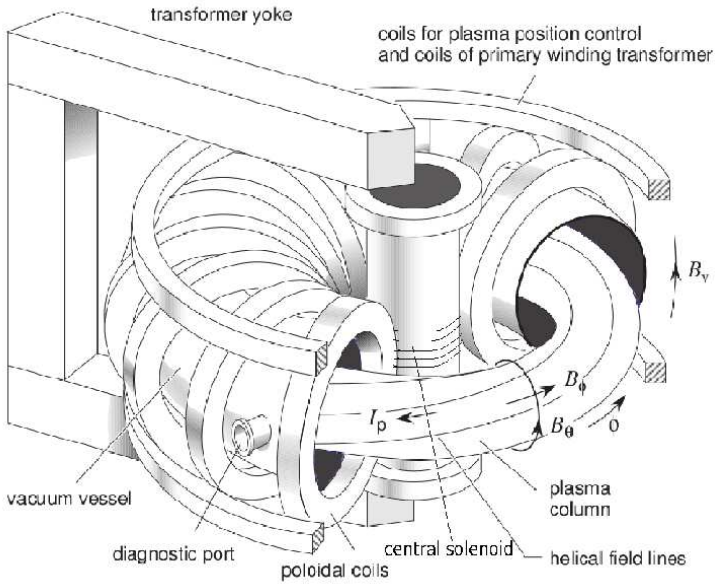


Figure 1.3: The tokamak and its confining magnetic set-up.

axisymmetric chamber, using a helical magnetic field, generated both by vertical coils and by the existence of a plasma current.
The tokamak geometry is the framework of the presented thesis.

## 1.2 The necessity to control the dynamics of energetic particles

To allow for sufficient fusion reactions to take place, the plasma power balance or **Lawson balance** needs to be reached, that is

$$\text{Losses} = P_{\text{losses}} + \frac{W_{\text{plasma}}}{\tau_E} = f_\alpha P_{\text{fusion}} + P_{\text{external}} = \text{Gains} \tag{1.2}$$

where $P_{\text{losses}}$ refers to unavoidable energy losses such as radiations, which are independent from the plasma transport properties. $W_{\text{plasma}}$ is the plasma energy content and $\boldsymbol{\tau_E}$ is the so-called **confinement time** which is a measure of the confinement quality, such that $W_{\text{plasma}}/\tau_E$ returns the power dissipated because of diffusion and convection processes. $P_{\text{fusion}}$ is the power liberated by fusion reactions, and $f_\alpha$ **is the fraction of fusion power which remains in the plasma**. Finally, $P_{\text{external}}$ corresponds to the external heating power needed to reach the balance. Frequently, one refers to this external power input using another quantity, the **amplification factor Q**,

$$Q = \frac{P_{\text{fusion}}}{P_{\text{external}}} \tag{1.3}$$

which is certainly a quantity one may want to optimize.

For this optimization, most fusion research aims at increasing the confinement time $\tau_E$. However, $f_\alpha$ may also be a critical parameter. Traditionally, $f_\alpha$ is estimated to be equal to 1/5. Indeed, neutrons, being neutral particles, have no chance to interact with the plasma or to be confined by the magnetic field. Consequently, this factor of 1/5 corresponds to the fraction of fusion energy carried by the alpha particles, and assumes that all this energy gets deposited on the bulk plasma. Several experimental observations however have shown that suprathermal particles, also referred to as **energetic or fast particles**, between 70 keV and a few MeV can be expelled from the confinement chamber without depositing their energy on the bulk plasma. In the DIII-D tokamak, the heating of ions to about 75keV using beam injection resulted in the expulsion of over 50 % of beam ions. In the TFTR tokamak (Tokamak Fusion Test Reactor [4]), ions heated by high frequency waves were expelled at high energy and even bored a hole in a vacuum port [5]. Recalling that alpha particles are liberated with energies of a few MeV, these observations suggest that **the fraction of fusion energy carried by the alpha particles may not be retained in the plasma, due the possible expulsion of alpha particles**. $f_\alpha$ could be much lower than 1/5, which would be detrimental for a reactor efficiency. Moreover, **a dangerous dynamics of the suprathermal particles is put to light by these experiments, which may strongly damage the chamber walls**. Hence the necessity to **control the dynamics of suprathermal particles**, and in particular of alpha particles, with the following goals:

- **Confining the energy of the fusion produced alpha particles**
- **Confining the suprathermal fuel ions and their energy.** External heating sources may bring fuel ions to suprathermal energies, but this process should not lead to their expulsion.
- **Slowing down suprathermal particles before they reach the plasma boundary**, in order to avoid materials damaging.
- **Avoiding a strong dilution of the fuel plasma by the alpha particles**. Even though it is of interest to keep the energy carried by the the alpha particles inside

the thermonuclear plasma, the presence of non-reacting particles degrades the plasma efficiency because of the related dilution. Ideally, one wants to get rid of the alpha particles once they have deposited their energy on the fuel plasma.

Present day experimental tokamaks mainly operate with pure deuterium plasmas, to avoid the hardships linked to the handling of radioactive tritium. Consequently, in all present day experiments, the power balance is achieved using external power, as the major heating source.

An objective of fusion research is of course to reduce the amount of external power to be provided (or in other words, to increase $Q$), an ideal situation being of course to build a self-consistent device, that is to reach the so-called **ignition** ($Q = +\infty$). A first step in this direction will be achieved by the next generation fusion tokamak **ITER** (*iter* meaning the way in latin), designed to be built around 2018 and intended to demonstrate the feasibility of fusion energy production. As can be seen in Tab. 1.1 where we compared ITER

| | Tore Supra | JET | ITER |
|---|---|---|---|
| Major radius $R_0$ (m) | 2.4 | 3.0 | 6.2 |
| Minor radius $r_0$ (m) | 0.7 | 1.2 | 2.0 |
| Plasma volume $V_p$ ($m^3$) | 25 | 155 | 830 |
| Maximum Plasma current $I_p$ (MA) | 1.7 | 5-7 | 15 |
| Toroidal field on axis $B_T$ (T) | 3.8 | 3.4 | 5.3 |
| Gas | D-D | D-D/D-T | D-D/D-T |
| Fusion power | ∼kW | 50kW/10MW | 500MW |
| Amplification factor $Q$ | $\ll 1$ | $\sim 1$ | $> 10$ |

Table 1.1: Tore Supra, JET and ITER parameters

objectives with current tokamaks, the French tokamak Tore-Supra and the Joint European Torus (JET), ITER will represent a quantitavive jump, from the point of view of scaling and performance, but it will also a qualitative jump, with a real attempt to extract energy from fusion reactions. Whereas $Q$ has not exceeded 1 in current devices, one of **ITER's goal is to achieve a $Q$ value of 10, that is, for $f_\alpha = 1/5$, to heat the plasma with twice as much fusion power as external power**. Consequently, ITER will be a major step in the understanding of the dynamics of alpha particles and suprathermal particles in general, for several reasons. First, suprathermal particles confinement will be studied in a confining chamber of realistic size. Secondly, first studies of a non-localized, self-organized heating source (the fusion energy carried by the alpha particles) will be possible. Then, interactions of alpha particles with the plasma collective behaviors will take place. And finally, experiments aiming at controlling the alpha particles dynamics will be possible.

In the way towards the understanding and control of ITER alpha particles dynamics, it is necessary to find models describing the interactions of suprathermal particles with the thermonuclear plasma.

## 1.3 Foretaste of the modelling difficulties

As explained in the previous section, an ideal situation would be to achieve the **deposition of the alpha particles energy** on the fuel plasma and to **tranport the slown down particles out of the plasma chamber**. These two processes may occur via **interactions with the main plasma**.

A favorable situation would be to have a time scale separation between the energy deposition and the transport of alpha particles, in order to ensure the particles do not reach the plasma boundary before they have delivered their energy. Unfortunately, the situation is not such. On the contrary, both the interactions at the origin of the energy deposition and at the origin of transport are spread over various time scales as well as various length scales. An attempt to summarize the types of interactions taking place between alpha particles and the main plasma is given in Fig. 1.4.

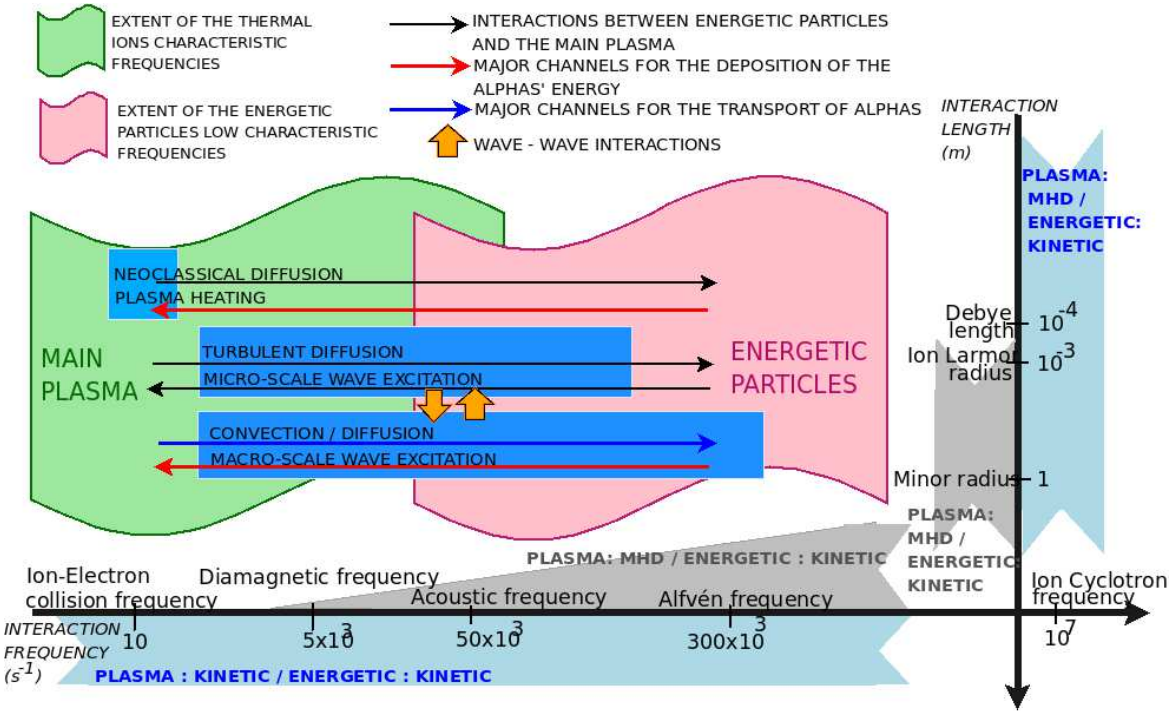


Figure 1.4: Time and length scales involved in the interactions between alpha particles and the main plasma.

Mainly, one may distinguish between

- short scale, individual Coulomb interactions, also simply called **collisions**, taking place inside a sphere of radius the **Debye length** of about $10^{-4}$m.

  Collisions allow some heating of the plasma electrons, and they induce a so-called **neoclassical transport**. However, this transport occuring with very low frequency and random directions is not expected to be dominant for suprathermal particles because of their high energies.

- micro-scale collective behaviors, taking place via the excitation of **micro-scale waves** with eigenfrequencies ranging from a few kHz to a hundred of kHz, and a broad radial spectrum ranging from about $10^{-4}$m to a few millimeters.

  Micro-scale waves are at the origin of the main thermal transport process, **turbulent diffusion**. However, they are not expected to be such important for suprathermal particles. Indeed, the typical **gyro-radius** of the suprathermal particles, that is, the characteristic radius of their gyromotion, is larger than a few millimeters. Consequently, the effects of micro-scale fluctuations is averaged out during one gyromotion of a suprathermal particle. For ITER, turbulent diffusion of suprathermal alphas has been estimated to be 20 times smaller than the one of thermal alphas [6]. Inversely,

alpha particles are not expected to induce a significative micro-scale activity (at least not directly), as long as their density remains limited. Hence, micro-scale waves may not be the most important channel for the alpha energy deposition.

- macro-scale collective behaviors, taking place via the excitation of **macro-scale waves**, with typical scale lengths of the order of several centimers to one meter, and typical eigenfrequencies ranging from a few kHz to 300 KHz.
  Due to their broad extent, these waves can interact with suprathermal particles. Moreover their eigenfrequencies correspond to the typical eigenfrequencies of the suprathermal particles, allowing for **resonances** and wave amplication to take place. Moreover, because of their broad extent, they can convect particles very rapidly on large distances. **Hence, macro-scale waves can be expected to be the main channel in the interaction of energetic particles with the plasma.**

Different plasma models are associated to the various time and length scales.

**Kinetic theories** describe the plasma collective motion in the 6 dimensional phase space using a distribution function $F(\mathbf{x}, \mathbf{v})$, which assumes a certain space or time averaging of the isolated charged particles [7] and of their associated discontinuous Coulomb potential. In quasineutral plasmas, the relevant averaging length is the **Debye length**, which represents the necessary distance for the Coulomb potential of an indidual charged particle to be screened by particles of the opposite charge. This way, individual behaviors get averaged. Nevertheless, the *cumulative* effects of collisions may still be retained. The main equation of kinetic theories is the **Boltzmann equation** with collision operator $\mathcal{C}$ and source $\mathcal{Q}$,

$$\frac{dF}{dt} = \mathcal{Q} + \mathcal{C} \cdot F \tag{1.4}$$

also called **Vlasov equation** when $\mathcal{C} \cdot F = 0, \mathcal{Q} = 0$. Eq. 1.4 can describe all time and length scales relevant to magnetized fusion plasmas phenomena of interest.

**Fluid theories** are based on the use of moments of the Boltzmann equation, that is, space dependant quantities of the form $c \int d\mathbf{v}\mathbf{v}^n f$ with $c$ a constant, $n \in \mathbb{N}$ (density, velocity...) and avoid the heavy calculation of the full velocity distribution. One major fluid description is the **Magneto-HydroDynamic (MHD) model** which describes the thermal plasma (electron and fuel ions) as a single fluid, simply with the use of density, velocity and pressure. MHD is appropriate for the description of **macroscopic interactions**, and for relatively **fast waves compared to the characteristic eigenfrequencies of the described populations**. The latter condition is called **hydrodynamic approximation**. It is often not so relevant to the electron dynamics but one may show that MHD still makes sense with minor error when the opposite limit is verified for the electrons. An important implication of the hydrodynamic approximation is that resonances may not occur between the described population and the waves. In the absence of resonances, the velocity distribution of particles cannot be broken, and the choice to describe only a few moments of distribution functions gets fully justified.

As explained earlier, macro-scale instabilities are the most direct interaction channel between energetic particles and the thermal plasma, and their characteristic interaction length is appropriate for MHD. Unfortunately, the hydrodynamic approximation is not verified for suprathermal particles, which followingly need kinetic modelling. For oscillations of the order of or below the acoustic frequency, MHD also becomes incomplete for the representation of the thermal plasma. Consequently, modelling the interaction of energetic particles with the thermal plasma requires a **mixing of MHD and kinetic theory** for modes oscillating around the Alfvén frequency, and **purely kinetic theory for lower frequencies**. For

both populations, **nonlinear effects** may play a role, and such effects can account for the transport of fast particles. Finally, the study may also get complicated by the possibility of **wave coupling between macro and micro waves**, which allow micro-waves to be an indirect channel in the transport and energy deposition of energetic particles.

## 1.4 Thesis outline

The topic of the PhD work presented here is the study of one type of macro-scale mode, known to interact strongly with energetic particles: the **Beta Alfvén Eigenmode (BAE)**.

BAEs are waves oscillating in the acoustic frequency range. This makes their study particularly challenging and important for the efficiency of burning plasmas. Indeed, in this frequency range, waves can resonate with both suprathermal particles and thermal ions. Consequently, **they may be a particularly good channel for a direct energy transfer from the suprathermal particles to the fuel ions**. Besides, the acoustic frequency is located at a cross-point between MHD studies and turbulent transport physics, which suggests **that acoustic waves could draw a link between the dynamics of energetic particles and the transport of the thermal plasma particles**.

During the lengthtime of the PhD work, we derived **the BAE dispersion relation** in a way which provides a direct description of the **mode structure** and using a **formalism which connects kinetic theory and MHD theory continuously**. Next, we analyzed the stability of BAEs in the presence of energetic ions. In a first attempt, a purely linear description was used, making possible the obtention of an **analytical linear criterion for BAE destabilization in the presence of energetic particles**, and the latter criterion was **compared with experiments, conducted in the Tore-Supra tokamak** during the time of PhD work. Finally, because the linear analysis revealed some features of the BAE stability which can be subject to a strong nonlinear modification, the question was raised of the possibility of a subcritical activity of the mode. In this direction, **a simple model was developed which gives some hints into the existence of metastable modes**.

Beyond the particular features of BAEs, general questions have been tackled, related to the dynamics of modes in the presence of energetic particles and from a broader perspective, in the presence of a resonant drive. The present thesis does not intend to forget this general framework. For this reason, we start our presentation with a review of the main physics involved in the interaction of energetic particles with macro/meso-scale waves, in *Chapter 2*, in order to define the points of relevance to be discussed in the analysis of BAEs: the role of geometry for the stability of waves with a *finite* frequency, the time scales involved, the required behaviors to retain in the modelling. In this chapter, fundamental concepts and notation of tokamak physics will be introduced.

The next chapters are more focused on the description and analysis of BAEs developed during the PhD work. *Chapter 3* explains the general "kinetic-MHD" variational model used for the modelling of BAEs. In *Chapter 4*, we derive the BAE dispersion relation and structure, using the previously defined framework. In *Chapter 5*, the results of our theoretical and experimental analysis of the BAE linear stability is presented. Finally, *Chapter 6* offers some directions for the nonlinear description of BAEs, and attempts to provide some preliminary response to the question of a possible nonlinear modification of the BAE stability properties.

*People talk fundamentals and superlatives and then make some changes of detail.*

Oliver Wendell Holmes Jr. (1841 - 1935)

# 2

# Fundamental concepts underlying the interaction of collective modes with energetic particles

We start this thesis with a basic review of the fundamental concepts underlying the interaction of energetic particles with a tokamak thermonuclear plasma.

The first part of this chapter is dedicated to the description of particle trajectories in a tokamak equilibrium, in a form which is particularly appropriate to understand particle resonant behaviors. This description will provide first insight into the tricky issue of energetic particles confinement.

Next, the interaction of suprathermal particles with the main plasma itself will be considered from a theoretical point of view, with an attempt to highlight and make accessible the most important results achieved in the modelling of this interaction, as well as the formalisms involved.

Finally, the experimental opportunities offered by the tokamak Tore-Supra with regards to this study will be depicted.

## 2.1 Magnetic configuration and particle trajectories

### 2.1.1 Magnetic configuration

#### General features

As already overseen in the thesis introduction, a tokamak thermonuclear plasma lies in an axisymmetric torus-like chamber, where charged particles are confined by a strong magnetic field. When the plasma cross-sections are approximately circular, its dimensions can be characterized by a **major radius** $R_0$ representing the plasma center and a **minor radius** $a$ represented in Fig. 2.1, but additional parameters such as elongation or ellipticity, not considered in this thesis, may be necessary to account for more complex cross-sections. The ratio of these two lengths is called the **inverse aspect ratio**,

$$\epsilon = \frac{a}{R_0} \tag{2.1}$$

and it is a measure of the importance of the effects related to the torus-like shape of the tokamak, compared to a purely cylindrical device. $\epsilon$ is a traditionnally considered to be a small parameter ($\sim 0.3$ in Tore-Supra).

At equilibrium (referred to with the notation $_{(0)}$), the tokamak magnetic configuration consists of well-defined embedded flux surfaces tangent to helical field lines, as illustrated in Fig. 2.1. The helicity of the field lines is necessary for a stable three dimensional plasma confinement, and it means that the magnetic field has components both in the axisymmetry direction, and in the meridian cross-sections. More explicitely, for any equilibrium magnetic

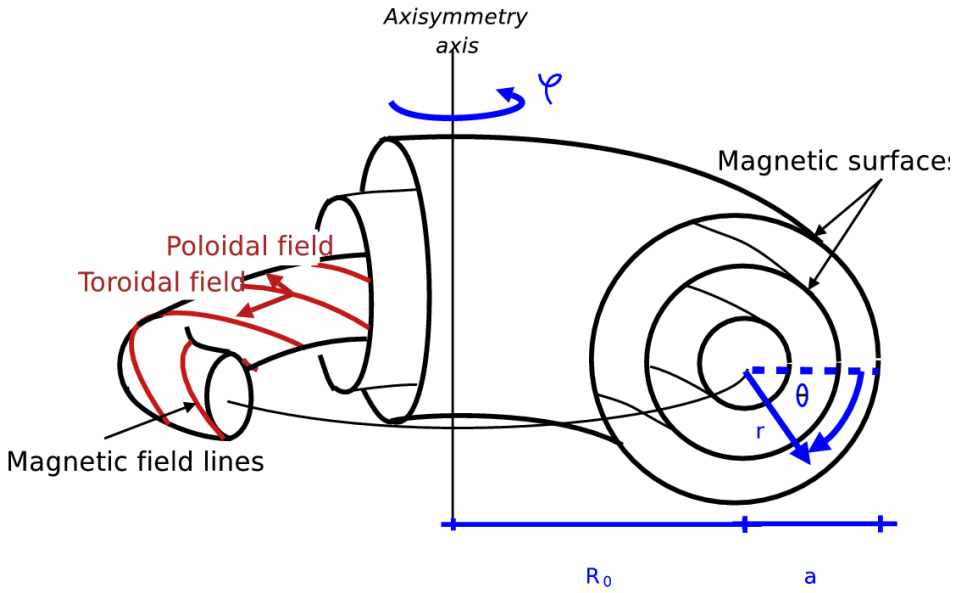


Figure 2.1: The tokamak core magnetic configuration and its traditional toroidal coordinates.

field $\mathbf{B}_{(0)}$ with the topological shape of a torus, there exists a set of coordinates $(-\Psi, \theta, \varphi)$ and a function $q(\Psi)$ such that

$$\mathbf{B}_{(0)} = \nabla\Psi \times \nabla(\varphi - q(\Psi)\theta), \tag{2.2}$$

where $\Psi$ is flux surface label (i.e, a function which is constant on magnetic surfaces) and can be understood as a radial coordinate, $\varphi$ is an angle which surrounds the device main vertical axis and defines the so-called **toroidal** direction, and $\theta$ is an angle which wraps the confinement chamber and defines the **poloidal** direction. One should also note that the word **toroidal** often also refers to the effects related to the torus configuration, in opposition to those related to an open cylindrical configuration. The field curvature towards the axisymmetry axis is an example of such toroidal effects.

Using this representation and vocabulary, the two characteristic components of the magnetic field can now be more accurately defined as a toroidal field $\mathbf{B}_{\mathrm{T}(0)} = -q(\Psi)\nabla\Psi \times \nabla\theta$, and a poloidal field $\mathbf{B}_{\mathrm{P}(0)} = \nabla\Psi \times \nabla\varphi$, which is typically small compared to $\mathbf{B}_{\mathrm{T}(0)}$, $\mathbf{B}_{\mathrm{P}(0)} \sim \epsilon\mathbf{B}_{\mathrm{T}(0)}$. In usual tokamak devices, the toroidal field is generated by external fields and the poloidal field by the generation of an equilibrium plasma current flows in the toroidal direction.

More precisely, it can be shown that in Eq. 2.2, $\Psi$ and $q$ are uniquely defined [8]. For a given flux surface, $-\Psi$ [1] is the poloidal flux crossing the ribbon-like surface $\mathcal{S}_\theta$ streched between the magnetic axis and the flux surface for a fixed value of $\theta$ (normalized to $2\pi$),

$$-\Psi = \frac{1}{2\pi}\int_{\mathcal{S}_\theta} ds\ \mathbf{B}_{(0)} \cdot \frac{\nabla\theta}{|\nabla\theta|}, \qquad (ds > 0). \tag{2.3}$$

If we now similarly define the toroidal magnetic flux going though $\mathcal{S}_\varphi$, a surface of constant $\varphi$ bounded by a given flux surface,

$$\Phi = \frac{1}{2\pi}\int_{\mathcal{S}_\varphi} ds\ \mathbf{B}_{(0)} \cdot \frac{\nabla\varphi}{|\nabla\varphi|}, \tag{2.4}$$

[1] The minus sign is a traditional convention made to allow a fast identification of $\Psi$ with the magnetic vector potential which is in the axisymmetry direction.

$q$ can be shown to be a flux surface label defined by

$$q \equiv -\frac{d\Phi}{d\Psi} = \frac{\mathbf{B}_{(0)} \cdot \nabla\varphi}{\mathbf{B}_{(0)} \cdot \nabla\theta}. \tag{2.5}$$

$q$ is an important parameter for tokamak studies, called the **safety factor**. It is a measure of the magnetic field helicity, whose absolute value precisely corresponds to the number of toroidal turns that a field line does while performing a single poloidal turn. For a plasma current flowing in the direction of the toroidal magnetic field, $(-\Psi, \theta, \varphi)$ is a right-handed coordinate system, and $q$ is positive.

Note that $\Phi$ and $q$, being flux surface labels, may be chosen as alternate *radial* coordinates. More commonly, the **radial coordinate** $r = a\sqrt{\Phi/\Phi(a)}$ is considered, since it can be shown to have an approximate regular behavior, close to the intuitive idea of a radius.

Using $\mathbf{r}$, we can define a commonly used quantity, the **shear** which is simply the normalized derivative of $q$,

$$s = \frac{r}{q}\frac{dq}{dr}. \tag{2.6}$$

Finally, we note that in a tokamak configuration, axisymmetry provides a simplified expression for the field. Indeed, $\varphi$ may be chosen to be the axisymmetry angle, such that the coordinate system $(-\Psi, \theta, \varphi)$ becomes partially orthogonal. Hence, $\mathbf{B}_{(0)}$ can be written

$$\mathbf{B}_{(0)} = \nabla\Psi \times \nabla\varphi + I\nabla\varphi, \tag{2.7}$$

with $I$ a flux label $I(\Psi) = R^2\mathbf{B}_{(0)} \cdot \nabla\varphi$, $R$ the distance to the axisymmetry axis [8].

### Simplified large aspect ratio equilibrium

The calculation of the flux surfaces arrangement involves the resolution of the so-called Grad-Shafranov equations [9]. For a circular set-up and with a large aspect ratio assumption $\epsilon^{-1} \gg 1$, the solution of the Grad-Shafranov equation to the second order in $\epsilon$ is a set of nested circular flux surfaces radially shifted in the torus outward direction. In a poloidal cross-section, the corresponding flux surfaces characteristic equations can be expressed in a simple way using the radius $R$ and the vertical direction $Z$ by

$$R = R_0 + r\cos\theta - \Delta(r), \quad Z = r\sin\theta, \tag{2.8}$$

where $\Delta$ is called the Grad-Shafranov shift. For simplicity, most subsequent computation make use of this approximation, sometimes with the additional assumption that $\Delta = 0$.

Applying Ampère's law, the toroidal field is found to be inversely proportional to $R$,

$$B_{\mathrm{T}(0)} = \frac{B_0 R_0}{R}, \qquad I(\Psi) = B_{\mathrm{T}(0)}R = B_0 R_0 \tag{2.9}$$

with $B_0$, the central field (taken at $R = R_0$ and $r = 0$). In the large aspect ratio limit with $\Delta = 0$, it follows that

$$B_{(0)} \approx B_0(1 - \frac{r}{R_0}\cos\theta), \qquad q = \frac{r}{R_0}\frac{B_{\mathrm{T}(0)}}{B_{\mathrm{P}(0)}} \tag{2.10}$$

### 2.1.2 Particle trajectories at equilibrium

Let us now describe the motion of a charged particle in the equilibrium electromagnetic field. As an addition to the magnetic field $\mathbf{B}_{(0)}$ described above, there may also be an equilibrium electric field $\mathbf{E}_{(0)} = -\nabla\phi_{(0)} - \partial_t \mathbf{A}_{\text{solenoid}}$, mainly induced by the magnetic flux generated in the tokamak central solenoid (see Fig. 1.3) for the plasma current generation.

From now on, we will make use of the words *perpendicular* and *parallel* to describe the plasma dynamics, and of the corresponding notations $\perp$ and $\parallel$. Unless otherwise noted, the latter adjectives should be understood with reference to the magnetic field, and more precisely to the equilibrum magnetic field, when a linear analysis is carried out.

#### Basic description of particle trajectories in a tokamak at equilibrium

As explained earlier, magnetic confinement is based on the idea that a magnetic field can enforce particles to follow its lines. More accurately, the perpendicular velocity of a charged particle immersed in a constant magnetic field is transformed into a rotational velocity around the field lines, whereas its parallel velocity is kept unperturbed. Hence its net parallel velocity. In a tokamak, the picture is more complicated because of the non-uniformity of the magnetic field and the presence of an electric field. Nevertheless, to the lower approximation, a charged species of a tokamak rotates around the magnetic field lines with a **gyrofrequency** $\boldsymbol{\Omega}_c$ and gyration or **Larmor radius** $\rho_\perp$ given by

$$\Omega_c = \frac{eB_{(0)}}{m}, \quad \rho_\perp = \frac{mv_\perp}{eB_{(0)}} \equiv \frac{v_\perp}{v_t}\rho \tag{2.11}$$

where $e$, $m$, $v_\perp$, $v_t$ are respectively the charge, the mass, the perpendicular and the thermal velocity of the species $s$. $\rho$ is more frequently used and called the **thermal gyroradius**, or simply gyroradius.

More precisely, when the magnetic field is almost uniform at the scale of the particle motion, ie.

$$\rho\frac{\nabla B_{(0)}}{B_{(0)}} \sim \frac{\rho}{L_p} \equiv \rho^* \ll 1 \text{ ($L_p$ is a typical equilibrium plasma scale)}, \tag{2.12}$$

which is typically the case in a tokamak (for electrons $\rho_e^* < 10^{-4}$, for thermal deuterium ions $\rho_i^* \sim 10^{-3}$ and for suprathermal ions $\rho_h^* \sim 10^{-2}$), the motion of a charged particle $\mathbf{x}$, can be divided into a small scale, fast gyrating motion and a larger scale, slower **guiding-center** motion $\mathbf{X}$, independent from the angle of the gyromotion (or gyroangle) $\gamma$,

$$\mathbf{x} = \mathbf{X} + \boldsymbol{\rho}, \text{ with } \boldsymbol{\rho} = O(\rho^*\mathbf{X}) \tag{2.13}$$

$$\dot{\mathbf{x}} = \dot{\mathbf{X}} + \dot{\boldsymbol{\rho}}, \text{ with } \dot{\boldsymbol{\rho}} \sim \dot{\mathbf{X}}. \tag{2.14}$$

When expanding the charged particle motion using Eq. 2.13, the guiding-center motion is found to depend only on its position $\mathbf{X}$ and of **two motion invariants**, its **magnetic moment** $\mu = mv_\perp^2/2B_{(0)}$ and its **energy** $\mathsf{E} = \mu B_{(0)} + mv_\parallel^2/2 + e\phi_{(0)}$, which may be assessed at the position $\mathbf{X}$ to the order considered in Eq. 2.14. Remark that if the invariance of $\mathsf{E}$ is exact in a conservative system at equilibrium, the invariance of $\mu$, derived from the expansion 2.13, is only verified to the $0^{th}$ order in $\rho^*$, and $\mu$ is thus often referred to as the **adiabatic invariant** [2]. To the expansion order considered in Eq. 2.14, this limit is not an issue.

A direct consequence of the invariance of $\mu$ is that some particles remain confined in the outer part of the confinement chamber as illustrated in Fig. 2.2. The latter particles are

[2] Note that $\mu$ is sometimes taken to be an invariant by definition, at any considered order in $\rho^*$. As will be clearer in the coming developments, it is equivalent to say that the guiding-center motion is taken to be independent of the gyroangle by definition. In this case, $\mu$ is not simply given by the expression $\mu = mv_\perp^2/2B_{(0)}$, and asymptotic developments exist.

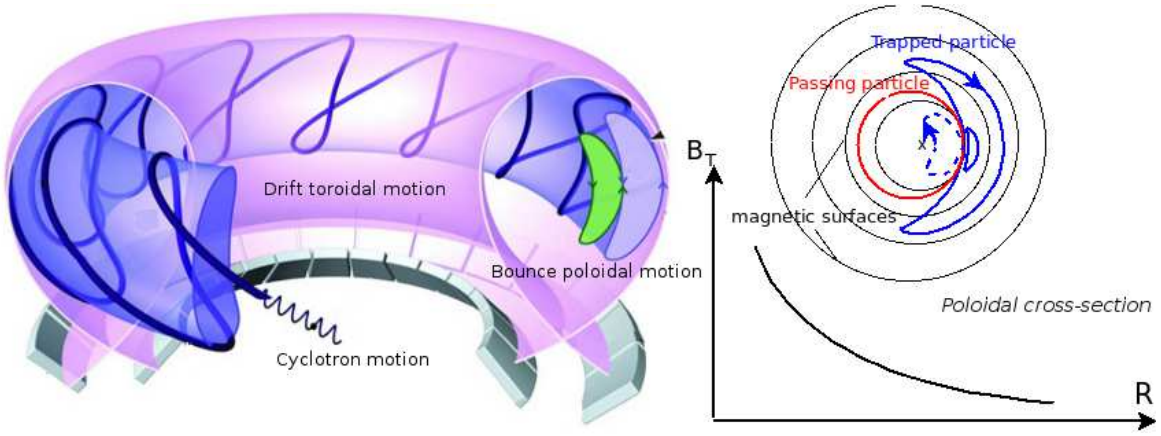


Figure 2.2: Particle trajectories in a tokamak. The left hand side picture illustrates the three angular components of a trapped particle trajectory. The right hand side picture is a poloidal projection of the trajectories of a passing and a trapped particle.

called **trapped particles** and their trajectories have the shape of a *banana* when projected onto a poloidal cross-section. To understand this behavior, we need to recall that the magnetic field of a toroidal configuration cannot be uniform, but varies like $1/R$ (Eq. 2.9). Let us now consider a particle characterized by the invariants $\mathsf{E}$ and $\mu$ and use the approximation that $B_{(0)} \approx B_{\mathrm{T}(0)}$, it directly comes that $\mu = (\mathsf{E} - mv_\parallel^2/2)/B_{(0)} \propto R(\mathsf{E} - mv_\parallel^2/2)$. Hence, if the particle approximately follows a helical field line and comes nearer to the axisymmetry axis, $R \to 0$, the simultaneous invariance of $\mathsf{E}$ and $\mu$ may enforce a cancellation of $v_\parallel$, which means that the particle (or more exactly its guiding-center) will bounce back to the outer region of the tokamak. If $v_\parallel$ does not cancel, the particle is called **passing particle**.

The existence of trapped particles is a first evidence that the motion of charged particles is not purely along the field lines. More explicitely, it can be shown that the guiding-center motion is, as expected, mainly parallel but that it also contains a **drift**. Explicitely,

$$\dot{\mathbf{X}} = v_\parallel \mathbf{b} + \mathbf{v}_g + O(\rho^{*2}\ v_t) \tag{2.15}$$

where $\mathbf{v}_g$, called the drift velocity, contains three physical components related to the presence of an electric field and to the magnetic field non-uniformities, $\mathbf{v}_g = \mathbf{v}_{\mathbf{E}\times\mathbf{B}} + \mathbf{v}_{\nabla B} + \mathbf{v}_c$ with

- $\mathbf{v}_{\mathbf{E}\times\mathbf{B}} = \frac{\mathbf{E}_{(0)}\times\mathbf{B}_{(0)}}{B_{(0)}^2}$ , the $\mathbf{E}\times\mathbf{B}$ drift
- $\mathbf{v}_{\nabla B} = \frac{\mu}{e}\mathbf{b}_{(0)} \times \frac{\nabla B_{(0)}}{B_{(0)}}$ , the grad-$B$ drift
- $\mathbf{v}_c = \frac{mv_\parallel}{eB_{(0)}}\mathbf{b}_{(0)} \times \boldsymbol{\kappa}$ , the curvature drift

where $\mathbf{b}_{(0)} = \mathbf{B}_{(0)}/B_{(0)}$, and $\boldsymbol{\kappa} = \mathbf{b}_{(0)} \cdot \nabla \mathbf{b}_{(0)}$ is the field local curvature. When $\mathbf{E}_{(0)}$ is chosen such that the $\mathbf{E}\times\mathbf{B}$ drift is only first order compared to $\rho^*$, which is the case in standard discharges (where $E_{(0)}$ is mainly parallel for toroidal current generation), $\mathbf{v}_g$ is shown to be only first order in $\rho^*$.

Note that the above developments would still be correct with slowly varying fields,

$$\frac{1}{\Omega_c}\frac{1}{B_{(0)}}\frac{dB_{(0)}}{dt} \sim \rho^*. \tag{2.16}$$

An additional drift associated with this time variation can be found in the litterature

- $\mathbf{v}_P = \frac{m}{e}\mathbf{b}_{(0)} \times \frac{d\mathbf{v}_g}{dt}$ , the polarization drift

but it is only second order in $\rho^*$ with our conventions.

It follows from the described drifts that the particle trajectories deviate from the field lines, which we represented in Fig. 2.2.

### Hamiltonian description of particle motion

Even if the direct expansion of the charged particle motion mentioned in the previous section may lead to a good physical understanding of its main dynamics, it rapidly becomes a hazardous work, when one wants to change the coordinate system, the geometry, add a perturbation or simply find higher order expressions.

For this reason, the developments to come will rather make use of the equivalent hamiltonian description of particle motion, which is particularly practical to unveil motion invariants or check the validity of their conservation, for example the energy conservation. The notions of Hamiltonian mechanics used in this thesis are summarized in Appendix A, and expressed using the conventions of Ref. [10], where a Lagrangian is mathematically a differential 1-form.

The motion of a charged particle immersed in a magnetic field, $\mathbf{B} = \nabla \times \mathbf{A}$ and an electric field $\mathbf{E} = -\nabla\phi - \partial_t \mathbf{A}$ in the six dimensional space-velocity phase space, is a Hamiltonian system, which can be expressed in the coordinate system $(\mathbf{x}, \mathbf{p}) = (\mathbf{x}, m\mathbf{v} + e\mathbf{A})$, with

$$\text{the } \textbf{Lagrangian} \quad \hat{\underline{\Gamma}}(\mathbf{x}, \mathbf{p}, t) = \mathbf{p} \cdot \mathsf{d}\mathbf{x} - \hat{H}\mathsf{d}t, \tag{2.17}$$

$$\text{the } \textbf{Hamiltonian} \quad \hat{H}(\mathbf{x}, \mathbf{p}, t) = \frac{|\mathbf{p} - eA|^2}{2m} + e\phi. \tag{2.18}$$

A Hamiltonian system described by the Lagrangian $\underline{\Gamma}(\mathbf{Z}, t) = \mathbf{\Gamma}(\mathbf{Z}, t) \cdot \mathsf{d}\mathbf{Z} - H(\mathbf{Z}, t)\mathsf{d}t$ with $\mathbf{Z} = (Z^a)_{a=1\ldots6} \in \mathbf{R}^6$ a phase-space coordinate system, verifies Hamilton's equations:

$$\frac{dZ^a}{dt} = [Z^a, H] + [Z^a, Z^b]\frac{\partial \Gamma_b}{\partial t} \tag{2.19}$$

where $[,]$ are called the **Poisson Brackets**.

The Poisson Brackets correspond to a bilinear antisymmetric function depending of the Lagrangian components $\mathbf{\Gamma}(\mathbf{Z}, t)$. They are correctly definined in Appendix A. Nethertheless, only two simple situations will be tackled in the thesis:

- When the values of the Poisson Brackets are known in a given coordinate system $\mathbf{Z} \in \mathbf{R}$, then for any function $f(\mathbf{Z}, t)$ and $g(\mathbf{Z}, t)$

$$[f, g] = \frac{\partial f}{\partial Z^a}[Z^a, Z^b]\frac{\partial g}{\partial Z^b}. \tag{2.20}$$

- When the coordinate system is **canonical**, that is, when the Lagrangian is of the form $\underline{\Gamma}(\mathbf{Z}, t) = Z_1 dZ_4 + Z_2 dZ_5 + Z_3 dZ_6 - H(\mathbf{Z}, t)\mathsf{d}t$, the expression of the Poisson Bracket is

$$[,] = \partial_{\boldsymbol{\mathcal{X}}}\partial_{\boldsymbol{\mathcal{P}}} - \partial_{\boldsymbol{\mathcal{P}}}\partial_{\boldsymbol{\mathcal{X}}} \tag{2.21}$$

where $\boldsymbol{\mathcal{X}} = (Z_1, Z_2, Z_3)$, and $\boldsymbol{\mathcal{P}}$ gathers the so-called momenta, $\boldsymbol{\mathcal{P}} = (Z_4, Z_5, Z_6)$.

The Lagrangrian describing the charged particle motion 2.17 is obviously expressed in canonical coordinates. Thus, Hamilton's equations 2.19 are easily computed,

$$\frac{d\mathbf{x}}{dt} = \partial_{\mathbf{p}}\hat{H} = \mathbf{p}/m \tag{2.22}$$

$$\frac{d\mathbf{p}}{dt} = -\partial_{\mathbf{x}}\hat{H} = e(\mathbf{E}+\mathbf{v}\times\mathbf{B}) + e\frac{d\mathbf{A}}{dt} \tag{2.23}$$

which shows that the Hamilton's equations are nothing but the usual Lorentz force balance. Nevertheless, we now have a powerful formalism to make coordinate transformations.

*~ Coordinate transformation in Hamiltonian systems & Application to the guiding-center transformation ~*
Hamilton's principle (see Appendix A) implies that the physics is conserved in a coordinate transformation, $\mathbf{Z} \to \mathbf{Z}'$, if there exists a total derivative $\mathsf{d}S$ [11],

$$\underline{\Gamma}'(\mathbf{Z}',t) = \underline{\Gamma}(\mathbf{Z},t) + \mathsf{d}S \tag{2.24}$$

Littlejohn [12] made use of this principle to derive the equations of motion for the guiding center in an equilibrium field $\mathbf{B}_{(0)}$. Starting from the Lagrangian $\hat{\underline{\Gamma}}$ of Eq. 2.17 and after successive modifications of the form 2.24, he found to the first order in $\rho^*$ the guiding-center relevant Lagrangian in the form

$$(\mathbf{x},\mathbf{p}) \to (\mathbf{X},\mu,v_\parallel,\gamma) \tag{2.25}$$

$$\hat{\underline{\Gamma}} \to \underline{\Gamma}_{\rm gc} = \mathbf{A}^*_{(0)}\cdot\mathsf{d}\mathbf{X} + \mu\mathsf{d}\gamma - H_{\rm gc}\mathsf{d}t$$
$$\text{with } H_{\rm gc} = \frac{1}{2}mv_\parallel^2 + \mu B_{(0)}(\mathbf{X}) + e\phi_{(0)}(\mathbf{X}), \tag{2.26}$$

and the corresponding basis Poisson Brackets,

$$\begin{array}{lllll} [X_i,X_j] &=& -(\nabla X_i\times\nabla X_j)\cdot\frac{\mathbf{b}_{(0)}}{eB^*_{(0)\parallel}}, & \left[\mathbf{X},mv_\parallel\right] &= \frac{\mathbf{B}^*_{(0)}}{B^*_{(0)\parallel}} \\ [\mu,X] &=& 0, & \left[\mu,v_\parallel\right] &= 0 \end{array} \tag{2.27}$$

where the $(^*)$ used by this author may be understood as a first order correction to the traditional fields: $\mathbf{A}^*_{(0)} = \mathbf{A}_{(0)} + (mv_\parallel/e)\mathbf{b}_{(0)}$, $\mathbf{B}^*_{(0)} = \nabla\times\mathbf{A}^*_{(0)}$, $B^*_{(0)\parallel} = \mathbf{b}_{(0)}\cdot\mathbf{B}^*_{(0)}$.

As required, this formulation leads to the same dynamics as the one described in the previous subsection. Indeed, expanding formulas 2.27 to recover the usual fields and keeping only first order corrections, it comes [3]

$$[X_i,X_j] = -(\nabla X_i\times\nabla X_j)\cdot\frac{\mathbf{b}_{(0)}}{eB_{(0)}}, \quad \left[\mathbf{X},mv_\parallel\right] = \mathbf{b}_{(0)} - \frac{mv_\parallel}{eB_{(0)}}(\boldsymbol{\kappa}\times\mathbf{b}_{(0)}) \tag{2.28}$$

which directly allows to recover the usual drifts

$$\frac{d\mathbf{X}}{dt} = [\mathbf{X},H_{(0)}] = v_\parallel\mathbf{b}_{(0)} + \mathbf{v}_c + \mathbf{v}_{\mathbf{E}\times\mathbf{B}} + \mathbf{v}_{\nabla B}\ .$$

Formulas 2.28 are the one used in the thesis, for their simplicity. However, it has to be noted that they do not conserve phase-space volumes exactly, contrary to formulas 2.27 [10].

[3] Note a useful formula: $\mathbf{b}\times\nabla\times\mathbf{b} = -\mathbf{b}\cdot\nabla\mathbf{b}$.

### Action-angle variables

In the previous section, we explained that a Hamiltonian description of particle motion could be powerful, and lead to simple insightful motion equations when expressed in canonical variables. However, when going from the particle variables $(\mathbf{x}, \mathbf{p})$ to the guiding-center variables $(\mathbf{X}, \mu, \mathsf{E}, \gamma)$, canonicity is lost. Fortunately, in the tokamak geometry, it is possible to display a **canonical system of variables which is consistent with the decoupling of the gyromotion and guiding-center motion**. Moreover, if follows from the tokamak periodicity in $\theta$ and $\varphi$ that the particle motion is quasiperiodic at equilibrium, and the chosen system of coordinates can be taken to be a system of **action-angle variables** $(\boldsymbol{\alpha}, \boldsymbol{J})$. Action-angle variables are a particular type of canonical variables appropriate for periodic systems where the "spatial" variables are angles and the momenta (or actions) are motion invariants, that is,

$$\dot{\mathbf{J}} = -\frac{\partial H_{(0)}}{\partial \boldsymbol{\alpha}} = 0, \quad \dot{\boldsymbol{\alpha}} = \frac{\partial H_{(0)}}{\partial \mathbf{J}} = \boldsymbol{\Omega}_{(0)}(\mathbf{J}) \tag{2.29}$$

Hence, this description does not only provide canonicity but also physical motion invariants, to which $\mu$ belongs. Moreover, the characteristic eigenfrequencies of the periodic particle motion can be directly derived, and the question of the time decoupling of the different periodic motion directly assessed. In particular, for the understanding of the resonances between waves and energetic particles, it is necessary to know these eigenfrequencies.

A derivation of the set of action-angle variables used in this thesis is provided in Appendix B.1, which closely follows Refs. [13, 14, 15]. The motion is found to be divided into three angular periodic motions

$$\boldsymbol{\alpha} = (\alpha_1, \alpha_2, \alpha_3) = \boldsymbol{\Omega}\ t = \boldsymbol{\alpha}_0 \quad + \boldsymbol{\Omega} \int_0^\theta \frac{d\theta}{\dot{\theta}} \tag{2.30}$$

(where $\boldsymbol{\alpha}_0$ stands for the initial phase-space position) with invariant eigenfrequencies

$$\begin{aligned}
\Omega_1 &= \Omega_b \oint \tfrac{d\theta}{2\pi} \tfrac{1}{\dot{\theta}}\ \dot{\gamma} && \approx \Omega_b \oint \tfrac{d\theta}{2\pi} \tfrac{1}{\dot{\theta}} \tfrac{eB_{(0)}}{m} \\
\Omega_2 &\equiv \Omega_b = 2\pi \left( \oint \tfrac{1}{\dot{\theta}} \right)^{-1} && \approx 2\pi \left( \oint \tfrac{1}{\mathbf{b}_{(0)} \cdot \nabla\theta\ v_\parallel} \right)^{-1} \\
\Omega_3 &= \Omega_b \oint \tfrac{d\theta}{2\pi} \tfrac{1}{\dot{\theta}}\ \dot{\varphi} && \approx \Omega_b \oint \tfrac{d\theta}{2\pi} \tfrac{1}{\dot{\theta}}\ \mathbf{v}_D \cdot \left[ -q'(\bar{\Psi})\theta \nabla\Psi + \nabla(\varphi - q(\bar{\Psi})\theta) \right] \\
&&& \quad + \delta_{\text{passing}}\ q(\bar{\Psi})\Omega_b
\end{aligned} \tag{2.31}$$

where the first angular motion is found to be related to the gyromotion $\gamma$, the second to the poloidal motion described by $\theta$ also called the **bounce motion**, and the third, called **precessional drift**, to the particle drift in the toroidal direction. The three angular motions can be clearly identified in the 3-D picture of Fig. 2.2. The *bounce integral* $(\Omega_b/2\pi) \oint (d\theta/\dot{\theta})...$, present in the eigenfrequencies expression, allows to remove the fields $\theta$-dependence. For passing particles, $\oint = \oint_0^{2\pi}$, whereas for trapped particles oscillating between the $\theta$-angles $[-\theta_0, \theta_0]$, $\oint = (1/2) \int_{-\theta_0}^{-\theta_0}$ (the full closed banana) $\approx \int_{-\theta_0}^{\theta_0}$.

The corresponding invariant momenta are

$$\begin{aligned}
J_1 &= \tfrac{m}{e}\mu \\
J_2 &= \oint \tfrac{d\theta}{2\pi} \tfrac{B_\theta}{B_{(0)}} m v_\parallel + e \oint \tfrac{d\theta}{2\pi} \Phi && \approx \oint \tfrac{d\theta}{2\pi} \tfrac{r^2}{qR_0}\ m v_\parallel + \delta_{\text{passing}}\ e\Phi(J_3) \\
J_3 &= e\Psi + \tfrac{I(\Psi)}{B_{(0)}} m v_\parallel && \approx e\Psi + R m v_\parallel
\end{aligned} \tag{2.32}$$

where $B_\theta$ is the covariant component of the field along $\theta$.

$J_1$ is nothing but the gyromotion adiabatic invariant, Similarly, $J_2$ is an adiabatic invariant and $J_3$ is an exact invariant related to the equilibrium axisymmetry in the toroidal direction, also simply called **toroidal momentum**.

We also provide in Eqs. 2.31 and Eqs. 2.32 some more approximate expressions of the invariants and motion characteristic frequencies, which are easier to use and interpret (This will be useful later on.). To make these approximations, we simply kept the lower order expressions in $\rho^*$ and $\epsilon$. Explicitely, we made use of the simplified expressions of the geometry given in section 2.1.1 and we neglected the drift motion when the parallel velocity had a finite contribution. This way a discontinuity appears between passing and trapped particles ($\delta_{\text{passing}} = 1$ for passing particles and 0 for trapped particles). The drift motion disappears in $\Omega_2$ and hence, the flux $\Phi$ becomes an invariant in the expression of $J_2$ for passing particles. The drift motion simply remains in the expressions of the toroidal drift, where we expanded the radial drift around a reference flux surface $\bar{\Psi}$.

Fully explicit expression of the equilibrium motion eigenfrequencies Eq. 2.31 can even be found within these approximations. The calculation of the normalized bounce and drift frequencies $\bar{\Omega}_b$ and $\bar{\Omega}_d$ such that

$$\Omega_2 = \Omega_b = \pm\frac{1}{qR_0}\sqrt{\frac{2\mathsf{E}}{m}}\bar{\Omega}_b, \quad \Omega_3 = \Omega_d + \delta_{\text{passing}} q(r)\Omega_b = \frac{q(r)}{r}\frac{E}{eB_0R_0}\bar{\Omega}_d + \delta_{\text{passing}} q(r)\Omega_b \quad (2.33)$$

is given in Appendix B.2 for the simplified geometry described in Eq. 2.1.1. We also give in this Appendix some more general expressions taken from Ref. [16] which contain effects of the Grad-Shafranov shift. The latter expressions are the one used in the thesis.

We now have a powerful description of the particle trajectories which, as explained earlier, is particularly appropriate for the computation of resonant behaviors.

Indeed, using the expression of the motion eigenfrequencies 2.31, one may directly catch the frequency range of the modes which may resonate and followingly exchange energy with the particles. As explained earlier $\Omega_1 \gg \Omega_2, \Omega_3$. Since $\Omega_3$ simply contains the lower order drift motion, we often get an additional time scale separation $\Omega_d < \Omega_b$. However, since $\Omega_b \propto \sqrt{\mathsf{E}}$, $\Omega_d \propto \mathsf{E}$, this separation is not strong for larger energies (orders of magnitude corresponding to our specific parameters of study will be provided later on in this thesis).

Moreover, we will see later on, that the non-conservation of the equilibrium invariants in the presence of a wave is the source of resonant wave-particle energy transfers: a computation of these transfers is consequently cleaner in the action-angle space.

Nevertheless, one should note that the action-angle variables may not allways be the most intuitive coordinates since they imply a mixing of space and velocity coordinates. For this reason, the energy invariant $\mathsf{E}$ is sometimes chosen instead of $J_2$. When doing this, another notation will be made use of, ie. ($\mu = J_1, \mathsf{E}, P_\varphi = J_3$), in order to make clear that $\mathsf{E}$ not $\mathbf{J}_2$ should be kept constant when deriving by $\mu$ or $P_\varphi$ (The $P_\varphi$ notation simply result from the remark that $J_3$ is nothing but the toroidal momentum, Appendix B.1.). Besides, noticing that $e\Psi/mRv_\parallel \sim (1/\rho^*)(\epsilon^2)(r/a)^3$, and taking $\rho^* \sim 10^{-3}, \epsilon \sim 0.3$ consistently with typical Tore-Supra parameters, it comes that far enough from the magnetic axis, $e\Psi$ dominates in the expression of $J_3$. Hence, it is often more convenient (and possible) to interpret $J_3$ as a purely radial coordinate.

### Application to energetic particle trajectories

We compared in Tab. 2.1 some features of the thermal and suprathermal particles' trajectories corresponding to a typical Tore-Supra discharge (where the suprathermal ions are

assumed to be heated by *Ion Cyclotron Resonant Heating in the minority heating scheme*) and to ITER parameters (where suprathermal particles are taken to be fusion born alpha particles). First, characteristic frequencies (corresponding to very trapped particles, $\bar{\Omega}_b \sim 1$, $\bar{\Omega}_d \sim 1$) are provided and put in parallel with the Alfvénic and acoustic frequency ranges. Next, typical gyration widths associated with the motion invariants are given: the Larmor radius and the banana width of trapped particles (considered here for marginally trapped particles, which display the largest width).

| | $D^+$ in TS ($E = 5$ keV) | $H^+$ in TS ($E = 300$ keV) | $D^+$ in ITER ($E = 15$ keV) | $\alpha$ in ITER ($E = 3.56$ MeV) |
|---|---|---|---|---|
| Acoustic range | $\sim 32$ kHz | | $\sim 21$ kHz | |
| Shear Alfvén range | $\sim 500$ kHz | | $\sim 190$ kHz | |
| $\Omega_c/2\pi$ | 28 MHz | 58 MHz | 40 MHz | 13 MHz |
| $\Omega_b/2\pi$ | 46 kHz | 500 kHz | 31 kHz | 270 kHz |
| $\Omega_d/2\pi$ | 0.4 kHz | 24 kHz | 0.12 kHz | 28 kHz |
| Larmor radius | 2.5 mm | 1.5 cm | 3.0 mm | 9.0 cm |
| Banana width | 8. mm | 4.5 cm | 1.0 cm | 30 cm |

Table 2.1: Features of the thermal and energetic ion trajectories in Tore-Supra and ITER, calculated with the values of Tab. 1.1, a normalized radius of 0.3, a density of $5e19$ m$^{-3}$ and $q = 1.0$.

Tab. 2.1 shows that the time scale separation between the gyromotion and guiding-center motion is fully verified for both energetic and thermal particles, but that the scale separation of the bounce and drift motions becomes less clear when going to higher energies. Besides, it confirms the idea developed in the thesis introduction that resonances are possible with the acoustic frequency range for both thermal and suprathermal particles, which makes this frequency range particularly important for the understanding of wave-particle resonances. In particular, resonances with macro-scale structures are expected to be more relevant since micro-scale perturbation ($\sim 1$ mm) fall below the typical Larmor radius of energetic particles.

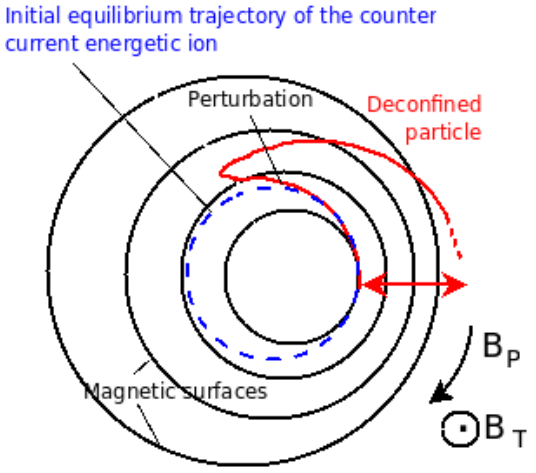


Finally, the calculation of the banana width of barely trapped particles gives a first insight in the particles confinement, because it is a measure of the deviation from the field lines. As can be seen in the table, the banana width of barely trapped energetic particles is a non-negligible fraction of devices' minor radius (5 cm/70cm in Tore-Supra, 0.3m/2m in ITER). We may already expect possible losses of confinement when a passing particle is slightly perturbed and gets slightly trapped (see the schematic on the side). Let us now analyze how such a perturbation may occur.

## 2.2 Theoretical review of energetic particle driven modes

We now review the main features of the interaction between energetic particles and the thermal plasma. It was explained earlier that energetic particles were expected to interact

preferably with macro-scale waves, which are traditionally described in the MHD formalism. After explaining some basics of MHD and MHD modes, we tackle the problem of the modes stability in the presence of an energetic particle drive. We display the particular geometric effects which stabilize these modes and lead to a classification between **gap modes** and **energetic particle modes (EPMs)**. Finally, various theories developed to explain the nonlinear evolution of these modes and the correlated transport of energetic particles will be depicted.

### 2.2.1 Basic Magneto-HydroDynamic waves

#### MHD equations, MHD energy principle

MHD is the traditional frame for the description of macroscopic instabilities ($>$ 1 cm in typical tokamak conditions). In the standard ideal MHD formalism, a quasi-neutral plasma of ions and electrons is described as a single fluid using three momenta, its mass density $\rho_M$, its velocity $\mathbf{V}$ and its scalar (isotropic) pressure $P$, and one vector field, the magnetic field $\mathbf{B}$. Ideal MHD equations are

$$\frac{d\rho_{\mathrm{M}}}{dt} + \rho_{\mathrm{M}} \nabla \cdot \mathbf{V} = 0 \tag{2.34}$$

$$\rho_{\mathrm{M}} \frac{d\mathbf{V}}{dt} + \nabla P = \mathbf{J} \times \mathbf{B} \tag{2.35}$$

$$\frac{dP}{dt} + \Gamma P \nabla \cdot \mathbf{V} = 0 \tag{2.36}$$

$$\mathbf{E} + \mathbf{V} \times \mathbf{B} = 0 \tag{2.37}$$

$$\nabla \times \mathbf{E} = -\frac{\partial \mathbf{B}}{\partial t} \tag{2.38}$$

$$\nabla \times \mathbf{B} = \mu_0 \mathbf{J} \tag{2.39}$$

$$\nabla \cdot \mathbf{B} = 0. \tag{2.40}$$

with $d/dt \equiv \partial_t + \mathbf{V} \cdot \nabla$.

The first three equations are the evolution equations of the three fluid moments, and Eq. 2.36 is the MHD pressure closure, characterized by the adiabatic compressibility coefficient $\Gamma$, equal to 5/3 for an isotropic pressure. Eq. 2.37 is the ideal Ohm's law which fully determines the electric field $\mathbf{E}$ as a function of $\mathbf{B}$. The last three equations result from the low frequency limit of Maxwell equations (no displacement current considered), and they define the plasma current $\mathbf{J}$ completely as a function of $\mathbf{B}$. In particular $\mu_0$ is the vacuum permeability.

Though not completely useful ($\mathbf{E}$ could be replaced directly in Eq. 2.38), Ohm's law contains important features of the MHD formalism. First, it directly returns that $E_{\|} = 0$, which means that charge separation is not considered to take place in the parallel direction. This condition will be refered to as the **MHD condition** in the remainder of the text. Secondly, after crossing with $\mathbf{B}$, it implies that $\mathbf{V}_\perp = \mathbf{E} \times \mathbf{B}/B^2$, showing that the MHD perpendicular velocity reduces to the fluid $\mathbf{E} \times \mathbf{B}$ drift, which simply results from the particles $\mathbf{E} \times \mathbf{B}$ drift (generalized here to non-equilibrium fields). The dominating character of the $\mathbf{E} \times \mathbf{B}$ drift is a major assumption of MHD, which is consistent with the hydrodynamic limit $\omega \to \infty$ [8]. Indeed, when fast fluctuations are considered $\partial_t \to +\infty$, $\mathbf{E} = -\nabla\phi - \partial_t \mathbf{A} \to \infty$, with $\mathbf{A}$ the vector potential ($\mathbf{B} = \nabla \times \mathbf{A}$). Hence drifts involving $\mathbf{E}$ becomes dominant compared to other effects involving spatial gradients only.

Let us now determine the linear normal modes (with eigenfrequency $\omega$) which may develop in an MHD plasma. For this, consider a fluctuation of eigenfrequency $\omega$ around a

known equilibrium state,

$$\begin{aligned} \rho_{\rm M} &= \rho_{\rm M(0)} + 2{\rm Re}\left(\rho_{\rm M\omega} e^{-i\omega t}\right), \qquad & \mathbf{V} &= 2{\rm Re}\left(\mathbf{V}_\omega e^{-i\omega t}\right), \\ P &= P_{(0)} + 2{\rm Re}\left(P_\omega e^{-i\omega t}\right), & \mathbf{B} &= \mathbf{B}_{(0)} + 2{\rm Re}\left(\mathbf{B}_\omega e^{-i\omega t}\right). \end{aligned} \tag{2.41}$$

A standard procedure to analyze these modes is to make use of a so-called **MHD energy principle**. Linearizing the MHD equations, and defining the MHD displacement $\boldsymbol{\xi}$ such that $\dot{\boldsymbol{\xi}} = \mathbf{V}$ ($-i\omega\boldsymbol{\xi}_\omega = \mathbf{V}_\omega$), the linearized MHD equations can be put in the form $\omega^2 \rho_{\rm M(0)}\, \boldsymbol{\xi}_\omega = \mathcal{F}(\boldsymbol{\xi}_{\boldsymbol{\omega}})$, with $\mathcal{F}$ a self-adjoint operator (for the scalar product, $(\mathbf{u},\mathbf{v}) \rightarrow \int d\mathbf{x}^3 \mathbf{u}^* \mathbf{v}$). Multiplying this equation by $\boldsymbol{\xi}_\omega^*$ and integrating over all space, it comes

$$\begin{aligned} \delta I \equiv \omega^2 \int d^3\mathbf{x} \frac{\rho_{\rm M}}{2} |\xi_\omega|^2 = \frac{1}{2}\int d^3\mathbf{x}\, \frac{|\mathbf{B}_{\omega\perp}|^2}{\mu_0} + \frac{1}{\mu_0}\left| B_{\omega\parallel} - \boldsymbol{\xi}_{\omega\perp}\cdot\nabla P_{(0)} \frac{\mu_0}{B_{(0)}}\right|^2 + \Gamma P_{(0)} |\nabla\cdot\boldsymbol{\xi}_\omega|^2 \\ - J_{(0)\parallel}(\xi_{\omega\perp}\times\mathbf{b}_{(0)})\cdot\mathbf{B}_\omega - 2(\boldsymbol{\xi}_\omega\cdot\nabla P_{(0)})(\boldsymbol{\kappa}\cdot\boldsymbol{\xi}_\omega^*) \\ = \frac{1}{2}\int d^3\mathbf{x}\boldsymbol{\xi}_\omega^*\ \mathcal{F}(\boldsymbol{\xi}_{\boldsymbol{\omega}}) \ \equiv\ \delta W_{\rm MHD} \end{aligned} \tag{2.42}$$

where $\delta I$ is the plasma kinetic energy, $\delta W_{\rm MHD}$ is called the **MHD potential energy**. Due to the self-adjointness of $\mathcal{F}$, $\omega^2$ and $\delta W_{\rm MHD}$ are directly shown to be real, and a given mode may either be purely oscillating and stable ($\omega \in \mathbf{R},\ \delta W_{\rm MHD} > 0$) or purely growing/damped ($\omega \in i\mathbf{R},\ \delta W_{\rm MHD} < 0$). With this energy formulation, one may directly determine the stability of the given equilibrium under a given perturbation $\boldsymbol{\xi}_\omega$.

Simple observation of Eq. 2.42 shows what may be the destabilizing features of a given equilibrium. The first three terms of $\delta W_{\rm MHD}$ are positive and hence, stabilizing. In particular, compressibility and magnetic field tension (included in $\mathbf{B}_{\omega\perp}$) act as restoring stabilizing forces. The two destabilizing mechanisms are included in the last two terms: the first one being related to the existence of an equilibrium current leads to so-called **current driven** , or **kink instabilities** and the second one depending on the respective sign of the pressure gradient compared to the field line curvature is the so-called **pressure driven**, or **interchange instabilities**.

### MHD waves in a uniform plasma

First insight into the nature of stable linear MHD waves can be obtained assuming a uniform magnetized equilibrium, $\mathbf{B}_{(0)}(\mathbf{x}) = \mathbf{B}_0$, $P_{(0)}(\mathbf{x}) = P_0$ ...

From the velocity equation, it clearly appears that the fluid inertia (the left hand side) has to balance pressure effects as well as the magnetic field tension, which enters $\mathbf{j}\times\mathbf{B}$. In linear analysis, two characteristic velocities appear, which account for this behavior,

$$\begin{aligned} &\text{the Alfvén velocity } v_A, \qquad v_A^2 = \frac{B_0^2}{\mu_0\rho_0} \\ &\text{and the sound velocity } c_s, \quad c_s^2 = \frac{\Gamma P_0}{\rho_0}, \end{aligned} \tag{2.43}$$

which respectively provide a measure for the restoring force induced by magnetic pressure, and the one resulting from compressibility (the kinetic pressure). In magnetized fusion plasmas, $c_s$ is smaller that $v_A$. The ratio of the plasma pressure to the magnetic pressure

$$\beta \equiv \frac{2\mu_0 P_0}{B_0^2} = \frac{2}{\Gamma}\frac{c_s^2}{v_A^2} \tag{2.44}$$

is a third important small parameter in magnetized fusion plasmas ($\sim 10^{-2}$ in Tore-Supra, where the typical values of the pressure and field are taken at the plasma center).

More precisely, linearizing the MHD equations to the first order in a perturbation of the form $\propto e^{i(\mathbf{k}.\mathbf{x}-\omega t)}$, three types of waves are found,

- the incompressible **shear Alfvén wave**, of dispersion relation

$$\omega^2 = k_\parallel^2 v_A^2 \tag{2.45}$$

This is a transverse wave, propagating in the parallel direction, where the perturbed magnetic field and perturbed velocity (parallel to each other) are perpendicular to the equilibrium magnetic field. Note that here $\omega^2$ is reminiscent from the mode inertia (as in Eq. 2.42), and $k_\parallel^2 v_A^2$ from the field line bending restoring force.

- the **fast** (+ sign in Eq. 2.46) and the **slow** (- sign in Eq. 2.46) **magnetosonic waves**

$$\omega^2 = \frac{k^2(v_A^2+c_s^2)}{2}\left(1 \pm \sqrt{1-\frac{4k_\parallel^2}{k^2}\frac{v_A^2 c_s^2}{(v_A^2+c_s^2)^2}}\right) \quad \begin{cases} k^2 v_A^2 \\ \\ k_\parallel^2 c_s^2 \end{cases} \text{ if } v_A \gg c_s \tag{2.46}$$

which couple kinetic and magnetic pressures.

In a tokamak configuration, the equilibrium parallel length scale is of the order of $R_0$ (or $qR_0$), whereas the typical equilibrium perpendicular is of the order of the minor radius $a$. Hence, for a large aspect ratio $1/\epsilon$, the tokamak geometry "naturally" leads to longer parallel scales, $k_\parallel \ll k_\perp$. When considering a perturbation, scale lengths may change significantly. However, interesting modes tend to be localized where $k_\parallel = 0$. In pure MHD plasmas, it simply comes from the fact that the magnetic field tension is proportional to $\propto k_\parallel v_A$ (it will be derived in a clean way in the course of the thesis, but the shear Alfvén wave dispersion already gives some indication of this) and stabilizing. Consequently, MHD instabilities are more easily excited where this tension cancels. When suprathermal particles are added to the picture, stable MHD modes may be driven unstable by energetic particles. Nevertheless, so-called resonant surfaces (verifying $k_\parallel = 0$) remain of interest because they can allow for a mode localization. Hence, it is often relevant to consider modes with $k_\parallel \ll k$. With the additional assumption of a low-$\beta$ plasma, a time separation appears between the three MHD waves,

$$k_\parallel c_s \ll k_\parallel v_A \ll k v_A. \tag{2.47}$$

Considering the energetic ions typical eigenfrequencies, it can be shown that resonances may occur between energetic ions and modes of the acoustic (or sound) and shear Alfv́en frequency ranges. This was illustrated in Tab. 2.1, where we compared the typical eigenfrequencies of suprathermal trapped particles with a typical value of the acoustic frequency range ($c_s/R_0$) and a typical value of the shear Alfvén frequency range ($v_A/R_0$).

### 2.2.2 Alfvén spectrum in a sheared plasma

#### Sheared plasmas and phase mixing

When moving to a non-uniform plasma, the situation is more complicated. The three MHD waves described above get fully coupled, and non-uniformity leads to non-coherent local behaviors at the origin of dispersion and damping.

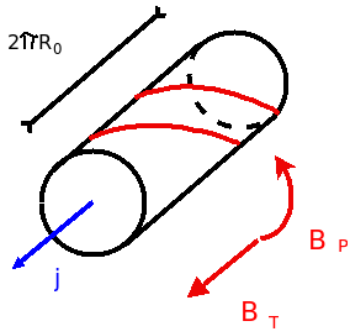


To picture this phenomenon, we make use of a cylindrical plasma of radius $a$ and length $2\pi R_0$, which can be seen as a tokamak plasma of null inverse aspect ratio, $\epsilon = 0$. Besides, we assume the plasma density to be uniform and the existence of a purely toroidal plasma current, localized at the cylinder center (for example with a current density $j(r) \propto (1-r/a)^2$). With $\epsilon = 0$, the equilibrium toroidal field (along the cylinder axis) is approximately uniform, $\mathbf{B}_{\mathrm{T}(0)}(\mathbf{x}) = B_0$, whereas the poloidal field is non-uniform (or *sheared*), $\mathbf{B}_{\mathrm{P}}(r)$.

This way, we obtain a cylindrical plasma with a sheared magnetic field, but one should note that the physics developed below can also be recovered with a more simple slab geometry and a sheared density (see Ref. [17]). The case developed here is simply more convenient for later developments to the tokamak geometry. To mimic the tokamak conditions, we also define an equivalent toroidal angle $\varphi$, such that $R_0\varphi$ holds as a coordinate for the toroidal direction and we assume that $B_{\mathrm{P}(0)}/B_{\mathrm{T}(0)} \sim \epsilon \ll 1$.

Let us now consider a linear normal mode. In a cylindrical configuration (characterized by an invariance in the direction of the cylindrical axis and in the $\theta$ direction), it is possible to take it of the form $\propto e^{i(\mathsf{m}\theta+\mathsf{n}\varphi)}$ with $(\mathsf{n},\mathsf{m})$ two integers. For this perturbation, it comes

$$ik_{\parallel} = \mathbf{b}_{(0)} \cdot \nabla\varphi \left(\mathsf{n} + \frac{\mathsf{m}}{q(r)}\right) \approx \frac{1}{R_0}\left(\mathsf{n} + \frac{\mathsf{m}}{q(r)}\right) \tag{2.48}$$

where we recall that $\mathbf{b}_{(0)} = \mathbf{B}_{(0)}/B_{(0)}$. The safety factor $q$ ($q(r) = (r/R_0)(B_{\mathrm{T}}/B_{\mathrm{P}})$ in the cylindrical limit) is a non-constant function of $r$ (we avoid the odd case where $\mathbf{B}_{\mathrm{P}} \propto r$). Hence, $k_{\parallel}$ is also a non-constant function of $r$, which means in particular that pure Alfvén waves $\omega = \pm k_{\parallel}(r) v_A$ cannot have a global structure. On the contrary, this equality seems to suggest that a **continuous frequency spectrum** of shear Alfvén waves exist, where each frequency is associated to a different radius (and an infinitely localized eigenfunction). In a global analysis however, this is not possible, which means that a wave cannot be a pure shear Alfvén wave. On the contrary, radial continuity enforces a mixing of the different polarizations involved in the three MHD waves described above.

To obtain a better understanding of the physics involved, we can expand the MHD equations using a perturbation of the form Eq. 2.41. Under the assumption that the considered perturbation verifies $k_{\parallel} \ll k_{\perp}$ and using that $\beta$ is a small parameter in magnetized fusion plasma, we already explained that the three classical MHD waves are characterized by a time scale separation. When only the first assumption is made, it is possible to focus on the lower frequency modes only, independently from the coupling to the fast magnetosonic branch. Such a decoupling leads to the so-called **shear Alfvén law** [8], which is an equation on the fluid vorticity, $\nabla \times \mathbf{V}$. Using the smallness of $\beta$ (to cancel sound wave effects) and $\epsilon$ (to simplify the differential operators), it is possible to express the shear Alfvén law using one unknown field only, the electric potential $\phi_\omega$. For general geometry, the shear Alfvén law reduces to

$$\begin{aligned} 0 = \nabla \cdot \left[\frac{\omega^2}{v_A^2}\nabla_\perp\phi_\omega\right] + B_{(0)}\nabla_\parallel\left\{\frac{1}{B_{(0)}^2}\nabla\cdot\left[B_{(0)}^2\nabla_\perp\left(\frac{1}{B_{(0)}}\nabla_\parallel\phi_\omega\right)\right]\right\} + \\ \mathbf{B}_{(0)}\times\nabla\left(\frac{1}{B_{(0)}^2}\nabla_\parallel\phi_\omega\right)\cdot\nabla\left(\frac{J_{(0)\parallel}}{B_{(0)}}\right) + \frac{2\mu_0}{B_{(0)}^2}\mathbf{B}_{(0)}\times\boldsymbol{\kappa}_{(0)}\cdot\nabla_\perp\left[\left(\frac{\mathbf{b}_{(0)}}{B_{(0)}}\times\nabla P_{(0)}\cdot\nabla_\perp\phi_\omega\right)\right] \end{aligned} \tag{2.49}$$

where we wrote $\nabla_\parallel = \mathbf{b}_{(0)}\cdot\nabla$, and generalized the definition of the Alfvén velocity to space dependent densities and magnetic fields, $v_A(r)$. A similar result will be derived later on. At

the moment, we can already identify the main physical components involved: inertia ($\propto \omega^2$), field line bending force ($\propto v_A^2 \nabla_\parallel^2$), kink ($\propto J_{(0)\parallel}$) and interchange ($\propto \boldsymbol{\kappa}_{(0)} \cdot \nabla P_{(0)}$).

Let us apply this equation to a cylindrical configuration, and perturbed quantities of the form $X_\omega^{\mathsf{m}} e^{i\mathsf{m}\theta + i\mathsf{n}\varphi}$. The cylindrical geometry enables $\boldsymbol{\kappa} = \kappa(r)\nabla r$, and the various $(\mathsf{m},\mathsf{n})$ Fourier components do not couple. Projection of Eq. 2.49 onto the $(\mathsf{m},\mathsf{n})$ harmonic returns

$$
\begin{aligned}
-\frac{d}{dr}\left\{ r^3 \left[\frac{\omega^2}{v_A^2} - (k_\parallel^{\mathsf{m}})^2\right] \frac{d}{dr}\left(\frac{\phi_\omega^{\mathsf{m}}}{r}\right)\right\} \;=\; & \omega^2 r^2 \frac{\phi_\omega^{\mathsf{m}}}{r}\frac{d}{dr}\left(\frac{1}{v_A^2}\right) \\
& + (1-\mathsf{m}^2)\left(\frac{\omega^2}{v_A^2} - (k_\parallel^{\mathsf{m}})^2\right)\phi_\omega^{\mathsf{m}} - \mathsf{m}^2 \frac{2\mu_0}{B_{(0)}^2}\frac{dP_{(0)}}{dr}\kappa_r \phi_\omega^{\mathsf{m}}.
\end{aligned}
\tag{2.50}
$$

This equation suggests the possibility of a smooth eigenfunction far from the **Alfvén resonance** condition, $\omega^2 = k_\parallel^{\mathsf{m}2} v_A^2$, but it shows that the existence of a surface of radius $r_A$ verifying the Alfvén resonance leads to a singularity in the mode structure.

Formally, the existence of an Alfvén resonance at $r = r_A$ can be treated using a perturbative two scale analysis separating the smooth and discontinuous structure variations of the mode [17]. Using temporarily the notation $\bar{E}_\omega^{\mathsf{m}} = \phi_\omega^{\mathsf{m}}/r$, the two scale analysis leads to the decomposition of the form $\bar{E}_\omega^{\mathsf{m}} = \bar{E}_{\omega 0}^{\mathsf{m}}(r_0) + \bar{E}_{\omega 1}^{\mathsf{m}}(r_0, r_1)$ where $\bar{E}_{\omega 1}^{\mathsf{m}} \ll \bar{E}_{\omega 2}^{\mathsf{m}}$, $r_0 \sim r$ is a slow variable similar to equilibrium quantities, and $r_1 \sim r - r_A$ is a fast variable, $\partial_{r_0} \ll \partial_{r_1}$. To the lower order,

$$
\frac{d}{dr_1}\left[ r^3 \left(\frac{\omega^2}{v_A^2} - (k_\parallel^{\mathsf{m}})^2\right)\frac{d\bar{E}_{\omega 1}^{\mathsf{m}}}{dr_1}\right] = 0 \quad \Rightarrow \quad \frac{d\bar{E}_{\omega 1}^{\mathsf{m}}}{dr} = \frac{C(r)}{\frac{d}{dr}\left(\frac{\omega^2}{v_A^2} - (k_\parallel^{\mathsf{m}})^2\right)\Big|_{r_A}(r - r_A)} \tag{2.51}
$$

$$
\Rightarrow \quad \bar{E}_{\omega 1}^{\mathsf{m}} \propto C(r)\ln|r - r_A| \tag{2.52}
$$

with C a slowly varying continuous function.

A **logarithmic singularity** appears close to the **Alfvén resonant surface** $r_A$, where $\omega^2 = k_\parallel^2 v_A^2$. Whereas the mode structure involves various polarizations away from $r_A$ (and in particular a radial dispersion), singularity can be understood as the excitation of a "pure" shear Alfvén wave at the Alfvén resonant surface. Since a shear Alfvén wave propagates in the parallel direction only (hence on a given radial surface), information gets accumulated at $r_A$, leading to the logarithmic singularity [18]. In particular, the singularity can be shown to be associated to a **discontinuity of the Poynting flux** [17, 19, 20]. Another way to understand the logarithmic behavior and the correlated development of **small scale structures** is to separate the plasma into various radial plasma shells characterized by its own eigenfrequency $\pm k_\parallel(r) v_A(r)$. Because each shell tends to respond better to a signal corresponding to its eigenfrequency, radial coherence is lost. This is called **phase-mixing** [21]. As a consequence of this lack of coherence, these shear Alfvén-like waves happen to be very localized. Hence, non-localized solutions are expected in Fourier space (ie: for the Fourier transform of $\bar{E}_\omega^{\mathsf{m}}(r)$), which in analogy with quantum mechanics are to be associated with a **continuous frequency spectrum** of solutions. The idea developed above is now justified.

Note that depending on the geometry, the surface where the Shear Alfvén law Eq. 2.49 presents a singularity, or *resonance*, may have a somewhat more complicated dispersion relation than $\omega = \pm k_\parallel v_A$. In the following, such surfaces will be called **Alfvén resonant surfaces**, and the spectrum of frequencies which can be solution of the corresponding dispersion relation, the **Alfvén continuous (resonant) spectrum**. Finally, the modes oscillating with a frequency of the continuous spectrum will be refered to as **continuum modes**. The latter notions are illustrated in Fig. 2.3, where we applied them to standard sheared q-profiles.

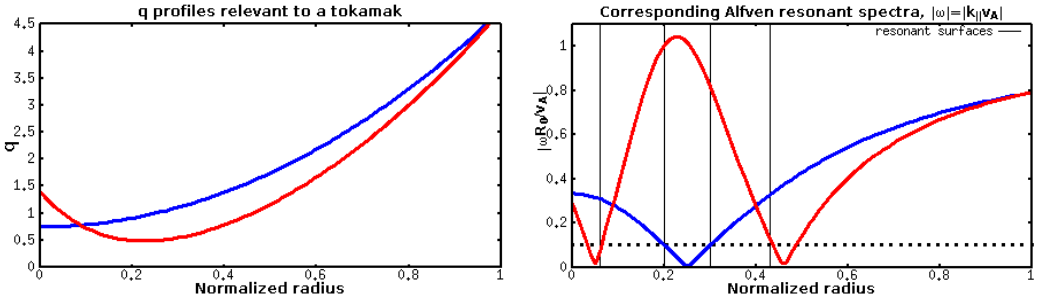


Figure 2.3: Typical sheared $q$ profiles of a tokamak and corresponding Alfvén resonant spectra for modes with a single poloidal and toroidal component, $(\mathsf{m}=-1,\mathsf{n}=1)$. As an example, the resonant surfaces for an acoustic mode ($\omega R_0/v_A \sim \beta \sim 0.01$) are indicated, and show where such a mode should display a singularity.

An important consequence of the singularity is that it implies a damping of the considered waves, called **continuum damping**. Recalling that MHD is only supposed to acccount for relatively large structures, this damping can physically be understood as a loss of information towards the small scales. We can already infer that moving to a kinetic description may eventually allow for some of these modes to live undamped (at least at the lowest order), the so-called **kinetic Alfvén waves**.

Interestingly however, it was shown that if an MHD mode is damped by continuum damping, and if the kinetic modelling of the wave displays a "strong" (kinetic) damping mechanism, the damping rate calculated by MHD does not differ from the one calculated with the kinetic formalism. In other words, the damping rate does not depend on the detailed process or on the details of the mode structure [19].

The verification of the existence of a damping and the computation of the resulting damping rate can be done using the interpretation of the MHD equations as an **energy relation**, in a similar fashion as for the derivation of the MHD energy principle. Multiplying Eq. 2.51 by $\bar{E}^{\mathsf{m}}_{\omega}$ and integrating over space under the assumption that there exists one single Alfvén resonance at $r_A$, it comes

$$\begin{aligned} -\delta W(\omega,\bar{E}^{\mathsf{m}}_{\omega}) &= \mathcal{P}\int rdr\left\{\left[r^2\left(\frac{d\bar{E}^{\mathsf{m}}_{\omega}}{dr}\right)^2+(\mathsf{m}^2-1)\bar{E}^{\mathsf{m}\ 2}_{\omega}\right]\left(\frac{\omega^2}{v_A^2}-(k^{\mathsf{m}}_{\parallel})^2\right)\right. \\ &\qquad \left.-\omega^2 r^2\bar{E}^{\mathsf{m}\ 2}_{\omega}\frac{d}{dr}\left(\frac{1}{v_A^2}\right)+\mathsf{m}^2\frac{2\mu_0}{B^2_{(0)}}\frac{dP_{(0)}}{dr}\kappa_r\bar{E}^{\mathsf{m}\ 2}_{\omega}\right\} \\ &= r^3\left[\frac{\omega^2}{v_A^2}-(k^{\mathsf{m}}_{\parallel})^2\right]\left(\frac{d}{dr}\bar{E}^{\mathsf{m}}_{\omega}\right)\bar{E}^{\mathsf{m}}_{\omega}\Big|_{r_A^-}^{r_A^+}=C(r)\bar{E}^{\mathsf{m}}_{\omega}|_{r_A^-}^{r_A^+} \end{aligned} \tag{2.53}$$

where the energy function used here can be easily identified as $\delta W(\omega,\bar{E}^{\mathsf{m}}_{\omega})=-\delta I+\delta W_{\mathrm{MHD}}$, and the last equation comes from Eq. 2.51. At the lowest order, the right hand side small scale singularity is usually assumed negligible compared to the expected large mode structure, and the main mode eigenfunction is found as a solution of $-\omega_0^2\delta W(\omega_0,\bar{E}^{\mathsf{m}}_{\omega 0})=0$. Expanding Eq. 2.53 to the next order, we can obtain the effect of the singularity on this eigenfunction. In particular, with the expansion $\omega=\omega_0+\delta\omega_r+i\gamma$, the damping rate is found to verify

$$-\frac{\partial(\delta W)}{\partial\omega_r}(\omega_0,\bar{E}^{\mathsf{m}}_{\omega 0})\ i\gamma=\frac{-i\pi\mathrm{Sgn}(\omega_0)\ C^2(r_A)}{\left|\frac{d}{dr}\left(\frac{\omega_0^2}{v_A^2}-(k^{\mathsf{m}}_{\parallel})^2\right)(r_A)\right|}. \tag{2.54}$$

Eq. 2.54 can be seen as an **energy balance**, where $\partial_r W$ is to be interpreted as the a measure of the **wave energy** of the low order solution of Eq. 2.53 [4], and the right hand side represents an energy well. Assuming in a first approximation that $\delta I \propto \omega^2$ and that $\delta W_{\mathrm{MHD}}$ has no dependance in $\omega$ (it may not be true in general since the structure of $\phi_\omega$ can depend on $\omega$), $-\partial_\omega \delta W(\omega_0, \bar{E}^{\mathsf{m}}_{\omega 0}) > 0$. Hence, $\gamma < 0$, the singularity implies a **damping**, as announced. This absorption of the wave energy suggested in the seventies that the coupling to the shear Alfvén spectrum, could be an interesting way to **heat the plasma by a direct injection of Alfvén type waves.**

Note that we can obtain a better idea of the damping time scales, coming back to the resolution of Eq. 2.51 which may be rewritten

$$\left(\partial_{tt} + (k^{\mathsf{m}}_{\parallel})^2 v_A^2\right) \partial_r \bar{E}^{\mathsf{m}} = C(r,t) \tag{2.55}$$

close to the continuum. Eq. 2.55 admits solutions of the form 2.55 $\partial_r \bar{E}^{\mathsf{m}}_\omega = C(r)\exp(\pm i k_\parallel v_A t)$ [17]. Consequently, when $t \to +\infty$, $\partial_r \to \pm i \partial_r (k^{\mathsf{m}}_{\parallel} v_A)\ t$ and diverges, reflecting the fact that the mode is characterized by a singularity. Finally

$$\bar{E}^{\mathsf{m}}_\omega = \pm \frac{C(r)}{i\partial_r (k_\parallel v_A)\ t}\ \ e^{\pm i k_\parallel v_A t}, \tag{2.56}$$

and the time behavior of the damping is observed to **be proportional to 1/t**.

### Gap Modes and Energetic Particle Modes (EPM) in toroidal geometry

From the previous section, we know that a mode is damped where Alfvén resonances occur. For example, let us consider a mode with $(\mathsf{n} = 1, \mathsf{m} = -1)$. We already explained that a mode often develops close to a surface where $k_\parallel = \mathbf{b}_{(0)} \cdot \nabla \varphi (\mathsf{n} + \mathsf{m}/q) = 0$, that is, where $q$ is rational, and in this case equal to one. Take for example $\omega$ to be an acoustic frequency, Alfvén resonance occurs for $|R_0 k_\parallel| = |\omega / v_A| \sim \beta$ ($\sim 0.01$ in Tore-Supra). Expanding $R_0 k_\parallel$ linearly around the $q = 1$ surface

$$|R_0 k_\parallel| \approx |R_0 k'_\parallel||\delta x| = |\mathsf{m}/q^2||q'||\delta x|, \tag{2.57}$$

and considering a standard monotonic Tore-Supra $q$ profile, two Alfvén resonances appear on both sides of the rational surface, with a typical distance to it $|\delta x| \sim 5$mm. This characteristic length is small for a macroscopic mode, and compared to Tore-Supra minor radius 0.7 m.

**In a toroidal geometry, various poloidal components** (various $\mathsf{m}$ numbers in the above decomposition) **are coupled together**, because the system is not fully invariant in the poloidal direction ($\epsilon \neq 0$). Due to this coupling which implies more global structures, continuum damping may be thought to be even more stabilizing than in cylindrical geometry. However, it is not the case because of the existence of **gaps in the shear Alfvén spectrum**, where a mode can live undamped.

From now on and until the end of this thesis, to avoid any ambiguity in the description of toroidal geometry and to allow for toroidicity induced poloidal coupling to be explicit, the quantities $\rho_s$ and $v_A$ need to be understood as independent from the poloidal angle $\theta$ ($\rho_s(r), v_A(r)$). In other words, the central field $B_0$ is used when assessing these quantities.

We may distiguish two types of conditions for a gap to occur [22]. Typical representations corresponding to the various types of modes described in this section are given in Fig. 2.4.

[4] We will come later to these ideas in subsection 3.1.2

- **Particular equilibrium properties naturally result in gaps in the Alfvén spectrum [23, 24, 25, 26].**

  Looking at the formula $\omega^2 = {k_\parallel^{\mathsf{m}}}^2 v_A^2$ for the localization of Alfvén resonances, it is obvious that some profiles are more favorable for the existence of modes with a large extent. A non-monotonic $q$ profile [26] and/or a non monotonic density profile may lead to finite minima of $k_\parallel^{\mathsf{m}2} v_A^2$. Below these minima, a mode with a frequency $\omega$ can have a rather large extent. An example of such modes are the **Reversed Shear Alfvén Eigenmodes** (RSAEs) [26, 27].
  Besides, some physical phenomena neglected in Eq. 2.49 (such as compressibility), can change the frequency localization of the Alfvén resonances. For example, when compressibility is taken into account the characteristic equation of the resonant spectrum has the form $\omega^2 = {k_\parallel^{\mathsf{m}}}^2 v_A^2 + \omega_0^2$ (in other words, the resonant spectrum is not purely of the shear Alfvén type but involves terms related to sound waves), and **Beta Alfvén Eigenmodes** with a eigenfrequency below $|\omega_0|$ are not damped.

- **Wave-wave coupling in toroidal geometry can allow for the existence of standing shear Alfvén waves.**

  We have explained earlier that the singularity induced by an Alfvén resonance at $r_A$ could be associated to the purely parallel phase velocity of shear Alfvén waves. Hence the idea that parallel transport and singularity vanishes if two shear Alfvén waves are coupled together to form a standing wave. This behavior may be visualized as the apparition of a *gap* in the shear Alfvén wave spectrum, as illustrated in Fig. 2.4.

  In toroidal geometry, the coupling of different poloidal harmonics directly leads to such types of gaps, called **toroidicity induced gaps**, and associated with **toroidal Alfvén Eigenmodes (TAE)** [28, 29].

The creation of the toroidicity induced gap appears directly when applying Eq. 2.49 to a toroidal geometry. In this equation, the divergence operator depends on $R = R_0(1 + (r/R_0)\cos\theta)$ and hence on $\theta$, which leads to poloidal coupling. Accordingly, poloidal coupling is found to involve terms proportional to the inverse aspect ratio, and the Right Hand Side (R.H.S.) of Eq. 2.49 can be put in the form [30]

$$-\frac{d}{dr}\left[r^3\left(\frac{\omega^2}{v_A^2} - (k_\parallel^{\mathsf{m}})^2\right)\frac{d}{dr}\left(\frac{\phi_\omega^{\mathsf{m}}}{r}\right)\right] - \frac{d}{dr}\left[r^3\bar{\epsilon}(r)\frac{\omega^2}{v_A^2}\frac{d}{dr}\left(\frac{\phi_\omega^{\mathsf{m}+1} + \phi_\omega^{\mathsf{m}-1}}{r}\right)\right] = R.H.S. \quad (2.58)$$

where $\bar{\epsilon}$ is of the order of and proportional to $\epsilon$.

Focusing on two neighboring poloidal components only, and making use of the previous notation $\bar{E}_\omega^{\mathsf{m}}$, this is again

$$-\frac{d}{dr}r^3\underline{\underline{D}}\frac{d}{dr}\begin{pmatrix}\bar{E}_\omega^{\mathsf{m}+1}\\ \bar{E}_\omega^{\mathsf{m}}\end{pmatrix} = R.H.S., \text{with } \underline{\underline{D}} = \begin{pmatrix}\omega^2/v_A^2 - (k_\parallel^{\mathsf{m}})^2 & \bar{\epsilon}(\omega^2/v_A^2)\\ \bar{\epsilon}(\omega^2/v_A^2) & \omega^2/v_A^2 - (k_\parallel^{\mathsf{m}+1})^2\end{pmatrix} \quad (2.59)$$

Far from the shear Alfvén resonances $\omega^2/v_A^2 - (k_\parallel^{\mathsf{m}/\mathsf{m}+1})^2$, the terms of the diagonal dominate ($\bar{\epsilon} \ll 1$), and the situation is close to the one of a cylinder.

The situation is different when both resonances are verified. The double cancellation of the resonant terms allows for both poloidal components to have similar, strong weights, and off-diagonal terms representing the poloidal coupling become of major importance. Consequently, the resonant spectrum (which leads to a singularity), of equation $\det(\underline{\underline{D}}) = 0$, does not cancel where both shear Alfvén waves couple. On the contrary, solving $\det(\underline{\underline{D}}) = 0$ displays a *gap*, represented in Fig. 2.4.

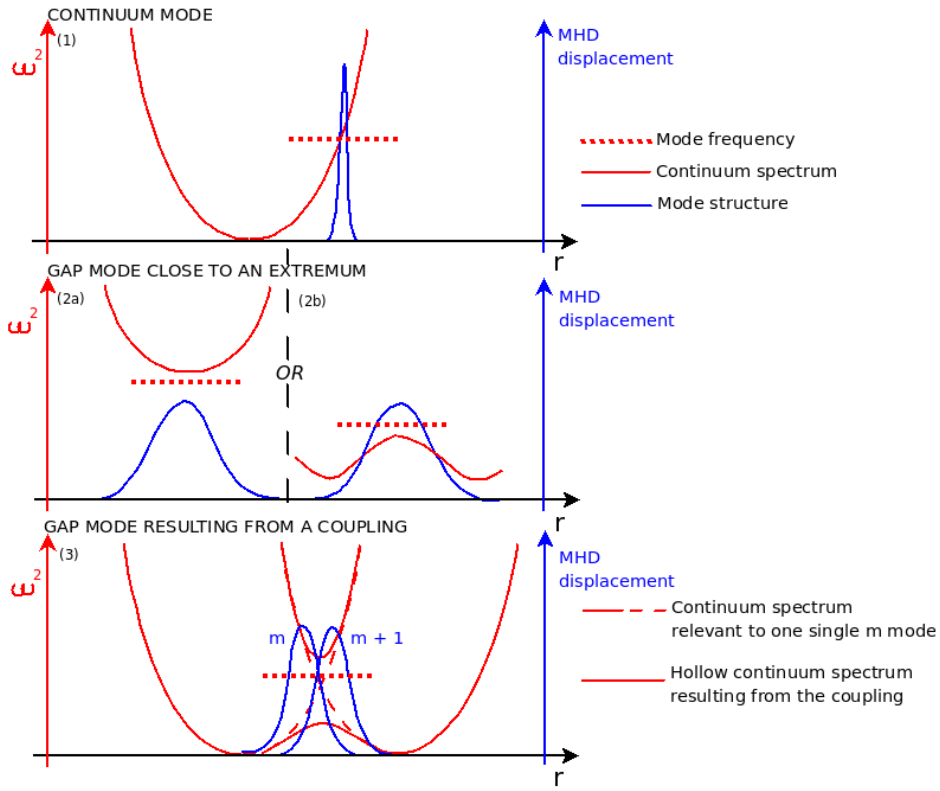


Figure 2.4: Continuum modes and gap modes.

Thanks to gaps, we now know that continuum damping may be avoided on relatively large radial extents. There remains to show that **radially localized modes** can live in these **frequency gaps**, which implies two necessary conditions on the frequency and on the existence of a *defect* able to localize a mode [31].

Such a study is classically carried out in Fourier space, where the Fourier transform of the radial dispersion equations (Eq. 2.51, 2.58), takes the form of a Schrödinger equation, and regular (ie, localized in radial space) localized (ie, non discontinous in radial space) solutions are looked for. In analogy with quantum mechanics localization in Fourier space, leads to a **discrete frequency spectrum**, in opposition to the shear Alfvén continuous spectrum.

Considering the above first type of gaps for example, it can be shown that localization is possible close to a point $r_0$, where $k_\parallel^{\mathsf{m}}$ is well approximated by $(k_\parallel^{\mathsf{m}})^2(r) = (k_\parallel^{\mathsf{m}}(r_0))^2 + (1/2)(k_\parallel^2)''(r-r_0)^2$, and in the presence of a defect. Such a situation occurs at the minimum of the $q$ profile where $k_\parallel'(r_0) = 0$ (leading to RSAEs) or close to a resonant surface where $k_\parallel^{\mathsf{m}}(r_0) = 0$. For RSAEs, the mode localization at the minimum of a $q$-profile leads to the so-called *Alfvén cascades*, that is to modes with a shifting localization and a shifting frequency, which follows the time variations of the $q$ profile.

Assuming for simplicity that $\mathsf{m} \gg 1$, and accordingly that equilibrium variations ($\sim r$) are negligible compared to radial variations of $k_\parallel$, and using the normalized radius, $\bar{r} = (r - r_0)(|\mathsf{m}|s_0/r_0)$ where $s_0$ is a characteristic value of the shear (defined in Eq. 2.6, and simply taken to be $s_0 = 1$ for when it cancels at the minimum of the $q$ profile), Eq. 2.51 takes the form

$$\frac{d}{d\bar{r}}\left\{\left[\bar{r}^2 - \Lambda^2\right]\frac{d}{d\bar{r}}\phi_\omega^{\mathsf{m}}\right\} = \frac{1}{s_0^2}[\bar{r}^2 - \Lambda^2]\phi_\omega^{\mathsf{m}} - \mathcal{G}\phi_\omega^{\mathsf{m}} \tag{2.60}$$

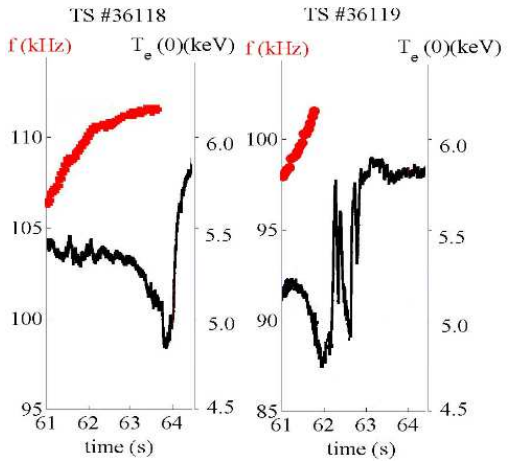


Figure 2.5: Frequency spectrum of Reversed Shear Alfvén Eigenmodes (RSAEs) identified in Tore-Supra [32]. Frequency cascading is associated to both density fluctuations and oscillations of the q-profile.

where $\Lambda^2 = (\omega^2/v_A^2 - k_\parallel^{\mathsf{m}}(r_0)^2) \times 2(\mathsf{m}^2 s_0^2/r_0^2)/(k_\parallel^2)''$, contains the information relative to the eigenfrequency.

Now taking the Fourier transform of $\phi_\omega^{\mathsf{m}}(\bar{r})$, ie, $\phi(\vartheta) = \int_{-\infty}^{+\infty} d\bar{r}\, \phi_\omega^m(\bar{r})\, e^{-i\bar{r}\vartheta}$ and using the change of variable, $\Psi(\vartheta) = \sqrt{1+s_0^2\vartheta^2}\phi(\vartheta)$, it comes

$$-\frac{\partial^2\Psi}{\partial\vartheta^2} + \left(-\Lambda^2 + \frac{s_0^2}{(1+s_0^2\vartheta^2)^2} - \frac{s_0^2\mathcal{G}}{(1+s_0^2\vartheta^2)}\right)\Psi = 0 \tag{2.61}$$

The condition for a mode to be in the gap (ie, to avoid singularity in Eq. 2.60) is $\Lambda^2 < 0$, which means that the mode eigenfrequency is in the outside region of the resonant spectrum curve (see Fig. 2.4). The condition for a mode localization depends on $\mathcal{G}$ and it is simply the necessary condition to create a localizing potential, in the Schrödinger like equation 2.61. As was shown in Ref. [33, 26, 27], various physical components can enter $\mathcal{G}$, and make possible the existence of localized modes in the frequency gaps: **these defects include equilibrium current [33], energetic particles [26] or toroidal effects** [27]...

Similarly, the dispersion relation of TAEs [34, 35] reads

$$-\frac{\partial^2\Psi}{\partial\vartheta^2} - \Lambda^2(1+\bar{\epsilon}cos\vartheta)\Psi + \frac{s_0^2}{(1+s_0^2\vartheta^2)^2}\Psi = 0 \tag{2.62}$$

where $s_0$ corresponds to the non-zero shear taken at the radial intersection of the two coupled shear Alfvén wave. Whereas $\bar{\epsilon}$ creates a gap, the finite shear $s_0$ is a defect which prevents a purely sinusoidal non-localized mode [36].

Finally, we have shown that global modes can develop in a toroidal plasma, which are not damped by continuum damping at the lowest order. As we will explain in the next section, these modes can be driven unstable by energetic particles. Besides, one should not forget these modes, which are damped in a pure MHD description, since the latter can be driven unstable when energetic particles are present. New modes can also result from the presence of energetic particles, such as *Energetic Geodesic Acoustic Modes* [37].

Following the MHD results presented so far, a separation is traditionnally made between:

- **Gap Modes** which live in a gap of the resonant Alfvén spectrum, and are not damped at the lowest order, so that only a small drive can excite them.

- **Energetic Particle Modes (EPMs)** which are damped or do not exist without a fair amount of energetic particles. EPM excitation is characterized by a relatively large threshold.

*A priori*, gap modes may be thought to be deleterious and dangerous modes. Indeed, the fact that they are only weakly damped makes them particularly easy to drive, but not very good candidates for transferring the energy of energetic particles to the thermal plasma. Moreover, their global structure can be particularly dangerous for the confinement of energetic particles, whose trajectories may be heavily modified by the mode fluctuations.

However, one should not forget that additional damping processes are missing in the above picture, which have an effect on the stability of gap modes. Example of such missing dampings are higher order **continuum damping at the plasma boundary** [36], **radiative damping** which occurs close to the resonant Alfvén spectrum, kinetic damping resulting from resonances with the thermal plasma, such as **ion Landau damping** [38] or **electron Landau damping** [39]. In particular, it is not possible to neglect ion Landau damping for the description of the Beta Alfvén Eigenmodes, although these modes are considered to be gap modes.

Moreover, it may not be fully meaningful to focus on gap modes only, if the population of energetic particles and the corresponding drive is *de facto* non negligible.

### Non-ideal effects

Before dealing with the interaction of the modes described above with energetic particles, let us simply make a few comments on the limits of ideal MHD used so far, for the description of the thermal plasma.

For this, let us recall the fundamental assumptions of MHD, given in the thesis introduction,

- the MHD time-scale validity: for low collisionality plasmas, MHD depends on the MHD hydrodynamic approximation, according to which $\omega$ is larger than the characteristic thermal plasma frequencies.

- the MHD spatial-scale validity: MHD only makes possible the description of macro-scale structures which are much larger than the thermal ion Larmor radius.

- the MHD closure: the plasma description is reduced to three moments in MHD, two scalars: the pressure and the density, and one vector field, the velocity. This relies in particular on the assumption that the plasma velocity distributions are always Maxwellians.

Two limits of ideal MHD directly follow the previous discussion, and call for kinetic modelling.

First, **continuum damping** which takes place in the Alfvén continous spectrum, can be seen as **conversion of macro-scale MHD waves to micro-scale kinetic waves** (when looking at the modes as propagative). This conversion does not necessarily enforce the use of kinetic theory because MHD damping rates are equal to kinetic damping rates, when kinetic waves are fully dissipated [19]. However, non-dissipated kinetic waves can exist inside the Alfvén continuous spectrum which do not present the same stability properties as gap or continuum modes [40]. Kinetic Toroidal Alfvén waves (KTAEs) are an example of such kinetic waves. More generally, kinetic effects such as **micro-scale effects, also called Finite Larmor Radius (FLR) effects** (that is, effects of the order of the few ion Larmor radii) enforce the existence a potential well in Eq. 2.61. It follows a discretization of the

Alfvén continuous spectrum [41] and the possibility for non-discontinuous radial modes to exist, as long as kinetic damping mechanisms are not too strong.

Secondly, **wave-particle resonances** are not appropriately modelled using MHD, because of the **hydrodynamic limit** and the consistent use of fixed Maxwellian shapes for the velocity distributions. Even if MHD is often reasonable outside of the hydrodynamic region, this extension may only be true when resonances are negligible. When continuum damping is null and kinetic resonant damping mechanisms become the major damping processes [38, 42] (ion Landau damping for example) kinetic modelling is desirable.

Finally, some physics is missing in MHD. We explained in section 2.2.1 that the **ideal MHD flow was purely a result of the $\mathbf{E}\times\mathbf{B}$ drift**, consistently with the hydrodynamic approximation. In particular the so-called diamagnetic flow (or velocity) which is related to pressure gradients is not taken into account. This assumption breaks when going to lower frequencies (see Fig. 1.4), and additional modes with a finite eigenfrequency come into place (such as **kinks oscillating with around the so-called diamagnetic frequency** in the **diamagnetic gap**). Similarly, MHD lacks charge separation in the parallel direction $E_{\|}=0$, and this may become an issue when electron inertia is non negligible.

### 2.2.3 Energetic particle drive

Let us move to the interaction of the modes described above with energetic particles. *A priori*, the idea that energetic particles can transfer energy to the thermal plasma modes is not obvious. On the contrary, first theories rather predicted that fast particles would stabilize MHD modes [43]. Because suprathermal are characterized by large eigenfrequencies, the idea was that they **could adapt to the mode fluctuations rapidly, and hence mitigate them**. However, first experiments designed to stabilize MHD kink modes with fast particles led to the excitation of unexpected new instabilities, the so-called **fishbone modes**.

What was later found for the latter kink modes is that they could indeed be stabilized by energetic particles, as long as their oscillation frequency verified $\omega \ll \Omega_{h,3}$ (which in general also implies $\omega \ll \Omega_{h,2}, \Omega_{h1}$, where $h$ stands for *hot* particles), and this was indeed interpretated as a mitigation effect induced by the fast response of the energetic particles [44]. However, the situation is strongly modified when resonances can take place $\omega \sim \Omega_{h,1}, \Omega_{h,2}, \Omega_{h,3}$. Nowadays, it is well known that a bounded frequency window exists, where fast particles are stabilizing for the kink instability [45, 44], but that both resonant damping and resonant drive can take place above this window.

A first intuition of the interaction of energetic particles with MHD modes can be obtained by the simple addition of a scalar pressure gradient corresponding to the hot particles in Eq. 2.35. When moving to the energy formulation, multiplication by $\boldsymbol{\xi}^*_\omega$ returns

$$-\boldsymbol{\xi^*}_\omega \cdot \nabla P_{h\omega} = -\boldsymbol{\xi}^*_\omega \cdot \mathbf{J}_{h\omega} \times \mathbf{B}_{(0)} = -i\omega\ \mathbf{J}_{h\omega} \cdot \mathbf{V}^*_\omega \times \mathbf{B}_{(0)} = i\omega\ \mathbf{J}_{h\omega} \cdot \mathbf{E}^*_\omega \tag{2.63}$$

where we neglected the fast ion velocity (assumption of closeness to the velocity balance) in the first equality, and made use of Ohm's law for the thermal plasma flow in the last one.

From Eq. 2.63, it appears that a **work** on the fast ion population has to be added in the energy relation Eq. 2.42 [44], and this work can lead to a **resonant wave-particle energy transfer**. This additional work implies a new term in the MHD energy relation, which is traditionally written with the notations

$$\delta W = -\delta I + \delta W_f + \delta W_k = 0 \tag{2.64}$$

where $\delta I$ represents inertia as in Eq. 2.42, $\delta W_f$ is a generalized MHD energy potential (supposed to contain all *fluid* behaviors), and $\delta W_k$ represents the contribution of the energetic

particles (which can only be modelled using *kinetic* theory). Eq. 2.64 has been given the name of **fishbone-like dispersion relation** [46, 47], and it can be shown to be of very general use in the study of the interaction of energetic particles with the thermal plasma, even when the plasma is given a kinetic description [48]. Even if the form of Eq. 2.64 may seem very intuitive, one should note that it implicitely contains an important feature of the physics at stake: the existence of two radial scales as in Eq. 2.51, which allows for a separation between localized inertial dynamics and longer scales associated with fluid behaviors and energetic particles.

There now remains to understand the effect of $\delta W_k$. Depending on the time scale involved, it can be either stabilizing or destabilizing.

- If the addition of a hot pressure were to be understood with traditional MHD, that is in the hydrodynamic approximation $\omega \gg \Omega_{h,1}, \Omega_{h,2}, \Omega_{h,3}$, one would expect a destabilizing effect. Indeed, we explained earlier that interchange instabilities were sensitive to the relative direction of the equilibrium field curvature compared to the one of the pressure gradient, and it may be shown that this feature favors instabilities in the outside part of the torus, that is in the low field side half part of the torus. Hence, energetic trapped particles which mainly evolve in the outside part of the torus (and are the dominant energetic particles under some heating processes like Ion Cyclotron Frequency Heating, ICRH) are destabilizing. However, the hydrodynamic approximation is not relevant.

- When $\omega \ll \Omega_{h,1}, \Omega_{h,2}, \Omega_{h,3}$, we already explained that stabilization could be expected.

- Now, $\omega \sim \Omega_{h,1}, \Omega_{h,2}, \Omega_{h,3}$ is a particular case where particles behave **resonantly** and can exchange energy with the mode. This response is called **resonant response** (whereas the two previous responses are referred to as **reactive responses**), and it may be either stabilizing or destabilizing.

Hence the importance of time scales...

Resonances are of particular interest, because they allow for **secular energy exchanges between particles and waves**. Such energy transfers come from the **non-conservation of the equilibrium motion invariants** of resonant particles. **Their magnitude and sign linearly depend on the gradients of the involved particle distribution function**. More precisely, if the distribution function of a hot particle population (but it is also the case for any other population) is $F_{h(0)}$, and resonance occurs for $\omega = \sum_i \mathsf{n}_i \Omega_{h,i}$, the gradients of interest can be shown (and in fact *will* be shown in chapter 5) to be the gradients $\mathsf{n}_i \partial_{J_i} F_{h(0)}$. Because the type of instabilities we are looking at are much slower than $\Omega_{h,1}$, it is reasonable to consider $\mathsf{n}_1 = 0$. Hence two types of mechanisms are usually distinguished for resonant drive or damping: energy induced transfers (with some subdivisions such as anisotropy induced excitation [49], or **Landau damping** [50] due to the negative energy slope of a thermal velocity distribution) and radial gradient induced energy transfers, related to the non-conservation of the third invariant.

An interesting point concerns the numbers $\mathsf{n}_i$ which are necessary for the resonant condition $\omega = \sum_i n_i \Omega_{h,i}$ to be met. *A priori*, the $\mathsf{n}_i$'s may span the whole range of integers, which somehow questions the possibility to avoid resonances. The question is all the more striking that the magnitude of the energy transfers is proportional to the $\mathsf{n}_i$'s, which suggests resonances may be more efficient when $\omega$ is well separated from the particle characteristic frequencies... In fact, this is not so because the $\mathsf{n}_i$'s cannot be taken independently from the wave structure it resonates with. It is possible to show that resonant drive by energetic particles is most efficient for medium $\mathsf{n}_i \sim$ 5-10 [51].

### 2.2.4 Nonlinear behaviors

We now know that interaction between energetic particles and some modes of the thermal plasma are possible. In particular, we put forward that a purely kinetic behavior, **wave-particle resonance**, can allow for an energy transfer from the energetic particles to the waves, which is of interest for the confinement of the alpha particles energy in burning plasmas.

Nevertheless, only a nonlinear analysis can tell us whether a wave can be sustained and act as an energy channel, or whether it is damped nonlinearly. Only a nonlinear analysis can tell us whether a mode will transport energetic particles and imply dangerous losses.

Classically, two kinds of nonlinearities are considered.

- **MHD nonlinearities** concern the thermal plasma and the mode structure and frequency nonlinear evolution.
- **Kinetic nonlinearities** concern the kinetic energetic response, related to its resonant behavior.

#### MHD nonlinearities

The fully nonlinear treatment of the MHD equations leads to the coupling of various perturbed fluid moments and fields, and can result in higher order poloidal components. This mechanism can be refered to as **mode-mode coupling**, and was analyzed for the TAE and for one type of EPM, called the **precessional fishbone mode** (a purely energetic mode, contrary to the previously mentionned **diamagnetic fishbones**).

For TAEs, mode-mode coupling (considered with a linear response of the energetic particles) has been shown to lead to a shift of the mode frequency out of the gap region, and hence to an increased damping and to a saturation [52]. For the precessionnal fishbones, mode-mode coupling leads to the generation of an $\mathsf{m} = 0$ plasma rotation and magnetic field, and displays a more ambiguous role of the nonlinearities. Far above the mode instability threshold, mode-mode coupling leads to saturation. However, close to threshold, MHD nonlinearities have been found to produce en explosive growth leading to a finite time divergence [53].

The latter behavior suggests a dominant role of MHD nonlinearities, under certain conditions. However, kinetic nonlinear theories are considered more successful at the moment, because number of observations could be related to their predictions.

#### Nonlinear saturation of gap modes via kinetic nonlinearities

$\sim$ *Nonlinear trapping* $\sim$

A successful explanation of the role of kinetic nonlinearities in the evolution of fast particle driven *gap modes* is based on the theory of **nonlinear particle trapping**. When a mode has a finite amplitude, energetic resonant particles can get trapped inside its structure (in six dimensional phase space) and their motion invariants are no longer conserved. If particles bounce inside the mode structure much faster than the mode growth, their trajectories are fully nonlinear and it is possible to solve for the energetic particle evolution and for the mode growth separately.

For a gap mode, the calculation of the mode growth can be done close to threshold, with a perturbative treatment of the energetic population. To the lower order, the linear real gap mode can is a solution of Eq. 2.64 and verifies $\delta W_L(\omega_0) = 0$, $\omega_0$ real.

If the mode linear structure can be assumed unchanged nonlinearly (MHD nonlinearities are neglected) but the resonant population of energetic particles is treated nonlinearly, ex-

pansion of the latter equation to the first order classically leads to an energy-like relation of the form [54]

$$(\partial_\omega \delta W_L)\ \delta\omega = -\delta W_{k,NL} - i\gamma_d \partial_\omega \delta W_L, \tag{2.65}$$

where the subscripts $L$ and $NL$ respectively stand for *linear* and *nonlinear*. $\delta W_{k,NL}$ represents the energetic particle kinetic response treated nonlinearly, and $\gamma_d$ accounts for first order background damping mechanisms, simply modelled with a constant rate in most studies of the nonlinear saturation of fast particle driven modes via nonlinear trapping.

Following the nonlinear trapping theory, Boltzmann equation Eq. 1.4 for the energetic particle distribution $F_h$ can be put in the form [55]

$$\frac{d\tilde{F}_h}{dt} - \mathrm{C}\cdot\tilde{F}_h = -\frac{\partial F_{h(0)}(\omega_0 + \mathrm{Re}(\delta\omega))}{\partial t} + (\mathcal{Q} + C\cdot F_h) \tag{2.66}$$

where $\tilde{F}_h = F_h - F_{h(0)}(\omega_0 + \mathrm{Re}(\delta\omega))$, and $F_{h(0)}$ stands for the value of the equilibrium distribution function where resonance occurs with $\omega_0 + \delta\mathrm{Re}\omega$ (a nonlinear shift of the frequency is allowed).

For a mode to be driven, the $\gamma_d$ related damping needs to be overcome by the energetic particle drive. Nonlinearly, particle trapping occurs and may be understood as the mixing of trajectories of neighboring particles. It results in a flattening of the gradients at the origin of the drive and eventually cancels the drive (see Fig. 2.6). Nethertheless, saturation of the mode amplitude can take place if some residual drive is conserved to balance $\gamma_d$ (and allow for $\mathrm{Im}(\delta\omega) = 0$ in Eq. 2.65). Two mechanisms have been identified to allow for a residual drive. When **collisions** ($C\cdot\tilde{F}_h$ in Eq. 2.65) are strong enough to reduce trapping, some driving slope is conserved. Otherwise, phase space structures resulting from trapping can move, (**or chirp**), in phase space ($\partial_t F_{h(0)}$ in Eq. 2.65). This chirping is to be associated to a mode frequency chirping and delivers some energy to the mode. These two saturation mechanisms are illustrated in Fig. 2.6, and they have been found to account for several experiments [49, 56].

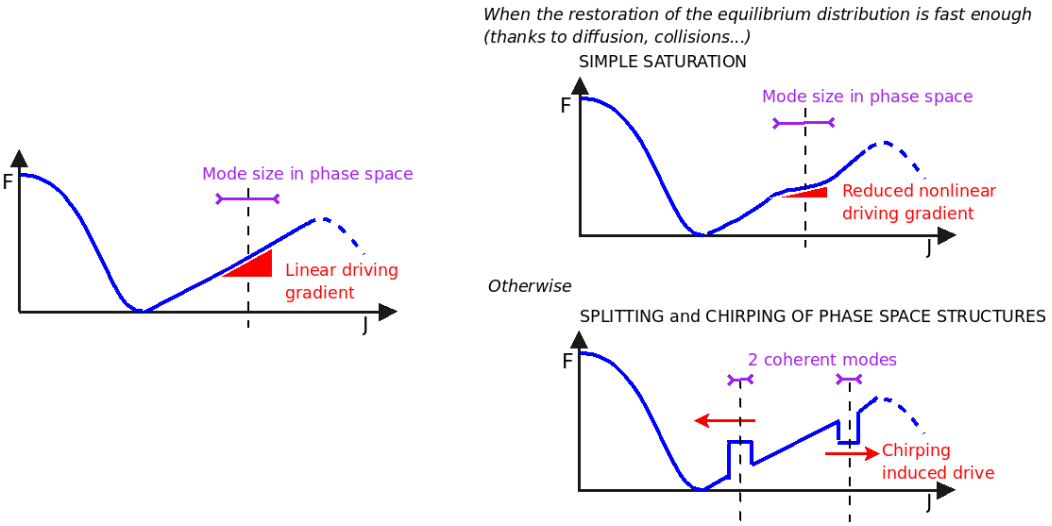


Figure 2.6: Two saturation regimes predicted for gap modes close to marginal stability: simple saturation and frequency chirping.

$\sim$ *Energetic particle transport* $\sim$
When a particle is nonlinearly trapped, breaking of one or several of its initial motion invariants, can lead to the situation pictured below Tab. 2.1, where a barely passing particle is scattered into a trapped particle (in the usual sense of section 2.1) and is no longer confined [56, 57]. If the phase space structure, where homogeneization occurs, extends in the radial direction, a particle can get **convected** radially. However, saturation due to nonlinear trapping has been shown to occur at low levels (meaning that the structure remains small) , and a strong radial transport can only occur if several modes are close by and their structures overlap . For example, an overlaping of the TAE and fishbone structures has been postulated in JET to explain the observation of energetic ion losses [58]. However, according to simulations [59, 60], a strong transport may only occur when a lot of modes are involved such that **stochastization** and hence diffusion [61] take place.

### Strongly nonlinear kinetic evolution of Energetic Particle Modes

When dealing with EPMs, the perturbative treatment of energetic particles presented in the previous section is no longer possible, and the mode characteristics (its structure and frequency) are strongly dependent on the energetic particle population itself. The latter feature prevents the use of a time scale separation between the mode and the fast particle evolutions, and leads to the resolution of time dependent equations. A possible form for the mode evolution has been suggested in Ref. [62]

$$\partial_\omega \delta W_L \; \partial_t \mathcal{A} = -\delta W_{k,NL}(t)\mathcal{A} - \Delta\mathcal{A} \tag{2.67}$$

where $\mathcal{A}(r,t)$ stands for the mode amplitude, $\Delta$ is a dispersive operator. Analogy with Eq. 2.65 is clear, but now the amplitude is made explicit in order to treat its time dependence on the same footing as the time evolution of $\delta W_{k,NL}(t)$. An additional feature of this model is that $\mathcal{A}$ is now given a radial dependence, which allows for a radial dispersion of the mode structure. Because the traditional variational formulation assumes that integration over has already been carried out, the $r$ dependence should be understood as a larger radial scale that the one corresponding to the mode size.

Since the time evolution of $\delta W_{k,NL}$ is now needed, a full evolution equation needs to be solved to get the energetic particle response, in agreement with Eq. 2.65. Because the time evolution of the mode is supposed to be as fast as the energetic particle evolution, nonlinear trapping does not have time to take place, such that the particle trajectories are **decorrelated** from the wave and the fast particle distribution can be treated with a formalism which has some analogy with a *quasi-linear* treatment. This calculation was carried out in [63] and returns a time evolution equation of the energetic particle population, which has the form

$$\partial_t \left[ \partial_t \left( \delta\hat{W}_{k,NL} \right) \mathcal{A}^2 \right] \propto \mathcal{A}^4 \qquad \text{with } \delta\hat{W}_{k,NL} \propto \frac{1}{\mathcal{A}^2}\delta W_{k,NL} \tag{2.68}$$

From Eq. 2.68, it appears that the typical nonlinear time verifies $\tau_{NL} \propto \mathcal{A}^{-1}$. The consequence is that nonlinear transport can be *balistic* (that is, faster than the traditional diffusive time, $\tau_{NL} \propto \mathcal{A}^{-2}$).

This analysis predicts a transition to a stronger (balistic) transport of energetic particles. In particular, it makes possible a strong and fast particle tranport corresponding to a simultaneous radial shift of both the energetic population and the mode structure, that may be seen as the radial propagation of an unstable front. This prediction is in agreement with the strong transport observed during the so-called ALEs (Abrupt Large amplitude Events) in the tokamak JT-60U.

## 2.3 Experimental and modelling tools for the study of energetic particle modes in Tore-Supra

Let us take a (short!) break from theory to present the experimental device, which was made use of during this work to proofcheck the theoretical predictions.

### 2.3.1 Tore-Supra

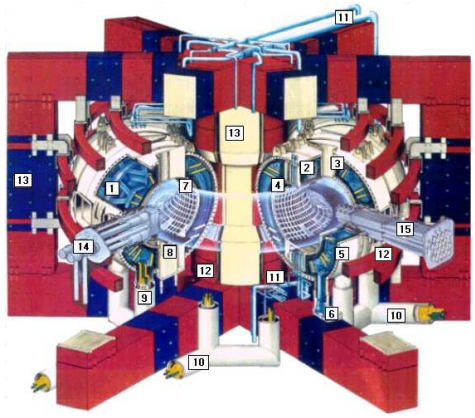

The tokamak Tore-Supra is a relatively large tokamak with a circular cross section, whose dimensions are described in Tab. 1.1. Its equilibrium configuration is well approximated by the embedded set of circular flux tubes with a shift, given in Eq. 2.8.

Tore-Supra discharges make use of deuterium only. The most basic tunable parameters are the toroidal magnetic field, the toroidal induction current and the plasma average density.

In standard Tore-Supra discharges, **the field** $B_{\mathrm{T}}$ belongs to $[2.2\mathrm{T}, 3.8\mathrm{T}]$ and can be tuned with precision ($\pm 10^{-3}\mathrm{T}$), but standard operation points $B_{\mathrm{T}} = 2.2, 2.8, 3.2, 3.8T$ are used (in particular for the tuning of the external heating sources).

**The toroidal plasma current** at the origin of the poloidal field, can be created using two mechasnisms. An **induction current** results from a varying vertical magnetic flux generated by the central solenoid (see Fig. 1.3). Induction is the easiest and most tunable mean to generate current, and it is in particular necessary to start the plasma. Standard Tore-Supra discharges can be tuned with a induction current between 0.6MA and 1MA. An additional current resulting from the injection of **High Frequency waves** in the plasma can be added to sustain the initial plasma current. This current source is usually more localized than induction, and allows for a control of the current radial profile.

Finally, the central density can be adjusted and belongs to the interval $[4 \times 10^{19}\mathrm{m}^{-3}, 7 \times 10^{19}\mathrm{m}^{-3}]$ in standard discharges.

A direct **heating** of the plasma occurs due to Joule's law and following the existence of a plasma current. Besides, injection of high frequency waves into the plasma can also improve the heating:

- **Ion Cyclotron Radio-frequency Heating (ICRH)** makes use of the ion cycloton resonance $\Omega_c$ to transfer energy to the plasma ions. However, requirements for the coupling of the waves with the plasma make easier the radio-frequency heating of an intermediate ion species, which deposits its energy on the plasma in a second step. In Tore-Supra, this intermediate species or **minority species** (representing 2 to 9% of the plasma ions) is usually taken to be hydrogen ions. Under ICRH heating, a tail of energetic hydrogen ions is formed and determining how they can transfer their energy to the main plasma is similar to the problem of transfering the alpha particles energy. Typical energy coupled to the plasma (deuterium + hydrogen) can reach 8MW in Tore-Supra.

- **Electron Cyclotron Radio-frequency Heating (ECRH)** makes use of the electron cyclotron resonance, and allows for a very localized and tunable heating of the plasma. In Tore-Supra, less that 1MW of ECRH can be coupled to the plasma.

- **Lower Hybrid (LH) waves** make use of the Landau resonance to transfer energy to the plasma. Their main use is to induce the plasma current, but they can also heat the plasma. In Tore-Supra, a maximum of 3 MW of LH can be reached at the moment.

### 2.3.2 Diagnostics

#### Overview

Various diagnostics are set up in Tore-Supra, which apply either for the measure of equilibrium parameters or for the measure of fluctuations.

Various equilibrium parameters can be measured. We give in the following a few examples of such diagnostics which are relevant to our topic. The density profile is accessed using Thompson scattering, interferometry or microwave reflectometry, with a typical error of 10%. The electron temperature profile is obtained using Electron Cyclotron Emission measurements, with an uncertainty below 5%. The measure of the minority fraction can be performed thanks to an analysis of the edge neutrals, but it is characterized by a strong error of about 50%. Finally, neutral Beam Injection allows for the measure of the ion temperature at one point of the plasma, but the diagnostic could not be used during our experiments.

Diagnostics with a high frequency acquisition (until 1MHz), can be used for the analysis of fluctuating MHD modes (typically, BAEs have a frequency of about 50 kHz, TAEs of about 200 kHz).

Tore-Supra core **microwave reflectometer** measures density fluctuations with eigenfrequencies below 300 kHz (its aquisition frequency is 1MHz) and with scale lengths longer than 1cm. The main advantages of this diagnostic are its high sensitivity (Relative density fluctuations, normalized to the main plasma density can be found as low as $\delta n/n \sim 10^{-4}$.), and the possibility to change the target radial location in one given discharge. Disadvantages come from some uncertainty on the targetted radial location and a relatively important noise. In the following, we provide some more details about this diagnostic, which was the main tool of the analysis performed in the thesis.

**Electron Cyclotron Emission (ECE)** makes possible the measure of electron temperature fluctuations, with scale lengths longer than 1cm, and with a good precision on the targetted radial location ($<$ 1cm). The current set-up in Tore-Supra allows two kinds of measurements. **Fast ECE** allows to catch fluctuations below 30 kHz, with a fast radial scan of the tokamak core. **ECE correlation** is used for higher frequencies (below 300 kHz), but simply allows to target one plasma radial location.

**Soft X-Rays diagnostics** measure the plasma emissivity which is a complex function of electron temperature, and of the densities of electrons and various ion species. Fluctuations below 100 kHz can be accessed. The main advantage of this diagnostic is that it is charaterized by several lines of sights (coming from the top and from the side of the machine) which scan a whole plasma cross-section simultaneously. A disadvantage is its lower sensitivity.

A main disadvantage of Tore-Supra diagnostics for the study of MHD fluctuations is the low performance of the Mirnov coils measurements (which do not detect fluctuations above a few KHz) due to protective tiles which surrounds the plasma chamber, and cut the magnetic signal. A detrimental consequence for MHD studies is the impossibility to access the toroidal numbers of the mode with frequencies above a few KHz.

### Microwave reflectometry

A microwave reflectometer makes use of the waves propagation properties in a plasma, and in particular of the notion of **cut-off layer**. The latter properties can be described using a so-called **wave index** $N$, which depends on the plasma (and in particular on its density) and on the wave characteristics. A cut-off layer is a layer where $N^2 = 0$, and it can be shown that a wave propagating in a region where $N^2 > 0$ which encounters a cut-off layer, gets reflected.

The idea of reflectometry is to inject waves in a plasma at well chosen frequencies which allow for them to be reflected, and then to measure the phase shift $\Phi_{\mathcal{R}}$ between the injected and the reflected wave. If the injected wave has a frequency $\omega_{\mathcal{R}}$, it directly comes that

$$\Phi_{\mathcal{R}} = 2\frac{\omega_{\mathcal{R}}}{c}\int_{R_{\mathcal{R}}}^{R_c} N(R,\omega_{\mathcal{R}})dR - \frac{\pi}{2}, \tag{2.69}$$

where $[R_{\mathcal{R}}, R_c]$ is simply the distance between the reflectometer ($\mathcal{R}$) and the cut-off layer.

A first use of the reflectometer is the determination of the equilibrium density profile. From the knowledge of $N(R,\omega_{\mathcal{R}})$ in Eq. 2.69, one can deduce the distance $[R_{\mathcal{R}}, R_c]$ and link it to the cut-off density. When modifying $\omega_{\mathcal{R}}$, the full equilibrium density profile can be reconstructed.

At fixed $\omega_{\mathcal{R}}$, that is for one targetted cut-off layer, the analysis of high frequency fluctuations can be linked to density fluctuations using Eq. 2.69. Assuming that the mode scale length is greater than the free space wavelength of the injected wave (typically $>$ 1cm), the cut-off layer is strongly enhanced by plasma fluctuations near this layer. Thus, in traditional configurations, the difference in phase shift (compared to the phase shift associated to the equilibrium) can be related to density fluctuations using [64]

$$\delta\Phi_{\mathcal{R}} = M_{\mathcal{R}}\sqrt{\pi}\,\frac{\omega_{\mathcal{R}}}{c}\left(\frac{1}{k_r \nabla N^2}\right)^{1/2}\frac{\delta n_e}{n_{e(0)}} \tag{2.70}$$

where $M_{\mathcal{R}} = n_e \partial N^2/\partial n_e$, and $\nabla N^2$ depend on the injected wave and need be assessed at the cut-off. $n_e$ is the electron density, and $k_r$ stands for the mode radial mode number (the calculation of Ref. [64] is done for a plane wave $\propto e^{ik_r x}$ ). Once the density fluctuations of a a mode has been extracted, $\delta n_e$, the MHD displacement can be obtained from $\delta n_e$ using the density transport equation. In its simplest form, it returns

$$\xi = \delta n_e / \frac{dn_e}{dr}. \tag{2.71}$$

The reflectometer used in this thesis sends waves in the tokamak equatorial plane (the horizontal plane cutting the torus chamber in two). It is configured to work with the higher cut-off of the so-called **X-mode**. This means that the injected wave refraction index verifies

$$N_X^2 = 1 - \frac{\omega_{pe}^2\left(1-\omega_{pe}^2/\omega_{\mathcal{R}}^2\right)}{\omega_{\mathcal{R}}^2 - \omega_{pe}^2 - \Omega_{ce}^2}, \tag{2.72}$$

and the injected wave frequencies are chosen to match the higher cut-off, of equation

$$\omega_{\mathcal{R}} = \frac{1}{2}\left(\sqrt{\Omega_{ce}^2 + 4\omega_{pe}^2} + \Omega_{ce}\right). \tag{2.73}$$

where $\Omega_{ce}$ is the electron cyclotron frequency and radially depends on the fiels, $\omega_{pe}$ is the electron plasma frequency and depends on the density, $\omega_{pe}^2 = n_e e^2/(m_e \epsilon_0)$ ($m_e$ the electron mass, $\epsilon_0$ the dielectric permittivity). In particular $M_{\mathcal{R}} \approx 2$.

The cross-section of the cut-off is represented in Fig. 2.7, where it appears that the plasma

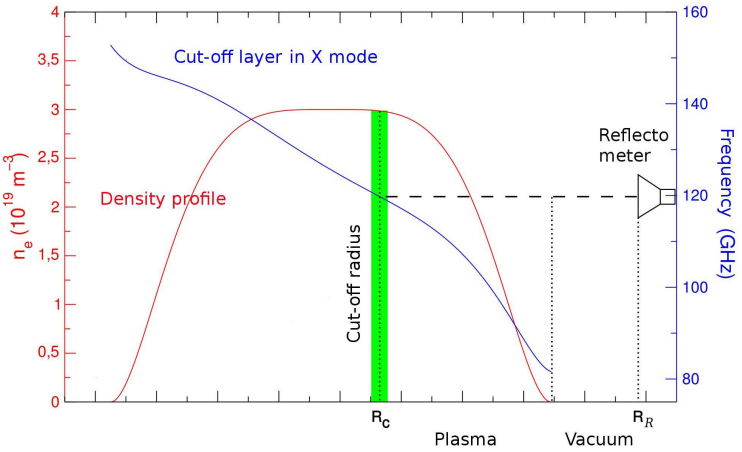


Figure 2.7: Schematic of the reflectometry set-up, and cut-off layer in X-mode.

can be scaned from the low field side (the outward part of the torus) to a third of the high field side, when the reflectometer frequency, $\omega_{\mathcal{R}}$ , is moved from 100 GHz to 140 GHz. In fact the radial extent which can be scaned by reflectometry depends on $B_{(0)\mathrm{T}}$ ( $B_{(0)\mathrm{T}} = 3.8$ T in Fig. 2.7) and does not allow to catch the core region for low fields. For these reasons, core reflectometry requires at relatively large field $B_{(0)\mathrm{T}} > 2.8$T.

For the study of fluctuations, we already mentionned an additional limitation of the reflectometry set-up to fluctuations of eigenfrequencies below 300 KHz (due to the reflectometry acquisition frequency, 1MHz). A final limitation is due to storage capacities. Two choices can be made:

- In *mode 1*, $\omega_{\mathcal{R}}$ can be increased by steps, such that a radial scan of the plasma can be done. In this case, steps cannot be longer 15 ms.
- In *mode 2*, a single radial point is targetted (more precisely, 3 points a later developments of the diagnostic), but a longer acquisition time is possible (until 0.5s).

### 2.3.3 CRONOS, PION

For the analysis of experiments, two codes have been used in this work.

**CRONOS** is a transport code which integrates various modules aiming at including MHD equilibrium requirements, the effects of multiple species in the plasma, and various heating sources [65]. It can be used either for the interpretation of experiments, or in a predictive way. In the interpretative mode, it reconstructs the plasma equibrium (and returns for example such quantities as the main ion or the electron temperature profiles $T_i$, $T_e$ or the $q$ profile), based on the experiments characteristics and on various diagnostic measurements.

To obtain a precise effect of ICRH, and in particular to obtain the ICRH fast ion distribution function, we made use of a Monte-Carlo code called **PION** [66], which takes as input various equilibrium parameters and returns the deposited ICRH power deposited on each species and the resulting deuterium and hydrogen distribution functions.

### 2.3.4 Experiments design

Any experiment involves a huge number of free parameters. We gave a sample of these parameters in section 2.3.1. One may be aware of some limitations on the range of parameters that can be reached.

In the study of fast particle driven modes, it is interesting to decouple equilibrium parameters (such as the field, the main plasma temperatures...), from the fast particle population. For that purpose, varying the source of suprathermal particles is of interest, but of course, one may check it is done independently from other parameters. In the experiments conducted in this work, the fast particle population is created using ICRH. As will be explained below, ICRH power coupling is dependent on equilibrium parameters as well.

We listed in the following limitations on the experiments parameters.

- **General limitations**

  Besides traditional technical limitations, such as the maximum current in the toroidal coils, or the maximum flux (which limits the discharge time lengths), the sustainability of a plasma depends on MHD stability, as we know. One strong limit on the density is the Greenwald density [67], $\beta_N \equiv (\beta/100) * (aB_0)/I_p(\mathrm{MA}) \leq 3\%$.

- **Power limitations**

  Power injection of heating waves in the plasma is of course limited by the capacitites of the antennas generating the waves. Besides, the resonant absorption of ion cyclotron or LH waves depends on plasma parameters. In particular, ICRH requires a relatively high density, and a window of minority fraction. This limits the possiblity to decouple the choice of these parameters. Finally, the expulsion of fast ions explained in the thesis introduction is particularly risky for the antennas, and has been found to induce detrimental localized heat loads.

- **Diagnostic requirements**
  Finally, the parameter extent is limited by the diagnostic requirement. We already explained that the use of core reflectometry is only possible for relatively large toroidal field, $B_0 > 3.2$ T.

## 2.4 Summary

*In this chapter, we presented some general physics of relevance for the understanding of the motion of energetic particles, and we reviewed important physics involved in the resonant excitation of waves with a finite frequency in tokamak, by energetic particles. Finally, we introduced the experimental device, Tore-Supra, where we conducted experiments to study the latter physics.*

*Important ideas can be retained:*

- *In the absence of perturbations, the motion of a particle in a tokamak can be divided into* **three periodic motions***, in general characterized by a time-scale separation, and appropriately described in a set of action-angle angles, which does not exactly match the natural geometric tokamak coordinates.*

  *In the presence of a wave, particles whose periodic motion match its oscillation frequency are* **resonant and can exchange energy with the wave. This allows energetic particles to drive macro- to meso- scale modes***.*

- *The natural formalism for the study of such macro- to meso- scale modes in a plasma is the MHD formalism and ordering, but MHD has some limitations. In particular, small scales cannot be reached by MHD, neither resonant phenomena.*

- *In a general sheared geometry, modes ocillating with a finite frequency are damped via phase-mixing (a process called* **continuum damping***) and hence stabilized. However, depending on geometry, some modes, the* **gap modes***, can avoid the latter damping. As a consequence, they can be very unstable and grow, with only a small amount of resonant drive by the energetic particles. For this reason, gap modes are the most dangerous modes, although other* **energetic particle modes** *can also be driven in the presence of a strong amount of energetic particle drive.*

- *Nonlinear descriptions are necessary to determine the effects of these instabilities on the plasma and in particular of the transport of energetic particles. Depending on the regime (the involved time scales and the amount of drive),* **different regimes of saturation and of particle transport can be predicted***.*

- *Experiments can be conducted in the Tore-Supra tokamak using various heating devices to create a population of fast particles. Diagnostics exist to catch some features of the modes that develop.*

*Equation (1.2-9) is a second order, nonlinear, vector, differential equation which has defied solution in its present form. It is here therefore we depart from the realities of nature to make some simplifying assumptions...*

Bate, Mueller, White, 1971, *Fundamentals of Astrodynamics*

# 3

# From the Gyrokinetic to the Magneto-HydroDynamic linear description of instabilities

We now describe the formalism and plasma model used in this thesis for the study of collective instabilities driven by energetic particles.

The theoretical review of the previous chapter indicated that MHD provides a good understanding of the main physics at stake in the interaction between macro-scale modes and energetic particles. However, we also indicated some limits of MHD in section 2.2.2.

For the study of Beta Alfvén Eigenmodes, of interest in this thesis, kinetic effects cannot be overlooked. The main reason is the expected important role of resonances with the thermal plasma, which we mentionned in the thesis introduction [38]. Besides, experiments display acoustic fluctuation frequencies very close to the MHD Alfvén continous spectrum, previously defined. This suggests that conversion to kinetic modes and small radial scales cannot be fully neglected.

Consequently, **a kinetic plasma model** is used in this thesis, for both the thermal plasma and the energetic population. The electric and magnetic field evolution equations, are taken into account using an equivalent **variational formulation** of Maxwell equations, in the same fashion as in Ref. [68]. Compared to Ref. [68], we bring some clarification of the coordinate systems used for the kinetic modelling, and the formulation is put in a form which can be directly related to the Shear Alfvén law, Eq. 2.49.

An advantage of a variational formulation is to provide an energy principle which directly extends the MHD kinetic energy principle to kinetic theory. When used as a dispersion relation, an energylike relation such as the MHD energy equation 2.42 provides a nice simple starting point to analyze the stability of a mode. For example, such simple conclusions on the stabilizing effect of various physical phenomena drawn ealier (for example the stabilizing effect of bended field line, via magnetic tension), can be generalized. However, one should note that moving to kinetic theory greatly modifies the form of the ideal MHD energy equation. In MHD, it takes the form $(\omega^2/2)\int d^3\mathbf{x}\ \rho_{\mathrm{M}}|\xi_\omega|^2 = (1/2)\int d^3\mathbf{x}\xi_\omega^*\mathcal{F}(\xi_\omega) = \delta W_{\mathrm{MHD}}$, with $\mathcal{F}$ a hermitian operator, and $\delta W_{\mathrm{MHD}}(\xi_\omega, \xi_\omega^*)$ a functional which does not explicitely depend on $\omega$. With kinetic effects included, the $\omega$ independence of the right hand side disappears in general. Worse, the dispersion relation $\mathcal{F}$ is no longer hermitian and the dispersion relation becomes fully complex.

A more technical advantage of the use of an integrated form of the Maxwell equations, is the possibility to switch easily from one coordinate system to another by a simple change of variables. In particular, a rigorous derivation of resonances with the particles eigenfrequencies (which is best understood in the action-angle variables) can be combined with a more geometric picture provided by the usual non-canonical guiding-center coordinates (which separates velocity and space coordinates).

We start this presentation by a general description of the variational principle, with an

attempt to provide some insight in the physical meaning involved when dealing with stability issues. Next, we explain the plasma kinetic model used in this work, the so-called **gyrokinetic model**, expanded here in the two coordinate system of interest to us, the action-angle variables and the non-canonical guiding-center variables introduced in the previous chapter. Finally, we combine the two models to display a gyrokinetic energy relation, and show how the MHD limit, leading to the traditional MHD energy equation, can be recovered.

## 3.1 Variational dispersion relation and instabilities

### 3.1.1 Variational formalism and energylike relation

For the instabilities of interest in this thesis, the electromagnetic fields can be described using the **low frequency Maxwell equations**

$$\nabla \cdot \mathbf{E} = -\frac{\rho}{\epsilon_0} \tag{3.1}$$

$$\nabla \times \mathbf{B} = \mu_0 \mathbf{j} \tag{3.2}$$

$$\nabla \cdot \mathbf{B} = 0 \tag{3.3}$$

$$\nabla \times \mathbf{E} = -\frac{\partial \mathbf{B}}{\partial t} \tag{3.4}$$

where the displacement current $\mu_0 \epsilon_0 \partial_t \mathbf{E}$ is neglected. The charged particles effects come into $\rho(\mathbf{x}, t) = \sum_s \rho_s(\mathbf{x}, t)$ and $\mathbf{j}(\mathbf{x}, t) = \sum_s \mathbf{j}_s(\mathbf{x}, t)$ which are the total charge density and total current density, summed over all the species $s$. From now on, the effects or properties of each species will be specified whenever there may be an ambiguity, with the convention that $s$ refers to any species, $s = i$ when the focus is on the thermal main ion, $s = e$ when it is on electrons and $s = h$ for the hot species.

Equivalently, it is possible to use the electric and magnetic vector potentials

$$\mathbf{E} = -\nabla\phi - \frac{\partial \mathbf{A}}{\partial t} \tag{3.5}$$

$$\mathbf{B} = \nabla \times \mathbf{A} \tag{3.6}$$

and a variational principle to solve Poisson and Ampère Eqs. 3.1, 3.2. Under the assumption that the studied domain is surrounded by an ideal conductor (such that there is no surface term in Eq. 3.7) and similarly as for the hamiltonian formulation of the particles motion, it is easy to see that Poisson and Ampère equations are equivalent to the extremalization of the electromagnetic action $\int dt\, \mathcal{L}$ under variations of the potentials $\mathbf{A}$ and $\phi$ (for fixed $\rho$ and $\mathbf{j}$), where $\mathcal{L}$ is the electromagnetic Lagrangian defined by

$$\mathcal{L}(\mathbf{A}, \phi) = \int d^3\mathbf{x} \left( \frac{\epsilon_0 \mathbf{E}^2}{2} - \frac{\mathbf{B}^2}{2\mu_0} \right) + \int d^3\mathbf{x} \left( \mathbf{j} \cdot \mathbf{A} - \rho\phi \right). \tag{3.7}$$

$\mathcal{L}$ clearly contains information on the fields energies $\propto \mathbf{E}^2$ and $\mathbf{B}^2$, whereas the second term of Eq. 3.7 can be interpreted as the interaction of the fields with the particles. If the term $\propto \mathbf{E^2}$ representing the electric field energy is neglected, extremalization by $\phi$ returns $\rho = 0$, that is **electroneutrality**. Since only collective perturbations are of interest to us (that is with wavelengths longer than the Debye length), the assumption of electroneutrality is made in the following.

For the study of electroneutral coherent perturbations, ie. for perturbed quantities of the form $X = X_\omega e^{-i\omega t} + c.c.$, a simpler variational form is the extremalization of the reduced

Lagrangian [68]

$$\mathcal{L}_\omega = -\int d^3\mathbf{x}\frac{\mathbf{B}_\omega^\dagger \mathbf{B}_\omega}{\mu_0} + \sum_s \mathcal{L}_{s\omega} \quad \text{with} \quad \mathcal{L}_{s\omega} = \int d^3\mathbf{x}\left(\mathbf{j}_{s\omega}\cdot\mathbf{A}_\omega^\dagger - \rho_{s\omega}\phi_\omega^\dagger\right) \tag{3.8}$$

under variations of the virtual potentials $\phi_\omega^\dagger$ and $\mathbf{A}_\omega^\dagger$, where $\mathcal{L}_{s\omega}$ represents again the interaction between the fields and the species $s$, and the virtual fields are chosen to cancel at the plasma boundary. Taking the $\omega$ component of Eqs. 3.1 and 3.2, and multiplying them respectively by $\phi_\omega^\dagger$ and $\mathbf{A}_\omega^\dagger$, it comes that $\mathcal{L}_\omega(\mathbf{A}_\omega, \phi_\omega, \mathbf{A}_\omega^\dagger, \phi_\omega^\dagger) = 0$ for any virtual fields $\phi_\omega^\dagger$, $\mathbf{A}_\omega^\dagger$, once the physical fields have been found. Inversely, when Eq. 3.8 is extremalized by these virtual fields, the $\omega$ component of Poisson and Ampere equations are directly recovered.

This variational principle is simpler than the one corresponding to Eq. 3.7 because the real physical fields are made completely independent from the virtual fields. In particular, using a self-consistent model for the particle fields, that is $\rho_{s\omega}(\phi_\omega, \mathbf{A}_\omega)$, $\mathbf{j}_{s\omega}(\phi_\omega, \mathbf{A}_\omega)$ is not in contradiction with the variational principle, whereas the previous procedure (where extremalization is with regards to $\phi$ and $\mathbf{A}$) requires the use a more **complete electromagnetic Lagrangian** including the particle energy. Of course, there is a cost to this simplicity. First, $\mathcal{L}_\omega$ is linear in $\phi_\omega^\dagger$, $\mathbf{A}_\omega^\dagger$, hence the idea of extremalization does not provide strong physical insight (it would have been different if extremalization would have correspond to minimization for example). Secondly, the physical interpretation of $\mathcal{L}_\omega$ is more ambiguous than the complete real electromagnetic Lagrangian, in particular when resonance come into play [69]. Nevertheless an **energylike relation** can still be displayed.

Since $\mathcal{L}_\omega(\mathbf{A}_\omega, \phi_\omega, \mathbf{A}_\omega^\dagger, \phi_\omega^\dagger) = 0$ is verified for any virtual field once the physical fields $\mathbf{A}_\omega$, $\phi_\omega$ have been determined, it is in particular true for $\phi_\omega^*$ and $\mathbf{A}_\omega^*$, if the latter cancel at the plasma boundary. Assuming an ideal surrounding conductor however, the latter verification is not necessary, and it directly comes from the integration of Maxwell equation that $\mathcal{L}_\omega(\mathbf{A}_\omega, \phi_\omega, \mathbf{A}_\omega^*, \phi_\omega^*) = 0$. Hence, we obtain an **energylike relation** similar to the one provided by MHD (built with the use of $\xi_\omega^*$). It is particularly interesting to recover such familiar quantities as the perturbed magnetic field energy $\int d^3\mathbf{x}|\mathbf{B}_\omega|^2/\mu_0$, which are closely related to the physical quantities.

However, the *linear* MHD energy principle which allows an easy determination of stability based on the sign of the different terms involved in the energylike relation cannot be extended in general. We explained that the linearized MHD equations could be put in the form $\omega^2\rho_{\mathrm{M}(0)}\ \boldsymbol{\xi}_\omega = \mathcal{F}(\boldsymbol{\xi\omega})$, with $\mathcal{F}$ a hermitian operator. When trying the same with the fields of interest in here, that is using a self-consistent linear model for the particle fields, $\rho_{s\omega}(\phi_\omega, \mathbf{A}_\omega)$, $\mathbf{j}_{s\omega}(\phi_\omega, \mathbf{A}_\omega)$, the electromagnetic fields equations can be put in the form $\mathcal{F}(\omega, \phi_\omega, \mathbf{A}_\omega) = 0$, but there is not garanty that $\mathcal{F}$ be hermitian, and the energylike relation and corresponding eigenvalues and eigenfunctions are in general fully complex. [1]

It is important to note that the variational procedure described above in Eq. 3.8, does not a priori assume any linearization, even one single $\omega$ was considered. Plasma nonlinearities certainly imply a mixing of various $\omega$. However, Maxwell equations return the electromagnetic fields as a linear function of the particle fields. Hence, for any field $X(t)$, $X_\omega$ can be understood as the Fourier transform of X ($X(t) = \int X_\omega e^{-i\omega t}d\omega$) and the $\omega$ component of Maxwell and Poisson equation can be extracted. Hence, the energy-like dispersion relation $\mathcal{L}_\omega(\phi_\omega, \mathbf{A}_\omega, \phi_\omega^*, \mathbf{A}_\omega^*)$ can be used in the nonlinear regime.

[1] Note that the use of the so called adjoint fields [69], that is of the solution of the adjoint operator $\mathcal{F}^\dagger$, instead of the conjugate fields provides another energy-like relation, from which one may derive some properties of the eigenvalues $\omega$. When $\mathcal{F}$ is hermitian, these adjoint fields are the same as the conjugates.

### 3.1.2 Physical interpretation of the energylike dispersion relation

Let us now try to have some insight in the physical meaning of the energylike relation.

Focusing on the particle part of the Lagrangian, the following relation comes out

$$\begin{aligned} -\int d^3\mathbf{x}\mathbf{j}_{s\omega}\cdot\mathbf{E}^*_\omega &= \int d^3\mathbf{x}\mathbf{j}_{s\omega}\cdot(\nabla\phi^*_\omega + i\omega\mathbf{A}^*_\omega) = i\omega\int d^3\mathbf{x}\,(\mathbf{j}_{s\omega}\cdot\mathbf{A}^*_\omega - \rho_{s\omega}\phi^*_\omega) \\ &= i\omega\mathcal{L}_{s\omega} \end{aligned} \tag{3.9}$$

where we made use of charge conservation $-i\omega\rho_{s\omega}+\nabla\cdot\mathbf{j}_{s\omega}=0$ in the second equality. Thus, the particle Lagrangian $\mathcal{L}_{s\omega}$ is found to be directly related to the **work** done by the electric field on the particles, from which wave-particle energy transfers follow. More precisely, considering the *real* total current and fields to have one single $\omega$ perturbed component, $\mathbf{j}_s = \mathbf{j}_{s(0)} + (\mathbf{j}_{s\omega}e^{-i\omega t} + cc.)$, $\rho_s = \rho_{s(0)} + (\rho_{s\omega}e^{-i\omega t} + cc.)$, and assuming $\omega$ to be real, the **net power transfer from the particles to the wave** (after averaging of the sinusoidal periodic variations on one period $T = 2\pi/\omega$) is found to be of the form

$$-\frac{1}{T}\int_0^T\int d^3\mathbf{x}\mathbf{j}_\mathbf{s}\cdot\mathbf{E} = -\int d^3\mathbf{x}\mathbf{j}_{s(0)}\cdot\mathbf{E}_{s(0)} - 2\omega\mathrm{Im}(\mathcal{L}_{s\omega}). \tag{3.10}$$

Since $-\int d^3\mathbf{x}\mathbf{j}_{s(0)}\cdot\mathbf{E}_{s(0)}$, is simply the energy transfer from the particles to the equilibrium fields (if there is any), the remaining term, $2\omega\mathrm{Im}(\mathcal{L}_{s\omega})$ appears like the power transfer from the wave to the particles of species $s$.

What about the real part of $\mathcal{L}_{s\omega}$? By analogy with a circuit component, the left hand side of Eq. 3.9 can be interpreted as the product of a complex current $\mathcal{I}$ and of a complex electric potential jump $\mathcal{U}$ considered in a certain plasma volume. Writing $\mathcal{Z}$, the impedance characterizing the plasma response (that is $\mathcal{U} = \mathcal{Z}\mathcal{I}$), the left hand side of Eq. 3.9 can be rewritten $-\mathcal{I}\mathcal{U}^* = -\mathcal{Z}|\mathcal{I}|^2$. In circuit theory, the impedance is usually put in the form $\mathcal{Z} = \mathcal{Z}_R + i\mathcal{Z}_I$, where $\mathcal{Z}_R$ and $\mathcal{Z}_I$ are respectively the electric component's *resistance* and *reactance*. Taking the imaginary part of Eq. 3.9 (still with $\omega$ real), it appears that $\mathrm{Re}(\mathcal{L}_{s\omega})$ corresponds to the reactance of the circuit component [69]. For this reason, $\mathrm{Re}(\mathcal{L}_{s\omega})$ is called the species **reactive response**, or **reactive energy**. It corresponds to the reactive response qualitatively described in section 2.2.3.

Finally, we find two types of responses. One response, the reactive response, behaves likes a reactance. Hence, it is not expected to modify the system energy, but energy may be "stored" or delivered. This response typically leads to exchanges between the equilibrium potential energy and the energy of waves. The other response is linked to energy transfers between waves and particles, and contains such effects as resonant excitation or damping, or dissipative effects such as collisions. When generalized to the Lagrangian 3.8 (not simply to the species $s$ Lagrangian $\mathcal{L}_{s\omega}$), $\mathrm{Im}(\mathcal{L}_\omega)$ can also contain continuum damping. This is obvious when looking at equation 2.54, if we admit that the Lagrangian $\mathcal{L}_\omega$ is not much different $\delta W$ given earlier (The link between the two will be made clearer in the following.). By analogy with circuit components, $\mathrm{Im}(\mathcal{L}_\omega)$ could be associated with *dissipation* (understood with a positive or negative sign). However, as noted in Ref. [70], the idea of dissipation is confusing. Indeed, $\mathrm{Im}(\mathcal{L}_\omega)$ contains resonant wave-particle energy transfers, which can be described by Vlasov equation (Eq. 1.4 with $\mathcal{C}\cdot F = 0, \mathcal{Q} = 0$). As will be explained in the following, Vlasov equation has a hamiltonian formulation, and hence should conserve energy. Thus, the idea of dissipation may be a bit misleading, and it is safer to simply say that $\mathrm{Im}(\mathcal{L}_\omega)$ contains resonances and dissipation (note that a complicated formalism has been developed to separate the two [71]). Nevertheless, because resonances and dissipation have similar behaviors (in particular, discontinuities introduced by resonances can be solved assuming a small order dissipation), it is often easier for physical interpretation to separate resonances

from the remaining plasma energy and look at them as external energy sources. This makes some sense when resonances are simply low order [69].

How can instabilities arise in such a system? Because we assumed the system to be closed (no surface terms in the Lagrangian), dissipation, sources, energy storage, are to be associated with the growth or damping of the plasma kinetic energy. In other words, $\omega$ can have an imaginary part, and **instabilities** are simply roots of the energylike dispersion relation with a positive imaginary part $\mathrm{Im}(\omega) > 0$.

When dissipation or resonances are negligible in the system, the type of instabilities which can arise come from the real part of the Lagrangian and they are called **reactive instabilities** [72]. In this case, it is demonstrated in Ref. [73] that the existence of a reactive instability is possible only in the presence of a **reactively active** species, that is, a population with a conductivity $\sigma_s$ such that such that $\partial_{\omega_r}(\mathrm{Im}\ \sigma_s) > 0$ ($\omega_r = \mathrm{Re}\omega$) for some real $\omega_r$ [2]. By definition, conductivity verifies $\mathbf{j}_s = \sigma_s \mathbf{E}$, such that Eq. 3.10 becomes. $-\int d^3\mathbf{x}\sigma_s|\mathbf{E}_\omega|^2 = i\omega\mathcal{L}_{s\omega}$. It seems reasonable to expand the definition of a reactively active species in the following way,

$$\partial_{\omega_r}\left(\omega_r \mathrm{Re}(\mathcal{L}_{s\omega})\right) < 0, \text{ for at least some real } \omega = \omega_r. \tag{3.11}$$

According to Ref. [73], because for such instabilities, no external source is feeding the system, energy conservation requires the instability to develop with a **negative energy**.

The idea of negative energy becomes clearer when dissipation or resonances (seen as energy sources) are added to the picture. Assume the energylike relation to be almost real (ie, with a lower order real expression $\mathcal{L}_{\omega(0)}$) with an approximate real root $\omega_{r0}$ ($\mathcal{L}_{\omega(0)}(\omega_{r0}) = 0$), and add a first order dissipation $\mathcal{L}_{\omega(1)}$ with $\mathrm{Im}\mathcal{L}_{\omega(1)} \neq 0$. Expansion close to $\omega_{r0}$ ($\omega = \omega_{r0} + \delta\omega_r + i\gamma$) returns

$$[\omega_{r0}\partial_{\omega_r}\mathrm{Re}\mathcal{L}_{\omega(0)}]\gamma = \partial_{\omega_r}(\omega_r \mathrm{Re}\mathcal{L}_{\omega(0)})\gamma = -\omega_{r0}\mathrm{Im}\mathcal{L}_{(1)}(\omega_{r0}). \tag{3.12}$$

The term in brackets in the first term is traditionally called the **wave energy density**, whereas the third term is easily recognized from Eq. 3.10 to correspond to a *source* of energy. Intuitively, one may expect an instability to grow when energy is fed into the system. This is the case for *positive energy waves* $[\omega_{r0}\partial_{\omega_r}\mathrm{Re}\mathcal{L}_{\omega(0)}] > 0$, but the existence of reactively active components verifying 3.11 or of reactive instabilities [72], suggests the possibility of waves with a negative energy density... which are damped when energy is provided to the system, as can be seen in Eq. 3.12[74]. Note that we already faced the difficulty to determine the sign of the wave energy in Eq. 2.54.

### Application to the fishbone-like dispersion relation, and to the special case of gap modes with a dominant m component

As will be made clearer later on, it is possible to link the Lagrangian to the more traditional $\delta W$ introduced in the previous chapter in a simple way

$$\mathcal{L}_\omega = -2\delta W \tag{3.13}$$

and hence to apply the remarks of the previous paragraph to the fishbone-like dispersion relation Eq. 2.64, $\delta W = -\delta I + \delta W_f + \delta W_k = 0$.

From the previous section, the interpretation of the fishbone-like dispersion relation is simpler when a well defined eigenmode (with a well defined stable structure and real frequency) can be determined for the non-resonant part of the dispersion relation, and when

[2] Note that the theorem used here, Foster reactance theorem, simply applies when there are no root on the real axis... which excludes a major candidate, MHD.

resonant excitation of the mode (or any other kind of drive or dissipation) can be treated perturbatively, like an external source. In particular, this description is legitimate for a gap mode close to **marginal stability**, that is, when only a small amount of resonant energetic particles interact with the mode.

The derivations carried out in this thesis make use of these two assumptions, and treat in particular the resonant excitation and damping as perturbative. Justifications or at least determination of validity domains for the latter assumptions will be provided. However, one should keep in mind that this approach breaks down if:

- the solution of the non-resonant dispersion relation is associated to a strong damping (for example for EPMs, defined in section 2.2.2) or it is reactively growing. In this case, marginal stability may only be reached for a sufficiently important resonant "source". And there is no garanty that even close to marginality a well defined mode can exist (depending on the strength characteristic time scales characterizing the drive and the damping mechanisms).

- the resonant energetic population is de facto non-perturbative. In this case, the eigenmode structure may be modified and it depends on the localization of the resonant drive for example.

In both cases, the wave cannot be separated from the resonant population and a wave energy density cannot be defined in a simple way.

Let us focus more precisely on gap modes with a dominant poloidal component and considered with the description of subsection 2.2.2. For such modes, the various terms involved in the fishbone-like dispersion relation can be given explicitely and we can try to see how our interpretation of the energylike dispersion applies.

In subsection 2.2.2, we saw that the radial structure of the modes could be described in Fourier space by a Schrödinger-like equation Eq. 2.60,

$$-\frac{\partial^2\Psi}{\partial\vartheta^2}+\left(-\Lambda^2+\frac{s_0^2}{(1+s_0^2\vartheta^2)^2}-\frac{s_0^2\mathcal{G}}{(1+s_0^2\vartheta^2)}\right)\Psi=0. \tag{3.14}$$

Here, we can recall that $\Lambda^2$ is related to inertia, $\Lambda^2=(\omega^2/v_A^2-k_\parallel^{\mathsf{m}}(r_0)^2)\times 2(\mathsf{m}^2 s_0^2/r_0^2)/(k_\parallel^2)''$, and needs to verify $\Lambda^2<0$ by definition of a gap mode. The other terms can be related to the fluid and kinetic potential energy, involved in the fishbone-like dispersion relation. Indeed, when multiplying Eq. 3.14 by $\Psi^*$, we can rebuild an energylike formula, which is directly proportional to the traditional MHD-like energy functional by Fourier transform properties (Parceval formula). The sign of the proportionality constant follows from the remark that $\omega^2$ (representing inertia) is multiplied by $(k_\parallel^2)''$ in the definition of $\Lambda^2$. It comes

$$\delta W_f+\delta W_k=C\sigma_\pm\left\{\int_0^{+\infty}d\vartheta\left(|\partial_\vartheta\Psi|^2+\frac{s_0^2|\Psi|^2}{(1+s_0^2\vartheta^2)^2}-\frac{s_0^2\Psi^*\mathcal{G}\Psi}{1+s_0^2\vartheta^2}\right)\right\}. \tag{3.15}$$

with $C$ some positive constant, and $\sigma_\pm=\mathrm{Sgn}(k_\parallel^2)''$.

If $\Lambda^2\ll 1$ and $\mathcal{G}\leq 1$, $\delta I$ can also be accessed. In this case, Eq. 3.14 can be solved independently for the inertia dependent terms and for the fluid terms, separating a "large $\vartheta$" and a "small $\vartheta$" region, as was done in Refs. [75, 38]. At large $\theta$ (or small *radial* scales), the fluid dependent terms are negligible, and the solution of Eq. 2.61 is a wave equation which has simple solutions of the form $\Psi_{\text{ext}}=\Psi_0\exp(i\Lambda\vartheta)$, with $\Lambda$ one of the (complex) roots $\Lambda^2$. When $\vartheta$ goes to 1, inertia becomes negligible in Eq. 2.61. The large $\vartheta$ solution can

be connected to the fluid (low $\vartheta$ region) solution $\Psi_{\rm in}$, using a matching of the slopes (see Fig. 3.1)

$$\begin{aligned} i\Lambda &= \frac{\Psi_{\rm ext}\partial_\vartheta\Psi_{\rm ext}|_{0+}}{\Psi_0^2} = \frac{\Psi_{\rm in}\partial_\vartheta\Psi_{\rm in}|_{+\infty}}{\Psi_0^2} = \frac{1}{\Psi_0^2}\int_0^{+\infty} d\vartheta \left( |\partial_\vartheta\Psi|^2 + \frac{s_0^2|\Psi|^2}{(1+s_0^2\vartheta^2)^2} - \frac{s_0^2\Psi^*\mathcal{G}\Psi}{1+s_0^2\vartheta^2} \right) \\ &= \left[\frac{1}{\Psi_0^2 C\sigma_\pm}\right](\delta W_f + \delta W_k), \text{ or equivalently } \delta I = \Psi_0^2 C\sigma_\pm i\Lambda \end{aligned} \tag{3.16}$$

where the slope $\partial_\vartheta\Psi_{\rm in}$ directly comes from an integration by part of Eq. 3.14. We now have the expression of $\delta I$!

Nevertheless, the story is not over, because we did not define what was the correct root to choose for $\Lambda$. In the following, we compare three criteria which can allow for such a determination, or more precisely, **we interpret two criteria which can be found in the litterature, with the ideas of negative/positive energy waves** developed in the previous paragraph:

- **The localization condition, which we presented as an existence condition for a gap mode to live in the previous chapter**.

  We explained that the traditional form of the existence criterion [26], [76] was a condition on $\mathcal{G}$ (explicitely of the form $\mathcal{G} > \mathcal{G}_0$) designed to create a sufficiently localizing Schrödinger well. The latter requirement can be reformulated as the necessity for the slope calculated in Eq. 3.16 to be negative, as illustrated in Fig. 3.1, or

  $$\mathrm{Im}\Lambda > 0. \tag{3.17}$$

  Note that the condition of localization in $\vartheta$-space only makes sense for a gap mode

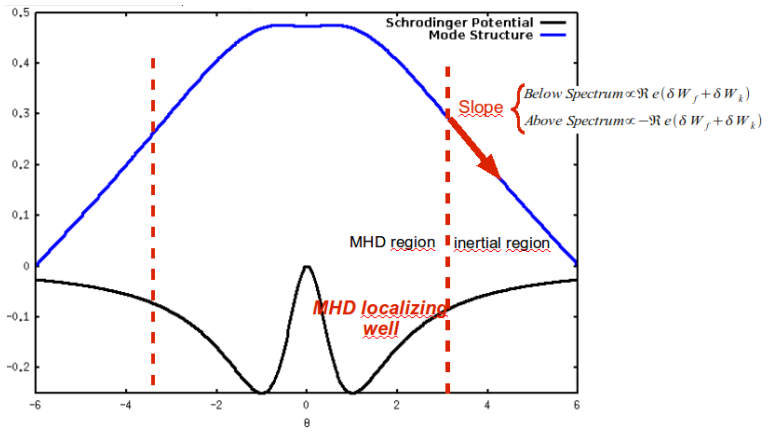


Figure 3.1: Schematic of a Fourier space localizing Schrödinger-like well and of a mode structure, relevant to a gap mode with a dominant poloidal mode number. The localization condition results from the necessity to overcome the central repulsive bump. For an inertia of the form of Eq. 3.16, the localization condition requires negative slope at the frontier between the inertial and MHD regions.

  $\gamma \geq 0$. If the wave is damped by continuum damping, such a condition is not relevant (the mode is peacked in radial space) and it may be necessary to expand it. We will not discuss negative $\gamma$ below.

- **The outgoing wave boundary condition** [77].
  This condition applies for equations of the form Eq. 3.14 which have been shown to

be quite general, when a two-scale separation between inertia and fluid terms applies [16]. It reads

$$\partial_{\omega_r} \mathrm{Re}\Lambda > 0. \tag{3.18}$$

Recalling that in $\vartheta$-space, the wave-like solution of 3.14 at large $\vartheta$ is proportional to $\propto \exp i\Lambda\vartheta$, the requirement 3.18 can be seen as the necessity for the wave to propagate towards the small radial scales, that is for its group velocity (in $\vartheta$-space) bring information to larger $\vartheta$.

- **The positivity of the wave energy density.**

  If the main $\omega$-dependence is carried by inertia, the positivity of the wave energy density close to a point $\omega_r$ (Eq. 3.12) reads

$$-\sigma_\pm \omega_r \partial_{\omega_r} \mathrm{Im}\Lambda > 0. \tag{3.19}$$

  Such a situation makes sense in the fishbone-like dispersion relation if the fast particles are simply perturbative and can be looked at as an external source, and $\delta W_f$ has no $\omega$-dependence (as it is the case for $\delta W_{\mathrm{MHD}}$).

Let us compare the three criteria. For simplicity, we use the reduced notations, $\Lambda^2 = \sigma_\pm(\omega^2 - \omega_0^2)$, $\delta I = \sigma_\pm i\Lambda$ where $\omega_0$ a constant. (The positive constants have no role in the following). Writing $\omega = \omega_r + i\gamma$, it comes $\Lambda_r^2 - \Lambda_i^2 = \sigma_\pm(\omega_r^2 - \gamma^2 - \omega_0^2)$, $\Lambda_r\Lambda_i = \sigma_\pm\omega_r\gamma$, and it follows

$$\partial_{\omega_r}\mathrm{Re}\Lambda = \gamma \mathrm{Im}\Lambda \frac{\sigma_\pm}{|\Lambda|^2}\left(1 + \frac{\sigma_\pm\omega_r^2}{(\mathrm{Im}\Lambda)^2}\right), \tag{3.20}$$

$$-\sigma_\pm\omega_r\partial_{\omega_r}\mathrm{Im}\Lambda = \mathrm{Im}\Lambda\frac{\omega_r^2}{|\Lambda|^2}\left(1 - \frac{\sigma_\pm(\mathrm{Re}\Lambda)^2}{\omega_r^2}\right). \tag{3.21}$$

For gap modes close to threshold, the fishbone like dispersion relation is almost real $\Lambda_r \to 0$, $\gamma \geq 0$, and we see that **the three criteria are equivalent for** modes which will be of interest to us in the following: modes oscillating with a frequency below the continuum spectrum (picture (2a) in Fig. 2.4) which verify $\sigma_\pm > 0$. In other words, **the localization and outgoing wave conditions simply select positive energy waves**. For the case of gap modes oscillating above the continuum spectrum (picture (2b) in Fig. 2.4), the situation is more ambiguous for the outgoing wave condition.

Let us finally see the consequences of the above criteria. When doing the assymptotic matching and using for example the localization constraint, it follows from the sign of $\mathrm{Im}\Lambda$

$$\mathrm{Re}(\delta W_f + \delta W_k) > 0, \quad \text{above the continuum spectrum} \tag{3.22}$$

$$\mathrm{Re}(\delta W_f + \delta W_k) < 0, \quad \text{below the continuum spectrum} \tag{3.23}$$

In the presence of an external drive, new instabilities can arise outside of the MHD unstable region. Similarly as for MHD instabilities $\delta W_{\mathrm{MHD}}$, they are characterized by a band of energy given by Eqs. 3.23. We will explain the signification of Eqs. 3.23 more precisely for BAEs.

## 3.2 Gyrokinetic description

The variational method presented above is simply a equivalent form of Maxwell equations. For self-consistent calculations, we now need to define a model for the plasma. In chapter 2,

it was explained that kinetic modelling was necessary for energetic particles, and could also be desirable for the main plasma. For the special case of Beta Alfvén Eigenmodes, several reasons call for a kinetic modelling of all the plasma species and will be listed in the next chapter.

In the following, we derive the so-called **linear gyrokinetic equation**, used in the latter analysis. Compared to traditional derivations [78, 79, 80, 10], the following one aims at providing a formulation, which **simultaneously applies to the non-canonical guiding center coordinates and to the action-angle coordinates** introduced in chapter 2. Such a formulation legitimates the subsequent simultaneous use of the two sets of coordinates in the variational formulas in section 3.3, which is useful for a clean derivation of resonances.

### 3.2.1 Basics of gyrokinetic theory

We indicated in the thesis introduction, chapter 1, that the collective behavior of a plasma species $s$ could be described using a six dimensional distribution function $F_s(\mathbf{x}, \mathbf{v})$, following Boltzmann equation 1.4. The so-called **drift-kinetic** and **gyrokinetic theories** are simplifications of the Boltzmann equation, which take advantage of the time scale separation between collective fluctuations and the fast gyromotion of a particle in a strongly magnetized plasma, to reduce the description to a 5 dimensional problem. Whereas drift-kinetic theories apply for smooth gradients compared to the species typical gyroradius $k_\perp \rho_s \ll 1$ (typically equilibrium characteristic gradients when $s = i$), **gyrokinetic theories are used for the modelling of perturbations with $\boldsymbol{k_\perp \rho_s \sim 1}$**. The latter ordering (when considered with respect to the thermal ions) is relevant to micro-scale perturbations, which characterize microturbulence. But gyrokinetic theories are also needed when perturbations are of the size of a few ion Larmor radii only, a scale which characterize the singularities of MHD modes.

The possibility to reduce the problem dimensionality is easy to understand when thinking of the separation between the slow **guiding-center** motion (renamed **gyrocenter** motion when a perturbation is present, because of the necessity to re-define the slow scale motion and the motion adiabatic invariant, in this case) and the fast gyromotion of a particle. If perturbations are slow compared to the fast gyromotion, it is *intuitively* possible to *time*-average this motion [3]. Hence, the gyroangle becomes a non-necessary variable, and the dimensionality gets reduced. Because a particle gyromotion (for given fixed gradients) is not too hard to compute, the *time*-averaging procedure can be directly linked to a *space*-averaging procedure along the gyromotion of typical size $\rho_s$, called **gyro-average**. The latter space-averaging procedure should not let think however that only perturbations with scales larger that $\rho_s$ can be modelled. Gyrokinetic theories are really designed to allow for small amplitude perturbations with $k_\perp \rho_s \geq 1$ (It makes sense for perturbation lengths which are fractions of $\rho_s$).

From the latter description, we already see that it will be necessary to choose an appropriate system of coordinate to describe the guiding-center (or gyrocenter) motion. And we provided two of them in subsection 2.1.2, the non-canonical guiding center variables $(\mathbf{X}, \mu, \mathsf{E}, \gamma)$, and the action-angle variables $(\boldsymbol{\alpha}, \mathbf{J})$.

#### Assumptions

Gyrokinetic theory is valid in the presence of a perturbation, and can be used for the modelling of instabilities. However, it has some requirements on both the equilibrium and perturbation structure.

[3] Note that this notion of *time-averaging* is rejected by the modern gyrokinetic theories, because it lets think that some information is lost when moving to the gyrokinetic frame. As will be explained in the next pages, the information relative to the fast gyro-angle can be kept in a coordinate transformation.

The main requirement is that the *unperturbed* plasma be strongly magnetized, that is the condition of Eq. 2.12,

$$\rho_s \frac{\nabla B_{(0)}}{B_{(0)}} \equiv \rho_s^* \ll 1 \tag{3.24}$$

which ensures the possibility to define a slow guiding-center motion and a fast gyromotion. Traditional gyrokinetic theories also consider the equilibrium electric field to be reduced

$$\frac{E_{(0)\perp,\,\parallel}}{v_{ts}B} = O(\rho^*) \text{ such that in particular } \frac{v_{\mathbf{E}\times\mathbf{B}}}{v_{ts}} = O(\rho_s^*) \tag{3.25}$$

The latter limitation on the equilibrium $\mathbf{E}\times\mathbf{B}$ drift is referred to as the **drift-kinetic ordering**[8], and it is opposed to the so-called **MHD ordering**, $v_{\mathbf{E}\times\mathbf{B}} \sim v_{ts}$ (this designation will be made clearer in section 3.4). The drift-kinetic ordering is usually valid in the plasma core, but may break at the edge where strong $\mathbf{E}\times\mathbf{B}$ flows are possible.

Gyrokinetic theories enable the description of perturbations with a limited amplitude (which cannot break the overall confinement), and a relatively limited frequency $\omega$ compared to the species gyrofrequency, $\Omega_{s,c}$. Explicitely, the following small parameters are used

$$\frac{\omega}{\Omega_{s,c}} \sim \epsilon_\omega \ll 1, \qquad \frac{\mathcal{X}_\omega}{\mathcal{X}_{(0)}} = \epsilon_\delta \ll 1, \tag{3.26}$$

where $\mathcal{X}$ stands for any charateristic quantity. However, as explained before, the mode length scale is allowed to be as small as the species gyroradius, but in the perpendicular direction only

$$\rho_s k_\perp = \epsilon_\perp \quad \text{arbitrary}, \qquad \frac{k_\parallel}{k_\perp} = \epsilon_\parallel \ll 1 \tag{3.27}$$

This restriction on $k_\parallel$ comes from the fact that perturbations with a large $k_\parallel$ are strongly stabilized by the magnetic field tension and consequently not very dangerous.

We now know all the small parameters involved in (linear and nonlinear) gyrokinetic theory [10]. An ordering which is relevant to core thermal ions is the following $\epsilon_\delta \sim \epsilon_\omega \sim \epsilon_\parallel \sim \rho^*$. For our derivations, we will assume $\rho_e^* \ll \rho_i < \rho_h \sim \epsilon_\delta \sim \epsilon_\omega \sim \epsilon_\parallel$, such that gyrokinetic theory applies to the three considered populations [79].

For our derivations, we will make use of the *linear* gyrokinetic equation, and simply retain first order terms in the perturbation ($\epsilon_\delta$). For a clean separation of the equilibrium and perturbed distribution function, $F_s = F_{s(0)} + f_{s\omega}$, the equilibrium distribution function needs to verify the (reasonable) orderings

$$\mu\partial_\mu F_{s(0)}|_{\mathbf{X},\mu,\gamma} \sim \mathsf{E}\partial_{\mathsf{E}} F_{s(0)}|_{\mathbf{X},\mu,\gamma} \sim P_\varphi \partial_{P_\varphi} F_{s(0)}|_{\mathbf{X},\mu,\gamma} = O(1). \tag{3.28}$$

For simplicity, we go a little bit further and assume the equilbrium distribution to be only slighty anisotropic, such that $\mu\partial_\mu F_{s(0)}|_{\mathbf{X},\mu,\gamma} = O(\epsilon_\delta)$.

Besides, for simplicity, no equilibrium electric field, no collisions and no sources will be considered in our derivation (A gyrokinetic treatment of collisions is a delicate task [81].).

### The gyro-average operator

The **gyro-average operator** is the space-averaging operator which allows to get rid of the details of the gyromotion, to retain only the slower motion relevant to the guiding-center (or

gyrocenter) dynamics,

$$J_0 \cdot = \frac{1}{2\pi}\int_0^{2\pi} d\gamma|_{\mathbf{X},\mathsf{E},\mu} \ ... = (1/2\pi)\int_0^{2\pi} d\alpha_1|_{\alpha_2,\alpha_3,\mathbf{J}} \ ... \ . \tag{3.29}$$

[4] A convenient form of this operator is given by its Fourier expression. Consider a function $\mathcal{F}(\mathbf{x})$ of Fourier transform $\mathcal{F}(\mathbf{k})$, and separate the particle gyromotion $\mathbf{x} = \mathbf{X} + \boldsymbol{\rho}$, with $\boldsymbol{\rho}$ the gyromotion of the form $\boldsymbol{\rho} = \rho_\perp(\cos\gamma\ \mathbf{e}_{\perp 1} + \sin\gamma\ \mathbf{e}_{\perp 2})$, with $\mathbf{e}_{\perp 1}$ and $\mathbf{e}_{\perp 2}$ two orthogonal unit vectors perpendicular to the magnetic field in $\mathbf{X}$. It comes

$$\begin{aligned} J_0 \cdot \mathcal{F}\ (\mathbf{X}) &= \int_0^{2\pi} d\gamma|_{\mathbf{X},\mathsf{E},\mu}\mathcal{F}(\mathbf{x}) = \int_{-\infty}^{+\infty} d\mathbf{k}\mathcal{F}(\mathbf{k})\int_0^{2\pi}\frac{d\gamma|_{\mathbf{X},\mathsf{E},\mu}}{2\pi}e^{-i\mathbf{k}\cdot\mathbf{X}-i\mathbf{k}\cdot\boldsymbol{\rho}(\gamma)} \\ &= \int d\mathbf{k}\mathcal{F}(\mathbf{k})\ e^{-i\mathbf{k}\cdot\mathbf{X}}J_0(k_\perp\rho_\perp) \end{aligned} \tag{3.30}$$

where $J_0()$ in the final term is the usual notation for the $0^{\text{th}}$ order Bessel function. Consequently, the gyro-average operator is found to be equivalent to a simple multiplication by a Bessel function in Fourier space (which justifies its notation $J_0$ !).

We represented the $J_0$ Bessel function in Fig. 3.2. Immediate physical insight can be

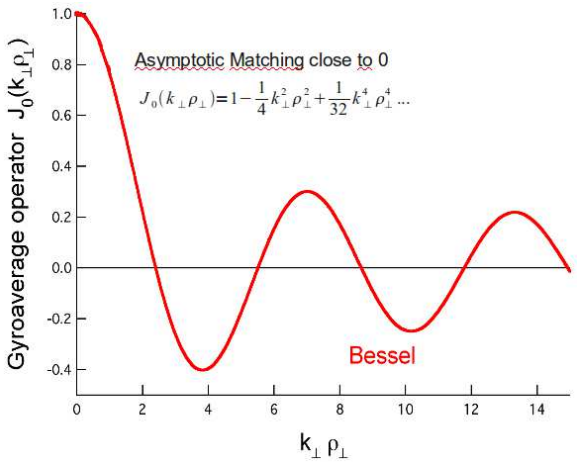


Figure 3.2: $0^{th}$ order Bessel function $J_0$.

obtained from this picture. When $k_\perp\rho_s \ll 1$, $J_0 \to 1$, the gyroradius of the particle is so small that it does not see any perturbation, and the gyro-averaging is nothing but the identity operator. When on the contrary, $k_\perp\rho_s \gg 1$, $J_0 \to 0$, the particle encounters several important variations of the fluctuation levels during its gyromotion. Thus, their averaged effect is null. Taking for example a perturbation of a few millimeters (a few thermal ion Larmor radii), the orderings $\rho_i \sim 1$mm, $\rho_e \sim 0.1$ mm, $\rho_h \sim 10$mm (energetic ions) show that the electron gyromotion should not modify the electron response to the mode, energetic ions will not be sensitive to the perturbation. For thermal ions, the effect of the gyromotion is more ambiguous, and requires a high order expansion of the gyro-average operator.

[4] Note that the equivalence of the two fast-angle averaging operators is not so trivial *a priori*, because two different fast angle systems could be defined for two different coordinate systems. Because the action-angle defined in this case, have been designed to match the traditional non-canonical guiding-center variables (in particular, $J_3$ depends on $(\Psi, E, \mu)$) equivalence is verified.

**Derivations of the gyrokinetic equation**

The gyrokinetic equation is *an* equation on a **5D distribution function**, expressed in a set of **equilibrium based coordinates** where one fast angle representing the fast gyromotion is not present. From this definition, no unicity is expected. Hence, a derivation of the gyrokinetic equation requires to define the basis coordinate system, as well as the relation between the analyzed 5D equation and the real 6D distribution function.

Two different approaches have been developed to display such a gyrokinetic equation. And their equivalence is not absolutely trivial *a priori*.

- **In traditional gyrokinetic theory**, Vlasov equation, $d_t F_s = 0$, is expressed in the equilibrium coordinates, for example in the guiding-center coordinates,

$$\frac{dF_s}{dt} = \frac{\partial F_s}{\partial t} + \frac{d\mathbf{X}}{dt} \cdot \frac{\partial F_s}{\partial \mathbf{X}} + \frac{d\mu}{dt} \cdot \frac{\partial F_s}{\partial \mu} + \frac{d\mathsf{E}}{dt} \cdot \frac{\partial F_s}{\partial \mathsf{E}} + \frac{d\gamma}{dt} \cdot \frac{\partial F_s}{\partial \gamma} = 0 \tag{3.31}$$

  and an equation on $J_0 \cdot F_s$ is derived based on a direct gyro-average of this equation [78, 79, 8]. The advantage of this method is that it offers a direct understanding of the orderings at stake from a single look at Eq. 3.31 (the range of $\partial_t \sim \omega$, or $\Omega$ for example, the order of the drifts in $\dot{\mathbf{X}}$...). However, this derivation is difficult because the $\gamma$-dependence needs to be handled at the same time in $F_s$ and in the total derivatives, which makes averaging a tough work, especially for nonlinear gyrokinetic theories.

- **Modern gyrokinetic theory** [10, 82] expands the idea underlying the definition of the equilibrium guiding-center coordinates, $\mathbf{Z}_{\rm gc}$, to the perturbed case. Making use of the techniques of the Hamiltonian formalism, and in particular, of the Lie transformations, they define the equations of motion of a *virtual* particle, the **gyrocenter** $\mathbf{Z}_{\rm gy}$, whose trajectory is independent from the fast gyroangle. Writing $\mathcal{T}$ the transformation $\mathcal{T} : \mathbf{Z}_{\rm gc} \rightarrow \mathbf{Z}_{\rm gy}$, the expression of Vlasov equation in the guiding-center variables is derived using

$$\frac{dF_{s,\rm gy}}{dt} = 0, \text{ where "}d_t\text{" is independent of } \gamma \tag{3.32}$$

$$\text{and} \quad F_{s,gc}(\mathbf{Z}_{\rm gc}) = F_{s,gy}(\mathcal{T} \cdot \mathbf{Z}_{\rm gc}) \tag{3.33}$$

  With this method, all the fast angle dependence is put in one single term, $\mathcal{T}$. Moreover, the use of a Hamitonian formalism ensures the conservation of energy and phase-space volumes.

### 3.2.2 Formulation of the linear gyrokinetic equation in a coordinate independent way

We now derive **the linear gyrokinetic equation** in a coordinate-independent form, **valid for a simultaneous use in the canonical action-angle coordinates** $(\boldsymbol{\alpha}, \mathbf{J})$ **and in the non-canonical guiding-center coordinates** $(\mathbf{X}, \mu, \mathsf{E}, \gamma)$.

We already explained that the action-angle variables were the appropriate coordinates to compute the particle eigenfrequencies, and as a consequence resonant behaviors. In linear theory, they are also a very convenient calculation tool because they allow for an explicit inversion of the Vlasov full time derivative (which, will greatly simplify our calculations). On the other hand, the non-canonical variables are closer to the fluid moments and to the geometric features of modes. For these reasons, we want to make sure that the *perturbed* fast-angle distribution function we will later introduce in the Lagrangian 3.8 makes sense

in both coordinate systems. The reason why this question is not fully trivial is that a perturbed distribution has *a priori* no reason to remain the same in a coordinate transformation $f_{\omega,\mathbf{Z}}(\mathbf{Z}) \neq f_{\omega,\mathbf{Z}'}(\mathbf{Z}')$.

The following derivation follows the same averaging method as traditional gyrokinetic theories, but will not fully overlook the lessons of modern theories. For purely linear derivations, it is indeed not needed to compute the full gyrocenter motion to concentrate all the gyroangle information. Only a *partial* coordinate transformation is necessary (and makes things much simpler than the traditional linear derivations [8]), which will be made in the following. Moreover, this *small* step will be observed to give the two coordinate systems of interest the same behavior. To make this small step, some classical formulas of Hamiltonian transformations are required, which can be found in Appendix A.

In any coordinate system $\mathbf{Z} = (Z^a)_{a=1...6}$, Vlasov equation for a species $s$ can be written in a hamiltonian form,

$$0 = \frac{dF_s}{dt} = \frac{\partial F_s}{\partial t} + \frac{dZ^a}{dt}\frac{\partial F}{\partial Z^a} = \frac{\partial F_s}{\partial t} - [H_s, F_s] - \frac{\partial \mathbf{\Gamma}_s}{\partial t} \cdot [\mathbf{Z}, F_s] \tag{3.34}$$

where we simply used Hamilton's equations Eq. 2.19, and the particle motion is described by the Hamiltonian $H_s$ and the Lagrangian $\underline{\mathbf{\Gamma}}_s = \mathbf{\Gamma}_s \cdot \mathsf{d}\mathbf{Z} - H_s \mathsf{d}t$.

At equilibrium, $\partial_t = 0$, $H_s = H_{s(0)} = \frac{1}{2}mv_\parallel^2 + \mu B_{(0)}$ and by definition of the action-angle variables, $H_{s(0)}$ is only a function of the three invariants $\mathbf{J}$. Expressed in the action-angle variables, Vlasov equation reads

$$[H_{s(0)}, F_{s(0)}] = -\partial_{\mathbf{J}} H_{s(0)} \cdot \partial_{\boldsymbol{\alpha}} F_{s(0)} = 0 \tag{3.35}$$

Since the particle eigenfrequencies $\partial_{\mathbf{J}} H_{s(0)} = \mathbf{\Omega}_{s(0)}$ are in general not null, $F_{s(0)}$ can also be taken to be a function of the $\mathbf{J}$ invariants only, or equivalently of the invariants ($\mu$, $\mathsf{E}$, $P_\varphi$).

Consider a perturbation, $H = H_{s(0)} + h_s$, $\mathbf{\Gamma}_s = \mathbf{\Gamma}_{s(0)} + \boldsymbol{\gamma}_s$, $F_s = F_{s(0)} + f_s$ (with $h_s$, $\gamma_s$ and $f_s$ first order quantities $\sim \epsilon_\delta$). For general, not necessarily canonical, coordinate systems, a perturbation can modify both the Hamiltonian and the Poisson bracket structure given by $\mathbf{\Gamma}_s$. The guiding-center/gyrocenter coordinate transformation consists in removing the fast-angle dependence of these two quantities, in order to display fast-angle free Hamilton's equations. In the nonlinear regime, this is necessary because of the complexity which results from the simultaneous mixing of three fast angle dependences in Eq. 3.34 (Due to the perturbation, fast-angle dependence may appear in $H_s$, in the Poisson brackets [,], and in $F_s$.). In the linear approximation however, second order perturbations are neglected, and only two fast angle dependences may get mixed together. Thus, it looks reasonable to use a simpler method. In the following, we make a transformation ($\mathbf{Z} \to \bar{\mathbf{Z}}$) removing the perturbation from the Poisson brackets (only), in order to concentrate the fast angle dependence of the $d_t$ operator in the Hamiltonian, and hence, ease the linear expansion.

From Appendix A.3, we know that this can be done using appropriate transformation generating functions (and a null gauge $S = 0$, for the notation of this Appendix). Equilibrium quantities are not modified by the transformation whereas the perturbed Hamiltonian becomes (Eq. A.22)

$$\bar{h}_s = h_s - (\boldsymbol{\gamma}_s - \bar{\boldsymbol{\gamma}}_s) \cdot \dot{\mathbf{Z}} \tag{3.36}$$

where we enforce $\bar{\boldsymbol{\gamma}}_s = 0$ to remove the perturbation from the Poisson bracket. In this new coordinate system, the perturbation (hence the fast angle dependence) disappears from the brackets such that the Vlasov equation can be linearized easily. To the first order in $\epsilon_\delta$, we obtain

$$\partial_t \bar{f}_s - \left[H_{s(0)}, \bar{f}_s\right] = \left[\bar{h}_s, F_{s(0)}\right] \tag{3.37}$$

where [,] are the *unperturbed* Poisson brackets.

We define $\bar{G}_s = \bar{f}_s - \partial_{\mathsf{E}} F_{s(0)} \bar{h}_s$. From Eq. 3.37, $\bar{G}_s$ verifies

$$\partial_t \bar{G}_s - [H_{s(0)}, \bar{G}_s] = -\partial_t \bar{h}_s \partial_{\mathsf{E}} F_{s(0)} + [\bar{h}_s, \mu] \partial_\mu F_{s(0)} + [\bar{h}_s, P_\varphi] \partial_{P_\varphi} F_{s(0)} \tag{3.38}$$

and has interesting characterics.

- $\bar{G}_s$ can be related to the initial distribution function, using Eq. (A.18). It comes $\bar{f}_s = f_s - (h_s - \bar{h}_s)\partial_{\mathsf{E}} F_{s(0)}$ such that $f_s = \partial_{\mathsf{E}} F_{s(0)} h_s + \bar{G}_s$.
- Eq. (3.38) does not depend on the coordinate system. On a one hand, the perturbed Hamiltonian $\bar{h}_s$ of a canonical system is equal to $h_s = e_s(\phi - \mathbf{v} \cdot \mathbf{A})$ (with $\phi$ and $\mathbf{A}$ perturbed potentials), and the suggested coordinate transformation $\mathbf{Z} \to \bar{\mathbf{Z}}$ is simply identity, since the bracket structure is by definition independent on the perturbation. In particular, $\bar{h}_s = h_s = e_s(\phi - \mathbf{v} \cdot \mathbf{A})$ for action-angle variables. On another hand, we displayed in Eq. 2.26 the particle Lagrangian for the non-canonical guiding-center variables. In fact, Littlejohn calculation of the guiding-center Lagrangian is valid in the presence of perturbed fields as well, such that a perturbation may enter both the Lagrangian symplectic structure $\mathbf{\Gamma}_s$, $\boldsymbol{\gamma}_s \cdot \dot{\mathbf{Z}} = \mathbf{A} \cdot \mathbf{v}$, and the Hamiltonian $h_s = e\phi_s$ [5]. Thus, $\bar{h}_s = e_s(\phi - \mathbf{v} \cdot \mathbf{A})$ in the non-canonical coordinates as well.

  Since the values taken by Poisson Brackets are not changed when the coordinate system is changed, the equality of the effective hamiltonians, shows that Eq. 3.38 is independent from the chosen set of guiding center coordinates. Thus, it should also be true for its solution $\bar{G}_s$.

Following the second point, one can choose to apply Eq. 3.38 to the action-angle variables, to evaluate the orderings at stake. Using the orderings of section 3.2.1, it clearly comes that the terms of the left hand side are respectively of the order of $\epsilon_\delta \omega$, $\epsilon_\delta \mathbf{\Omega}_{s(0)} \cdot \partial_{\boldsymbol{\alpha}}$, and the terms of the right hand side of the order of $\epsilon_\delta \omega$, $\epsilon_\delta \rho_s^* \Omega_{s,1} \partial_{\alpha_1}$, $\epsilon_\delta \Omega_{s,3} \partial_{\alpha_1}$. As a consequence, the fast angle dependent part of $\bar{G}_s$ ($\partial_{\alpha_1} \neq 0$) may only be low order in $\rho_s^* \leq \epsilon_\delta$. And to the first order in $\epsilon_\delta$, it is only needed to retain the gyro-averaged part of $\bar{G}_s$. The problem is reduced to the equations

$$f_s = \partial_{\mathsf{E}} F_{s(0)} h_s + J_0 \cdot \bar{G}_s \quad \text{with} \tag{3.39}$$

$$\partial_t \left(J_0 \cdot \bar{G}_s\right) - [H_{s(0)}, J_0 \cdot \bar{G}_s] = -\partial_t (J_0 \cdot \bar{h}_s) \partial_{\mathsf{E}} F_{s(0)} + [J_0 \cdot \bar{h}_s, P_\varphi] \partial_{P_\varphi} F_{s(0)}. \tag{3.40}$$

Eq. 3.40 can be called the linear gyrokinetic equation, and it is related to the perturbed distribution function by Eq. 3.39. As can be seen in the latter equation, a fast angle contribution has been retained in the expression of the perturbed distribution function ($\propto h_s$). The latter contribution is called the **adiabatic term**, whereas $\bar{G}_s$ is the **non-adiabatic term**. As shown by this derivation, $\bar{G}_s$ can be used for our two reference coordinate systems, but from Eq. 3.39, it clearly appears that it is not the case for $f_s$($h_s$ being different in the two sets of coordinates).

### Application to action-angle variables

In action-angle variables, a linear perturbation can be Fourier expanded. Taking the perturbation to one single frequency $\omega$, we can write

$$h_{s\omega} = \sum_{\mathbf{n}} h_{s,\mathbf{n}\omega}(\mathbf{J})\, e^{i\mathbf{n}\cdot\boldsymbol{\alpha}} + c.c.\ , \qquad f_{s\omega} = \sum_{\mathbf{n}} f_{s,\mathbf{n}\omega}(\mathbf{J})\, e^{i\mathbf{n}\cdot\boldsymbol{\alpha}} + c.c.\ . \tag{3.41}$$

[5] In Eq. 2.26, $B_{(0)}$ shall not be expanded to include perturbed quantities because it is simply a result of the definition of $\mu$.

Eq. (3.40) returns for each triplet $\mathbf{n} = (\mathsf{n}_1, \mathsf{n}_2, \mathsf{n}_3)$,

$$(J_0 \cdot \bar{G})_{s,\mathbf{n}\omega} = \delta_{\mathbf{n}=\mathbf{n}^*} \ \frac{\omega \partial_{\mathsf{E}} F_{s(0)} + (F_{s(0)}/T_{s(0)})\ \mathsf{n}_3 \Omega_{*s}}{\omega - \mathbf{n}\cdot\mathbf{\Omega}_s}\ h_{s,\mathbf{n}\omega} \tag{3.42}$$

where $\Omega_{*s}$ is the **diamagnetic frequency** $\Omega_{*s} = T_{s(0)}\partial_{P_\varphi} \ln(F_{s(0)}) = T_{s(0)}\partial_{J_3|\mathsf{E}} \ln(F_{s(0)})$ and contains effects related to equilibrium pressure gradient (For later use, we also use the practical notation $\mathbf{\Omega}_{*s} \equiv (0, 0, \Omega_{*s})$.). $T_{s(0)}$ is the species $s$ equilibrium temperature. In order to remain general and to considere non-Maxwellian distribution functions, we generalize the definition of the temperature writing

$$-\frac{1}{T_{s(0)}} = \partial_{\mathsf{E}} \ln F_{s(0)} \tag{3.43}$$

where $T_{s(0)}$ may be a function of the three equilibrium motion invariants. Finally, $\mathbf{n}^*$ refers to any triplet with $\mathsf{n}_1 = 0$. The condition $\mathbf{n} = \mathbf{n}^*$ results from the gyro-average, which corresponds to the removal of any component with $\mathsf{n}_1 \neq 0$ in the action-angle Fourier space.

#### Application to the guiding-center non-canonical variables

In order to compute Eq. 3.40 in the non-canonical variables $(\mathbf{X}, \mathsf{E}, \mu, \gamma)$, we need to use the unperturbed fundamental Poisson brackets given in Eq. 2.28. It directly comes

$$\left(\partial_t + v_\parallel \nabla_\parallel + \mathbf{v}_{gs}\cdot\nabla\right) J_0 \cdot \bar{G}_s = \left(-T_{s(0)}\partial_{\mathsf{E}} F_{s(0)} \partial_t + F_{s(0)} \mathbf{v}_{*s}\cdot\nabla\right) \frac{J_0 \cdot \bar{h}_s}{T_{s(0)}} \tag{3.44}$$

Here,

$$\mathbf{v}_{*s} = \frac{T_{s(0)}}{e_s B_{(0)}} \left(\mathbf{b}_{(0)} \times \frac{\nabla F_{s(0)}}{F_{s(0)}}\right) \tag{3.45}$$

is the velocity counter-part of the previously defined diamagnetic frequency, and it is simply called the **diamagnetic velocity** ($i\mathbf{n}\cdot\mathbf{\Omega}_{*s} \equiv \mathbf{v}_{*s}\cdot\nabla$). $\mathbf{v}_{gs}$ is naturally the usual drift derived from the equilibrium Hamiltonian Eq. 2.15, with a null $\mathbf{E}\times\mathbf{B}$-drift (no perpendicular electric field is considered for simplicity).

## 3.3 A gyrokinetic energy functional for the study of shear Alfvén waves

Now that we have determined the plasma response, it can be introduced in the Lagrangian 3.8. In the following section, we expand the electromagnetic Lagrangian with the gyrokinetic plasma response, in order to study modes of the shear Alfvén type. More precisely, we focus on modes with eigenfrequencies $\omega \leq v_A/qR$ ($1/qR$ being the natural $k_\parallel$ scale length), but no lower bound (in a sheared plasma $k_\parallel$ *a priori* varies radially and may cancel).

Considering the time scale separation $k_\parallel v_A \ll k_\perp v_A$, it means in particular that our developments to come will not take into account fast magnetosonic waves. Nethertheless, we already said that the lower shear Alfvén frequency range was more relevant to the energetic particle eigenfrequencies.

For simplicity, we also assume the various species equilibrium distribution to be even in $v_\parallel$, such that there cannot be any equilibrium current in particular. Recalling that the equilibrium distribution functions need to be functions of motion invariants, $F_{(0)}(\mu, \mathsf{E}, P_\varphi)$, this property is verified if we make the approximation $P_\varphi \approx e\psi$.

### 3.3.1 Conventions for the study of waves of the shear Alfvén type

From now on, perturbations will be considered with a single frequency $\omega$. It can be shown that for frequencies which are small compared to the one of compressional Alfvén waves, the perturbed parallel magnetic field verifies

$$B_{\omega\parallel} = -\mu_0 \frac{\nabla P_{(0)} \times \mathbf{b}_{(0)}}{B_{(0)}^2} \cdot \frac{\nabla_\perp \phi_\omega}{i\omega}, \tag{3.46}$$

where $P_{(0)}$ is the total plasma pressure. An easy way to understand this equality is to consider the perpendicular pressure balance in Eq. 2.35 (under the assumption that the left hand side inertia does not adjust fast enough) along with the incompressible pressure state equation, or to cancel the second term of the MHD principle 2.42, which can be seen as the oscillating energy of compressional Alfvén waves (whereas the first and the third terms are to be associated respectively with the shear Alfvén and sound waves).

Using Eq. 3.46, a nice simplification appears. The problem is found to be equivalent to a simpler problem with a reduced perturbed hamiltonian $\bar{h}_s = e_s(\phi_\omega - v_\parallel A_{\omega\parallel})$ (with no perpendicular magnetic potential), under the condition that the drift velocity be replaced by

$$\mathbf{v}_{gs} = \frac{1}{e_s B_{(0)}} \left( m_s v_\parallel^2 + \mu B_{(0)} \right) \left( \mathbf{b}_{(0)} \times \frac{\nabla B_{(0)}}{B_{(0)}} \right) \tag{3.47}$$

or in other words, to take the curvature drift proportional to the $\nabla B$ drift.

This condition is often understood as a low $\beta$ approximation, because it leads to a simultaneous disappearing of the perturbed parallel field $B_{\omega\parallel}$ and of the difference between the two drifts in the equations, (and the two are proportional to $\beta$, as can be seen for example for $B_{\omega\parallel} \propto \mu_0 P_{(0)}/B_0^2$ in Eq. 3.46). But this cancellation is better understood as a compensation of the two effects. A more rigorous derivation of Eqs. 3.46 and 3.47 is given in Ref. [68] .

The **problem is now reduced to two scalar fields**, the electric potential and the parallel magnetic potential. For the study of MHD like modes, it is interesting to make use of two different scalar fields $(\psi, \mathcal{E})$, defined by [83]

$$\nabla_\parallel \psi = -\partial_t A_\parallel \qquad \text{and} \qquad \mathcal{E} = \psi - \phi \ . \tag{3.48}$$

Obviously, $\psi$ is directly related to $A_\parallel$, whereas $\mathcal{E}$ can be linked to the parallel electric field. Indeed $E_\parallel = -\mathbf{b}_{(0)} \cdot \nabla\phi - \partial_t A_\parallel = \mathbf{b}_{(0)} \cdot \nabla\mathcal{E} = 0$, such that the **ideal MHD constraint** $E_\parallel = 0$ can be directly inferred from $\mathcal{E}$.

Note that the definitions of $\psi$ and $\mathcal{E}$ are somehow ambiguous when $\nabla_\parallel = 0$. Considering one tokamak mode of toroidal mode number $\mathsf{n}$ and one of its poloidal component of number $\mathsf{m}$ ($\propto \psi_\omega^{\mathsf{m}}(r) \exp(i(\mathsf{m}\theta + \mathsf{n}\varphi))$, $k_\parallel$ is again $\nabla_\parallel = ik_\parallel = \mathbf{b}_{(0)} \cdot \nabla\varphi(\mathsf{n} + \mathsf{m}/q)$ (Eq. 2.48). Because $q$ is sheared, $\nabla_\parallel$ may only be null on some surfaces unless $\mathsf{n} = \mathsf{m} = 0$. Consequently the derivations to come are only valid for $(\mathsf{n}, \mathsf{m}) \neq (0, 0)$, but they can also apply to the electrostatic limit (taking $\psi = 0$).

### 3.3.2 Lagrangian reduction

**Expression of the field and and particle terms**

The Lagrangian field component can be calculted in the reference fields $(\psi_\omega, \mathcal{E}_\omega)$,

$$\begin{aligned}\mathbf{b}_{(0)}\cdot\nabla\times\mathbf{B}_\omega &= \mathbf{b}_{(0)}\cdot\nabla\times\nabla\times(A_{\omega\parallel}\mathbf{b}_{(0)}) = \nabla_\parallel\left(B_{(0)}\nabla_\parallel\left(\frac{A_{\omega\parallel}}{B_{(0)}}\right)\right) - \mathbf{b}_{(0)}\cdot\nabla^2(A_{\omega\parallel}\ \mathbf{b}_{(0)})\\ &\approx -\nabla_\perp^2 A_{\omega\parallel} = -\frac{1}{i\omega}\nabla_\perp^2\nabla_\parallel A_{\omega\parallel}\end{aligned} \tag{3.49}$$

where the approximation is valid for $\mathbf{B}_{(0)} \approx \mathbf{B}_{\mathrm{T}(0)}$.

The Lagrangian particle terms, $\mathcal{L}_{s\omega}$, require to express the charges and currents using Vlasov equation, in the gyrokinetic approximation. This can be done easily in the action-angle canonical variables, and it returns

$$\mathcal{L}_{s\omega} = \int d^3\mathbf{x}\frac{n_{s(0)}e_s^2}{T_{s(0)}}|\phi_\omega|^2 - \sum_{\mathbf{n}=\mathbf{n}^*}\int d\Gamma\frac{F_{s(0)}e_s^2}{T_{s(0)}}\frac{\omega-\mathbf{n}\cdot\mathbf{\Omega}_{*s}}{\omega-\mathbf{n}\cdot\mathbf{\Omega}_s}\left|J_0\cdot\left(\phi - v_\parallel A_\parallel\right)_{\mathbf{n}\omega}\right|^2. \tag{3.50}$$

We recover the particle adiabatic response in the first term, whereas the second term is obviously resonant.

■–
To derive Eq. 3.50, we can for example express the perturbed particle velocity in the canonical system $(\mathbf{x}, \mathbf{p} = m_s\mathbf{v} + e_s\mathbf{A})$ where the expression of the perturbed velocity is easily found to be $\mathbf{v}_{s\omega} = (-e_s/m_s)\mathbf{A}_\omega = (-e_s/m_s)A_{\omega\parallel}\mathbf{b}_{(0)}$ to derive the perturbed linear destributions of charges and currents,

$$\begin{aligned}\mathbf{j}_{s\omega} &= e_s\left(\int d^3\mathbf{p} f_{s\omega}\mathbf{v}_s + F_{s(0)}(\tfrac{-e_s}{m_s}\mathbf{A}_\omega)\right)\\ \rho_{s\omega} &= e_s\int d^3\mathbf{p} f_{s\omega}.\end{aligned} \tag{3.51}$$

The perturbed particle Lagrangian for the species $s$ becomes

$$\mathcal{L}_{s\omega} = e_s\int d\Gamma f_{s\omega}\mathbf{v}_s.\mathbf{A}_\omega - \tfrac{e_s^2}{m_s}\int d\Gamma F_{s(0)}|\mathbf{A}_\omega|^2 - \int d\Gamma f_{s\omega}e_s\phi_{s\omega} \tag{3.52}$$

where $d\Gamma = d^3\mathbf{x}$ is a phase space volume element.

We can now switch to another canonical set of variables, $(\boldsymbol{\alpha},\boldsymbol{J})$, such that $d\Gamma = d^3\boldsymbol{\alpha}d^3\mathbf{J}$, and use the linear gyrokinetic approximation $f_{s\omega} = \partial_E F_{s,eq}h_{s\omega} + J_0\cdot\bar{G}_{s\omega}$, Eq.3.42 to find

$$\begin{aligned}\mathcal{L}_{s\omega} =& -\frac{e_s^2}{m_s}\int d\Gamma F_{s(0)}|A_{\omega\parallel}|^2 - e_s\int d\Gamma J_0\cdot\bar{G}_{s\omega}(\phi_\omega - v_\parallel A_{\omega\parallel})\\ &+ e_s^2\int d\Gamma\frac{F_{s(0)}}{T_{s(0)}}\left(|v_\parallel A_{\omega\parallel}|^2 + |\phi_\omega|^2 - v_\parallel(\phi^*_{\omega\parallel}A_{\omega\parallel} + \phi_{\omega\parallel}A^*_{\omega\parallel})\right)\\ =& \int d^3\mathbf{x}\frac{n_{s(0)}e_s^2}{T_{s(0)}}|\phi_\omega|^2 - e_s\int d\Gamma\left(J_0\cdot\bar{G}_{s\omega}\right)\left[J_0\cdot\left(\phi_\omega - v_\parallel A_{\omega\parallel}\right)\right]^*\end{aligned} \tag{3.53}$$

Note that the last equality is valid for an equilibrium distribution which is even in $v_\parallel$ (Note that it is possible to relax this assumption to include current driven modes, overlooked in this analysis [68]). –■

Eq. (3.50) is the usual expression for studying the stability of drift waves. To study electromagnetic modes, it is convenient to reformulate the resonant term using the fields $\psi$ and $\mathcal{E}$ which can be compared to the MHD orderings. We made the expansion using the more tractable action-angle Fourier expansion, but with an attempt to introduce elements of the traditional guiding-center coordinates, in order to recover some traditional fluid and kinetic results, in the following parts. This expansion is explained in smaller characters below.

■–
To carry out the expansion of Eq. (3.50), we constantly made use of the coordinate independence of the operators involved in the linear gyrokinetic equation to switch from action-angle variables to the non-canonical guiding-center coordinates. Expansion of the perturbed Hamiltonian

$$\begin{aligned}\frac{1}{e_s}J_0\cdot\bar{h}_{s\omega} =& J_0\cdot(\phi_\omega - v_\parallel A_{\omega\parallel}) = J_0\cdot(\phi_\omega + \frac{v_\parallel\nabla_\parallel\psi_\omega}{-i\omega})\\ =& J_0\cdot\left[\frac{-i\omega + v_\parallel\nabla_\parallel + \mathbf{v}_{gs}\cdot\nabla}{-i\omega}\psi_\omega - \frac{\mathbf{v}_{gs}\cdot\nabla}{-i\omega}\psi_\omega - \mathcal{E}_\omega\right]\\ =& J_0\cdot\left[\frac{\partial_t - [H_{s(0)},\cdot]}{-i\omega}\psi_\omega - \frac{\mathbf{v}_{gs}\cdot\nabla}{-i\omega}\psi_\omega - \mathcal{E}_\omega\right]\\ \left(\frac{1}{e_s}J_0\cdot\bar{h}_{s\omega}\right)_{\mathbf{n}=\mathbf{n}^*} =& \left[\frac{-i\omega + i\mathbf{n}\cdot\mathbf{\Omega}_s}{-i\omega}\psi_{\omega\mathbf{n}}\right] - \left[\frac{\mathbf{v}_{gs}\cdot\nabla}{-i\omega}\psi_\omega + \mathcal{E}_\omega\right]_{\mathbf{n}}\end{aligned} \tag{3.54}$$

leads to

$$\begin{aligned}\mathcal{L}_{s\omega} =& +\int d^3\mathbf{x}\frac{n_{s(0)}e_s^2}{T_{s(0)}}|\phi_\omega|^2 - \sum_{\mathbf{n}^*}\int d\Gamma\frac{F_{s(0)}e_s^2}{T_{s(0)}}\left(1+\frac{i\mathbf{n}\cdot\mathbf{\Omega}_{*s}}{-i\omega}\right)\left(1-\frac{i\mathbf{n}\cdot\mathbf{\Omega}_s}{-i\omega}\right)|\psi_{\omega\mathbf{n}}|^2\\ &+\sum_{\mathbf{n}^*}\int d\Gamma\frac{F_{s(0)}e_s^2}{T_{s(0)}}\left(1+\frac{i\mathbf{n}\cdot\mathbf{\Omega}_{*s}}{-i\omega}\right)(\psi_{\omega\mathbf{n}}\mathcal{E}^*_{\omega\mathbf{n}} + \psi^*_{\omega\mathbf{n}}\mathcal{E}_{\omega\mathbf{n}})\\ &-\sum_{\mathbf{n}=\mathbf{n}^*}\int d\Gamma\frac{F_{s(0)}e_s^2}{T_{s(0)}}\frac{\omega-\mathbf{n}\cdot\mathbf{\Omega}_*}{\omega-\mathbf{n}\cdot\mathbf{\Omega}_s}\left|\left(\frac{\mathbf{v}_{gs}\cdot\nabla\psi_\omega}{-i\omega}+\mathcal{E}_\omega\right)_{\mathbf{n}}\right|^2.\end{aligned} \tag{3.55}$$

where we suppressed any integration term even in the parallel velocity $v_\parallel$. Rewriting $(\mathcal{E}^*_{\omega\mathbf{n}}\psi_{\omega\mathbf{n}} + \mathcal{E}_{\omega\mathbf{n}}\psi^*_{\omega\mathbf{n}}) = |\mathcal{E}_{\omega\mathbf{n}}|^2 + |\psi_{\omega\mathbf{n}}|^2 - |\phi_{\omega\mathbf{n}}|^2$, and using electroneutrality:

$$\sum_s\int d^3\mathbf{p}(F_{s(0)}e_s^2/T_{s(0)})\mathbf{v}_{*s} = \mathbf{b}_{(0)}\times\nabla\left(\sum_s e_s\int d^3\mathbf{p}F_{s(0)}\right) = 0 \tag{3.56}$$

and moving to the non-canonical guiding-center variables, we finally get an MHD-like energy principle 3.57 –■

We can finally put the Lagrangian in a form which unavoidably reminds us of the MHD energy functional.

$$\begin{aligned}\mathcal{L}_\omega =& -\int d^3\mathbf{x}\frac{1}{\mu_0}\left|\frac{\nabla_\perp\nabla_\parallel\psi_\omega}{-i\omega}\right|^2 + \sum_s\int d\Gamma\frac{F_{s(0)}e_s^2}{T_{s(0)}}|\mathcal{E}_\omega|^2\\ &+\sum_s\int d\Gamma\frac{F_{s(0)}e_s^2}{T_{s(0)}}\left(1+\frac{\mathbf{v}_{*s}\cdot\nabla}{-i\omega}\right)\left[(1-J_0\otimes J_0)(|\phi_\omega|^2 - |\mathcal{E}_\omega|^2)\right]\\ &+\sum_s\int d\Gamma\frac{F_{s(0)}e_s^2}{T_{s(0)}}(J_0\cdot\psi_\omega)^*\left(\frac{\mathbf{v}_{gs}\cdot\nabla}{-i\omega}\right)(J_0\cdot\psi_\omega)\\ &+\sum_s\int d\Gamma\frac{F_{s(0)}e_s^2}{T_{s(0)}}\left(\frac{\mathbf{v}_{*s}\cdot\nabla(J_0\cdot\psi_\omega)}{-i\omega}\right)^*\left(\frac{\mathbf{v}_{gs}\cdot\nabla(J_0\cdot\psi_\omega)}{-i\omega}\right)\\ &-\sum_s\sum_{\mathbf{n}=\mathbf{n}^*}\int d\Gamma\frac{F_{s(0)}e_s^2}{T_{s(0)}}\frac{\omega-\mathbf{n}\cdot\mathbf{\Omega}_*}{\omega-\mathbf{n}\cdot\mathbf{\Omega}_s}\left|J_0\cdot\left(\frac{\mathbf{v}_{gs}\cdot\nabla\psi_\omega}{-i\omega}+\mathcal{E}_\omega\right)_{\mathbf{n}}\right|^2\end{aligned} \tag{3.57}$$

In Eq. 3.57, the notation used for the non-resonant part needs some clarification: the form $\hat{L}(fg)$, with $f$ and $g$ two scalar fields should be understood as the effect of a hermitian operator $\hat{L}(fg) = \hat{L}(gf) = f(\hat{L}g)$, and the $\otimes$ symbol stands for a bilinear function such that $(A\otimes B)(fg) = (Af)\times(Bg)$ for $f$, $g$ two scalar fields.

In this functional, we can recognize the first term to be the magnetic tension or **magnetic field line bending term**. The next three contributions are to be associated with **inertia** and include **polarization (with Finite Larmor Radius corrections), and diamagnetic effects, related to $\mathbf{v}_{*s}$**. The fifth term is the MHD-like **interchange drive**, and the last term which is not present in MHD, describes the wave-particle resonant interaction.

### Application to a thermal plasma

We now apply the kinetic energy functional 3.57 to a purely thermal plasma with one single ion species $i$ (and no energetic particles). In other words, the electron and ion thermal equilibrium distribution functions are assumed to be Maxwellians with respect to energy, ie:

$$F_{s(0)} = \frac{n_{s(0)}\left(P_\varphi\right)}{\left[2\pi m_s T_{s(0)}\left(P_\varphi\right)\right]^{3/2}} \exp\left\{-\frac{E}{T_{s(0)}\left(P_\varphi\right)}\right\}. \tag{3.58}$$

where $n_{s(0)}$ is the species density and $T_{s(0)}$ is the species temperature. $T_{s(0)}$ is in agreement with the definition of the temperature given earlier 3.43, but it now depends on $P_\varphi$ only.

Moreover, we assume that $P_\varphi = e_s\Psi + R_0 m_s v_\parallel \approx e_s\Psi$ such that $P_\varphi$ is close to a *radial* coordinate (such that we can write the density and the temperature to be functions of $r$ only, $n_s(r)$ and $T_s(r)$). Doing this, the particles radial drift away from their reference magnetic surface is neglected. Because this approximation is more problematic for trapped particles, it is often called the **thin banana width approximation**. Using the conservation of $P_\varphi$, $\delta P_\varphi = 0 = (e_s B_0)((r/R_0)\delta r + \rho_s(\delta v_\parallel/v_{ts}))$, this approximation is observed to scale like $(R_0/r)\rho_s$ for trapped particles and may not be valid at the center (for ions). However, it is usually a good approximation for passing particles (with a reduced $\delta v_\parallel$). With the latter approximation, the Maxwellian Eq. 3.58 is similar to the more natural idea of thermal equilibrium (ie, a velocity Maxwellian at a given position, as is used in MHD for example). However, one should not forget that in general, the equilibrium distribution has to be taken a function of the invariants, and that $P_\varphi$ does not rigously correspond to a position .

Finally, the ion and electron populations can be combined in the Lagrangian under a few reasonable assumptions. If there is no additional population, electroneutrality at equilibrium implies $n_{i(0)} = n_{e(0)} \equiv n$. Besides, we assume that $|\nabla T_{i(0)}|/T_{i(0)} \approx |\nabla T_{e(0)}|/T_{e(0)}$, and use the notation $e = e_i = -e_e$.

We now focus on modes with typical wavelengths going from a few ion Larmor radii to the mesocale $k_\perp a \leq 0.1$. More precisely, we assume the following orderings to be verified, $\nabla n/n \sim |\nabla T_{(0)}|/T_{(0)} \ll k_\perp < 1/\rho_i$, such that equilibrium variations can be removed at the scale of the perturbation of interest. Combining all the assumptions, it comes

$$\begin{aligned}
\mathcal{L}_\omega = &- \int d^3\mathbf{x} \frac{1}{\mu_0}\left|\frac{\nabla_\perp\nabla_\parallel\psi_\omega}{-i\omega}\right|^2 + \int d^3\mathbf{x}\frac{ne^2}{T_{i(0)}}\left(1+\frac{1}{\tau_e}\right)|\mathcal{E}_\omega|^2 \\
&+ \int d^3\mathbf{x}\frac{ne^2}{T_{i(0)}}\left\langle\left(1+\frac{\mathbf{v}_{*i}\cdot\nabla}{-i\omega}\right)(1-J_0\otimes J_0)\right\rangle\left(|\phi_\omega|^2-|\mathcal{E}_\omega|^2\right) \\
&- \int d^3\mathbf{x}\frac{ne^2}{T_{i(0)}}\left\langle\left(\frac{\mathbf{v}_{gi}\cdot\nabla}{-i\omega}\right)(1-J_0\otimes J_0)\right\rangle|\psi_\omega|^2 \\
&+ \int d^3\mathbf{x}\frac{ne^2}{T_{i(0)}}\left\langle\left(\frac{\mathbf{v}_{*i}\cdot\nabla}{-i\omega}\right)\left(\frac{\mathbf{v}_{gi}\cdot\nabla}{-i\omega}\right)(\tau_e+J_0\otimes J_0)\right\rangle|\psi_\omega|^2 \\
&- \sum_s\sum_{\mathbf{n}=\mathbf{n}^*}\int d\Gamma\frac{F_{s(0)}e_s^2}{T_{s(0)}}\frac{\omega-\mathbf{n}\cdot\mathbf{\Omega}_{*s}}{\omega-\mathbf{n}\cdot\mathbf{\Omega}_s}\left|J_0\cdot\left(\frac{\mathbf{v}_{gs}\cdot\nabla\psi_\omega}{-i\omega}+\mathcal{E}_\omega\right)_{\mathbf{n}}\right|^2
\end{aligned} \tag{3.59}$$

where $\langle ...\rangle = (1/n_{i(0)})\int d^3\mathbf{p}F_{i(0)}...$, $\tau_e = T_{e(0)}/T_{i(0)}$. In deriving Eq. 3.59, the drift-kinetic equation for the electrons, $J(k_\perp\rho_e) = 1$, has been used and the $J_0$ notation of Eq. 3.59 should be understood as the thermal ion relevant gyro-average operator. The identity Eq. 3.59 will be the starting point of our analysis of BAEs.

Before, analyzing Eq. 3.59, it is relevant to check its validity. Several non-variational gyrokinetic formulations exist, which have been developed for the study of shear Alfvén type waves [83, 84, 38]. One should normally recover similar equations when applying the variational principle, and extremalizing $\mathcal{L}_\omega$ under variations of $\phi^*_\omega$ and $A^*_{\omega\parallel}$, or almost equivalently under variations of $\psi^*_\omega$ and $\mathcal{E}^*_\omega$ [6].

And indeed, one can recover the equations of Ref. [41]. Differentiation according to $\mathcal{E}^*_\omega$ at fixed $\psi^*_\omega$ returns a **modified electroneutrality equation**

$$-\left(1+\frac{1}{\tau_e}\right)\mathcal{E}_\omega+\left\langle\left(1+\frac{\mathbf{v}_{*i}\cdot\nabla}{-i\omega}\right)(1-J_0^2)\right\rangle\psi_\omega=-\sum_s\frac{T_{s(0)}}{ne_s}\left\langle J_0\cdot K_s\right\rangle \tag{3.60}$$

with $K_s$ the solution of *a* **linear gyrokinetic equation**

$$\left(\partial_t+v_\parallel\nabla_\parallel+\mathbf{v}_{gs}\cdot\nabla\right)K_s=\frac{F_{s(0)}e_s}{T_{s(0)}}\left(\partial_t+\mathbf{v}_{*s}\cdot\nabla\right)\left[J_0\cdot\left(\frac{\mathbf{v}_{gs}\cdot\nabla\psi_\omega}{-i\omega}+\mathcal{E}_\omega\right)\right]. \tag{3.61}$$

Differentiation according to $\psi^*_\omega$ at fixed $\mathcal{E}^*_\omega$ returns the **vorticity equation**

$$\begin{aligned}-\frac{v_A^2}{\omega^2}\nabla_\parallel(\rho_i^2\nabla_\perp^2)\nabla_\parallel\psi_\omega+\left\langle\left(1+\frac{\mathbf{v}_{*i}\cdot\nabla}{-i\omega}\right)(1-J_0^2)\right\rangle\phi_\omega-\left\langle\left(\frac{\mathbf{v}_{gi}\cdot\nabla}{-i\omega}\right)(1-J_0^2)\right\rangle\psi_\omega\\ -\frac{\rho_i^2v_A^2}{\omega^2}\mathbf{b}_{(0)}\times\nabla\left\langle\beta\right\rangle\cdot\nabla_\perp\left(\mathbf{b}_{(0)}\times\kappa\cdot\nabla_\perp\psi_\omega\right)=\sum_s\frac{T_{s(0)}}{ne_s}\left\langle\left(\frac{\mathbf{v}_{gs}\cdot\nabla}{-i\omega}\right)J_0\cdot K_s\right\rangle\end{aligned} \tag{3.62}$$

where in $v_A^2=B_0^2/\mu_0nm_i$ (the field is taken at the plasma center), again $\beta=2\mu_0n(T_{i(0)}+T_{e(0)})/B_0^2$ takes into account electrons and ions. Eqs. 3.60, 3.61 and 3.62 are in agreement with the equation of Ref. [41].

Note that we can recognize in the vorticity equations some terms of the Shear Alfvén Law 2.49, now expanded to include diamagnetic, FLR and resonant behaviors.

## 3.4 Link with MHD

The **MHD ordering** is traditionally recognized to be appropriate for a large **total** $\mathbf{E}\times\mathbf{B}$-drift velocity

$$\frac{\mathbf{E}\times\mathbf{B}}{B^2}\sim v_{ti} \tag{3.63}$$

and it is for this reason opposed to the **drift-kinetic ordering**

$$\frac{\mathbf{E}\times\mathbf{B}}{B^2}\sim\rho_i^*v_{ti} \tag{3.64}$$

which we made use of to derive the linear gyrokinetic equation [8]. We already explained in the first paragraph of section 2.2.1 that a strong $\mathbf{E}\times\mathbf{B}$ flow was to be associated with the requirement of fast dynamics. The consequence of this ordering is that several terms considered to be low order compared to the $\mathbf{E}\times\mathbf{B}$ related effects (diamagnetic terms, $E_\parallel$) are not present in MHD, and this appears both when studying equilibrium properties and fluctuations. In particular, in the presence of a coherent fluctuation of frequency $\omega$, the previously defined MHD displacement can be directly related to the electromagnetic fields fluctuations, via the $\mathbf{E}\times\mathbf{B}$ fluctuations only (constrained by the ideal Ohm's law),

$$\boldsymbol{\xi}_\omega=\frac{\mathbf{B}_{(0)}\times\nabla\phi_\omega}{-i\omega}. \tag{3.65}$$

[6] The word *almost* here is simply used to recall the indetermination of $\psi^*_\omega$ where $k_\parallel=0$, which results from its definition. As will be clearer in Eq. 4.25, this may have an impact.

Despite this ordering difference, we can recover the **low $\beta$ limit of the MHD energy equation** 2.42, when cancelling the parallel electric field ($\mathcal{E}_\omega = 0$) and keeping enough terms to retain the $\mathbf{E}\times\mathbf{B}$ drift only. In our functional, $\mathbf{E}\times\mathbf{B}$ fluctuations correspond to second order terms in $k_\perp\rho_i$, and neglecting lower order terms kills any diamagnetic effects other than the interchange drive. This possibility to recover the MHD limit is to be related to the fact that our linear expansion of the MHD equations assumed a null equilibrium electric field and was consequently not in contradiction with the drift-kinetic ordering.

A clean way to proceed is to use the **hydrodynamic approximation** and to adopt the limit $\omega \to +\infty$. This ordering increases the relative weight of the electromagnetic potential term $|\mathcal{E}_\omega|^2$ in the functional and consequently implies its cancellation while extremalizing by $\mathcal{E}^*_\omega$. It also cancels diamagnetic effects since $\omega_*/\omega = (\mathbf{V}_{*i}\cdot\mathbf{k})/\omega \to 0$. Besides, the hydrodynamic ordering $\omega \gg k_\parallel v_{te} \gg k_\parallel v_{ti}$ removes any resonance. Finally, to the second order in $\rho_i k_\perp$, the Lagrangian given in Eq. 3.59 reduces to

$$\begin{aligned}\mathcal{L}_\omega = &- \int d^3\mathbf{x}\frac{1}{\mu_0}\left|\frac{\nabla_\perp\nabla_\parallel\psi_\omega}{-i\omega}\right|^2 + \int d^3\mathbf{x}\frac{ne^2}{T_{i(0)}}\rho_i^2\left|\nabla_\perp\psi_\omega\right|^2 \\ &+ \int d^3\mathbf{x}\frac{ne^2}{T_{i(0)}}(1+\tau_e)\left\langle\left(\frac{\mathbf{v}_{*i}\cdot\nabla}{-i\omega}\right)\left(\frac{\mathbf{v}_{gi}\cdot\nabla}{-i\omega}\right)\right\rangle|\psi_\omega|^2 \\ &- \int d^3\mathbf{x}\frac{1}{B_0^2}\left|\frac{\mathbf{b}_{(0)}\times\kappa\cdot\nabla\psi_\omega}{-i\omega}\right|^2\left[\sum_s T_{s(0)}\int d^3\mathbf{p}F_{s(0)}\left(\frac{m_s v_\parallel^2+\mu_s B_{(0)}}{T_{s(0)}}\right)^2\right]\end{aligned} \tag{3.66}$$

or again

$$\begin{aligned}\mathcal{L}_\omega = &- \int d^3\mathbf{x}\frac{1}{\mu_0}\left|\frac{\nabla_\perp\nabla_\parallel\psi_\omega}{-i\omega}\right|^2 + \int d^3\mathbf{x}\frac{1}{\mu_0 v_A^2}\left|\mathbf{b}_{(0)}\times\nabla_\perp\psi_\omega\right|^2 \\ &+ 2\int d^3\mathbf{x}\frac{1}{B_0^2}\left(\frac{\mathbf{b}_{(0)}\times\nabla P\cdot\nabla_\perp\psi_\omega}{-i\omega}\right)\left(\frac{\mathbf{b}_{(0)}\times\kappa\cdot\nabla_\perp\psi_\omega}{-i\omega}\right)^* \\ &- \int d^3\mathbf{x}\frac{c_s^2}{\mu_0 v_A^2}\left|2\frac{\mathbf{b}_{(0)}\times\kappa\cdot\nabla\psi_\omega}{-i\omega}\right|^2\end{aligned} \tag{3.67}$$

where $\left\langle J_0^2\right\rangle(.) \equiv \Gamma_0(.)$ has been approximated by its asymptotic limit close to 0, to the order $k_\perp^2\rho_s^2$. $c_s^2 = \Gamma\left(T_{e(0)}+T_{i(0)}\right)/m_i$ is the **MHD sound speed**, with $\Gamma$ the adiabatic compression index (similar to Eq. 2.43). Note that our kinetic derivation gives $\Gamma = 7/4$, which is different from the value of 5/3 found in the usual 3-D adiabatic pressure equation of state. This difference is the result of the temperature anisotropy between the parallel and perpendicular directions implied by the form of $\mathbf{v}_{gs}$ we considered. However, if we now neglect anisotropy, the usual value of $\Gamma$ can be shown to be recovered.

The Lagrangian of Eq. (3.67) is directly recognized as

$$\mathcal{L}_\omega = -2\delta W_{\text{MHD}} + \omega^2\int d^3\mathbf{x} n m_i\left|\boldsymbol{\xi}_\perp\right|^2 \tag{3.68}$$

where we deduced $\boldsymbol{\xi}$ from Eq. 3.65 and $\delta W_{\text{MHD}}$ is a reduced form of the MHD energy functional 2.42, similar to the one developed in Ref. [84] and called the Slow Sound Approximation. One easily identifies the first three terms of Eq. 3.67 as the field line bending tension, kinetic energy, and interchange. The $B_\parallel$ stabilization of Eq. 2.42 is missing due to the low $\beta$ approximation. Finally, using Eqs. 3.65, it comes

$$\nabla\cdot\boldsymbol{\xi} = \nabla\cdot\boldsymbol{\xi}_\perp = \frac{1}{B_{(0)}^2}\left(\mathbf{B}_{(0)}\times\nabla\times\mathbf{B}_{(0)} - \nabla B_{(0)}^2\right)\cdot\boldsymbol{\xi}_\perp = 2\boldsymbol{\kappa}\cdot\boldsymbol{\xi} \tag{3.69}$$

and the last term is directly recognized as the compressibility related term of Eq. 2.42. It is interesting to note that in this approach, **compressibility is intimately related to geometry** via curvature, $\boldsymbol{\kappa}$.

It is worth noting a difference between the direct derivation of $\delta W_{\mathrm{MHD}}$ starting from the MHD equations and the kinetic derivation provided here. This difference explains that the MHD energy functional can only be recovered with an approximation, the Slow Sound Approximation (SSA) of Ref. [84], corresponding to $\omega \gg c_s/R$ and similar to the hydrodynamic limit $\omega \gg \mathbf{n}\cdot\boldsymbol{\Omega}_s$ assumed in here.

In MHD, the removal of the SSA displays a resonant term which is reminiscent of the wave-particle kinetic resonances, and behaves in a similar fashion as the Alfvén resonant continum. This term is associated to a so-called **Slow Sound Continuum** corresponding to $\omega^2 = k_\parallel^2 c_s^2$. It can be recovered from kinetic resonances of the form $0 = \omega - \mathbf{n}\cdot\boldsymbol{\Omega}_i = \omega - k_\parallel v_\parallel$ (relevant to passing ions, when $\omega \sim k_\parallel c_s$), with the *formal* substitution

$$\mathcal{R}_{kinetic} = \frac{1}{m_i}\Gamma\left[T_{e(0)} + T_{i(0)}\frac{1}{4\Gamma}\left\langle\left(\frac{m_i v_\parallel^2 + \mu B_{(0)}}{T_i}\right)^2\left(\frac{\omega}{\omega - k_\parallel v_\parallel}\right)\right\rangle\right] \tag{3.70}$$

$$\longrightarrow \mathcal{R}_{fluid} = c_s^2\frac{\omega^2}{\omega^2 - k_\parallel^2 c_s^2} \tag{3.71}$$

in the resonant term of Eq. 3.59 (where we simply assumed $\mathcal{E} = 0$, considered all ion resonances to be of the form $\omega - k_\parallel v_\parallel$, and neglected electron resonances $\omega \ll \mathbf{n}\cdot\Omega$ to derive the first equation above). With this substitution, the fluid and kinetic approaches can be made consistent, and the form of Eq. (6) of Ref. [84] and Eqs.(2) and (3) of Ref. [85] can be recovered. Nevertheless, one should note that such a substitution makes sense in the limit $k_\parallel v_\parallel/\omega \longrightarrow 0$ only, also associated to a **high-q** limit ($k_\parallel \propto 1/q$), that is, close to the SSA. In this limit, resonances do not occur but *transit corrections* may result from Eqs.3.70 and 3.71, which are similar in fluid and kinetic theories,

$$\mathcal{R}_{kinetic} \approx c_s^2\left(1 + \frac{6}{7(1+\tau_e)^2}\frac{k_\parallel^2 c_s^2}{\omega^2}\right) \approx \mathcal{R}_{fluid} \approx c_s^2\left(1 + \frac{k_\parallel^2 c_s^2}{\omega^2}\right). \tag{3.72}$$

Otherwise, when $\omega^2$ approaches $k_\parallel^2 c_s^2$, the MHD Slow Sound Continuum arises. But the latter is not fully consistent with collisionless kinetic theory, and it is consequently safer to directly start with the more precise kinetic formalism.

The MHD functional 3.67, with the transit corrections 3.72 is relevant to study shear Alfvén waves or $n = 0$ electrostatic modes in the MHD-SAA limit. This system has been studied extensively [84, 86], and it shows how finite compressibility modifies the Alfvén spectrum and forces the occurence of a low frequency gap where the BAE can exist, even when the slow sound continuum is not taken into account [84]. In the next chapter, we study the equivalent kinetic functional to investigate tokamak acoustic modes and we underline the role of kinetic effects.

## 3.5 Summary

*In this chapter, we presented the kinetic formulation, later used in the thesis for the study of Beta Alfvén Eigenmodes.*

- *Using a variational principle, we explained that Maxwell equations could be put in the form of a complex* **energy balance**, *which allows to compute particle-wave energy transfers, and to define the notion of wave-energy density, and positive energy waves.*

  *We saw in particular, that waves with a* **positive energy density** *could be driven* **unstable**, *when the sign of particle to wave energy resonant energy transfers was positive.*

  *Next, in a effort to understand this idea of positive energy density, we compared it with some requirements of gap modes, classically used in the litterature [35, 77]: the idea that gap modes should be* **localized in the radial Fourier space** *(that is to say not discontinuous in the "normal" radial space, by definition) or the idea that* **energy propagation should be towards the small scales** *[77]. Our conclusion was that* **all three requirements were equivalent for gap-like modes**, *with a dominant* m *component.*

- *Next, we derived the kinetic response of plasma particles to an electromagnetic fluctuation, using the traditional gyrokinetic framework. In this work, we made use of some properties of Hamiltonian transformation to make a derivation of the linear gyrokinetic equation in a* **form which simultaneously applies for action-angle variables and for the non-canonical guiding center variables**, *which is appropriate to deal with resonances.*

- *We finally combined this gyrokinetic response with the variational formulation of Maxwell equations, to display an* **energylike relation, which extends the traditional MHD energy equation**.

  *In this work, we chose to write this energylike relation in a form which directly applies to MHD-like fluctuations. This allowed us to* **recover the classical equations used for the study of shear-Alfvén type waves [41], as well as the MHD functional as a limit**.

*What is the "Beta-induced Alfvén Eigenmode?"*
Heidbrink, Phys. Plasmas 6, 1147 (1999)

# 4 The Beta Alfvén Eigenmode

The question raised by W. W. Heidbrink in a paper of 1993, reveals the ambiguity surrounding the nature of the Beta Alfvén Eigenmode. The latter ambiguity reflects the complexity of the acoustic frequency band where resonances are possible with both thermal and suprathermal particles (see Fig. 1.4) and where various physical effects (compressibility, effects related to the previously defined diamagnetic terms, sound waves) can enter into play.

The main goal of this chapter is to provide a kinetic description of the mode, with an attempt to clarify the physics involved in its dispersion relation and structure, and in particular the role of some kinetic effects which are missing in MHD, such as Finite Larmor Radius (FLR) effects. A related objective is to compare BAEs with other modes traditionally recognized to oscillate in the acoustic frequency range, to allow for an unambiguous identification of BAEs in experiments. Based on this analysis, an interpretation of some acoustic modes observed in the Tore-Supra tokamak will be given.

The chapter is organized as follows. An introduction presents some basic observations of the mode and the particular features of our description. Sections 4.2, 4.3 and 4.4 contain the derivation of the mode frequency and structure, and respectively present the approximations, the local inertial physics and the global structure and dispersion relation of Beta Alfvén Eigenmodes. Section 4.5 compares BAEs with well known modes involved in transport studies, the so-called Geodesic Acoustic Modes (GAMs). Finally, Section 4.6 presents the acoustic modes observed in Tore-Supra and offers an interpretation for their identification.

From now on and until the end of the thesis, we get rid of the subscript $_{(0)}$ to refer to the equilibrium, whenever there is no possible confusion. In particular, $T_i, T_e, v_{ti}, \tau_e, n_h$ will have to be understood as equilibrium quantities.

## 4.1 Introduction

### 4.1.1 A variety of modes in the acoustic frequency range

Recently, quasi-coherent modes have been observed in Tore-Supra in the **acoustic frequency range [87, 88], that is with a frequency of the order of** $v_{ti}/R_0 \sim c_s/R_0$. Their identification requires to understand the types of modes that can develop in this range.

**BAEs** are traditionally recognized to be **electromagnetic fluctuations with finite** (m, n) mode numbers, oscillating with an acoustic frequency in a **gap of the Alfvén resonant spectrum induced by compressibility** (The last term of Eq. 3.67, possibly with the correction Eq. 3.72). The name comes from the dual physics which is associated with the mode existence: the presence of an *Alfvén* resonant spectrum (symbolized by the frequency $\omega_A \equiv v_A/qR \approx v_A/R_0$) and *compressibility* which is at the origin of the mode

*acoustic* frequency ($\omega_{BAE} \sim v_{ti}/R_0$). Indeed, taking the ratio of these two characteristic frequencies, *beta* is recovered : $4v_{ti}^2/v_A^2 = \beta$.

First observations of BAEs were performed in the TFTR and DIIID tokamaks [89] in the presence of energetic ions heated by Neutral Beam Injection, and the modes were found to have a strong deleterious impact on the confinement of the energetic population [90]. Later, BAEs, likely driven by finite amplitude magnetic islands, were also identified in the tokamaks FTU [91, 92] and TEXTOR [93]. Finally, in JET, a high frequency branch of the fishbone modes was observed to oscillate with typical BAE frequencies [94, 95], and may be associated to the same compressible physics as the BAE.

Nevertheless, other modes have been predicted and/or observed in the acoustic frequency range.

An important example is **Geodesic Acoustic Modes (GAMs)**. GAMs are well-established modes in turbulent transport studies, which are thought to strongly interact with turbulence [96, 97, 98, 99, 100, 101, 102]. They are usually taken to be acoustic oscillations with **a main** $(\mathsf{n} = 0, \mathsf{m} = 0)$ **component** and related to the same physics as BAEs: **geometry related compressibility**. Because the existence of GAMs is strongly related to turbulent dynamics, and because electrostatic fluctuations dominate turbulence, they are usually thought to be well described in the **electrostatic limit** (that is, with negligible magnetic fluctuations). Some experimental oscillations, obtained with non-magnetic diagnostics, have been identified as GAMs: in DIII-D using Beam Emission Spectroscopy [103], in JIPT-IIU [104], JFT-2M [105] and T-10 [106] using heavy ion beam probes, in Asdex-Upgrade by Doppler reflectometry [107] and in the Heliac H1 using Langmuir probes [108]. Nevertheless, more recent experiments also reported the existence of $(\mathsf{n} = 0, \mathsf{m} = 0)$ magnetic fluctuations with an acoustic frequency, and the latter were also refered to as GAMs [109].

Other modes, BAAEs (Beta Alfvén Acoustic Eigenmodes), electromagnetic modes with lower frequencies than BAEs and related to the shear of the tokamak equilibrium [85, 110], modes related to diamagnetic effects (ITG/Ion Temperature Gradient or AITG/Alfvén Ion Temperature Gradient [41, 111]), as well lower branches of RSAEs (the Reversed Shear Alfvén Eigenmodes [76], already presented in chapter 2) are also expected in the acoustic frequency range.

This variety makes the study of the acoustic frequency range particularly challenging and controversial.

### 4.1.2 An ambiguous interpretation of BAEs

Soon after the first observations of BAEs, the existence of a **compressibility induced gap** in the MHD resonant Alfvén spectrum was identified [84, 86] with MHD codes (For illustration, such a gap has been calculated in Fig. 4.1 for a Tore-Supra relevant discharge).

Analytically, when compressibility is added but the Slow Sound Continuum is neglected (see section 3.4), it is easily shown that the local Alfvén resonant spectrum of a mode with a main finite $(\mathsf{m}, \mathsf{n})$ component takes the form

$$\Lambda^2 \equiv \frac{\omega^2 - \omega_{BAE}^2}{\omega_A^2} = q^2 R_0^2 (k_\parallel^{\mathsf{m},\mathsf{n}})^2 \qquad \text{instead of} \qquad \Lambda^2 \equiv \frac{\omega^2}{\omega_A^2} = q^2 R_0^2 (k_\parallel^{\mathsf{m},\mathsf{n}})^2 \tag{4.1}$$

(with $\omega_A = v_A/qR_0$) close to the surface where $k_\parallel^{\mathsf{m},\mathsf{n}}$ cancels, which can also be seen as modification of inertia (or the necessity to define a **generalized inertia** $\Lambda^2$). Moreover, $\omega_{BAE}$ is an acoustic frequency (of the order of the experimental observations) which slightly

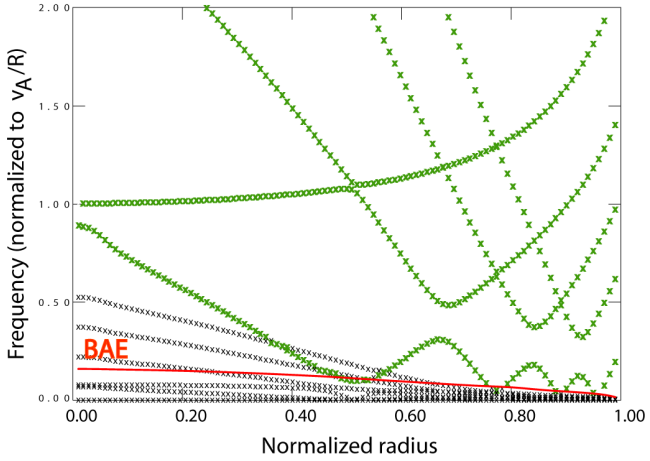


Figure 4.1: Continuum spectrum calculated with CSCAS [86], based on the CRONOS transport reconstructed equilibrium for shot #42039 ($t \sim 9.5$s), whose main characteristics can be found in Figs. 5.4 and 5.5. The spectrum is plotted for a mode with a toroidal mode number $n = 1$ and and an assumed compressibility of 1.67. The green curves correspond to the lines of the Alfvén spectrum, the black curves to the slow continuum.

varies depending on the chosen MHD-like model,

$$\begin{array}{lcll} \omega_{BAE}^2 & = & 2c_s^2/R_0^2 & \text{- in the MHD-SAA.} \\ \omega_{BAE}^2 & = & (v_{ti}^2/R_0^2)(7/2+2\tau_e) & \text{- when ions only are in the hydrodynamic limit and anisotropy is considered, } \Gamma = 7/2, \end{array} \quad (4.2)$$

such that gap modes are possible below $\omega_{BAE}$ ($\omega < \omega_{BAE}$). Next, the existence of an extremum of the resonant spectrum where $(k_\parallel^{\mathsf{m},\mathsf{n}})^2$ cancels, makes reasonable the existence of a discrete mode in this gap (with the same arguments as those given in the derivation of Eq. 2.61), and the interpretation of BAEs as gap modes close to an extremum pictured in Fig. 2.4 (schematic 2.b).

This description is interesting because it shows that compressibility, which is usually thought to be *stabilizing* (it is a positive contribution to $\delta W_{\text{MHD}}$ 2.42) can have a destabilizing impact on MHD stable modes. However, this picture is somehow limited and has been subject to controversy.

- A first reason is that neglecting the Slow Sound Continuum in the MHD formalism only makes sense if the mode frequency verifies $\omega \gg k_\parallel c_s$ for any relevant poloidal component of the mode. In particular, for the mode sidebands (which are absolutely necessary for computating compressibility), $k_\parallel^{\mathsf{m}\pm1} \approx \pm 1/qR_0$, where $k_\parallel^{\mathsf{m},\mathsf{n}} = 0$. Hence, it is not clear that for an acoustic mode, the approximation that the Slow Sound Continuum has no effect can apply.

  For this reason, an alternate interpretation of the gap represented in Fig. 4.1 has been given, attributing this gap to a *coupling between a sound wave of poloidal number* $\mathsf{m}\pm1$ *and an Alfvén wave of poloidal number* $\mathsf{m}$, in the same fashion as for the TAE gap [86] (the coupling of two Alfvén waves). This interpretation is reasonable in MHD and indeed, it was shown that the MHD Slow Sound Continuum impacts on the shape of the compressibility induced gap.

  However, we explained in section 3.4, that a kinetic description was more reasonable for describing the resonant regime $\omega \sim c_s/qR_0 \sim v_{ti}/qR_0$ [89, 38]. For this reason,

the MHD picture of a coupling between a sound wave and an Alfvén wave can be misleading.

First, a resonant condition of the form $\omega - k_{\parallel}^{\mathsf{m},\mathsf{n}}(r)v_{\parallel} = 0$ (a certain curve in the $(r, v_{\parallel})$ space) is generally less localizing radially than a resonant condition of the form $\omega^2 - (k_{\parallel}^{\mathsf{m},\mathsf{n}}(r))^2 c_s^2 = 0$ (a line in $(r, v_{\parallel})$ phase space, parallel to $r = 0$)), even if it is true that for a thermal population, the first resonant condition is usually more active where $v_{\parallel} \sim v_{ts}$, which also tends to enforce some radial localization.

Secondly, $c_s \ll v_A$ leads to a cross point of the Alfvén and Slow Sound Continua which is very close to the resonant surface, such that the mode is expected to have a dominating $\mathsf{m}$ component rather than two poloidal components of equal weight (like it is the case for TAEs).

- A second reason is that several experiments [109, 112] return mode frequencies which are close to the values of $\omega_{BAE}$ given by the formulas 4.2, that is close to the continuum spectrum. It is in particular the case for the modes observed in Tore-Supra, as will be shown later on. We already explained that in this case, small scales (FLR) which may only be accessed with kinetic theory, become important [41].

  More generally, for a given generalized inertia $\Lambda^2$, closeness to the resonant spectrum can be associated to the closeness to the roots of the $\Lambda^2 = 0$. For this reason, the roots of this generalized inertia have been given a special name, **accumulation points** [35]. With a resonant spectrum of the form $\Lambda^2(\omega) = q^2 R_0^2 (k_{\parallel}^{\mathsf{m},\mathsf{n}})^2$, it is clear that accumulation points separate the resonant spectrum $\Lambda^2 > 0$ from the frequency where discrete gap modes can take place $\Lambda^2 < 0$ (see again Fig. 2.4). In this sense, the generalized inertia defined in here is fully consistent with the $\Lambda^2$ defined in Eq. 2.61.

- Finally, this picture does not take into account some physics which can be relevant to the acoustic frequency range, and which is not included in MHD. For example, it is interesting *a priori* to keep $E_{\parallel}$ because it contributes to resonances (see the numerator of the resonant term in Eq. 3.59) and hence wave-particle energy transfers. Secondly, such modes as ITG/AITG may only be found when diamagnetic terms are included [77].

The multiplicity of mode names given in the previous subsection results from the diverse physics involved, but in a lot of parameter ranges, these physical features need to be considered simultaneously. Moreover, as will be clearer in the following (and in particular in Eq. 4.53) the addition of kinetic effects, such as high order FLR, imply a degeneracy removal of the MHD modes [41]. It follows that from a kinetic point of view, an infinite spectrum usually needs to be substituted to the picture of well defined separated discrete modes (though in general, **accumulation points** may be displayed). For this reason, more recent analysis favor a more global description of the mode spectrum rather than a separate description of each possible mode [42].

### 4.1.3 Objectives of the performed derivation

In the first part of this work, we will calculate the BAE dispersion relation using the **variational gyrokinetic energy principle of Eq. 3.59**, with an attempt to catch some missing kinetic features of the MHD model which are relevant to modes on Tore-Supra, and to provide a description of the mode structure.

First, the use of Eq. 3.59 will make possible a separation between the electron and ion responses, which is important when dealing with frequencies of the order of the thermal particles equilibrium characteristic frequencies.

Next, to derive its geometry, the **mode will be expanded into its various poloidal Fourier components $\mathsf{m}$, and FLR effects will be calculated to a high order**, relevant to fluctuations which are close to $\omega_{BAE}$, that is, close to the resonant spectrum. Earlier MHD [84] and kinetic [38, 41] derivations of BAEs were carried out in the **ballooning formalism**, briefly explained in Appendix D. In the work presented here, the Fourier expansion in the poloidal components (only) will return the coupling between poloidal sidebands which is intrinsically related to compressibility and makes possible an analysis of the relative weight of the sidebands involved. Moreover, the mode radial structure will be calcultated directly in a possibly more intuitive way.

Nevertheless, the following calculation will not provide the complete calculation of the Slow Sound Continuum related resonance, and **transit corrections only** (with the correct *kinetic* coefficients though) will be provided, which are relevant to the high-$q$ limit. The full computation of the Slow Sound Continuum related resonances (ie, of resonances with the passing ions, see section 3.4) has been done in Ref. [38], and the additional effect of resonances with trapped ions can also be found in the literature [42]. Besides, diamagnetic effects (negligible for typical Tore-Supra parameters) will not be taken into account.

With these methods and approximations, the results of Eq. 4.2 will be recovered and extended.

In a second part, a comparison of BAEs with electrostatic GAMs will be performed, and the degeneracy of BAEs and GAMs, developed in Ref. [113] analyzed in the light of our formalism.

## 4.2 Approximations of the derivation

In the following, we study BAEs in a simplified **circular equilibrium** using a poloidal and toroidal Fourier component expansion.

Concerning equilibrium, we take advantage of the smallness of $\beta$, $r/R_0$ and $L_p/R_0$ (Recall that $L_p$ a typpical equilibrium plasma poloidal scale at the mode location) considering $r/R_0 \sim \beta$ and $L_p/R_0 >\sim \beta^{1/4}$. The different choices made for $L_p/R_0$ and $r/R_0$ (which one could have choosen with the similar ordering $\epsilon \sim \sqrt{\beta}$, following the given numerical values provided earlier) come from the fact that modes on Tore-Supra have been observed at the plasma center ($r \sim 0.2a$), where equilibrium gradients are flatter. A consequence of the smallness of $r/R_0$ is that the operators $\nabla_\perp$, $\nabla_\parallel$ and $J_0$ which follows, are to be understood as independent on $\theta$. Moreover we take $q \sim s \sim \tau_e \sim 1$.

For the *linear* description of modes, axisymmetry enables the selection of one single $\mathsf{n}$ component whereas toroidicity implies poloidal coupling, such that we can simply write the various field quantities in the form

$$\phi_\omega = \sum_{\mathsf{m}} \phi_\omega^{\mathsf{m}}(r) \exp(i\mathsf{m}\theta + i\mathsf{n}\varphi). \tag{4.3}$$

In particular, with the notation $\nabla \equiv i\mathbf{k}$, $k_r$ needs to be understood as an operator whereas $k_\theta = \mathsf{m}/r$ for the poloidal component $\mathsf{m}$. Next, BAEs (as well as GAMs) are considered to belong to the acoustic frequency range $\omega \sim v_{ti}/R_0$ with a meso-scale structure $1/L_p \ll \mathbf{k}_\perp \approx (k_r, k_\theta) \ll 1/\rho_i$.

For BAEs in particular, we expand the computation close to a surface $r_s$ [1] where

[1] Often called *resonant* surface, but not to be confused with the Alfvén resonant surface.

$k_\parallel^{\mathsf{m}}(r_s) = 0$ (without neglecting neighboring radial variations) where localization is reasonable, as explained above. Since the $\mathsf{m}$ poloidal component corresponding to the latter surface is likely to be dominant in this area, we refer to it as the mode *main poloidal component*. From now on, we also use the notation $\mathsf{m}$ to refer to this component (whereas $\mathsf{m} \pm 1, \pm 2$ will be used for its sidebands). Taking $k_\theta = \mathsf{m}/r$, we finally consider $\rho_i k_\theta \sim \beta$ ($\mathsf{m}$ from 1 to 10), but we do not enforce the radial scale, following the remark that a two-scale structure is expected to arise from this study (see section 2.2.2).

### 4.2.1 The energy functional in the acoustic frequency region

Let us first reduce the functional Eq. 3.59 to a simpler expression valid in the acoustic frequency range (hence, for both for BAEs, GAMs or BAAEs at this point).

For $\omega \sim v_{ti}/R_0$, **diamagnetic effects** verify

$$\frac{\mathbf{n}\cdot\mathbf{\Omega}_{*i}}{\omega} \equiv \frac{\mathbf{v}_{*i}\cdot\mathbf{k}}{\omega} \sim \frac{\rho_i v_{ti} k_\theta / L_p}{(v_{ti}/R_0)} = (\rho_i k_\theta)\left(\frac{R_0}{L_p}\right) \sim< O(\beta^{3/4}) \tag{4.4}$$

In general, the ordering we use makes diamagnetic terms negligible in the acoustic frequency range (this will be clearer in the next paragraph).

Secondly, we know from subsection 3.2.2 that the resonance $\omega/(\omega - \mathbf{n}\cdot\mathbf{\Omega}_s)$ in action-angle variables, is equivalent to the *operator* $(-i\omega)(-i\omega + v_\parallel\nabla_\parallel + \mathbf{v}_{gs})^{-1}$. For **electrons** characterized by a large thermal velocity, $T_e \sim T_i \Rightarrow v_{ti}/v_{te} \sim \sqrt{m_e/m_i} \sim 0.02 \sim 2\beta$. Hence, for the natural length scale $k_\parallel \sim 1/qR_0$ ($q \sim 1$) and for finite $\mathsf{m}$ and $\mathsf{n}$ mode numbers,

$$\frac{k_\parallel v_{te}}{\omega} \sim \frac{v_{ti}}{v_{te}} \sim \beta \tag{4.5}$$

and the resonant operator is found to be dominated by the parallel component, whose role is to make the resonance negligible. In other words, for the scaling $k_\parallel \sim 1/qR_0$, electrons move faster than the mode phase velocity such that their *non-adiabatic response* cancels. Very close to the resonant surface where $k_\parallel^{\mathsf{m}}$ cancels for the main component, the assumption of **electron adiabaticity** can be challenged (even if it remains valid for the resonant terms which involve poloidal sidebands...not all of them). For simplicity however, we assume this assumption to be valid in the whole extent of the studied domain, as long as the main poloidal component has a finite $\mathsf{m}$ (hence $\mathsf{n}$) mode number.

Note however that the latter assumption is not correct for GAMs, whose main component verifies $k_\parallel^{\mathsf{m}=0} = 0$ ($\mathsf{n} = 0$) and falls into the opposite *hydrodynamic* limit.

With the above assumption, $\mathbf{n}\cdot\mathbf{\Omega}_{*i} \ll \omega \sim v_{ti}/qR_0 \ll k_\parallel v_{te}$, the functional reduces to

$$\begin{aligned}\mathcal{L}_\omega = &-\int d^3\mathbf{x}\frac{1}{\mu_0}\left|\frac{\nabla_\perp\nabla_\parallel\psi_\omega}{-i\omega}\right|^2 + \int d^3\mathbf{x}\frac{ne^2}{T_{i,eq}}\left(|\mathcal{E}_\omega|^2 + \frac{1}{\tau_e}\left|\tilde{\mathcal{E}}_\omega\right|^2\right)\\ &+\int d^3\mathbf{x}\frac{ne^2}{T_{i,eq}}\left\{(1-\Gamma_0)(|\phi_\omega|^2 - |\mathcal{E}_\omega|^2) - \left\langle\left(\frac{\mathbf{v}_{gi}\cdot\nabla}{-i\omega}\right)(1-J_0^2)\right\rangle|\psi_\omega|^2\right\}\\ &-\sum_{\mathbf{n}=\mathbf{n}^*}\int d\Gamma\frac{e^2F_{i,eq}}{T_{i,eq}}\left(\frac{\omega}{\omega-\mathbf{n}\cdot\mathbf{\Omega}_s}\right)\left|J_0\cdot\left(\frac{\mathbf{v}_{gi}\cdot\nabla\psi_\omega}{-i\omega} - \mathcal{E}_\omega\right)_{\mathbf{n}}\right|^2.\end{aligned} \tag{4.6}$$

In order to make this expression valid for GAMs as well, we simply introduced the modified field $\tilde{\mathcal{E}}_\omega = \mathcal{E}_\omega - \langle\mathcal{E}_\omega\rangle_{\theta,\varphi}$ ($\mathcal{E}_\omega =$ for finite ($\mathsf{n}$, $\mathsf{m}$) components), which stands for the remaining

resonant electrostatic term involved in the conservation of the GAM main poloidal component.

### 4.2.2 Two scale-separation and inertial layer

In order to assess the importance of the terms of the functional Eq. 4.6, there remains to determine the radial scales. In the following, we simply focus on BAEs. For these modes, a special role is played by the *field line bending tension* which is characterized by a radial dependence, $k_\parallel^{\mathsf{m}}(r)$. Close to the resonant surface where $k_\parallel^{\mathsf{m}}(r_s)=0$, we can expand $k_\parallel$

$$k_\parallel^{\mathsf{m}} \approx k_\parallel^{\mathsf{m}\,\prime}\, x = -\frac{1}{qR_0} k_\theta s x, \qquad \text{with } x=(r-r_s) \tag{4.7}$$

where the shear $q, s$ are assessed at $r_s$. This radial variation is at the origin of the shearing effect of section 2.2.2 and of the related apparition of two scales.

More precisely, the orderings of the various terms of the functional 4.6 are shown in Tab. 4.1, where, as explained in Eq. 4.2, compressibility may be combined with inertia

| Field line bending | Inertia | High order Larmor radius effects | Interchange | Resonant terms linked to compressibility |
|---|---|---|---|---|
| $\frac{(\rho_i k_\perp)^2 (qR_0 k_\parallel)^2}{\beta}$ | $(\rho_i k_\perp)^2$ | $(\rho_i k_\perp)^4$<br>$(\rho_i k_\perp)^2 (\rho_i k_\theta)\frac{R_0}{L_p}$ | $(\rho_i k_\perp)(\rho_i k_\theta)\frac{R_0}{L_p}$ | $\frac{\omega-\mathbf{n}\cdot\mathbf{\Omega}_*}{\omega-\mathbf{n}\cdot\mathbf{\Omega}_s}(\rho_i k_\perp)^2$ |

Table 4.1: Orderings of the functional terms. The Lagrangian terms are of the order of $\mathcal{L}\sim\int d\mathbf{x}(ne^2/T_i)$ times the values given in the table.

and lead to a *generalized inertia* $\Lambda^2$, such that (with the table conventions) $(\rho_i k_\perp)^2 \to (\omega_A/\omega)^2\Lambda^2(\rho_i k_\perp)^2$.

We know from section 3.4 that MHD corresponds to the case where FLR are simply expanded to the order $(\rho_i k_\perp)^2$. This limited expansion is at the origin of the apparent *continuum damping* which characterizes MHD, and comes from disregarding small scales. In order to model smaller scales and catch in a same picture gap modes and continuum modes, the relevant next order is $(\rho_i k_\perp)^4$. As expected, the relevance of such scales is related to closeness to the MHD resonant spectrum or closeness to an accumulation point: indeed, when matching the $(\rho_i k_\perp)^4$ order with generalized inertia, it comes

$$\Lambda^2 \sim \beta(\rho_i k_\perp)^2 \ll 1. \tag{4.8}$$

With a similar matching, now of the field line bending term with $(\rho_i k_\perp)^4$, the radial scale which is relevant to 4th order FLR is obtained

$$(\rho_i k_\perp)^2 (qR_0 k_\parallel)^2/\beta \sim (\rho_i k_\perp)^4 \;\Rightarrow\; \rho_i k_\perp \sim \rho_i k_r \sim \beta^{1/4} \gg \rho_i k_\theta, qR_0 k_\parallel^m \sim \beta^{3/4}. \tag{4.9}$$

It now clearly appears that small scales are localized in a region around $r_s$ of typical length $1/k_r \sim \rho_i \beta^{-1/4}$ (a few millimeters), which is large enough to contain the Alfvén resonant surfaces (where $\Lambda^2 = (qR_0 k_\parallel)^2$ if $\Lambda^2$ is *positive*) where MHD predicts a discontinuity for continuum modes.

This particular region where strong gradients are expected will be called **inertial region** because it contains inertia. Away from this region, that is for larger $r \sim 1/k_r$, terms involving $k_r$ get smaller and can no longer balance the field line bending tension, such that $\rho_i k_r \to 0$. Other terms, which are less dependent on $k_r$, come into play and can set up the relevant

radial scale, usually a macro scale relevant to MHD. For this reason this "external region" will be refered to as **MHD region**, but one should note that it does no longer contain either inertia or compressibility. In particular a lower limit exist on $\rho_i k_\perp \geq \rho_i k_\theta \sim \beta$, which limits the mode radial extent to $1/k_r \sim 1/k_\theta \sim 0.1 - 1\text{m}$.

With this estimate of the mode radial scale, we can assess the validity of the approximations announced earlier.

To the relevant lower order of the functional terms ($\sim \beta$ following Tab. 4.1), neglecting diamagnetic terms (understood as any term involving $\Omega_*$) is justified. Higher order diamagnetic corrections are uncessary because of the scaling 4.4, whereas interchange is only a very lower order term with the assumption $L_p/R_0 > \beta^{1/4}$. In the MHD region, this latter choice is possibly debatable and it may be more reasonable to consider $L_p/R_0 \sim a/R_0 \sim \beta^{1/2}$, such that interchange may be the higher order effect to balance field line bending, at the relevant scale $1/k_r \sim \rho_i \beta^{-1/2}$.

Inversely, neglecting the Slow Sound continuum is not fully consistent, but will be done for simplicity. In the derivation, we will simply consider transit corrections with the ordering $k_\parallel v_\parallel/\omega = O(\rho_i k_\perp)$ which can simply make sense in a high q limit. Note that a purely formal ordering using 1/6 fractions of $\beta$ can be developed, but using such an ordering does not change anything in the story...

## 4.3 Derivation of the BAE characteristic equation in the inertial layer

In this part, we focus on the inertial region only.

### 4.3.1 Determination of the relevant fields

From the previous section, we can derive the relevant field poloidal components, using a Fourier expansion and extremalization of the functional 4.6. Expansion to the fourth order FLR effects makes necessary a Fourier expansion to the second order sidebands, such that 2 scalar fields $(\psi_\omega, \mathcal{E}_\omega)$ for 5 poloidal components: $\mathsf{m}, \mathsf{m} \pm 1, \mathsf{m} \pm 2$.

This calculation is done in Appendix C with the addtional assumption on the **sidebands symmetry**

$$\psi_\omega^{\mathsf{m}+1} = -\psi_\omega^{\mathsf{m}-1}, \psi_\omega^{\mathsf{m}+2} = \psi_\omega^{\mathsf{m}-2}, \mathcal{E}_\omega^{\mathsf{m}+1} = -\mathcal{E}_\omega^{\mathsf{m}-1}, \mathcal{E}_\omega^{\mathsf{m}+2} = \mathcal{E}_\omega^{\mathsf{m}-2} \tag{4.10}$$

This asssumption on the sidebands parity is made possible by the approximation $qR_0 k_\parallel^{\mathsf{m}\pm1} = qR_0 k_\parallel^{\mathsf{m}} \pm 1 \approx \pm 1$ which is consistent with the order of accuracy of our calculation ($(\rho_i k_\perp)^4 \sim \beta$) and leads to the degeneracy of the poloidal sidebands. Note however that this degeneracy removal is also consistent with the inverse parity choice $\psi^{\mathsf{m}+1} = \psi^{\mathsf{m}-1}, \psi^{\mathsf{m}+2} = -\psi^{\mathsf{m}-2}$..., but that the latter choice does not return modes with an acoustic frequency [114].

This expansion returns the following estimates,

$$\begin{array}{rclcrcl} \psi_\omega^{\mathsf{m}+1/\mathsf{m}+2} & = & O((\rho_i k_\perp)^4 \psi_\omega^{\mathsf{m}}) & , & \mathcal{E}_\omega^{\mathsf{m}} & = & O((\rho_i k_\perp)^5 \psi_\omega^{\mathsf{m}}), \\ \mathcal{E}_\omega^{\mathsf{m}+1} & = & O((\rho_i k_\perp) \psi_\omega^{\mathsf{m}}) & , & \mathcal{E}_\omega^{\mathsf{m}+2} & = & O((\rho_i k_\perp)^2 \psi_\omega^{\mathsf{m}}) \end{array} \tag{4.11}$$

We conclude that close to a resonant surface, the main poloidal component $(\mathsf{n}, \mathsf{m})$ of a BAE mode is close to satisfy the MHD constraint $\mathcal{E}_\omega^{\mathsf{m}} = 0$, while its $\mathsf{m} \pm 1, 2$ satellites are almost electrostatic. Since the same derivation can be done at a neighboring resonant surface, this

means that the mode extension of the vector potential is smaller than the one of the electric potential.

Moreover, to our order of accuracy (4th order in $\rho_i k_\perp \sim \beta$), it comes $\mathcal{E}_\omega^m = \psi_\omega^{m+1} = \psi_\omega^{m+2} = 0$, which means in particular that the problem is reduced to the determination of three field components only $\psi_\omega^m, \mathcal{E}_\omega^{m+1}$ and $\mathcal{E}_\omega^{m+2}$, instead of 6.

### 4.3.2 Derivation

We can now develop the Lagrangian 4.6 to the 4th order in $(\rho_i k_\perp)$ using the fields $\psi_\omega^{\mathsf{m}}$, $\mathcal{E}_\omega^{\mathsf{m}+1}$, $\mathcal{E}_\omega^{\mathsf{m}+2}$ and determine the expression of the sideband fields as functions of the main poloidal vector potential $\psi_\omega^{\mathsf{m}}$.

■–

In a cylidrical equilibrium, the curvature verifies $\mathbf{b}_{(0)} \times \kappa = -\frac{\mathbf{1}}{\mathbf{R_0}} \left[\sin(\theta)\,\mathbf{e_r} + \cos(\theta)\,\mathbf{e}_\theta\right]$ and implies a coupling of poloidal components via the $\mathbf{v}_{gi} \cdot \nabla$ operator such that for any poloidal number $\mathsf{m}'$,

$$(\mathbf{v}_{gi} \cdot \nabla \psi_\omega)^{\mathsf{m}'} = i \sum_{\epsilon=\pm 1} \omega_{gi,\epsilon} \psi_\omega^{\mathsf{m}'+\epsilon} \tag{4.12}$$

where $\omega_{gi,\epsilon}$ is an operator defined as $\omega_{gi,\epsilon} = \frac{1}{2} v_{gi}(+i\epsilon k_r + \frac{\mathsf{m}'+\epsilon}{r}) \approx i\epsilon \frac{v_{gi} k_r}{2} \equiv +i\epsilon\omega_{di}$. $ik_r$ stands for the $\partial_r$ operator and $v_{gi} = \frac{-1}{eB_{(0)}R_0}\left(m_i v_\parallel^2 + \mu_i B_{(0)}\right)$.

Using formula 4.12 and in the absence of transit corrections, Eq. 4.6 takes the form $\mathcal{L}_\omega = \int d^3\mathbf{x} \frac{ne^2}{T_i} L_\omega$, with

$$\begin{aligned} L_\omega = &-\rho_i^2 \frac{v_A^2}{\omega^2} \nabla_\parallel \nabla_\perp^2 \nabla_\parallel |\psi_\omega^m|^2 + (1-\Gamma_0)\,|\psi_\omega^m|^2 + 2\left(1-\Gamma_0+\tau_e^{-1}\right)\left[\left|\mathcal{E}_\omega^{m+1}\right|^2 + \left|\mathcal{E}_\omega^{m+2}\right|^2\right] \\ &- 2iK_1\left[\psi^m \mathcal{E}_\omega^{m+1*} - \psi^{m*}\mathcal{E}_\omega^{m+1} + \mathcal{E}_\omega^{m+2}\mathcal{E}_\omega^{m+1*} - \mathcal{E}_\omega^{m+2*}\mathcal{E}_\omega^{m+1}\right] \\ &- 2K_2\left[|\psi_\omega^m|^2 + 3\left|\mathcal{E}_\omega^{m+1}\right|^2 + \psi_\omega^m \mathcal{E}_\omega^{m+2*} + \psi^{m*}\mathcal{E}_\omega^{m+2}\right] \\ &- 6iK_3\left[\psi_\omega^m \mathcal{E}_\omega^{m+1*} - \psi_\omega^{m*}\mathcal{E}_\omega^{m+1}\right] - 6K_4\,|\psi_\omega^m|^2, \end{aligned} \tag{4.13}$$

and $K_n = \left\langle \left[\frac{\omega_{di}}{\omega}\right]^n J_0^2 \right\rangle \sim (\rho_i k_\perp)^n$. If small order transit effects are added, the following additional terms should be added to $L_\omega$,

$$L_{\omega\parallel} = -2L_0\left(\left|\mathcal{E}_\omega^{m+1}\right|^2 + 4\left|\mathcal{E}_\omega^{m+2}\right|^2\right) - 2iL_1\left[\psi_\omega^m \mathcal{E}_\omega^{m+1*} - \psi_\omega^{m*}\mathcal{E}_\omega^{m+1}\right] - 2L_2\,|\psi_\omega^m|^2 \tag{4.14}$$

where $L_n = \left\langle \left(\frac{v_\parallel}{qR_0\omega}\right)^2 \left[\frac{\omega_{di}}{\omega}\right]^n J_0^2 \right\rangle$, where the transit operators have been assumed to be of order $L_n \sim (\rho_i k_\perp)^{n+2}$.

Next, extremalization with respect to $\mathcal{E}_\omega^{m+1*}$ and $\mathcal{E}_\omega^{m+2*}$ yields

$$\begin{aligned} \mathcal{E}_\omega^{m+1} &= i\tau_e\left[(K_1 + L_1 + 3K_3) + 4\tau_e K_1 K_2 - \tau_e K_1(1-\Gamma_0-L_0-K_1^2\tau_e)\right]\psi_\omega^m \\ &+ O\left((\rho_i k_\perp)^4 \psi_\omega^m\right) \end{aligned} \tag{4.15}$$

$$\mathcal{E}_\omega^{m+2} = -iK_1\tau_e \mathcal{E}_\omega^{m+1} + K_2\tau_e\psi_\omega^m + O\left((\rho_i k_\perp)^3 \psi_\omega^m\right) \tag{4.16}$$

The sidebands are now easily expressed as functions of the main poloidal component$\psi_\omega^{\mathsf{m}}$, and the Lagrangian can simply be written

$$\begin{aligned} L_\omega = &\left[-\rho_i^2 \frac{v_A^2}{\omega^2}\nabla_\parallel \nabla_\perp^2 \nabla_\parallel + (1-\Gamma_0) - 2K_2 - 6K_4 - 2L_2 - 2\tau_e\left(K_1^2 + K_2^2\right)\right. \\ &\left. - 2\tau_e\left(2K_1L_1 + \tau_e K_1^2 L_0 - \tau_e(1-\Gamma_0)K_1^2 + 5\tau_e K_1^2 K_2 + 6K_1K_3 + \tau_e^2 K_1^4\right)\right]\,|\psi_\omega^m|^2. \end{aligned} \tag{4.17}$$

There remains to calculate the explicit expressions of the operators $K_n$'s and $L_n$'s. If we make use of the notation $b = \rho_i^2 k_r^2$, $\Omega = \frac{\omega R_0}{v_{Ti}}$, $\zeta = \frac{v_\parallel}{v_{Ti}}$, $h = \frac{v_\perp^2}{2v_{Ti}^2}$ in the following paragraphe only, it easily comes that

$$\langle ... \rangle = \int_{-\infty}^{+\infty} \frac{d\zeta}{\sqrt{2\pi}} e^{-\zeta^2/2} \int_0^{+\infty} dh e^{-h} ... \tag{4.18}$$

$$\frac{\omega_{di}}{\omega} = -\frac{\sqrt{b}}{\Omega}\frac{h+\zeta^2}{2} \tag{4.19}$$

$$J_0^2 = 1 - bh + \frac{3}{8}b^2h^2. \tag{4.20}$$

Hence,

$$\begin{array}{lcllcl} \Gamma_0 & = & \left\langle J_0^2 \right\rangle_i = 1 - b + \frac{3}{4}b^2 & K_1 & = & -\frac{\sqrt{b}}{\Omega}\left(1 - \frac{3}{2}b\right) \\ L_0 & = & \frac{1}{q^2\Omega^2}\left(1 - b + \frac{3}{4}b^2\right) & K_2 & = & \frac{7}{4}\frac{b}{\Omega^2}\left(1 - \frac{13}{7}b\right) \\ L_1 & = & -\frac{1}{q^2\Omega^2}\frac{\sqrt{b}}{\Omega}\left(2 - \frac{5}{2}b\right) & K_3 & = & -\frac{9}{2}\frac{b\sqrt{b}}{\Omega^3} \\ L_2 & = & \frac{1}{q^2\Omega^2}\frac{b}{\Omega^2}\left(\frac{23}{4} - \frac{33}{4}b\right) & K_4 & = & \frac{249}{16}\frac{b^2}{\Omega^4}. \end{array} \tag{4.21}$$

Substituting these expressions into Eq. 4.17 directly returns the functional Eq. (4.22). –■

The result is

$$\mathcal{L}_\omega = -\int d^3\mathbf{x}\frac{ne^2}{T_i}\frac{\omega_A^2}{\omega^2}\psi_\omega^{\mathsf{m}*}\left[(qR_0)^2\rho_i^2\nabla_\parallel\nabla_x^2\nabla_\parallel + \Lambda^2\rho_i^2\nabla_x^2 + \sigma\rho_i^4\nabla_x^4\right]\psi_\omega^{\mathsf{m}} \tag{4.22}$$

where

$$\Lambda^2 = \frac{\omega^2}{\omega_A^2}\left[1 - \left(\frac{v_{ti}}{\omega R_0}\right)^2\left(\frac{7}{2} + 2\tau_e\right) - \frac{1}{q^2}\left(\frac{v_{ti}}{\omega R_0}\right)^4\left(\frac{23}{2} + 8\tau_e + 2\tau_e^2\right)\right] \tag{4.23}$$

$$\sigma = \frac{\omega^2}{\omega_A^2}\left[\frac{3}{4} - \left(\frac{v_{ti}}{\omega R_0}\right)^2\left(\frac{13}{2} + 6\tau_e + 2\tau_e^2\right) + \left(\frac{v_{ti}}{\omega R_0}\right)^4\left(\frac{747}{8} + \frac{481}{8} + \frac{35}{2}\tau_e^2 + 2\tau_e^3\right)\right] \tag{4.24}$$

$\Lambda^2$ is obviously the fluid-like *generalized inertia* announced earlier, whereas $\sigma$ stands the high order FLR.

To determine the relevant equation for $\psi_\omega^{\mathsf{m}}$, there remains to extremalize according to $\psi_\omega^{\mathsf{m}*}$. Some caution is necessary when dealing with electromagnetic waves because of the ambiguous definition of $\psi_\omega^{\mathsf{m}*}$ at the resonant surface, which simply determines $\psi_\omega^{\mathsf{m}*}$, modulo a delta function. Hence, the clean use of the variational principle, originally based on variations of $\mathbf{A}_\omega^*$ rather than $\psi_\omega^*$, leads to the eigenmode equation

$$\left[(qR_0)^2\rho_i^2\nabla_\parallel\nabla_x^2\nabla_\parallel + \Lambda^2\rho_i^2\nabla_x^2 + \sigma\rho_i^4\nabla_x^4\right]\psi_\omega^{\mathsf{m}} = C \tag{4.25}$$

where the C constant is some constant which results from this indetermination.

The form of this eigenmode equation is fully consistent with the one found by F. Zonca *et al.* in Eq. (9) of Ref. [41] for their description of the BAE inertial region, where the effects of the C constant disappears in their formalism because the inertial region corresponds to large $\theta$ value, in the ballooning representation. The coefficients found by these authors,

$$\Lambda^2 \text{ and } Q^2 = (k_\theta\rho_i s)^2\sigma \tag{4.26}$$

have been verified to asymptotically match ours when diamagnetic effects are neglected and the real, high q limit is taken [113]. Hence formulæ 4.23 and 4.24 provide simple tractable expressions, relevant to the high q limit.

At this point, we can already link our kinetic derivation to the fluid result of Eq. 4.1. In the absence of the 4th order term in Eq. 4.25, a resonant continuum mode (characterized by a discontinuity) can be excited if $\Lambda^2 > 0$, at the localization where $\Lambda^2 = (qR_0k_\parallel^{\mathsf{m}})^2$, and a gap exists for $\Lambda^2 < 0$. $\Lambda^2$ given in Eq. 4.23 is of the form 4.1 with the additional small order transit correction $\propto 1/q^2$, and hence allows for a gap below the accumulation point

$$\omega^2 < \omega^2_{\text{accumulation point}} \approx \omega_{BAE}^2\left[1 + \frac{1}{q^2}\frac{23/2 + 8\tau_e + 2\tau_e^2}{7/2 + 2\tau_e}\right] \tag{4.27}$$

$$\text{with } \omega_{BAE} = \left(\frac{v_{ti}}{R_0}\right)\sqrt{\frac{7}{2} + 2\tau_e} \tag{4.28}$$

When now fourth order terms are added, discontinuity at the origin of continuum damping disappears, and the separation between gap modes and continuum resonant modes looses significance. More precisely, we can say that small scale kinetic effects offer a continuous description of the boundary between gap modes and continuum resonant modes. Note that it is the same 4th order expansion which makes possible the existence KTAEs mentionned in subsection 2.2.2.

## 4.4 Dispersion relation and structure of the Beta Alfvén Eigenmode

As explained in subsection 4.2.2, Eq. 4.25 is only valid in a narrow *inertial* region around the mode main resonant surface, whereas *incompressible MHD-like terms* are expected to play a more important role away from this resonant surface.

We now determine the **solutions of Eq. 4.25 which can match the solutions of the incompressible ideal MHD region**, usually constrained by boundary conditions. For this, we use a classical matching procedure [13] from which we derive the **mode structure in real (radial) space**. As will be shown in the following for modes with a given parity, the asympotic behavior of the ideal MHD region close to a resonant surface depends on *two* coefficients only (note that the latter coefficients are not necessarily the mode amplitude and slope close to the resonant surface), which reduce the degrees of freedom offered by the inertial equation via asymptotic matching. More precisely, matching these *two* coefficients makes possible to display a *univocal* relation linking the mode frequency and wave numbers, the mode **dispersion relation**, derived below.

In the following, the focus is on the resolution of the inertial layer solution. For this reason, only a reduced model will be used of for the ideal incompressible region, which overlooks the geometry difficulties related to the treatment of broad mode structures. Nevertheless, the latter model is sufficient to describe a mode asymptotic structure close to a resonant surface, where strong radial gradients start to dominate (see Appendix D). Also, putting aside the details of radial profiles non uniformity along with our assumption of *symmetry of the poloidal components* Eq. 4.10, makes possible to assume eigenmodes to have a given (radial) parity in the surrounding of the resonant surface, which is convenient for a clearer presentation of the following presentation.

### Ideal incompressible solution

We explained in section 4.2.2 that MHD-like contributions can set up the larger scale of the mode. When $\rho_i k_r$ gets smaller, the poloidal wave number number $\rho_i k_\theta \sim \beta$ in the field line bending tension, or the interchange drive can set up the leading order. For this reason, we choose to keep these two terms in the ideal incompressible region. Vorticity (Eq. 3.62) reduces to

$$\nabla_\parallel \nabla_\perp^2 \nabla_\parallel \psi_\omega + \mathbf{b}_{(0)} \times \nabla \langle \beta \rangle \cdot \nabla_\perp \left( \mathbf{b}_{(0)} \times \boldsymbol{\kappa} \cdot \nabla_\perp \psi_\omega \right) = 0 \tag{4.29}$$

In order to avoid the lengthty character of a poloidal Fourier expansion, we solve this equation in the **ballooning representation, which makes possible a 1-D treatment** of this equation (instead of the traditional 2D treatment in the $(r, \theta)$ space). The basics of the ballooning formalism are presented in Appendix D. Following this Appendix, when the perpendicular gradients are much larger than the parallel gradients (which is the case for modes with a large toroidal mode numbers $\mathsf{n}$, or close to regions where radial gradients are strong), it is possible to transfom Eq. 3.62 into an equation which depends on one single

variable $\vartheta \in [-\infty, +\infty]$. $\vartheta$ is an extension of the geometrical poloidal angle $\theta$, regarded as a coordinate along the magnetic field, and the transformed field $\psi(\vartheta)$ can be understood as the Fourier transform of $\psi_\omega^{\mathsf{m}}(x/k_\theta s)$, where $\mathsf{m}$ is the main mode poloidal component we are focusing on, and the quantity $s$ is assessed at the mode resonant surface. In other words, $\psi(\vartheta) = \int_{-\infty}^{+\infty} |k_\theta s| dx\, \psi_\omega^m(x) e^{-ik_\theta s x}$.

Following Appendix D, the ballooning transformation in an equilibrium with circular flux surfaces, returns

$$\nabla_\parallel \rightarrow \frac{1}{qR_0}\partial_\vartheta \tag{4.30}$$

$$-\nabla_\perp^2 \rightarrow k_\perp^2 = k_\theta^2 + k_r^2 = k_\theta^2(1 + s^2\vartheta^2) \tag{4.31}$$

$$\mathbf{b}_{(0)} \times \boldsymbol{\kappa} \cdot \nabla_\perp \rightarrow \frac{-ik_\theta}{R_0}(\cos\vartheta + s\vartheta \sin\vartheta) \tag{4.32}$$

where again $s$ and $q$ are assessed at the localization of the $\mathsf{m}$ resonant surface. Finally, the ballooning representation of vorticity is

$$-\partial_\vartheta(1 + s^2\vartheta^2)\partial_\vartheta\psi - \alpha(\cos\vartheta + s\vartheta\sin\vartheta)\psi = 0 \tag{4.33}$$

where $\alpha = -q^2 R_0 \partial_r \beta$.

Using the additional transformation $\Psi = \sqrt{1 + s^2\vartheta^2}\,\psi$, vorticity finally takes a simpler form

$$-\partial_{\vartheta\vartheta}\Psi + \frac{s^2}{(1 + s^2\vartheta^2)^2}\Psi - \frac{\alpha}{1 + s^2\vartheta^2}(\cos\vartheta + s\vartheta\sin\vartheta)\Psi = 0 \tag{4.34}$$

The form of Eq. 4.34 is obviously the same as the one of Eq. 2.61 and it can be understood as a Schrödinger potential well.

Since, we now really want to determine the mode structure and an univocal dispersion relation, we now go a little bit further than what was done in Eq. 3.16, and display the mode **asymptotic behavior** close the mode resonant surface, which corresponds to large $\vartheta$ when working in the ballooning (/Fourier) space.

We can extract the non-periodic part of the solutions of Eq. 4.34 at large $\vartheta$ using solutions of the form $\vartheta^\delta$. It directly comes that the non-periodic large $\vartheta$ asymptotic behavior of a solution of Eq. 4.34 can be put in the form [115],

$$\Psi = \Psi_- + \Delta\Psi_+, \text{with} \quad \begin{array}{l} \Psi_- \sim \hat{\Psi}_0(\vartheta)|\vartheta|^{1/2-\nu} \text{ for large } \vartheta \\ \Psi_+ \sim \hat{\Psi}_0(\vartheta)|\vartheta|^{1/2+\nu} \end{array} \tag{4.35}$$

with $\nu = \sqrt{1/4 - \alpha/s^2}$, $\Delta$ a constant depending on boundary conditions, $\hat{\Psi}_0(\vartheta) = \Psi_0$ for even parity modes and $\hat{\Psi}_0(\vartheta) = \Psi_0 \mathrm{Sgn}(\vartheta)$ for odd parity modes.

When it is small, the $\Delta$ constant has a simple meaning. We already saw that we could access the MHD energy functional multiplying by the Schrödinger-like equation by $\Psi^*$ and integrating by parts. More precisely, we can write

$$\Psi^* \partial_\vartheta \Psi = \delta W_{\mathrm{MHD}}^{bal}(\Psi) \tag{4.36}$$

for modes with a given parity, with $\delta W_{\mathrm{MHD}}^{bal}$ the ideal MHD energy potential relevant to the ballooning representation. Using that $\psi(\vartheta)$ is the Fourier transform of $\psi_\omega^{\mathsf{m}}(x/k_\theta s)$ along with Parceval identity, it is easy to see that $\delta W_{\mathrm{MHD}}^{bal}$ related to the traditional MHD energy potential by

$$\delta W_{\mathrm{MHD}}^{bal} = \frac{|k_\theta s|}{2\pi R_0 r_s}\frac{1}{\rho_i^2 k_\theta^2}\frac{T_i}{ne^2}\frac{\omega^2}{\omega_A^2}\delta W_{\mathrm{MHD}} \tag{4.37}$$

So, to the first order, Eq. 4.36 returns [2]

$$\Delta = \delta W^{bal}_{MHD}(\Psi_-)/|\Psi_0|^2 \equiv \delta\hat{W}_{\rm MHD}/|s| \tag{4.38}$$

From now on, we assume that $\Delta$ is small [3], and that the same is true for $\alpha/s^2$, in agreement with the ordering of subsection 4.2.2. It follows that $\nu \sim 1/2$, and $\Psi_- \sim \hat{\Psi}_0$ at large $\theta$. Making such a substitution is equivalent to the "constant-$\Psi$" approximation used in Ref. [35], and allows a first estimate of $\delta\hat{W}$ of the form

$$\delta\hat{W}_{\rm MHD} = \int_0^\infty d\vartheta \left[\frac{s^2}{(1+s^2\vartheta^2)^2} - \frac{\alpha(\cos\vartheta + s\vartheta\sin\vartheta)}{(1+s^2\vartheta^2)}\right] \tag{4.39}$$

Finally, coming back to $\psi$, the *large* $\vartheta$ behavior of the ideal incompressible MHD part is

$$\psi(\theta) \sim \frac{\hat{\Psi}_0(\vartheta)}{s}\left(\frac{1}{|\vartheta|} + \frac{\delta\hat{W}_{\rm MHD}}{|s|}\right). \tag{4.40}$$

We can directly deduce the small $x$ behavior of the ideal solution close to the resonant surface, taking the inverse Fourier transform as in Ref. [116, 115].

For modes with the **tearing parity** (odd $\psi$), the ideal small $x$ behavior is

$$\psi^{\mathsf{m}}_\omega(x) \sim i\frac{\Psi_0}{2s}{\rm Sgn}(x)\left(1 + \frac{2}{\pi}\frac{\delta\hat{W}_{\rm MHD}}{|s|}\frac{1}{|k_\theta s||x|}\right) \tag{4.41}$$

For modes with the **twisting parity** (even $\psi$), it comes

$$\psi^{\mathsf{m}}_\omega(x) \sim \frac{\Psi_0}{s}\left(\frac{\delta\hat{W}_{\rm MHD}}{|s|}\frac{\delta(x)}{|k_\theta s|} - \frac{1}{\pi}\ln|x|\right) \tag{4.42}$$

There now need to verify if and under what condition solutions of the inertial layer can smoothly connect to the MHD solution.

### Solutions of the inertial region and asymptotic matching

We restrict the resolution of the inertial equation 4.25 to the case $\sigma \geq 0$, or equivalently $Q^2 \geq 0$. This is a reasonable assumption for usual conditions, and frequencies of the order of the accumulation point ($\sigma(\omega_{BAE}) > 0$ for $\tau_e > 5.45$).

Expanding as usual $k_\parallel$ close to the resonant surface, $k_\parallel = -k_\theta s x/qR_0$, the inertial layer eigenmode equation can be written in a simplified Weber-like form

$$\partial_{\bar{x}}\left(-\bar{x}^2 - a + \frac{1}{4}\partial_{\bar{x}\bar{x}}\right)\partial_{\bar{x}}\psi^{\mathsf{m}}_\omega = \frac{C}{k_\theta^2 s^2} = C_\infty \tag{4.43}$$

where $a = -\Lambda^2/2\sqrt{Q}$ and $\bar{x} = x/L_I$, with $L_I$ a **typical size of the inertial region**,

$$L_I = \sqrt{2Q}/|k_\theta s|. \tag{4.44}$$

[2] We define here a *normalized* MHD energy which is independent from the mode amplitude, $\delta\hat{W}_{\rm MHD}$. We introduce $|s|$ simply to recover the normalization of Ref. [16]

[3] This assumption is consistent with our earlier assumption of closeness to the BAE accumulation point $\Lambda \to 0$ because of the matching of Eq. 3.16

For modes with the *tearing* parity, $C_\infty = 0$. Eq. (4.43) becomes $\left(-\bar{x}^2 - a + \frac{1}{4}\partial_{\bar{x}\bar{x}}\right)\partial_{\bar{x}}\psi_\omega^{\mathsf{m}} = C'_\infty$. For $a > -1/2$, it has a unique explicit solution for $\partial_{\bar{x}}\psi_\omega^{\mathsf{m}}$ which cancels at infinity (in agreement with the requested asymptotic behavior of the ideal solution)

$$\partial_{\bar{x}}\psi_\omega^{\mathsf{m}} = -C'_\infty \int_0^1 dt(1-t)^{-\frac{3}{4}+\frac{a}{2}}(1+t)^{-\frac{3}{4}-\frac{a}{2}}e^{-t\bar{x}^2} \tag{4.45}$$

and this solution has the following large $\bar{x}$ asymptotic behavior,

$$\begin{aligned}
\psi_\omega^{\mathsf{m}}(\bar{x}) &\sim \mathrm{Sgn}(\bar{x})\left(\frac{C'_\infty}{|\bar{x}|} + \int_0^\infty \partial_{\bar{x}}\psi_\omega^{\mathsf{m}}\right) \\
&= C'_\infty \mathrm{Sgn}(\bar{x})\left(\frac{1}{|\bar{x}|} - \frac{\sqrt{\pi}}{2}\int_0^1 dt\ (1-t)^{-\frac{3}{4}+\frac{a}{2}}(1+t)^{-\frac{3}{4}-\frac{a}{2}}t^{-\frac{1}{2}}\right) \\
&= C'_\infty \mathrm{Sgn}(\bar{x})\left(\frac{1}{|\bar{x}|} - \frac{\pi}{2\sqrt{2}}\frac{\Gamma(\frac{1}{4}+\frac{a}{2})}{\Gamma(\frac{3}{4}+\frac{a}{2})}\right)
\end{aligned} \tag{4.46}$$

It can be matched to the asymptotic behaviors of the ideal region taking the dispersion relation

$$-2\sqrt{Q}\frac{\Gamma(\frac{3}{4}-\frac{\Lambda^2}{4Q})}{\Gamma(\frac{1}{4}-\frac{\Lambda^2}{4Q})} = \frac{\delta\hat{W}_{\mathrm{MHD}}}{|s|}. \tag{4.47}$$

Similarly, an explicit form of the inertial solution can be found for the even parity modes. For $a > -3/2$, the unique even solution which cancels at infinity is

$$\partial_{\bar{x}}\psi_\omega^{\mathsf{m}} = -C_\infty \bar{x}\int_0^1 dt(1-t)^{-\frac{1}{4}+\frac{a}{2}}(1+t)^{-\frac{1}{4}-\frac{a}{2}}e^{-t\bar{x}^2} \tag{4.48}$$

and we want to match this solution to the ideal MHD region. We first note from the eigenmode equation (4.43) considered in the large $\bar{x}$ region, that the dominant large $\bar{x}$ behavior of $\partial_{\bar{x}}\psi_\omega^m$ is equal to $-C_\infty/\bar{x}$, announcing the logarithm behavior of $\psi_\omega^{\mathsf{m}} \sim -C_\infty \ln|\bar{x}|$, and leading to a first matching condition to the ideal solution

$$C_\infty = \frac{\Psi_0}{\pi s} \tag{4.49}$$

To recover the relevant coefficient corresponding to the ideal $\delta$-function behavior and hence obtain a second matching condition, we first notice that the ideal behavior can be rewritten $\psi_\omega^{\mathsf{m}}(\bar{x}) + C_\infty \ln|\bar{x}| \sim (C_\infty \pi\delta\hat{W}_{\mathrm{MHD}}/(|s|\sqrt{2Q}))\ \delta(x)$. The corresponding matching condition is

$$\int_{-\infty}^{+\infty} d\bar{x}\ (\psi_\omega^{\mathsf{m}} + C_\infty \ln|\bar{x}|\ ) = \frac{C_\infty \pi}{\sqrt{2Q}}\frac{\delta\hat{W}_{\mathrm{MHD}}}{|s|} \tag{4.50}$$

After integration by parts and under the assumption that $a > 1/2$, the right hand side becomes
$-\int_{-\infty}^{+\infty}(\bar{x}\partial_{\bar{x}}\psi_\omega^{\mathsf{m}} + C_\infty)\ d\bar{x}$

$$\begin{aligned}
&= -C_\infty \int_{-\infty}^{+\infty} d\bar{x}\int_0^1 dt(1-t)^{-\frac{5}{4}+\frac{a}{2}}(1+t)^{-\frac{5}{4}-\frac{a}{2}}\left[(-\frac{1}{4}+\frac{a}{2})(1+t) + (\frac{1}{4}+\frac{a}{2})(1-t)\right] \\
&= -C_\infty \frac{\pi}{\sqrt{2}}\left[(-\frac{1}{4}+\frac{a}{2})\frac{\Gamma(-\frac{1}{4}+\frac{a}{2})}{\Gamma(\frac{1}{4}+\frac{a}{2})} + (\frac{1}{4}+\frac{a}{2})\frac{\Gamma(\frac{3}{4}+\frac{a}{2})}{\Gamma(\frac{5}{4}+\frac{a}{2})}\right] = -C_\infty\sqrt{2}\pi\frac{\Gamma(\frac{3}{4}+\frac{a}{2})}{\Gamma(\frac{1}{4}+\frac{a}{2})}
\end{aligned} \tag{4.51}$$

This leads to the exact same dispersion relation as found for the tearing parity, ie Eq. (4.47).

We finally arrived at the same dispersion relation found in Ref. [41] in the ballooning representation, and we recovered the equivalence between even and odd parity modes, discovered for a large class of asymptotic problems using the Fourier transformation [115]. In addition, this derivation produces an image of the BAE radial structure in real space, and shows how high radial gradients, characterizing the inertial region, can connect to lower gradients of the incompressible ideal MHD region, when the accumulation point is approached. An illustration of such a structure is given in Fig. 4.2 for the twisting parity. A similar two-scale structure could be displayed for the tearing parity, with a **step like**-shape, as suggested by the *constant* asymptotic behaviors in the ideal region in Eq. 4.41.

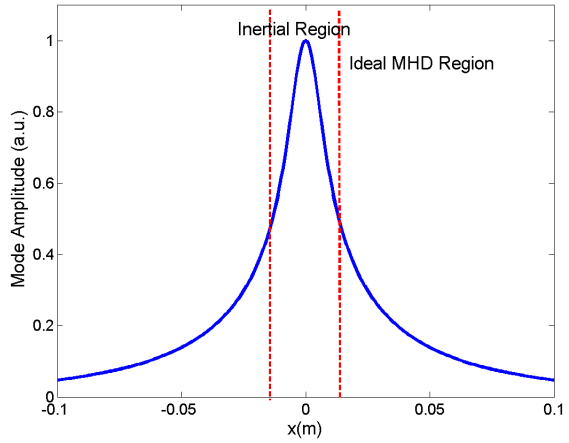


Figure 4.2: Typical scales of the mode radial structure for the twisting parity. The curve is a numerical solution of the equation $\partial_{\bar{x}}\left(-\bar{x}^2 - a + \frac{1}{4}\partial_{\bar{x}\bar{x}}\right)\partial_{\bar{x}}\psi_\omega^{\mathrm{m}} = (\sqrt{2|Q|}/s)^2\ \bar{x}^2\psi + (\alpha/s^2)\psi$ where the contributions of both the inertial region and the ideal region have been kept. The parameters used are $\beta = 2\%$, $\alpha/s^2 = 0.5$ and $\sqrt{2|Q|}/s \sim (\rho_i k_\theta)^{3/4} \sim \beta^{3/4}$.

### 4.4.1 Discussion

*∼ Structure of the Alfvén Spectrum ∼*

From the form of the BAE dispersion relation Eq. 4.47, we can make some comments on the role of 4th order kinetic terms on the structure of the Alfvén spectrum.

First, as was pointed out in Ref. [41], when $\Lambda^2$ is sent to $+\infty$ in the BAE dispersion relation 4.47, the fluid case given in Eq. 3.16 is recovered,

$$i|s|\Lambda = \delta\hat{W}_{\mathrm{MHD}} \tag{4.52}$$

(and we now have a clean definition of the constants of proportionality used before).

When now $\Lambda^2 \to 0$, then $\delta\hat{W}_{\mathrm{MHD}} \to 0$ and higher order FLR come into play. In particular, for a very small $\delta\hat{W}_{\mathrm{MHD}}$, the dispersion relation Eq. 4.47 can be expanded and returns the solutions

$$\Lambda^2 = (4l+1)Q + (2/\pi)\sqrt{Q}\ [(\Gamma(l+1/2)/\Gamma(l+1))\delta\hat{W}_{\mathrm{MHD}}/|s|\ ]\ , \tag{4.53}$$

with $l$ a positive integer [41], at the origin of an infinite number of discrete solutions for the mode frequency $\omega$. Hence, the image of a separation between a discrete spectrum of

*undamped* modes below the accumulation point ($\approx \omega_{BAE}$), and a continuum spectrum of *damped* modes above this point, is replaced by a continuous description of the frequency spectrum, where an infinite number of discrete *undamped* solutions exist. What we found in this calculation (for $Q^2 \geq 0$) is that high order FLR enforce a *finite* (small) size for the structures, such that radial discontinuity (and the correlated damping) are no longer relevant. In other words, the mode is localized in the Fourier $\vartheta$ space, and solution spectrum is consequently discrete. Higher order FLR are said to **discretize the continuum**.

In particular, for $l = 0$ and $\delta\hat{W}_{\text{MHD}} = 0$, the solution is approximately $\omega^2 \approx \omega_{BAE}^2 + \omega_A^2 \rho_i |k_\theta s| \sqrt{\sigma(\omega_{BAE})}$. This can also be rewritten $\omega^2 = \omega_{BAE}^2 + k_\parallel^2 v_A^2$ with $k_\parallel$ assessed at the typical mode extent enforced by high order FLR and given in Eq. 4.44, such that the local coupling of the continuum shear Alfvén type wave with compressibility appears.

$\sim$ *Around the causality constraint* $\sim$
We explained in subsection 3.1.2 that the sign of a wave energy density could be a difficult issue, and often required the use of an additional *constraint* (a localization constraint, or an equivalent localization constraint...). In particular, for gap modes expected to oscillate with a frequency *below* the continuous Alfvén spectrum and with a generalized inertia of the form $\Lambda^2 \propto \omega^2 - \omega_0^2$, we saw that causality implied $\text{Sgn}(\delta W_f + \delta W_k) = \text{Sgn}(\delta\hat{W}_{\text{MHD}}) < 0$, in agreement with the fact that $\delta\hat{W}_{\text{MHD}}$ was to be associated with the mode slope at the frontier between ideal and inertial regions, as was shown in Fig. 3.1. Neglecting transit terms, the BAE inertia clearly enters this category, and (undamped) gap modes are consequently expected to verify $\text{Sgn}(\delta\hat{W}_{\text{MHD}}) < 0$.

Recalling that $\delta\hat{W}_{\text{MHD}}$ defined here is incompressible (compressibility has been moved to the generalized inertia), a way to understand the causality constraint, is to rewrite the full (normalized) MHD energy, $\delta W_{\text{MHD}}^{full} = \delta\hat{W}_{\text{MHD}} + \delta W_{\text{compressible}}$, where we know $\delta W_{\text{compressible}} > 0$. It follows that

- MHD unstable modes verify $\delta W_{\text{MHD}}^{full} < 0$
- MHD gap modes occur for $0 \leq \delta W_{\text{MHD}}^{full} \leq \delta W_{\text{compressible}}$

and the role of **compressibility clearly appears to be stabilizing for MHD type instabilities, but destabilizing from the point of view of continuum damping**.

In this derivation however, we displayed undamped modes with a positive $\delta\hat{W}_{\text{MHD}}$ (the odd solutions provided above have a validity range which extends to $a > -3/2$ and allows for a positive $\delta\hat{W}_{\text{MHD}}$ in Eq. 4.47. This is due to high order FLR. However, these effects do not completely modify the previous picture. $\delta\hat{W}_{\text{MHD}}$ can still be associated with the mode slope at the junction between the inertial and ideal MHD regions. However, now, inertia itself can enforce localization, as illustrated in Fig. 4.3.

## 4.5 The degeneracy of Beta Alfvén Eigenmodes and Geodesic Acoustic Modes

We explained in the introduction of this chapter that a reason for the complexity of the acoustic range is the variety of modes and mode names which have been attributed to acoustic oscillations. We compare in this section the well known GAMs with BAEs, where again GAMs are acoustic oscillations with a main $\mathsf{m} = 0, \mathsf{n} = 0$ component, which corresponds to usual case treated in transport theories. More precisely, it is possible to display an **electrostatic** acoustic solution of our equations, with a main $\mathsf{m} = 0, \mathsf{n} = 0$ component. Our following comparison will have to be understood as a comparison between **electrostatic**

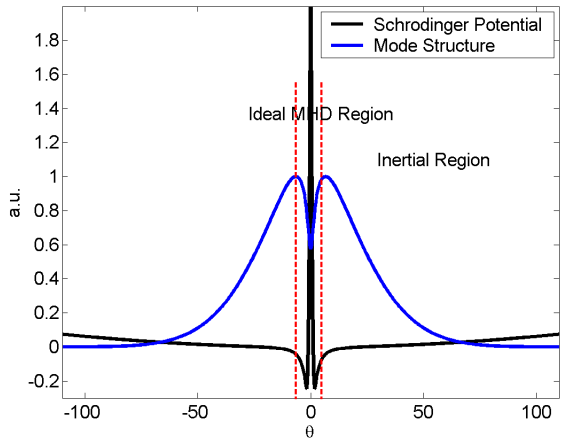


Figure 4.3: Schematic of the Fourier space localizing Schrödinger-like well and structure of a BAE close to the BAE accumulation point, for the twisting parity.
The effect of high order Finite Larmor Radius is to enforce the localization condition in Fourier space, or in other words to set-up a finite small radial scale. Thanks to high order FLR, localization is possible even if the slope of the mode at the boundary between the inertial and MHD regions is not negative.

**GAMs taken in the electrostatic limit and BAEs**. Hence, if not otherwise noted, the word GAM will have to be understood in the electrostatic limit.

We show how the **degeneracy of the BAE and GAM dispersion relations**, claimed in Ref. [113], can be understood in the light of our formalism. Even if the difference between GAMs and BAEs may be thought to be small (it is simply a difference in mode numbers), the idea of a degeneracy is not so trivial, because a change in mode numbers modifies the response of the electrons in the wave frame. In particular, for our derivation of BAEs, we used the time scaling

$$k_{\|} v_{ti} \ll \omega \ll k_{\|} v_{te} \tag{4.54}$$

(where $k_{\|}$ is understood as an operator and stands for any of the poloidal components), which leads to an *adiabatic* electron response and a *hydrodynamic* ion response. Electron adiabaticity can obviously not hold for $\mathsf{m} = 0, \mathsf{n} = 0$.

Such a degeneracy can have important implications. As will be clearer in the next chapter, mode excitation by fast particles is easier for modes with finite $(\mathsf{n}, \mathsf{m})$ than for $(\mathsf{n} = 0, \mathsf{m} = 0)$ modes. If the BAE/GAM degeneracy is verified, then we could expect wave-wave coupling to lead to an excitation of GAMs, which are well known to have an impact on turbulent transport.

### 4.5.1 The BAE/GAM degeneracy

#### Basis of the BAE/GAM degeneracy

We start our analysis with Eq. 4.6, which applies for both GAMs and BAEs.

As follows from the preliminary comments, a major difference between BAEs and GAMs is the electron response to the main $\mathsf{m} = 0, \mathsf{n} = 0$ field component.

For GAMs in the electrostatic limit, the electron adiabatic response, ie. the term proportional to $(1/\tau_e)|\tilde{\mathcal{E}}^{\mathsf{m}}_{\omega}|^2$ in Eq. 4.6, is balanced by the last term of Eq. 4.6, when the latter is calculated for $\omega \gg \mathbf{n}^* \cdot \mathbf{\Omega}_e$. Consequently, the **total electron response cancels**.

Inversely, for BAEs, we assumed the electron response to be fully adiabatic, such that the $(1/\tau_e)|\mathcal{E}^{\mathsf{m}}_\omega|$ term should *a priori* be conserved. However, electron adiabaticity ($\omega \ll k_\parallel v_{te}$) exactly means that electrons respond very *fast* to the perturbation in the parallel wave frame (ie. following the wave phase velocity in the parallel direction), and can cancel parallel charge separation and the correlated parallel electric field, $E_\parallel = 0$. Consistently, we found from our derivations of BAEs that $\mathcal{E}^{\mathsf{m}}_\omega = 0$, such that the electron reponse is null in the functional Eq. 4.6.

So finally, the difficulty for the electron response disappears.

From a more formal point of view, we found that the BAE problem could be reduced to the determination of three fields, $\psi^{\mathsf{m}}_\omega, \mathcal{E}^{\mathsf{m}+1}_\omega$ and $\mathcal{E}^{\mathsf{m}+2}_\omega$, instead of 6. The same is true for electrostatic GAMs, for which it is necessary to determine the three components of $\phi_\omega = -\mathcal{E}_\omega$. Using the approximations of section 4.2 (without any necessity to relate small parameters to $\beta$ since the field line bending tension now cancels for the main mode), the development of the GAM functional exactly returns Eq. 4.13 with the following substitution

$$\phi^{\mathsf{m}+1/\mathsf{m}+2}_{\omega,\mathsf{GAM}} = -\mathcal{E}^{\mathsf{m}+1/\mathsf{m}+2}_{\omega,\mathsf{BAE}}, \qquad \phi^{\mathsf{m}}_{\omega,\mathsf{GAM}} = \psi^{\mathsf{m}}_{\omega,\mathsf{BAE}}, \tag{4.55}$$

It follows that the inertial BAE Lagrangian given in Eq. 4.22 and the characteristic equation 4.25 hold for GAMs as well, **to the 4th order in** $\rho_i k_r$.

In this sense, we observe a degeneracy of the BAE and GAM modes. It does not mean however that the two modes have the exact same eigenfunctions. In particular, for GAMs, $k^{\mathsf{m}}_\parallel = 0$ in Eq. 4.25. The field line bending and interchange ($k_\theta = 0$) terms do not enforce the existence of a larger radial scale where $(\rho_i k_r)^2$ terms become negligible, as it is the case for BAEs. Hence, if is makes sense to neglect equilibrium profiles radial variations (as we have done until now), there is no need to distinguish two regions.

Finally, we obtained that **the BAE/GAMdegeneracy is verified at the local points where** $k^{\mathsf{m}}_{\parallel,\mathsf{BAE}} = 0$**, in the case where diamagnetic effects are negligible.**

### Limits of the BAE/GAM degeneracy

In order to capture the full extent of the BAE/GAM degeneracy, we may come back to some of our assumptions to see which one may be considered weaker.

**Diamagnetic effects** $\propto \mathsf{n}$ will clearly not have the same effects on GAMs and BAEs. However, in the range of parameters depicted here, their removal has been justified. Weaker assumptions may be the **electron adiabaticity** or the **GAM electrostatic feature**. In particular, we took electrostaticity as a starting point. Since Eq. 4.25 has solutions for $\mathsf{n} = 0, \mathsf{m} = 0$, the electrostatic limit is not incorrect. However, we did not prove that electromagnetic fluctuations are impossible for GAMs (in the general sense).

One of the basis of the BAE/GAM degeneracy derived above is the possibility to reduce the problem to the description of three poloidal components only. The cancellation of $\psi^{\mathsf{m}+1/\mathsf{m}+2}_\omega$ is reasonable and weakly depends on the main mode numbers. Indeed, it comes from Eq. C.5 of the Appendices, that the cancellation of an $\mathsf{m}_i$ ($i \in (\mathsf{m}, \mathsf{m}+1, \mathsf{m}+2)$) magnetic fluctuation is valid when $qR_0 k^{\mathsf{m}_i}_\parallel/\beta$ is large . Since $qR_0 k^{\mathsf{m}_i}_\parallel \approx \pm 1$ or $\pm 2$, regardless on the main mode poloidal component, it is reasonable to take $\psi^{\mathsf{m}+1,\mathsf{m}+2}_\omega = 0$.

Consequently, four fields remain

$$\psi^{\mathsf{m}}_\omega, \mathcal{E}^{\mathsf{m}}_\omega, \mathcal{E}^{\mathsf{m}+1}_\omega, \mathcal{E}^{\mathsf{m}+2}_\omega, \tag{4.56}$$

and our model for BAEs considers $\mathcal{E}^{\mathsf{m}}_\omega = 0$, whereas GAM electrostaticity leads to $\psi^{\mathsf{m}}_\omega = 0$. What we verified, is that the cancellation of one of these two components leads to same final

dispersion equation.

However, these cancellations can break.

- $\mathcal{E}^{\mathsf{m}}_{\omega} = 0$ relies on the fast (massless) response of the electrons (see Eq. C.5), to the $\mathsf{m} = 0, \mathsf{n} = 0$ fields. This cannot hold for GAMs (in the opposite). For BAEs, it may also be questioned because electron adiabaticity cannot really be considered to any order, in particular close to a resonant surface. **Electron inertia** may lead to some corrections of the BAE dispersion relation which do not behave the same way for (n=0,m=0) modes and for finite $\mathsf{n}$ modes. These ideas have been developed in Ref. [117].

- $\psi^{\mathsf{m}}_{\omega} = 0$ relies on the importance of $qR_0 k^{\mathsf{m}}_{\parallel}/\beta$ which is not verified for an $(\mathsf{n} = 0, \mathsf{m} = 0)$ component. It means that the electrostaticity of GAMs is not enforced.

Electromagnetic GAMs were found in JET experiments described in Ref. [109]. To the extent of our analysis, there is no garanty that they may have the same dispersion as the one we derived for BAEs. In Ref. [109] however, the classical MHD BAE dispersion relation was used, and we already said that it was in agreement with our calculation. The reason for this agreement is simply that the authors of this article started from an MHD formalism... hence with $\mathcal{E}^{\mathsf{m}}_{\omega} = 0$ assumed *a priori*.

### 4.5.2 The GAM eigenmodes

We already discussed the locality of the BAE/GAM degeneracy. In particular, the GAM eigenmodes do not need to be the same as the one we described above. The GAM charateristic equation 4.25 can be rewritten $(\Lambda^2 \rho_i^2 \nabla_x^2 + \sigma \rho_i^4 \nabla_x^4)\psi^{\mathsf{m}}_{\omega} = 0$, which simply leads to a wave-like solution

$$\omega^2 \approx \omega^2_{BAE} + \omega^2_A \sigma(\omega_{BAE}) \rho_i^2 k_r^2 \tag{4.57}$$

characterized by the group velocity

$$v_{gr} = \frac{\partial \omega}{\partial k_r} = \frac{T_i}{eBR}\sqrt{\frac{7}{2} + 2\tau_e}\frac{\omega^2_A}{\omega^2_{BAE}}\sigma(\omega_{BAE})\rho_i k_r \tag{4.58}$$

In general standard conditions (for which $\sigma(\omega_{BAE}) \geq 0$), this means an outward propagation, but it is interesting to note that a change of sign of $\sigma(\omega_{BAE}) \geq 0$ is *a priori* not impossible for special conditions.

So, contrary to BAEs, GAMs are not localized to our order of approximation. In reality, a radial shearing effect similar to the one described in section 2.2.2 can take place (leading in particular to conversion to kinetic waves), if the radial variation of equilibrium profiles is not neglected. In this case, the continuous spectrum is simply $\Lambda^2 = 0$, or $\omega^2 = \omega^2_{BAE}(r)$ and similarly as for usual gap modes with a main $\mathsf{m}$ poloidal component, localization is possible where $(\omega^2_{BAE})' = 0$ [109, 113].

### 4.5.3 Distinguishing BAEs from GAMs

If we are to believe the BAE/GAM degeneracy, distinguishing them based on their oscillation frequency may be an issue, since both modes eigenfrequencies are expected be dominated by $\omega_{BAE}$ whereas the distinguishing corrections $k_r$, $\delta\hat{W}_{\mathrm{MHD}}$ are experimentally subject to strong errorbars.

Hence, instead of considering their frequency to distinguish BAEs and GAMs, it is more relevant to look at their **structure**.

With our definitions, the main difference between BAEs and GAMs is their toroidal mode number, but unfortunately the latter cannot be accessed in Tore-Supra, as explained in section 2.3.2.

The radial structure of the BAEs and GAMs also differs. We showed in this paper that BAEs are radially localized, whereas GAMs tend to have a wave structure. This property of the GAMs, which we found here in the electrostatic limit, is intrisically linked to the cancellation of the field line bending term, and could consequently be relevant for GAMs with a magnetic component. It makes sense as long as equilibrium profiles do not present a localizing extremum.

Finally, we explained that the chosen symmetry Eq. 4.10 was relevant to the acoustic frequency range, when the shear is limited. It indicates that both the structure of electrostatic GAMs and the *inertial* structure of BAEs are characterized by a poloidal symmetry $\psi_\omega \approx \psi_\omega^{\mathsf{m}} + 2i\psi_\omega^{\mathsf{m}+1}\sin\theta...$, and this property was also found to be relevant to GAMs with electromagnetic fluctuations (in Ref. [114]). For BAEs however, this symmetry does no longer hold in the MHD ideal region, where interchange starts being effective and implies a coupling to the $\cos\theta$ parity. A consequence of this difference in poloidal polarization is that the observation of fluctuations in the torus equatorial plane (where $\theta = 0$) can only be caused by BAEs, which are sensitive to diamagnetic or interchange terms, in particular in the ideal MHD region.

## 4.6 Identification of acoustic modes observed in Tore-Supra

Our previous analysis makes possible the analysis of the acoustic oscillations measured in Tore-Supra.

### 4.6.1 Characteristics of Tore-Supra acoustic modes

First acoustic fluctuations of the density [88, 118] and the temperature [87] were performed in 2005. During the PhD work, new experiments were conducted which will be reported on in this thesis.

Tore-Supra modes have been observed in the presence of ICRH Heating in the hydrogen minority heating scheme (see section 2.3.1), in various equilibrium conditions. Typical observation conditions were for a central toroidal field $B_0 \in [2.8, 3.8]$ T, a central density $n_0 \in$ [4.8e19, 5.5e19] $\mathrm{m}^{-3}$, a hydrogen minority fraction $f_{min}$ (fraction of the hydrogen density to the main ion density, deuterium) $\in [3, 10]$ %, and an ICRH power $P_{ICRH} \in [1.5, 5.0]$ MW.

We represented in Fig. 4.4 a typical observation performed with X-mode reflectometry, in *mode 2* (see section 2.3.2) using 15ms windows for each radius. We also represented in this set of figures the central temperature $T_0$ which is subject to a series of crashes and relaxations, called **sawtooth oscillations**. Sawtooth oscillations are well known macroscopic tokamak **MHD oscillations** which systematically occur in Tore-Supra standard dicharges (in the presence of ICRH power or not) on which we will be spending some more time in the next chapter. As will be shown, the stability of BAEs has been observed to depend on the sawtooth dynamics, which calls for some caution when describing the modes.

With the parameters given above, Tore-Supra modes have been found to belong to the frequency range [45, 65] kHz, in agreement with the **acoustic frequency** $\propto v_{ti}/R_0$, as illustrated in the left hand side of Fig. 4.4.

Shot #41925: $B_0 = 3.80T$, $n_0 = 5.04e19m^{-3}$, $I_p = 0.95MA$, $P_{LH} = 0.0MW$, $P_{ICRH} = 3.9MW$, $f_{min} = 4.8\%$

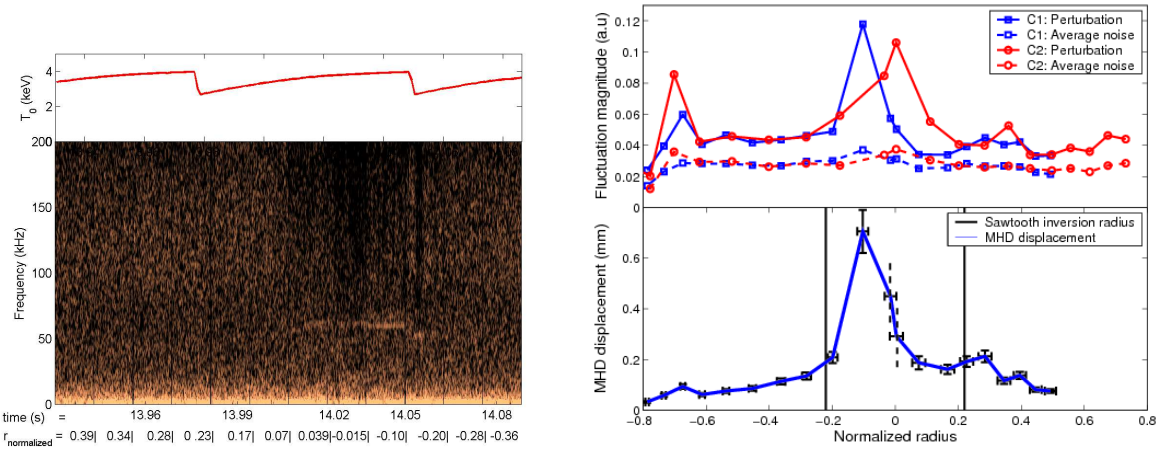


Figure 4.4: In the left hand side figure, the time spectrum of density oscillations has been plotted, for the different radii successively targetted by the reflectometer. -/+ are used to distinguish high field side radii from low field side radii.
In the right hand side figure, the mode radial structure is obtained from the determination of the maximum density fluctuation level measured at each radius, in the acoustic frequency range. The picked maximum acoustic fluctuations (*full lines*) and average ambient fluctuation level (*dotted lines*) are obtained from two reflectometry channels, C1 (*squares*) and C2 (*circles*). The MHD displacement corresponding to the fluctuations given by C1 is derived using Eq. 2.71. Horizontal error-bars correspond to a reflectometer in X-mode. Unbounded vertical errorbars indicate a prohibitive uncertainty at the plasma center.

A typical mode structure, derived from the measure of the acoustic fluctuation level is represented on the right of Fig. 4.4, as a function of the normalized radius $r/a$, where $a$ is the plasma radius.

In order to get rid of the role of the sawtooth dynamics (which can be expected to play a role in the mode amplitude), two channels of the reflectometer have been used, targetting different radii at different times. The main features of the observed are well illustrated by the figure: a **macroscopic scale of several centimeters** (in general 1 to 15cm), **a central localization bounded by the** $q = 1$ **surface** (identified in these figures by the sawtooth inversion radius) and **a relatively low amplitude** (with an estimated maximum MHD displacement of the order of one millimeter) even for large ICRH power input ($P_{ICRH} = 3.9$MW in shot #41925). In several shots, we could find some indications that the mode fluctuations were stronger in the torus high field side, but this was not a systematic observation.

### 4.6.2 Identification

#### Analysis of the frequency spectrum

Let us now examine the **mode frequency spectrum**. Our orderings for the acoustic frequency range apply well to Tore-Supra, and it is consequently reasonable to expect diamagnetic effects to play a minor role. Hence, it makes sense to postulate that the measured fluctuations are of the BAE/GAM type. To make this verification, we plotted in Fig. 4.5 the experimental frequency spectrum as a function of the dominant contribution to the BAE/GAM frequency, $\omega_{BAE}$ (Eq. 4.28), using the (ECE) experimental measure of $T_e$ and the assumption that $T_i = 0.8T_e$. The latter assumption, verified for shot #42039 (a reference shot for our subsequent analysis) using the CRONOS transport code [65] (which returned $T_i = 0.82T_e$ for this shot), is reasonable in Tore-Supra for the densities covered in these experiments (ie, *large* densities, which allow sufficient collisions between electrons and ions

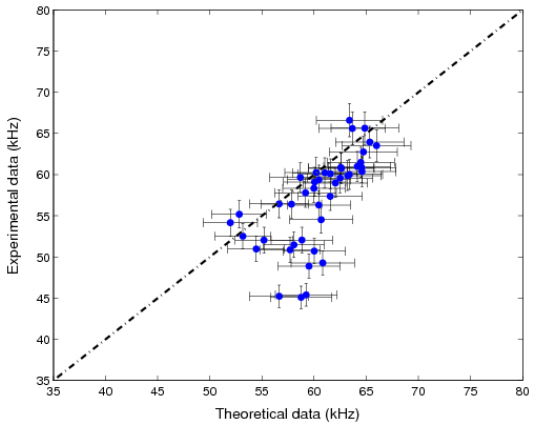


Figure 4.5: Comparison of $\omega_{BAE}$ with the experimental frequencies (averaged over 10ms windows, to avoid the details of the mode frequency evolution faster than the temperature relaxation time) between 40kHz and 80kHz and exceeding a signal/noise value of 3., for the full set of our experiments with $P_{LH} = 0$. Horizontal errorbars correspond to an assumed 30% error on the value of $T_e/T_i$.

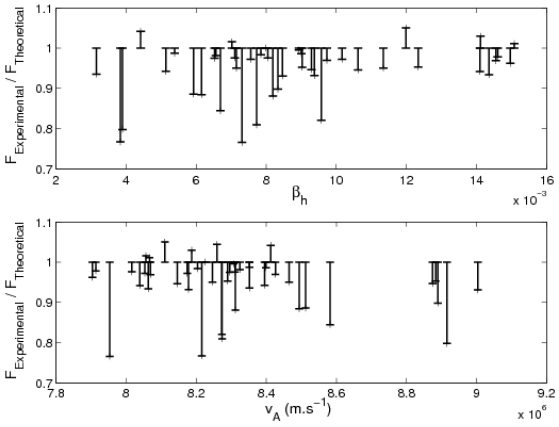


Figure 4.6: Distance of experimental points to $\omega_{BAE}$ as a function of the Alfvén velocity $v_A$, and the estimated normalized fast ion pressure $\beta_h$.

to allow $T_i$ to be no too far from $T_e$). What this shows, is that **ions are not cold in our experiments**. More precisely, an average over 10ms windows of the spectrum and values of $\omega_{BAE}$ has been used to avoid the details of the sawtooth dynamics (which could modify $\delta\hat{W}_{\mathrm{MHD}}$ in the BAE dispersion relation), and simply portray the main tendencies of the modes frequency.

Fig. 4.5 shows a good agreement between the experimental data and $\omega_{BAE}$, with an error which does not exceed 10% in most cases and may be attributed to a 30% incertainty on the knowledge of $T_e/T_i$. In particular, the increase of the mode frequency with temperature is well reproduced. **This validates the assumption that the observed modes belong the BAE/GAM family**.

Note however that the fact that most experimental points are below $\omega_{BAE}$ (as was also found in [91] and [92]) may suggest the necessity to add some corrections to the BAE/GAM formula 4.28: Alfvénic [90], diamagnetic or finite Larmor radius corrections [92], or the effect of energetic particles [37] (entering the BAE dispersion relation in $\delta\hat{W}_{\mathrm{MHD}}$ for example). To investigate the role of such effects, the distance of the experimental points to $\omega_{BAE}$ is plotted in Fig. 4.6, as a function of the Alfvén velocity $v_A$, the normalized energetic ion pressure $\beta_h = 2\mu_0 n_h T_h/B_0^2$ (The estimate of $\beta_h$ used for this experimental work will be described more clearly in the next chapter.). No obvious contribution of $v_A$ or $\beta_h$ is unveiled by this analysis. In particular, it was shown in [37] that a new branch of the GAM family, called **Energetic Geodesic Acoustic Mode**, and characterized by a much lower frequency (of about half or a third of $\omega_{BAE}$) was reached for sufficiently high values of $\beta_h$. No such behaviour in discriminated in Fig. 4.6, and we can consequently exclude the possibility that the modes studied in here are purely energetic modes, similar to EGAMs.

### GAMs or BAEs?

There remains to distinguish between BAEs and GAMs. As explained earlier, the toroidal mode number of acoustic modes cannot be identified in Tore-Supra. However, following

section 4.5.3, we can find some clues indicating that the observed are BAEs rather than GAMs.

First, Tore-Supra reflectometry measurements are performed in the tokamak equatorial plane, where GAM fluctuations are expected to be negligible.

Secondly, in all the conducted shots, modes were found to be localized with a (possibly off-axis) maximum inside the $q = 1$ surface. This suggests a role of the rational $q$ surfaces (possibly resonant surface). Moreover, we know that GAM localization depends on the existence of an extremum of $\omega_{BAE}(r)$. Accordingly, in experiments showing GAMs with a global structure or simulations of GAMs , the existence of GAMs was related to either a non-monotic $q$ profile [109], or non-monotonic temperature profile [86]. Such non-standard conditions are not expected in our experiments, which correspond in most cases to discharges with on axis ICRH heating (and without any off-axis current drive).

Finally, as will be clearer in the next chapter, the excitation of an $\mathsf{n} = 0, \mathsf{m} = 0$) mode by energetic particles is a difficult process, and most experimental observations of GAMs with a global structure performed until now, required specific heating conditions (counter injection of Neutral Beam Ions [119] or high field ICRH heating [109]). In our experiments, the mode excitation did not require such constraining heating characteristics.

As a conclusion, **Tore-Supra acoustic modes are identified as BAEs.**

## 4.7 Summary

*In this chapter, we derived the dispersion relation and structure of Beta Alfvén Eigenmodes, in the absence of energetic particles, using a kinetic model for the plasma, which retained high order Finite Larmor Radius effects and low order transit effects, corresponding to the approximation $\omega \gg v_{ti}/qR_0$, but no diamagnetic effects.*

- *Our derivation of the* **BAE dispersion relation** *carried out using a decomposition of the mode structure onto its poloidal Fourier components returned the same dispersion relation as the one found in Ref. [77] using the ballooning formalism, if the latter is taken in the high q-limit, without diamagnetic effects.*

- *The calculation of the* **mode structure** *was carried out explicitely, displaying the mode two-scale radial structure, where one may distinguish an* **inertial region** *dominated by strong radial gradients and a* **smoother region corresponding to MHD scales**. *In particular, it allowed to determine the typical size of the inertial region (correctly assessed with the kinetic formalism) as well as the geometric constants of relevance, which enter the dispersion relation, both for modes with an even shape and modes with an odd shape around the mode inertial layer.*

- *Next, we compared Beta Alfvén Eigenmodes with Geodesic Acoustic Modes. We showed that the* **eigenmode equation of both modes is degenerate**, *because of a formal similarity between the electrostatic limit and the approximate cancellation the parallel electric field for BAEs, the so-called MHD property.*

- *As a consequence of the BAE/GAM degeneracy, the two modes are not easy to distinguish in Tore-Supra. Thus, we studied the features that can be analyzed in experiment for that purpose and concluded that* **the modes found in Tore-Supra are BAEs**.

*Let us now determine the effects of a fast particle population on the modes stability.*

*Les théories ont causé plus d'expériences que les expériences n'ont causé de théories.*

Joseph Joubert (1754-1824)

# 5

# Linear stability of Beta Alfvén Eigenmodes in the presence of energetic particles

Let us finally approach the problem of the role of energetic particles in the modification of the stability properties of a plasma. We already mentioned the possibility of introducing a contribution of the energetic particles in the mode dispersion relation to build up the **fishbone-like dispersion relation** in Eq. 2.64, where we essentially replaced the traditional $\delta W_{\mathrm{MHD}}$ of the MHD energy principle, by $\delta W_f + \delta W_k$, without much justification. It is tempting to make the same manipulation in the BAE dispersion relation Eq. 4.47 which obviously couples an inertial part and energy potential energy $\delta\hat{W}$. We already anticipated some modifications of the mode behavior involved by such an additional contribution in the previous chapters, such as the destabilization of MHD modes by the energetic particles, as well as the emergence of new modes (such as the EGAMs mentioned in subsection 4.6.2) when the energetic particle contribution becomes important. The aim of this chapter is to study the **linear stability of BAEs in the presence of energetic particles**.

We start this chapter with an analytical computation of the BAE fishbone-like dispersion relation in a relevant way for the study of Tore-Supra modes, using a **perturbative approach to add damping mechanisms neglected so far, and the effect of energetic particles**. For acoustic modes $\sim v_{ti}/R_0$, resonances with passing thermal ions $\mathbf{n}*\cdot\boldsymbol{\Omega_i} \sim v_{ti}/qR_0$, the so-called **ion Landau damping**, are expected to be the main damping process, whereas the energetic particle drive can provide the driving source. The perturbative treatment of damping follows the small order expansion of the transit effects performed in the previous chapter, and it makes some sense if $\omega^2_{BAE} = (T_i/m_i)(7/2\tau_e + 1) \gg (T_i/m_i)(1/q^2)$. For stability studies (that is to say, when studying the closeness to **marginal stability**, where damping and drive compensate), it is consistant to make use of a perturbative approach for the energetic population as well. Nevertheless, the form of the energetic particle contribution provided below can be extended to the general case. From the competition of driving and damping mechanisms, it is possible to deduce the **BAE stability threshold**.

Next, we compare the calculated threshold with experiments. In this work, **experiments were conducted in order to allow for a systematic and statistical analysis of the experimental conditions and tunable parameters which favor the BAE destabilization, in the presence of a population of ICRH heated ions**. Earlier stability analysis were conducted for Toroidal Alfvén Eigenmodes (TAEs) [39, 120] or fishbones [94, 16]. For BAEs, the major point is the role of Landau damping, which can be important and get close to the validity limit of the perturbative approach, for the type of experiments performed. Landau damping was even thought to prevent the apparition of modes in the acoustic frequency range. And indeed, in the tokamak JET, the observation of global GAMs was reported to be possible only when thermal ions were "cold", hence in a regime of low Landau damping [109]. A legitimate question is whether the same is required for the excita-

tion of BAEs. A second interesting point for BAEs is the **localization of damping**, which depends on the mode structure and can differ significantly from TAEs.

In the experiments presented here, various global and local parameters have been varied to determine the conditions for BAE excitation and the precise role of these parameters in the excitation. In a first part, the role of **global macroscopic parameters** is studied, based on a statistical analysis of various shots designed to keep homothetic plasma profiles. Next, attention is given to the **effects of a $q$ profile and fast ion profile modification, in order to estimate in particular the role of the fast population anisotropy**.

## 5.1 Computation of the fishbone-like dispersion relation relevant to Tore-Supra Beta Alfvén Eigenmodes

### 5.1.1 The fishbone-like dispersion relation applied to Beta Alfvén Eigenmodes

In the absence of energetic particles and neglecting damping mechanisms, the BAE dispersion relation has been found in Eq. 4.47, to be divided into an inertia related part, and an incompressible MHD-like region. This separation mimics the traditional MHD energy relation Eq. 2.42, but contains an additional spatial information, according to which inertial terms are concentrated where high radial gradient are present, that is, inside a layer of typical size (see Eq. 4.44)

$$L_I = \sqrt{2Q}/|k_\theta s| \sim \left(\frac{\rho_i}{k_\theta s}\frac{\omega_{BAE}}{\omega_A}\right)^{1/2}. \tag{5.1}$$

The additive form of the Lagrangian Eq. 3.8, which is simply related to the traditional MHD energy relation (by Eq. 3.68, $-1/2\mathcal{L}_\omega = -(\omega^2/2)\int d\mathbf{x}^3 n m_i |\xi|^2 + \delta W_{\text{MHD}}$ ) tells us that if we now want to add energetic particles related effects, it makes sense to simply add the energetic particle Lagrangian $-1/2\mathcal{L}_{h\omega}$ to the MHD dispersion relation.

In principle of course, the addition of an extra population of particles could modify both the inertia and MHD structure, as well as the various orderings we made use of for the calculations of the previous chapter. However, an estimate of $L_I$ given in Eq. 5.1 returns values of the order of a few mm in Tore-Supra, whereas the gyroradius of suprathermal ions (typically with energies between 100 keV and 1MeV) is of the order of $\rho_h$ ∼10mm. For this reason, energetic ions are not expected to interact with the mode inertial structure, as was also argued in Ref. [75], and their contribution can simply be added to the larger scale structure.

Traditionally, the non-resonant contribution of energetic particles is summed up to the thermal plasma MHD part, to form a real energy potential $\delta W_f = \delta W_{\text{MHD}} - (1/2)\mathcal{L}_{s\omega}^{non-res}$ which contains all the *fluid*-like contributions, whereas the resonant (*kinetic*) contributions from the energetic particles is computed separately, $\delta W_k = -(1/2)\mathcal{L}_{h\omega}^{res}$. Following Eq. 3.57, an expression for the resonant Lagrangian of a species $s$ can be taken to be [1]

$$\mathcal{L}_{s\omega}^{res} = \sum_{\mathbf{n}=(0,\mathsf{n}_2,\mathsf{n}_3)} \int d^3\mathbf{x} d^3\mathbf{p}\; e_s^2 \frac{\omega\partial_{E|\mu} + \mathsf{n}_3\Omega_{*s}/T_s}{\omega - \mathbf{n}\cdot\mathbf{\Omega}_s} F_s \left| \left(\frac{\mathbf{v}_{gs}\cdot\nabla\psi_\omega}{-i\omega} + \mathcal{E}_\omega\right)_{\mathbf{n}} \right|^2 \tag{5.2}$$

and now have the three announced contributions of the fishbone-like dispersion relation Eq. 2.64, an inertia ( / or generalized inertia) term which we can note $\delta I$, a fluid-like contribution $\delta W_f$ and a kinetic energetic particle term, $\delta W_k$.

[1] Note that the separation between between a non-resonant contribution and a resonant contribution is not univocal, and that a different cut-off could have been made.

For consistency with the previous notation and with the literature [16], we use a normalized form of the generalized MHD relation, consistent with the normalizing constants of Eq. 4.37 and Eq. 4.38, that is, we multiply the MHD relation by

$$\hat{C} = \frac{\mu_0}{B_0^2}\frac{R|k_\theta|}{2\pi r_s}q^2\left(\frac{\omega^2 B_0^2 s^2}{k_\theta^2 \Psi_0^2}\right), \tag{5.3}$$

to obtain the normalized fishbone-like dispersion relation

$$\delta\hat{W} \equiv -\delta\hat{I} + \delta\hat{W}_f + \delta\hat{W}_k = 0. \tag{5.4}$$

where in particular, $\delta\hat{W}_f = \delta\hat{W}_{\mathrm{MHD}} - (\hat{C}/2)\mathcal{L}_{h\omega}^{non-res}$, and $\delta\hat{W}_{\mathrm{MHD}}$ corresponds to the quantity used in Eq. 4.47. Again, the quantities of Eq. 5.3, $k_\theta = \mathsf{m}/r, s, q$, need to be assessed close to the main resonant surface of the BAE, $r = r_s$. $\Psi_0/s$ is a characteristic value of the mode amplitude, whose relation to the mode MHD structure has been calculated in Eq. 4.41 and 4.42 for modes with a given parity. In particular, for the tearing parity, the last parenthesis of Eq. 5.3 can be rewritten $1/\delta\xi_0$ where $\delta\xi_0$ represents the jump of the radial MHD displacement close to the mode inertial region.

Let us calculate now determine the different terms involved in Eq. 5.4 more precisely.

### 5.1.2 The energetic particle term

In this section, we compute the resonant Lagrangian 5.2 for a population of energetic particles ($s = h$), relevant to a Tore-Supra ICRH heated plasma.

#### Energetic particle equilibrium distribution functions

When ICRH heating is used in the hydrogen minority scheme, hydrogen ions are accelerated in the *perpendicular* direction, where the resonance condition $\omega_{ICRH} = \Omega_{c,h} = eB_{(0)}/m_h$ or $R = eB_0R_0/(m_h\omega_{ICRH})$ is met, that is on a *vertical surface of constant R*. To the lower approximation (and in particular in the absence of MHD activity), these hot ions are thought to release their energy on electrons, via collisions, such that an equilibrium is reached when the local ICRH input power, $P_{ICRH}(r)$ is balanced by the energy released on electrons $\propto \nu_{he}n_hT_h$, with $\nu_{he}$ the collision frequency between the heated particles and the electrons. Our formalism assumes the existence of an *equilibrium* distribution function for the hot particles, which makes sense as long as the growth rate of the considered MHD modes $\gamma$ is smaller than $\nu_{he}$ and than the typical particle characteristic frequency. In our range of parameters (typically close to threhold, for stability analysis), it is a reasonable assumption, $\gamma \ll \omega_r <\sim \Omega_{h,1\ldots3}$ (for $\omega = \omega_r + i\gamma$).

Following the heating, a tail of hot hydrogen ions is expected, and it has been found to be well approximated by a Maxwellian of temperature $T_h > T_i \sim T_e$ [45]. Moreover, at the location where resonance occurs, the energy of the resulting population of hot particles is dominated by its perpendicular energy, such that the equilibrium invariant $\mu/E \sim 1/B_{(0)}$ is almost independent on the hot particle.

Consistently, a traditional analytic fit for a population of ICRH heated ions is the **anisotropic Maxwellian**,

$$F_h(r,\lambda,\mathsf{E}) = \tilde{n}(r)f_\lambda(\lambda-\lambda_0)e^{-\mathsf{E}/T_h(r)} \tag{5.5}$$

where $f_\lambda$ is a highly picked function in 0 often taken to be a $\delta$-function [45], and $\lambda_0$ is a constant defining the resonant surface $R/R_0 = \lambda_0$. As required, $F_h$ has been expressed as

a function of **three equilibrium invariants**, here chosen to be the radial coordinate $r$ (invariant with the assumption of small orbit width), the energy $\mathsf{E}$, and $\lambda = \mu B_0/\mathsf{E}$. The word **anisotropic** refers to the dependence in $\lambda$ (or $\mu$) of the distribution function.

Taking $f_\lambda$ such that $\int d\lambda f_\lambda = 1$, it is possible to rewrite the equilibrium distribution function 5.5 as a function of the more traditional characteristic quantities of a distribution function. From Appendix E.2.1, it comes

$$\tilde{n}(r) = \frac{n_h(r)}{(2\pi m_h T_h)^{3/2}} \frac{2}{< \bar{\Omega}_b(\lambda, r) >_\lambda} \quad \text{with} \quad < ... >_\lambda = \int_0^{1+r/R} d\lambda f_\lambda. \tag{5.6}$$

### Derivation of the energetic particle term

When a mode oscillates with a real frequency $\omega_r$ ($\omega = \omega_r + i\gamma$), different populations of particles can resonate with it. As a consequence, $\delta\hat{W}_k$ is the sum of many resonances, which are seen from Eq. 5.2 to be of the form $\omega - \mathbf{n}^* \cdot \mathbf{\Omega}_s = 0$ with $\mathbf{n}^* = (0, \mathsf{n}_2, \mathsf{n}_3)$. The latter terms come from the the projection of the fields structure, typically expressed in the $(r, \theta, \varphi)$ coordinate system, onto the particle relevant coordinates, the action-angle variables, and they can be an infinite number. However, **only a few of them are at the same time relevant to the population of particles in place, and with a non-negligible field component**.

First, considering a BAE with a single finite $\mathsf{n}$ number, it can be shown that the only field components which do not cancel verify $\mathsf{n}_3 \neq \mathsf{n}$ (more details are given in Appendix E.2.2). To determine the relevant values of $\mathsf{n}_2$, the BAE frequency $\omega_{BAE}$, estimated to be an approximation for $\omega_r$, is plotted in Fig. 5.1, along with the typical numerical values of the equilibrium characteristic frequencies $(\Omega_{s,b}, \Omega_{s,d})$ relevant to ICRH heated hydrogen ions (with typical energies between 100keV and a few hundreds keV) and thermal ions, using the expressions of the *normalized* drift and bounce frequencies (Eq. B.29) given in Appendix B.2. It comes from Fig. 5.1 that the most effective resonance with hot ions are of the form

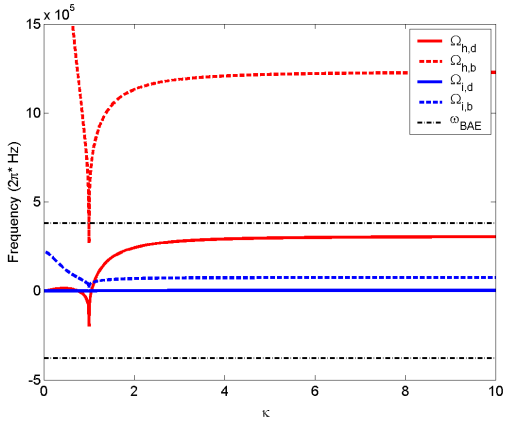


Figure 5.1: Equilibrium characteristic frequencies, calculated assuming $R_0 = 2.45$m, $q = 1$, $s = 0.1$, $r = 0.14$m, 400keV hot hydrogen ions, and 3keV thermal ions. Those quantities are given as function of the pitch angle $\kappa^2 = 2(r/R)\lambda/\left(1 - (1 - r/R)\lambda\right)$, such that $\kappa > 1$ corresponds to trapped particles, and $\kappa < 1$ to passing particles.

$\omega - \mathsf{n}\Omega_{h,d} = 0$, because $\Omega_{h,b} \gg \omega_{BAE}$. For $\omega_r \mathsf{n} > 0$, trapped ions are the only candidates for this excitation. Instead, for $\omega_r \mathsf{n} < 0$, resonance may be achieved by all types of particles presenting a drift reversal. For low shear, it means that passing ions (taking $\mathsf{n}_2 = -\mathsf{n}$, $q \approx 1$) and marginally trapped ions can resonate with the mode. In the following, only the

case with $\omega_r \mathsf{n} > 0$ is considered. Indeed, it can be argued that for standard profiles with a negative radial gradient (as expected in our experimental conditions), a mode with $\omega_r \mathsf{n} < 0$ is damped and not excited by the energetic population. This argument will be made clearer in the following paragraphs.

Following these remarks, it appears meaningful to simply keep resonances of the form ($\mathsf{n}_1 = \mathsf{n}_2 = 0$, $\mathsf{n}_3 = \mathsf{n}$) and **fast trapped ions**. As an addition, **the MHD-constraint**, $\mathcal{E}_\omega = 0$, which is verified out of the inertial region in the absence of the fast ions, is assumed to be valid when fast ions are added as well. In the approximation of **thin banana** ($k_r \delta_b \ll 1$ with $\delta_b$ the particle banana widths) for the energetic ions, which is partly justified in the MHD region, and after some calculations given in Appendix E.2, the energetic contribution reduces to

$$\begin{aligned} \delta\hat{W}_k &= -2^{3/2}\pi^2 \mathsf{m} q(r_s)^2 m_h^{3/2} \frac{\mu_0}{B_0^2} \times \\ &\int_0^a \frac{1}{r_s^2} r dr |\bar{\xi}|^2 \int_{1-r/R}^{1+r/R} d\lambda \bar{\Omega}_d^2 \bar{\Omega}_b \int_0^{+\infty} \frac{d\mathsf{E}}{\mathsf{E}-\mathsf{E}_{res}} \mathsf{E}^{5/2} \left( \mathsf{E}_{res} \partial_{\mathsf{E}|\mu} - \frac{1}{\bar{\Omega}_d} R_0 \partial_r \right) F_h \end{aligned} \tag{5.7}$$

where $\bar{\xi} = \xi/(k_\theta \Psi_0/B_0 \omega s)$ with $\xi = k_\theta \psi_\omega^{\mathsf{m}}/B_0\omega$, is the normalized MHD displacement, associated with the field main poloidal component. $\mathsf{E}_{res}$ is the necessary energy to meet the resonant condition $\omega - \mathsf{n}\Omega_{h,d} = 0$,

$$\mathsf{E}_{res} = \frac{r}{\mathsf{n} q(r)} \frac{e_h B_0 R_0}{\bar{\Omega}_d} \omega. \tag{5.8}$$

Eq. 5.8 is in agreement with Eq. 8 of Ref. [46].

It is already possible to make a few physical comments based on the form of Eq. 5.8, to get a first feeling of the role of an energetic population in the drive of a mode. Assuming a mode of frequency $\omega = \omega_r + i\gamma$ to be purely oscillating ($\gamma = 0$), resonance occurs for $\mathsf{E} = \mathsf{E}_{res}(\omega_r)$, which is at the origin of a discontinuity in Eq. 5.8. Solving this discontinuity is traditional for the treatment of wave-particle interaction.

First, we note that the discontinuous function $1/(\mathsf{E} - \mathsf{E}_{res})$ can be replaced by the well-defined *principal value* distribution $\mathcal{P} \cdot \int_0^{+\infty} d\mathsf{E}/(\mathsf{E} - \mathsf{E}_{res})$ to give a meaning to Eq. 5.8. Nevertheless, in order for $\delta\hat{W}_k(\omega)$ to be analytic in the complex plane ($\omega \in \mathbb{C}$), the proper substitution is $1/(\mathsf{E}-\mathsf{E}_{res}) \longrightarrow \mathcal{P} \cdot \int_0^{+\infty} d\mathsf{E}/(\mathsf{E}-\mathsf{E}_{res}) \pm i\delta$, where the sign preceeding $\delta$ needs to be defined. The traditional way to determine this sign is to make use of an argument of **causality** [7]. Looking at a fluctuation field $\mathcal{F}_\omega = \mathcal{F}(\omega)$, as the Laplace transform of a time dependent field $\mathcal{F}(t) = \int_{\omega=\omega_r+i\gamma} d\omega_r \mathcal{F}(\omega) \exp(-i\omega t)$, cancellation of the signal at $t = -\infty$ (the origin of time) requires $\gamma > 0$. This means that the function $\mathcal{F}_\omega$ needs to have a physical meaning in the upper half plane only. Hence, if one wants to define an analytic function in the whole complex plane, one first needs to define such dispersion relation in the upper half plane and continue it in the lower half plane, analytically. In our case, the integration over $\mathsf{E}$ is well defined in the upper half plane for $\omega = \omega_r + i\gamma$, $\gamma > 0$. When now $\gamma$ is sent to 0, it comes

$$\frac{1}{\mathsf{E} - \mathsf{E}_{res}(\omega_r + i\gamma)} \quad \underset{\longrightarrow}{\gamma \ll \omega_r} \quad \frac{1}{\mathsf{E} - \mathsf{E}_{res}(\omega_r)} + \frac{i\mathsf{E}_{res}(\gamma)}{(\mathsf{E} - \mathsf{E}_{res}(\omega_r))^2} \tag{5.9}$$

The imaginary part is positive, and so should be the sign in front of the delta function.

As expected, this resonant behavior is at the origin of a **wave-particle energy transfer**. Indeed, we know from Eq. 3.10, that for $\omega \approx \omega_r$, $\omega_r \mathrm{Im}(\delta\hat{W}_k(\omega_r)$ is positively proportional to the energy transfer from the hot particles to the wave ($-2\omega_r \mathrm{Im}\mathcal{L}_{s\omega}$), and it is the resonance which allows this imaginary part to be finite.

More precisely, we observe that the amplitude and sign of the energy transfer depend on the existence of **gradients of the equilibrium distribution function**, $\partial_r F_h$ and $\partial_{\mathsf{E}} F_h$ [2]. For $\mathsf{E}_{res} \sim T_h$ (that is for the type of hot population expected to resonate with the mode), the **contribution of the radial gradient is dominant**. Typically, the ratio of the first to the second term in the second parenthesis of Eq. 5.8, is of the order of $\omega/\Omega_{*h} \sim (\mathsf{E}_{res}/T_h)(R_0/L_{ph}) \sim 1/\epsilon$ (neglecting anisotropy as a first approximation), where $L_{ph}$ is a typical radial gradient of the hot particle distribution function. For this reason, the localization extent of a heating mechanism is of importance in the drive of a mode.

In particular, keeping the hot ion radial gradient induced drive only, it follows that the **the sign of the energy transfer from the hot particles to the wave is given by** $-\mathrm{Sgn}(\mathbf{m}\boldsymbol{\omega_r}\boldsymbol{\partial_r F_h}) = \mathrm{Sgn}(\mathbf{n}\boldsymbol{\omega_r}\boldsymbol{\partial_r F_h})$. We recover the announced idea that only waves with $\omega_r \mathsf{n} > 0$ can be excited.

A second result announced in the previous chapter is the difficulty to excite GAMs. For $\mathsf{n} = 0$ modes, radial gradient induced excitation as well as resonance with the particle drift motion are not possible. However, because of anisotropy, it was shown in Ref. [109], that the energy derivative $\mathsf{E}_{res}\partial_{\mathsf{E}|\mu}$ could be larger than $O(1)$ (For clarity, the contribution of anisotropy to the energy derivative is the second term of the brackets in Eq. 5.11), and such excitation is not inconsistent with a resonance with passing hot ions. It remains that excitation of GAMs could only be found in very special conditions.

To make comparisons with Tore-Supra experiments, it is useful to apply further simplification. First, we assume the hot ion distribution to be an **anisotropic Maxwellian**, that is, of the form defined in Eq. 5.5.

Secondly, in the absence of the observed modes toroidal and poloidal mode numbers, we assume the mode MHD structure to be a **kink with** $(\mathsf{m}, \mathsf{n}) = (-1, 1)$ **poloidal component**.

As explained earlier, a kink mode is an incompressible MHD instability driven by the equilibrium current. In a tokamak and for discharges with a standard monotonic $q$-profile, $(\mathsf{m}, \mathsf{n}) = (-1, 1)$ kink modes are common modes, which are in particular at the origin of sawtooth crashes. Such modes are usually recognized to have an odd step-like structure [121] with a discontinuity localized at the mode resonant surface, ie $\boldsymbol{\xi} = \boldsymbol{\xi}_0$ for radii $q(r) < 1$ and $\boldsymbol{\xi} = \boldsymbol{\xi}_0$ for $q(r) > 0$.

We know from the previous chapter that the BAE inertial region can connect with both an even or an odd step-like structure, and we showed that even modes with a frequency which is close to the BAE accumulation point tend to be very localized. Because our experiments (Fig. 4.4) show rather extended structures, in agreement with a localization inside the $q = 1$ surface, it is reasonable to expect the BAE to have an odd structure and an inertial layer localized on the $q = 1$. A second argument to justify this choice is the remark that sawtooth oscillations are found in our experiments (periodically excited before the sawtooth crashes). It means that in the types of equilibria set up in our experiments, the kink typical structure is to be associated with a small *incompressible* $\delta W_{MHD}$, which again is in agreement with the fact that BAE oscillations are found close to the BAE accumulation point. Finally, observations of $\mathsf{n} = 1$ modes oscillating with an acoustic frequency have been performed in the JET tokamak, where the toroidal mode number could be measured [16]. It is reasonable to postulate a similar physics here.

[2] Note that the lack of gradient along the third invariant $\partial_\mu$ simply comes from the fact that our definitions are gyroaveraged.

With the above assumptions, the energetic particle term takes the form

$$\begin{aligned}\delta\hat{W}_k &= -\pi q(r_s)^2 \mathsf{m} \int_0^a \frac{1}{r_s^2} r dr |\bar{\xi}|^2 \beta_h \int_{1-r/R}^{1+r/R} d\lambda \frac{\bar{\Omega}_b \bar{\Omega}_d^2}{<\bar{\Omega}_b>_\lambda} \times \\ &\left\{ -\frac{\mathsf{E}_{res}}{T_h} Z_5 f_\lambda - \frac{\mathsf{E}_{res}}{T_h} Z_3 \lambda f'_\lambda \right. \\ &\left. -\frac{1}{\bar{\Omega}_d}\left[ \frac{R\partial_r n_h}{n_h} Z_5 - \frac{R_0 \partial_r <\bar{\Omega}_b>}{<\bar{\Omega}_b>} Z_5 + \frac{R_0 \partial_r T_h}{T_h}\left(Z_7 - \frac{3}{2} Z_5\right)\right] f_\lambda \right\}\end{aligned} \tag{5.10}$$

with $\beta_h = 2\mu_0 n_h T_h / B_0^2$, and $Z_p(y_0) = (1/\sqrt{\pi}) \int_{-\infty}^{+\infty} dy y^{p+1} \exp(-y^2)/(y^2 - y_0^2)$, for $y_0^2 = \mathsf{E}_{res}/T_h$. In particular, the function $Z$, such that $Z(y_0) = y_0 Z_{-1}(y_0)$, is the *Fried et Conte function*, and

$$\begin{aligned} Z_3(y_0) &= \tfrac{1}{2} + y_0^2 + y_0^3 Z(y_0), \\ Z_5(y_0) &= \tfrac{3}{4} + \tfrac{y_0^2}{2} + y_0^4 + y_0^5 Z(y_0), \quad Z_7(y_0) = \tfrac{15}{8} + \tfrac{3}{4} y_0^2 + \tfrac{y_0^4}{2} + y_0^6 + y_0^7 Z(y_0). \end{aligned} \tag{5.11}$$

### 5.1.3 Inertia and Landau damping

A partial computation of inertia, $\delta\hat{I}$, was done in the previous chapter where resonance related energy transfers were absent. In this approximation, $\delta\hat{I}$ was found to be purely real and of the form

$$\begin{aligned}\delta\hat{I} &= \frac{\hat{C}}{2} \int_{inertia} d^3\mathbf{x} \frac{ne^2}{T_i} \frac{\omega_A^2}{\omega^2} \psi_\omega^{\mathsf{m}*} \left[ (qR_0)^2 \rho_i^2 \nabla_\parallel \partial_r^2 \nabla_\parallel + \Lambda^2 \rho_i^2 \partial_r^2 + \left(\frac{Q}{k_\theta \rho_i s}\right)^2 \rho_i^4 \partial_r^4 \right] \psi_\omega^{\mathsf{m}} \\ &= \begin{cases} i\Lambda |s(r_s)| & \text{for large } \Lambda^2 \\ -2\sqrt{Q}\, \frac{\Gamma(3/4 - \Lambda^2/4Q)}{\Gamma(1/4 - \Lambda^2/4Q)} |s(r_s)| & \text{for } \Lambda^2 \longrightarrow 0 \end{cases}\end{aligned} \tag{5.12}$$

where $\Lambda^2$ and $Q^2$ two real functions of $\omega$, representing generalized inertia and high order finite Larmor radius effects, given by Eqs. 4.23, 4.24 and 4.26. When they are purely real, $\Lambda^2$ and $Q^2$ can be also interpreted as a measure of the **inertia length**. Indeed, when $\Lambda^2$ is large such that the term in $Q^2$ is negligible in Eq. 5.12, the balance of field line tension and generalized inertia returns a typical inertia length, $L_I \sim |\Lambda|/|k_\theta s(r_s)|$. When $\Lambda^2 \to 0$, the case considered in chapter 4, high order FLR come into play and are able to set up a new relevant inertia length, given in Eq. 5.1, $L_I \sim \sqrt{Q}/|k_\theta s(r_s)|$.

However, as mentioned in the chapter introduction, resonance (and resonance induced energy transfers) with thermal ions can be expected in the acoustic frequency range, as also suggested by Fig. 5.1, for very passing particles ($\kappa^2 \ll 1$ in this figure). As will be shown, resonance with passing thermal ions, can lead to a damping characterized by a resonance of the form $\omega - \mathbf{n}^* \cdot \mathbf{\Omega}_i = \omega - k_\parallel v_\parallel$, which has been given the name of **Landau damping**. Landau damping explains the existence of a threshold for BAE excitation, even for modes which are in the compressibility induced BAE gap (represented in Fig. 4.1 for a Tore-Supra discharge) and escape continuum damping, or for modes which are close to the BAE gap edge (ie, close to $\omega_{BAE}$) and likely to exhibit an undamped kinetic structure.

A precise calculation of $\delta\hat{I}$ including a non-perturbative treatment of Landau damping can be found in Refs. [77, 92]. In this analysis, a much simpler perturbative model is used, valid for large $\omega q R/v_{ti}$, and more tractable for statistical comparisons with experiments. With this approximation, the *real* dispersion relation given in Eq. 5.12 is lower order, and Landau damping can be introduced at the same order as the previous transit effects, corresponding to the real part of the resonant term.

For passing ions, $\Omega_{i,2} \approx v_\parallel/qR_0$, $\Omega_{i,3} \approx v_\parallel/R_0$. Relevant resonances are with the sidebands, $\mathsf{n}_2\Omega_{i,2} + \mathsf{n}_3\Omega_{i,3} = (\mathsf{m}/q + \mathsf{n})(v_\parallel/R_0) = k_\parallel^{\mathsf{m}\pm1} v_\parallel \approx \pm v_\parallel/qR_0$, close to the main mode resonant surface. The computation of Landau damping which results from the latter resonances follows the same logics as described for the resonances with energetic ions. It is developed in Appendix E.3, starting from the resonant lagrangian 5.2. It returns

$$\begin{aligned} \frac{\hat{C}}{2}\mathrm{Im}(\mathcal{L}_{i\omega}^{res})(\omega) &= \frac{\hat{C}}{2}\int d^3\mathbf{x}\frac{ne^2}{T_i}(\rho_i\partial_r\psi_\omega^{\mathsf{m}})^2\delta_I \\ \text{with } \delta_I &= \frac{\sqrt{\pi}}{2\sqrt{2}}\left(q\frac{v_{ti}}{R\omega}\right)e^{-\frac{1}{2}\left(\frac{qR\omega}{v_{ti}}\right)^2}\left[2+2\left(\left(\frac{qR\omega}{v_{ti}}\right)^2+2\tau_e\right)+\left(\left(\frac{qR\omega}{v_{ti}}\right)^2+2\tau_e\right)^2\right]. \end{aligned} \tag{5.13}$$

Let us analyze the expression 5.13. It is already clear that the calculated resonant behavior implies an energy tranfer from the wave to the particles because $\mathrm{Sgn}(\omega_r\mathrm{Im}(\mathcal{L}_{i\omega}^{res})) > 0$. A wave with a positive energy is consequently **damped**.

For $\omega \approx \omega_r$ in the acoustic frequency range, $\delta_I$ is of the order of 1 (at the limit of the perturbative treatment) and should not vary significantly for high density ICRH experiments, because the BAE frequency is proportional to $v_{ti}/R_0$. A more important role may be expected from the mode radial gradient included in the term $(\rho_i\partial_r\psi_\omega^{\mathsf{m}})^2$. The presence of this radial gradient gives a major importance to the inertial region characterized by high radial gradients, and explains why **Landau damping may be considered to be mainly an inertial phenomenon** and integration reduced to the inertia region $\int \longrightarrow \int_{inertia}$. Note however that this reduction is consistent with the ordering of $\delta\hat{W}_k$ (calculated in the MHD region), only in the perturbative frame, that is for $\delta_I < 1$. Beyond this limit, an argument of localization of the Landau resonance condition should be invoked instead, to restrict Landau damping to the inertial region. It results that Landau damping can be put in the form

$$\frac{\hat{C}}{2}\mathrm{Im}(\mathcal{L}_{i\omega}^{res}) \approx \frac{\omega^2}{\omega_A^2}\delta_I(r_s)\frac{2\pi}{k_\theta}\int_{inertia} dr(\partial_r\bar{\xi})^2 \approx \frac{\omega^2}{\omega_A^2}\delta_I(r_s)\frac{c_0}{k_\theta L_I} \tag{5.14}$$

where $c_0$ is a constant of order 1 depending on the details of the inertia structure, and the integration is approximated by $c_0/2\pi L_I$. In this form, the role of the mode inertia length $L_I$ is clearly put forward. In particular, the precise computation of high order finite Larmor radius effects, which is necessary for a correct estimate of $L_I$ when $\Lambda^2 \to 0$ finds a justification here.

We may even be more precise, noticing that the addition of the resonant inertia imaginary part Eq. 5.13 to the real inertia Eq. 5.12 allows the direct inclusion of Landau damping in the "generalized inertia":

$$\mathrm{Re}(\Lambda^2) \longrightarrow \Lambda^2 = \mathrm{Re}(\Lambda^2) + i(\omega^2/\omega_A^2)\delta_I(r_s). \tag{5.15}$$

This way, a direct estimate of the inertial energy $d\hat{I}$ is given by formulas 5.12, where now $\Lambda$ is to be understood as the square root of a complex function of $\omega$. In particular, a direct assessement of the $c_0$ constant above follows,

$$\mathrm{Im}(\delta\hat{I}) \approx \begin{cases} \frac{1}{2}\frac{\omega^2}{\omega_A^2}\delta_I(r_s)\frac{1}{k_\theta L_I}, & k_\theta s(r_s)L_I = |\mathrm{Re}(\Lambda)|, \quad \text{for large } \Lambda^2 \text{ and } \omega < \omega_{BAE} \\ \frac{\sqrt{\pi}}{2}\frac{\omega^2}{\omega_A^2}\delta_I(r_s)\frac{1}{k_\theta L_I}, & k_\theta s(r_s)L_I = |\sqrt{Q}|, \quad \text{for } \Lambda^2 \longrightarrow 0^+ \end{cases} \tag{5.16}$$

The estimate of Landau damping for the various models, that is formulas 5.12 with the *complexified inertia* and formulas 5.16, is plotted in Fig. 5.2. The expressions of Landau damping with the inertia length are observed to be good approximations in their validity

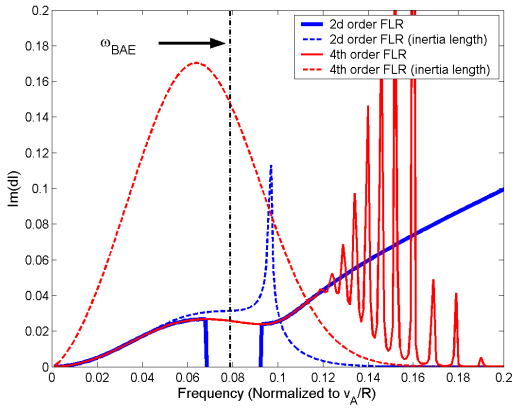


Figure 5.2: Inertia localized damping, $\mathrm{Im}(\delta\hat{I})$, as a function of the real frequency $\omega_r$ for the different models given by formulas 5.12 and 5.16. Below $\mathrm{Re}(\Lambda^2) = 0$ represented by the divergence of the blue dotted curve, damping is to be attributed to Landau damping, whereas continuum damping dominates for $\mathrm{Re}(\Lambda^2) > 0$.

areas. The one including 2D order FLR effects diverges where $\Lambda^2 = 0$ (slighty shifted from $\omega_{BAE}$ due to the high-q correction). More interestingly, the role of high order finite Larmor radius effects clearly appears. Close to $\Lambda^2 = 0$, the inclusion of 4th order finite Larmor radius effects is shown to be necessary to compute Landau damping appropriately. Because it is the frequency region where experimental points have been found, the **4th order FLR model is used in our subsequent analysis**, that is, the second equation of Eq. 5.12, with the complexified inertia Eq. 5.15.

### 5.1.4 The fluid energy

The incompressible MHD energy corresponding to a kink structure has in toroidal geometry has been calculated in Ref. [121] for discharges with a monotonic q-profiles. It reads

$$\delta\hat{W}_f = 3\pi(1-q(0))\left(\frac{13}{144} - \beta_p^2(r_s)\right)\frac{r_s^2}{R_0^2}. \tag{5.17}$$

## 5.2 Simplication of the threshold for comparison with experiments

The BAE excitation **threshold** can now be deduced from 5.4. Close to threshold ($\omega = \omega_r + i\gamma$ with $|\gamma| \ll |\omega_r|$), the dispersion relation can be expanded to the first order: $\delta\hat{W}(\omega_r + i\gamma) = 0 = i\gamma(\partial/\partial\omega_r)\delta\hat{W}(\omega_r) + \delta\hat{W}(\omega_r)$ to the first order. It follows,

$$\gamma\frac{\partial}{\partial\omega_r}\mathrm{Re}(\delta\hat{W}) = -\mathrm{Im}(\delta\hat{W}) \tag{5.18}$$

where we know that the right hand side is related to the wave-particle energy transfer ($P_{wave\to s} = 2\omega_r\mathrm{Im}(\mathcal{L}_{s\omega}^{res})$ ), and hence not surprisingly determines if the wave is damped ($\gamma < 0$) or excited ($\gamma > 0$). For a wave with *positive energy* (see section 3.1.2), $\omega_r\partial\mathrm{Re}(\delta\hat{W})/\partial\omega_r < 0$ and in agreement with the causality constraint, the excitation condition simply becomes $\omega_r\mathrm{Im}(\delta\hat{W}(\omega_r)) > 0$. Since $\mathrm{Sgn}(\mathrm{Im}(\delta\hat{W})) = -\mathrm{Sgn}(\mathrm{Im}(\mathcal{L}_\omega))$, this simply means that instability occurs for a positive energy transfer from the particles to the wave.

We now assume $\mathrm{Re}(\delta\hat{W}) \gg \mathrm{Im}(\delta\hat{W})$, consistently with the above *perturbative* calculation of Landau damping, such that the lower order solution of $\delta\hat{W}(\omega_r) = 0$ is well approximated by

$\omega_{BAE}$. Hence, excitation occurs for $\mathrm{Im}(\delta\hat{W}_k)(\omega_{BAE}) > \mathrm{Im}(\delta\hat{I})(\omega_{BAE})$. Under the simplifying assumption that the mode is more localized than the fast ion distribution, such that global characteristic values of the fast ion distribution $(T_h, n_h ...)$ may be considered instead of precise radial distributions, and considering the effect of the radial pressure gradient to be dominant in Eq. 5.11, this condition reduces to

$$\frac{\beta_h}{\beta_i}\left(\frac{R_0}{L_{ph}}\right)\left(\frac{L_I}{r_s}\right) > \frac{c_0(7/2+2\tau_e)\delta_I}{\pi^{3/2}\Omega_{h,d}(\lambda_0)\delta_h(T_h/\mathsf{E}_{res})}. \tag{5.19}$$

Here $L_{ph}$ is again a typical radial gradient length of the hot ion distribution. $\delta_h$ is a function of $(T_h/\mathsf{E}_{res})$ which takes the form $\delta_h(T_h/\mathsf{E}_{res}) = \mathcal{P}(\sqrt{\mathsf{E}_{res}/T_h})\exp(-\mathsf{E}_{res}/T_h)$, with $\mathcal{P}$ a polynomial derived from the imaginary part of the last bracket of 5.11. When only the contributions of the radial density and temperature gradients are kept, $\mathcal{P}$ is equal to

$$\mathcal{P}(\sqrt{\frac{\mathsf{E}_{res}}{T_h}}) = \left(\frac{\mathsf{E}_{res}}{T_h}\right)^{5/2}\left\{L_{ph}\frac{\partial_r n_h}{n_h}|_{r_s} + L_{ph}\frac{\partial_r T_h}{T_h}|_{r_s}\left(\frac{\mathsf{E}_{res}}{T_h}-\frac{3}{2}\right)\right\}. \tag{5.20}$$

$\delta_h$ makes the excitation easier when $T_h <\sim \mathsf{E}_{res}$ (The optimal values of $T_h/\mathsf{E}_{res}$ is 0.24 for the case of a dominating temperature gradient, as also illustrated in Fig. 5.9) and it is typically of order 1 when the optimal value of $E_{res}/T_h$ is reached.

The form of Eq. 5.19 is similar to the TAE excitation threshold calculated in [39] but it includes the additional role of the inertia length $L_I$, which is to be related to the fact that the frequencies of interest $\omega \sim \omega_{BAE}$ are small compared to $\omega_A$. Interestingly, it appears that for $T_h/\mathsf{E}_{res}$ slightly below 1 (achievable in Tore-Supra) and for $\omega \sim \omega_{BAE}$ (leading to $\delta_I \sim 1$), the right hand side of 5.19 is of order 1. Hence, it seems possible to access the **threshold in Tore-Supra experimental conditions** described subsection 4.6.1.

To allow for an easy comparison of the computed threshold with experimental observations, we now want to **link the parameters of Eq. 5.19 with measurable quantities**. *When* it is possible to assume the plasma shape, the shape of the fast ion distribution ($R_0/L_{ph}$ in particular), the $q$ profile ($r_s$ in particular) and $T_e/T_i$ to be constants, scalings can be used:

$$\begin{aligned} &L_I \propto \sqrt{Q}, && \omega_{BAE} \propto \sqrt{T_e}, \\ &n_h T_h \propto P_{ICRH}/\nu_{he} && \text{with } \nu_{he} \propto n_0/T_e^{3/2} \end{aligned} \tag{5.21}$$

where the second line follows our previous description of the ICRH induced equilibrium distribution function given in section 5.1.2 and $\nu_{he}$ is again the ion-electron collision frequency. Taking the hot particle distribution to be mainly made out of hydrogen ions, it also comes that $n_h \propto f_{min} n_0$, and Eq. 5.19 becomes

$$c_1 n_0^{1/4}\frac{P_{ICRH}}{n_0^2}\frac{T_e}{B_0} > c_3/\delta_h\left(c_2\frac{1}{f_{min}}\frac{P_{ICRH}}{n_0^2}\frac{T_e}{B_0}\right) \tag{5.22}$$

where we conserved the right and left hand sides of 5.19, such that $c_1, c_2, c_3$ are unambiguously defined as the proportionality coefficients between the physical quantities of Eq. 5.19 and the measurable quantities: $T_e$ (taken at the center), $n_0$ (the central density) and $f_{min}$, respectively measured by ECE, reflectometry and neutrals detection diagnostics.

In this formula, all tunable parameters are found to have an ambiguous role in the excitation, depending on the distance to the resonance condition $T_h/E_{res} \sim 1$. In particular, the **B-field, known to favor the excitation of energetic particle modes such as precessional fishbones (characterized by an excitation condition of the form** $\beta_h >$

$\beta_{h0}$ [45]) **has a reduced role on the BAE excitation threshold**. More precisely, if we make use of the rough scaling law $n_0 T_e \sim B_0 f(n_0, P_{ICRH})$ with $f$ a given function, $B_0$ disappears in the threshold for fixed values of $n_0$ and $P_{ICRH}$. Note that the same is not true for TAEs, for which a similar derivation shows a non-negligible but ambiguous impact of the $B$-field. In particular, it is easy to see that taking $\omega \propto B_0/\sqrt{n_0}$ (for TAEs) in the left hand side of 5.19 makes the resonance condition $T_h/\mathsf{E}_{res} \sim 1$ harder to reach for higher $B_0$. One should notice however that the role of $B_0$ in the left hand side of Eq. 5.22 *depends on the model* chosen for the inertia. Again, a correct description of the inertia length appears important to understand the mode excitation. This idea will be further discussed.

## 5.3 A solver for the dispersion relation

In order to evaluate and solve the fishbone-like dispersion relation, we wrote a c++ program using the Matpack library [122] for the computation of integrals and special functions. The program takes as input equilibrium parameters calculated from the CRONOS and PION codes, to calculate the various terms of the fishbone like dispersion relation.

The program can assess the dispersion relation for a chosen value of the frequency $\omega_0$ and deduce the mode stability, or find the roots of the dispersion relation in a circle of center $\omega_0 \in \mathbb{C}$ and radius $|\delta\omega|$ given by the user, using Davies method [123]. The input and output parameters of the solver are given in Tab. 5.1 .

| | | |
|---|---|---|
| **Input** | • Equilibrium data reconstructed by CRONOS or experimental diagnostics | -$B_0$, $R_0$, $q(r), \tau_e(r_s), n(r_s)$ |
| | • Hydrogen distribution function computed by PION and projected onto an anisotropic Maxwellian | -$n_h, T_h, \lambda_0$<br>-$\Delta\lambda$ (the typical width of $f_\lambda$) is set up by the user |
| | • User defined mode characteristics | -$(\mathsf{m}, \mathsf{n}), \omega_0 + \delta\omega$<br>-Radial Structure: Kink/Numerical |
| | • Model | -Inertia: w/wo high order FLR<br>-$\delta\hat{W}_k$: w/wo anistropy drive $f'_\lambda$<br>-Value of $\delta\hat{W}_{\mathrm{MHD}}$ |
| **Output** | • Simple estimate of stability | $\delta\hat{W}_k(\omega_0)$, $\delta\hat{I}(\omega_0)$,<br>$\mathrm{Re}(\omega_0)\mathrm{Im}(\delta\hat{W}(\mathrm{Re}\omega_0)) > 0$ ? |
| | • Search of dispersion relation roots in circle of center $\omega_0$ and radius $\|\delta\omega\|$ | Roots |

Table 5.1: Inputs and outputs of the dispersion relation root solver.

## 5.4 Comparison of the theoretical threshold with experiments carried out in the Tore-Supra tokamak

### 5.4.1 Objectives of the experimental campaign

To analyze the BAE stability and in particular estimate the relevance of the thresholds described by Eqs. 5.19 and 5.22, experiments were performed to determine the experimental excitation thresholds of BAEs in Tore-Supra, for **various equilibrium parameters**. Two aims were given to this study:

- Identify the role of *global* parameters, $B_0, n_0, f_{min}$, when profiles are kept homothetic.
- Analyze some effects related to a profile modification, for example a modification of the $q$-profile.

### 5.4.2 Experimental settings

#### Scenari and parameters

Experimental conditions were varied around the **reference parameters**: $B_0 = 3.8$T, $I_p = 1$MA, $n_0 = 5e19\text{m}^{-3}$, $P_{ICRH} = 2.5$MW, $f_{min} = 4\%$, for which earlier observations of BAEs could be performed. To determine the thresholds for BAE excitation, ICRH power was increased step by step with an attempt to keep the other parameters fixed (In reality, these parameters cannot be kept fixed as explained in subsection 2.3.4, which limits the range of parameters which can be explored), using long enough steps to allow for equilibrium parameters to reach steady-state $\sim 3.5s$. Fig. 5.3 displays a typical scenario used during our set of experiments.

First, equilibrium conditions were modified, with an attempt to keep profiles homothetic. For this, pure ICRH discharges were used, keeping the ratio $I_p/B_0$ constant to limit modifications of the $q$-profile. Three values were considered for the field, $B_0 = 2.8/3.2/3.8$T, three (target) values for the central density $n_0 = 4.5/5/5.5e^{19}\text{m}^{-3}$. The minority fraction, $f_{min}$ was varied from 2.5% to 10%, whereas $P_{ICRH}$ was increased from 0 to $5.5MW$ with 0.5MW steps. Next, additional experiments were conducted to determine a possible role of the shape of the $q$ profile, controlled by some input of LH power (already indicated to make possible the generation of a localized current), $P_{LH} = 0.0/1.2/2.2$MW.

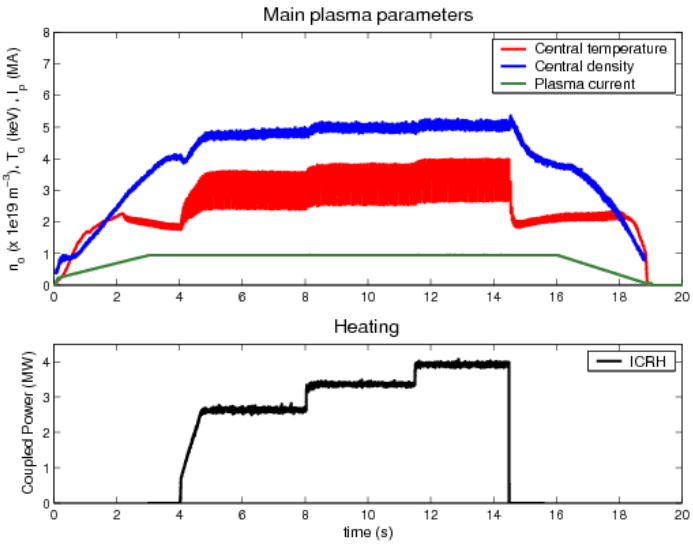


Figure 5.3: Time evolution of the main plasma parameters in shot #41925.

#### Diagnostic set up

Various fluctuation diagnostics have been set up for the experiments: reflectometry, ECE fluctuation diagnostics, interferometry, soft X rays, designed to measure fluctuations in the last half second of each ICRH step. Even if some observations could be performed on the

electron temperature (after a heavy post-treatment though, see Fig. 5.5), the best observations were achieved with reflectometry which proved high sensitivity. For this reason, most of the following analysis is based on reflectometry. The two modes of the reflectometry diagnostics (described in subsection 2.3.2) were used to obtain the long time evolution of the mode during a whole sawtooth period, as well as its radial structure and to allow for the mode detection over a broad radial range.

### 5.4.3 General qualitative features of the mode stability

Before entering quantitave considerations, let us describe some features of the occurence of BAEs in our discharges, qualitatively.

#### BAE stability and sawtooth dynamics

We already mentioned the existence of sawtooth oscillations in all of our discharges, that is, oscillations of the central temperature characterized by a sudden crash and a slower restoration of about 20s (Fig. 5.4 and 4.4). The reason for these crashes is that our equilibria are inside the limit where pure MHD incompressible kink instabilities are unstable (that is $\delta\hat{W}_f < 0$ in Eq. 5.17). Kink instabilities (which can be identified easily on fluctuation diagnostics, with a real frequency of around 3kHz) grow such that central confinement gets lost: it is the sawtooth crash. Following this drop of the central temperature, the plasma gets MHD stable ($\delta\hat{W}_f > 0$) and the central temperature can be restored until MHD marginal stability $\delta\hat{W}_f = 0$ is reached once again.

As a consequence, despite our attempts to reach steady-state conditions for each ICRH step, sawtooth oscillations does not allow to rigorously talk about a constant central temperature, or a constant density. Moreover, the presence of BAEs was found to be influenced by the sawtooth oscillations. This influence is well illustrated in Fig. 5.4 and 5.5, which are typical observations we made. As observed in these figures, the mode is more intense at the beginning and at the end of the sawtooth period, where the mode frequency also appears to grow (sometimes faster than the temperature relaxation time).

For the statistical analysis of the conditions for BAE destatbilization, we will not be considering the details of the sawtooth dynamics. In particular, the so-called central temperature will be a time average of the central temperature, whereas the presence of BAEs will have to be understood as the presence of the mode at the end of each sawtooth period. Because our statistical analysis makes use of "scalings", this choice seems reasonable.

For more detailed analysis (the detailed analysis carried out for shot #42039 in the following), the temperature and $q$ profiles computed by CRONOS will be used, which corresponds to the equilibria prior to the sawtooth crash.

#### BAE stability and LH Heating

A second striking feature which appeared during our experiments is the role of LH power. As shown in Fig. 5.6, the mode amplitude is signicantly enhanced in the presence of LH heating ($P_{LH} = 2.1MW$). This phenomenon was found to be particularly obvious close to marginal stability, suggesting a reduction of the mode excitation threshold with the introduction of LH heating. In some shots, the modes also appeared to be radially extended in the presence of LH power.

Even if LH power implies some additional heating of the ion population, it is not expected to produce ions with sufficient energies to excite acoustic modes. Hence, these observations suggest that the addition of LH power modifies *equilibrium* properties in a way which favors

Shot #42039, $t \sim 9.5s$: $B_0 = 3.80T$, $n_0 = 4.45e19m^{-3}$, $I_p = 0.95MA$, $P_{LH} = 0.0MW$, $P_{ICRH} = 3.1MW$, $f_{min} = 8\%$

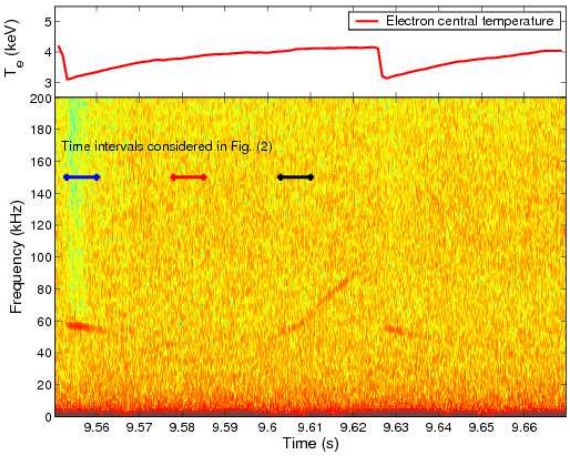


Figure 5.4: Reflectometry spectrogram at the plasma center for shot #42039. In this picture, the time interval [9.56 9.62] corresponds to a typical sawtooth period.

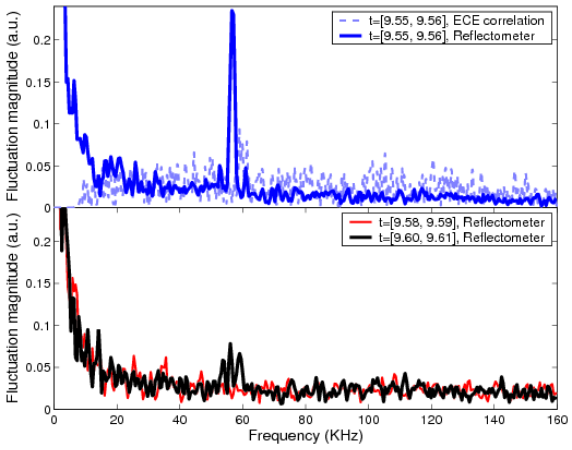


Figure 5.5: Fluctuation spectra corresponding to the time intervals shown in Fig. 5.4, taken at the plasma center. The plotted ECE correlation spectrum results from the correlation of the 10 first ms of each sawtooth period between $t = 9s$ and $10s$ (necessary to discrimate the mode) and the filtering of the perturbations below 10 kHz.

Shot #42806: $B_0 = 3.86T$, $n_0 = 4.65e19m^{-3}$, $I_p = 0.95MA$, $P_{LH} = 0.0MW$, $P_{ICRH} = 1.7MW$, $f_{min} = 5.5\%$
Shot #42815: $B_0 = 3.86T$, $n_0 = 4.75e19m^{-3}$, $I_p = 0.95MA$, $P_{LH} = 2.2MW$, $P_{ICRH} = 1.7MW$, $f_{min} = 4.7\%$

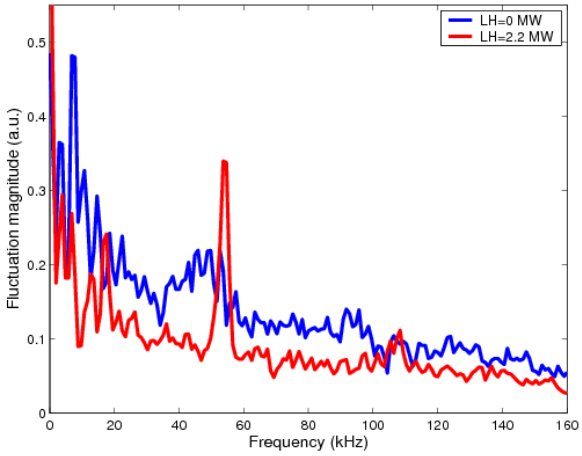


Figure 5.6: Modification of the BAE density fluctuation spectrum with the introduction of LH power.

the mode excitation.

### 5.4.4 Single case analysis

We first start the comparison with a particular case analysis to verify the above claim that the threshold condition Eq. 5.19 is accessible for relatively standard parameters, using the numerical tool described in section 5.3.

The studied case is shot #42039, analyzed at two different times, $t \sim 7s$ and $t \sim 14s$, corresponding to two different levels of ICRH power, but similar equilibrium parameters. The main experimental parameters of the shot are given in Fig. 5.8. The q-profile was found from a CRONOS simulation to be almost parabolic, with a $q = 1$ surface localized at a normalized radius of 0.35, and a central value consistent with q=0.7 (within the code errorbars). From an experimental point of view, modes were observed with reflectometry in both cases, and the first set of experimental conditions ($t \sim 7s$) was found to be close to marginal stability (when increasing the power lever step by step).

The features of the fast ion distribution calculated by PION are given in Fig. 5.7, where it appears that relatively large values of the fast ion pressure can be reached (for comparison, $\beta_i \sim 0.2 - 0.3\%$), and that the resonant condition $T_h/E_{res} \sim 1$ (more precisely optimal for $T_h/E_{res} \sim 0.25$ for a dominant temperature gradient as illustrated in Fig. 5.9) is accessible, which makes the resonant drive reasonable. As also appear in this figure, the localization of fast particles is slightly off-sxis. Now, from the comparison of the two experimental

Shot #42039, $t \sim 7s$: $B_0 = 3.80T$, $n_0 = 4.37e19m^{-3}$, $I_p = 0.95MA$, $P_{LH} = 0,0MW$, $P_{ICRH} = 2.3MW$, $f_{min} = 8\%$
Shot #42039, $t \sim 14s$: $B_0 = 3.80T$, $n_0 = 4.54e19m^{-3}$, $I_p = 0.95MA$, $P_{LH} = 0.0MW$, $P_{ICRH} = 4.6MW$, $f_{min} = 8\%$

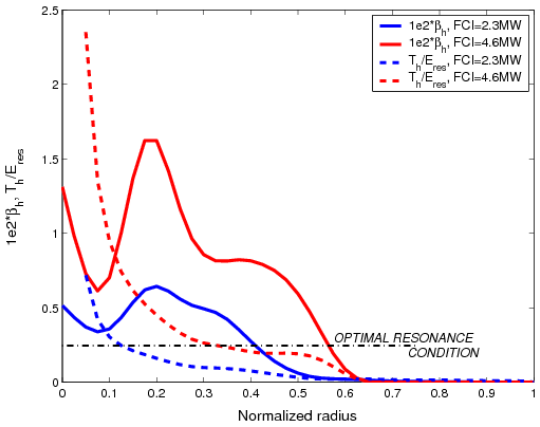


Figure 5.7: Radial profiles of the fast ion normalized pressure and resonance parameter $T_h/E_{res}$, for different power input.

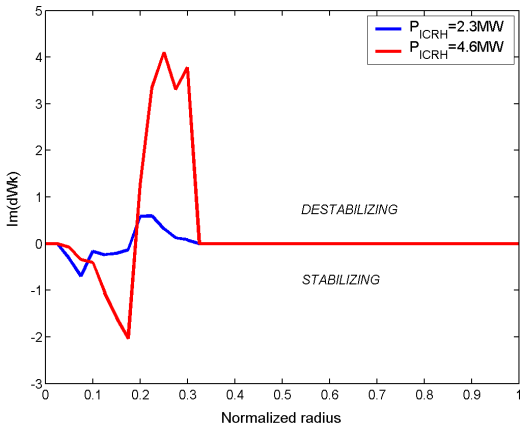


Figure 5.8: Radial profile of the fast ion induced wave-particle energy transfer, $\mathrm{Im}(d\hat{W}_k(\bar{r}))$, for different power input. $\mathrm{Im}(d\hat{W}_k(\bar{r}))$ verifies $\int_{\bar{r}} d\bar{r}\mathrm{Im}(d\hat{W}_k(\bar{r})) = \mathrm{Im}(d\hat{W}_k)$ with $\bar{r}$ the normalized radius.

conditions, it appears that the introduction of ICRH power can have an effect on the two free parameters involved in the threshold Eq. 5.19: the fast ion pressure $\beta_h$ and the resonance condition which is better met a higher power ($t \sim 14s$) between the normalized radii 0.2 and 0.35, where the fast ion pressure profile presents a negative slope.

The corresponding profiles for the drive are given in Fig. 5.8. The drive appears to be very sensitive to the gradients of the fast particle radial pressure, as expected. Only regions characterized by a negative radial gradient of the fast ion population (see the form of $\beta_h$ in Fig. 5.7) lead to a drive, whereas positive gradients lead to damping. Consequently, a

stronger off-axis heating could be expected to be stabilizing for the modes described here, even for large values of $P_{ICRH}$. Finally, in agreement with the shapes of the fast particle distribution functions, the drive at higher power is three times as strong as in the lower power case.

Let us now compare drive and damping, calculated with the previously defined expressions of $\delta\hat{I}$ (with 4th order FLR), and of $\delta\hat{W}_k$. (without anisotropy [3] ). For the marginal conditions ($t \sim 7s$) and the experimental value of the mode oscillation frequency $\omega_r^{\exp}/2\pi = 55kHz$, it comes

$$\mathrm{Im}\delta\hat{I}(\omega_r^{\exp}) = 0.024 \qquad \mathrm{Im}\delta\hat{W}_k(\omega_r^{\exp}) = 0.026 \tag{5.23}$$

which seems to suggest a good agreement between theory and experiment. Indeed, from this calculation, the mode appears to be rightfully excited, and close to marginal stability.

Note that the use of the dispersion relation solver of section of 5.3 as a root solver is unfortunately much less conclusive at the moment. For a choice of $\delta\hat{W}_{\mathrm{MHD}} = 0$ (consistent with the assumption of an $(-1, 1)$ kink structure for the BAE, a structure which is obviously close to marginal MHD stability as proved by the presence of sawtooth oscillations), the calculated solution of the dispersion relation $(\omega_r^{\mathrm{sol}}, \gamma^{\mathrm{sol}})$ is

$$\omega_r^{\mathrm{sol}}/2\pi = 66\mathrm{kHz} \qquad \gamma^{sol}/\omega_r^{\mathrm{sol}} = -1.6 \times 10^{-3}, \tag{5.24}$$

which implies that the mode is damped, and that some corrections to the dispersion relation needs to be provided to avoid the difference between the computed and the experimental values of the oscillation frequency (In particular, the perturbative treatment of Landau damping is questionable). Nevertheless, the root solver, being currently still under a testing phase (for dispersion relations with multiple roots), caution is necessary at the moment.

In any case, the comparison between theory and experiments confirms the closeness to marginal stability for the shot #42039 at $t \sim 7s$. This case will be considered as a reference in the following.

### 5.4.5 Statistical analysis of the role of global parameters

#### Procedure

In this part, we compare the observation of BAEs with the threshold calculated in Eq. 5.22, taking the marginal experimental conditions described above as a reference to define the constants $c_1$, $c_2$ and $c_3$, defined there. Such analysis can be seen as an experimental proof-check of the perturbative treatment of the excitation and damping of BAEs.

In the following, $c_1$ and $c_2$ are adjusted to match the experimental data of shot #42039 at time $t \sim 7s$ with the computed value of the fast ion distribution calculated by the code PION at the normalized radius of maximum excitation, 0.25. $c_3$ is made consistent with the ratio of $\delta\hat{I}$ and $\delta\hat{W}_k$ computed for shot #42039, that is

$$c_3 = c_1 n_0^{1/4} \frac{P_{ICRH}}{n_0^2} \frac{T_e}{B_0} \delta_h \times \frac{\delta\hat{I}}{\delta\hat{W}_k} \tag{5.25}$$

where $\delta\hat{I}$ and $\delta\hat{W}_k$ are the values given in Eq. 5.23.

The theoretical threshold is compared with the experimental mode onset, defined as the existence of a time coherent signal/noise value exceeding 2, on the reflectometry diagnostic.

[3] Anisotropy is usually taken to be a limited effect and to be relevant only with very particular heating conditions [109, 119] With the $\delta$-function used as a model for the fast ion distribution, we do not want to introduce an artificially strong anisotropy induced excitation.

### Results

The results of the mode investigation are given in Fig. 5.9. On this plot, the onset of modes

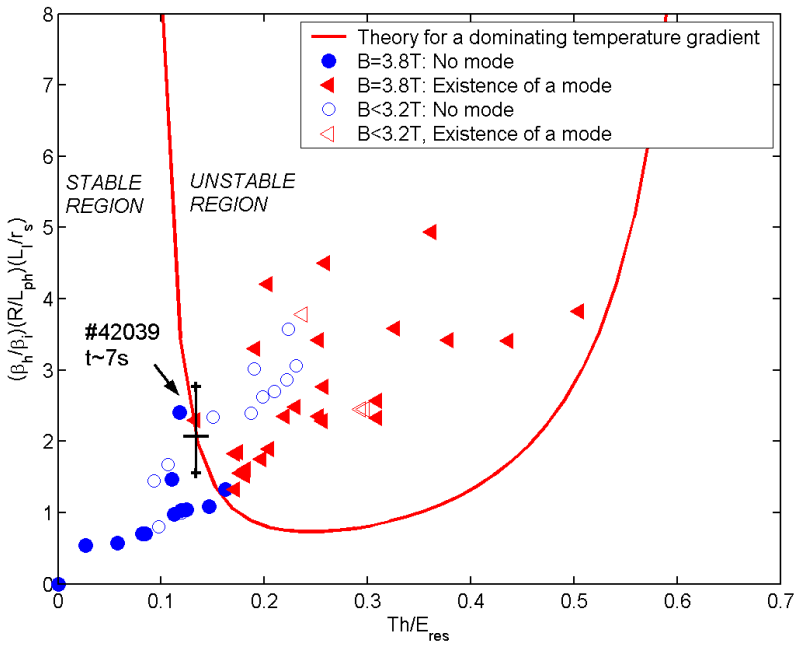


Figure 5.9: BAE apparitions in Tore-Supra discharges, compared to the theoretical prediction. A "mode observation"corresponds to a coherent signal/noise value exceeding 2. The pointed dot corresponds to the case $\#42039, t \sim 7s$.

has been reported as a function of the two degrees of freedom involved in 5.22, based on the scalings used to establish this formula and on the assumption that $c_1$, $c_2$ and $c_3$ do not significantly vary during the experiments. The horizontal error-bar stands for the relative mismatch between the observed localization of the threshold (close to the dot representing shot #42039 at time $t \sim 7s$) and the numerical computation of it derive from Eq. 5.23. Though quite small, it is observed to induce a possibly large error in the vertical direction due to the sensitivity of $\delta_h(T_h/E_{res})$ in Eq. 5.25. The theoretical threshold has been plotted assuming a dominating radial temperature gradient $L_{ph} = L_{Th}$. Keeping only the radial temperature gradient in formula 5.20, the threshold curve reads

$$\mathcal{Y} = c_3/\delta_h(\mathcal{X} = T_h/E_{res}) = c_3/(E_{res}/T_h)^{5/2}(E_{res}/T_h - 1.5)e^{-E_{res}/T_h} \tag{5.26}$$

where $(\mathcal{X}, \mathcal{Y})$ stand for the abcissa and ordinate of the graph. From the full PION computation of the fast ion distribution carried out for shot #42039, the consideration of a dominating temperature gradient is reasonable. Interestingly, **the vertical shape of the plotted theoretical curves close to $T_h/E_{res} \sim 0.1$ implies that a sufficiently high hot ion temperature is the major necessary condition for the mode onset** whatever the hot ion pressure.

As can be seen in this figure, a good agreement appears between theory and experiment for the fixed large magnetic field $B_0 = 3.8T$, which gives some confidence in the computed orders of magnitude of Landau damping and excitation. The agreement is particularly striking considering the rather large extent of the investigated values of the minority fraction. The role of the latter parameter is indeed well illustrated by the reference shot #42039 at time

$t \sim 7s$, experimentally observed to be marginally unstable in spite of a relatively large power input $P_{ICRH} = 2.3MW$ but a high minority fraction $f_{min} = 8\%$. For similar equilibrium parameters and for more standard minority fractions $f_{min} \sim 4\%$, modes could be observed with a power input $P_{ICRH} = 1.5MW$. Hence, the **perturbative framework appears to have some relevance, at least to estimate the qualitative relative effect of global macroscopic parameters**.

For lower field, excitation is seen in Fig. 5.9 to be harder than expected by theory. As explained in section 5.2, the model used in this threshold assessment does not imply a clear role of the magnetic field, in contradiction with the experimental observation. This may suggest the relevance of using a different model for the inertia length. In particular, because the latter (very small) length may evolve significantly in the nonlinear regime, an improvement of the stability analysis may be considered towards a nonlinear description of the BAE structure. However, considering the important shift of the threshold for lower fields, found experimentally in Fig. 5.9, this model modification is likely to be insufficient and other possibilities such as a harder mode detection for lower magnetic field may provide simpler explanations.

### 5.4.6 Detailed additional analysis

Though less systematically studied, some interesting phenomena were put forward in our experiments, enhancing the role of additional parameters neglected so far. In the following, attention is given to the role of the shear and fast ion distribution anisotropy.

The modification of the shear $s$ is the best candidate to explain the drop of the excitation threshold in the presence of LH heating, described in subsection 5.4.3. Indeed, the level of LH heating is not expected to heat the fast ions to relevant energies for resonance with an acoustic mode. Hence, the noted threshold reduction is more likely to be linked to a modification of equilibrium parameters. Besides, this interpretation is in agreement with the discontinuous presence of the mode in the course of the sawtooth period shown in 5.4. To better understand this role, we computed numerically the values of the excitation and damping for different artificial $q$ profiles. Starting from the parameters of shot $\#42039, t \sim 7s$, we tested various parabolic $q$ profiles with a fixed $q = 1$ surface, and different central values and computed the resulting values of the drive and damping. The results of this analysis are given in 5.10 and 5.11. As can be seen in Fig. 5.10, a flatter $q$ profile tends to decrease both the excitation $d\hat{W}_k$ and damping $d\hat{I}$. This behaviour of the damping is easy to understand noticing that $L_I \propto \sqrt{s(r_s)}^{-1}$ and hence $\delta I \propto \sqrt{s(r_s)}$. To understand the origin of the drop of $d\hat{W}_k$, we plotted in Fig. 5.11, the parameters of Eq. 5.19 which are sensitive to a $q$ profile modification. The major parameter modified here is obviously the bounce frequency, which is an affine function of $s$. The simultaneous drop of the drive $\mathrm{Im}(d\hat{W}_k)$ and of the damping $\mathrm{Im}(d\hat{I})$ with a flattened $q$ profile does not allow to explain the decrease of the BAE excitation threshold non ambiguously. However, as can be seen in Fig. 5.10, the graphs representing the drive and the damping are characterized by different curvatures. $\delta\hat{I}$ appears to be concave and $\delta\hat{W}_k$ to be convex, which is consistent with the interpretation of these behaviours. This situation enables the two curves to cross twice, meaning that an increase of the shear may induce either an easier or a harder mode excitation, depending on the starting point. Such a situation can be postulated to explain the mode onset at the beginning ($s \sim 0$ at the center) and at the end of a sawtooth period.

The fast ion anisotropy may also play a role in the stability analysis. First, as can be seen in (E.17), anisotropy may induce an energy gradient and hence a mode excitation. With

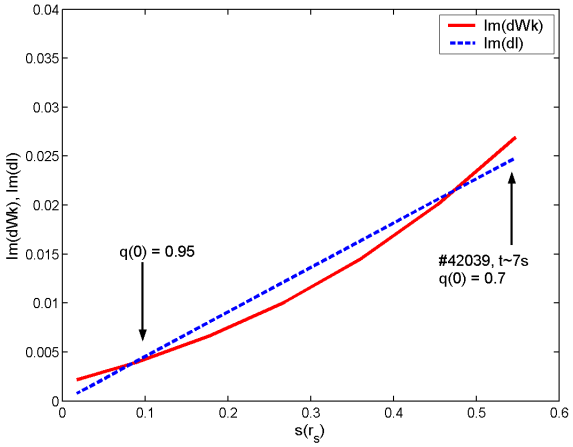


Figure 5.10: Effect of modification of the shear (taken at the resonance layer) on the drive and damping. In the main picture, fixed parameters correspond to shot#42039, with $P_{ICRH} = 2.3MW$. The second picture is a speculative schematic of a possible configuration, commented in the core of the paper.

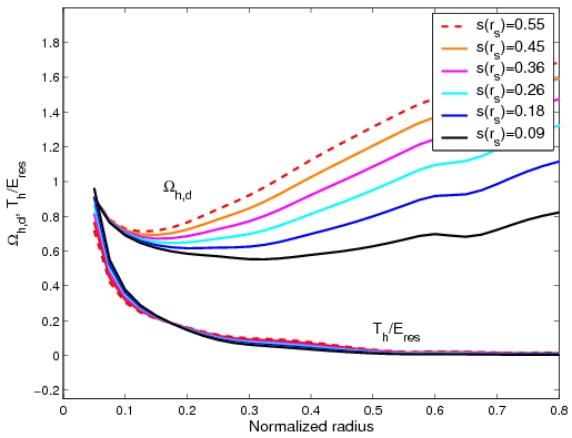


Figure 5.11: Effect of a modification of the shear on the drift frequency $\Omega_{h,d}$ and resonance parameter $T_h/E_{res}$ radial profiles.

the parameters of shot #42039 at time $t \sim 7s$ and taking a $\delta$-function to model the fast ion pitch angle $f_\lambda = \delta(\lambda - \lambda_0)$, anisotropy is seen to imply a factor of 2 on the mode drive. Although the $\delta$-function may seem to be a poor model, this important factor may reveal a certain role of this excitation mechanism.

The fast ion anisotropy also gives some importance to the heating localization. As an addition to the modification of the characteristic radial gradients of the fast ion population noted above, a modification of the heating localization changes the particle pitch-angle $\lambda_0$. To assess this phenomenon, we plotted in 5.12 the values of $\mathrm{Im}(\delta\hat{W}_k)$ for different values of $\lambda_0$ (and artificially fixed radial gradients) starting from the parameters of shot #42039 at marginal stability. As can be seen in Fig. 5.12, a lower drive may be expected for a

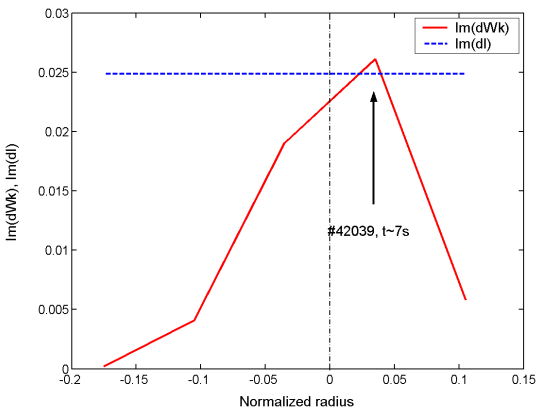


Figure 5.12: Effect of modification of the anisotropy parameter $\lambda_0$ on the drive and damping. $\lambda_0$ gives some hint into the localization of the ICRH heating.

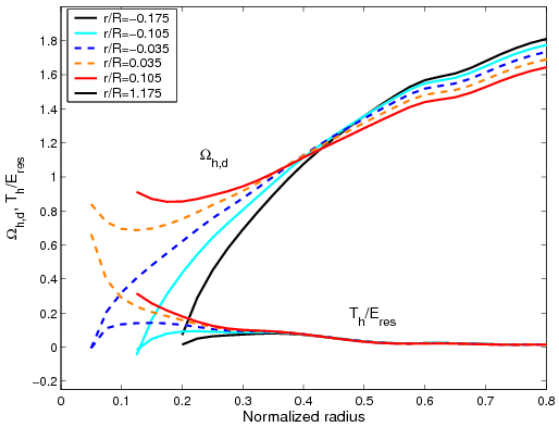


Figure 5.13: Effect of modification of the anisotropy parameter $\lambda_0$ on the drift frequency $\Omega_{h,d}$ and resonance parameter $T_h/E_{res}$ radial profiles.

high field side heating localization. The explanation of this behaviour is given in Fig. 5.13,

where it appears that the resonance condition is better met when fast particles are more strongly trapped and $\bar{\Omega}_{h,d}$ subsequently enhanced. Though not fully realistic, Figs. 5.12 and 5.13 show a non-negligible role of the particles pitch-angle and of the radial variation of the precession frequency $\Omega_{h,d}$, often taken to be constant in the theoretical assessment of the energetic particle drive. This idea of a role the heating localization was suggested to us by experimental observations, but a cleaner experimental investigation of this phenomenon still needs to be carried out.

## 5.5 Summary

*In the present chapter, the BAE excitation threshold was calculated using analytic expressions for the energetic particle drive and for ion Landau damping, and it was compared with experiments conducted on the Tore-Supra tokamak both qualitatively and quantitatively.*

- *In the perturbative framework, the calculation of the threshold was found to involve different parameters relative to the energetic particle distribution as well as to equilibrium parameters. These parameters could be reduced to* **two degrees of freedom** *which depend on experimental macroscopic tunable parameters (the density, the magnetic field, the minority fraction and level of ICRH heating), under the assumption that radial profiles are homothetic, from one experiment to the other.*

- *This made possible a statistical comparison of the calculated BAE threshold with experiments. This comparison returned a fair agreement between theory and experiment, which confirms the* **orders of magnitude of the computed damping and excitation mechanisms** *involved in the BAE stability, and the rough* **global role of the above macroscopic tunable parameters**. *The* **necessity to meet the resonant condition appeared to be the most determining factor for the mode destabilization**, *in agreement with both theory and experiment.*

- *More surprisingly, the conducted analysis highlighted an ambiguous* **role of the shear** *in the BAE excitation, which may give some explanation to the discontinous onset of the mode in the course of a sawtooth period.*

- *Nevertheless, the threshold analysis as well as the theory/experiment comparison also pointed out some missing physics of the threshold calculated here.*

  *First, the strong role of the inertial layer (narrow) size in the assessment of Landau damping suggests that the mode stability can be modified when moving to the* **nonlinear framework**, *because strong gradients are usually not expected to survive nonlinearly.*

  *Next, our model cannot explain the higher threshold for BAE destabilization at lower $B_0$-field. Neither can it explain the increase of the BAE frequency at the end of the sawtooth periods. The* **perturbative treatment of Landau damping**, *used here, should definitely be seen as weak point, considering the orders of magnitude involved. Moreover,* **diamagnetic effects**, *neglected in this analysis, have recently been postulated for the increase of the BAE frequency at the end of the sawtooth period, observed in the Asdex Upgrade tokamak as well [124]. Although the latter effects are a priori negligible in our experimental conditions, it may be interesting to assess such a claim.*

  *Thus, both a non-perturbative treatment of Landau damping and diamagnetic effects are currently being implemented in the BAE dispersion relation, following the derivations given in Ref. [77]. Further theory-experiment comparisons are also planned in the next experimental campaigns.*

*One interesting point suggested by the* **analytic** *calculation of the BAE threshold is the possibility of a* **nonlinear** *modification of stability. This is the motivation for the preliminary nonlinear developments conducted in next chapter, where indeed one process for the apparition of subcritical activity will be proposed.*

*However, one should note that the analysis to come is not directly suggested by the* **theory-experiment comparison** *given here, which does not not advocate for the existence of a subcritical activity.*

*On doit exiger de moi que je cherche la vérité, mais non que je la trouve.*

Denis Diderot (1713-1784)

# 6 Towards a nonlinear description

In this chapter, we address the problem of the *nonlinear* description of Beta Alfvén Eigenmodes, in order to get some ideas about their **saturation mechanisms** and the related **transport of energetic particles**. The goal of the following presentation is not to provide a full picture of the nonlinear evolution of BAEs. It is an attempt to enlight some difficulties related to the descripton of nonlinear *kinetic* behaviors, analyze the applicability of the most classical interpretation of fast particle saturation, that is the *nonlinear trapping* briefly outlined in subsection 2.2.4, and finally investigate some intrinsic difficulties of BAEs. More specifically, two ideas are focused on. First, we consider the possible existence of **metastable saturated modes**, related to the nonlinear trapping of resonant particles. Next, some thoughts are given to the effects of a nonperturbative treatment of damping and excitation.

In the first section, we explain how it is possible to extend the nonlinear energy principle displayed in the previous chapters. Next, we come back to the theory of *nonlinear trapping* in order to determine its meaning and validity for BAEs. Finally, the analysis of metastable modes is carried out in section 6.3, whereas some observations and ideas related to the consideration of non-perturbative damping and excitation are developed in section 6.4.

## 6.1 Formulation of a nonlinear energy principle

In linear analysis, perturbed solutions are *eigenfunctions* of eigenvalue $\omega$, proportional $\propto \exp(i\omega t)$. For such types of perturbations, we displayed in subsection 3.1.1 of chapter 3, an energylike dispersion relation, derived from the linear expansion of the low-frequency Maxwell equation,

$$\begin{aligned} 0 = \mathcal{L}_\omega(\phi_\omega, \mathbf{A}_\omega, \phi_\omega^\dagger, \mathbf{A}_\omega^\dagger) &= -\int d^3\mathbf{x} \frac{\mathbf{B}_\omega^\dagger \mathbf{B}_\omega}{\mu_0} + \sum_s \int d^3\mathbf{x} \left( \mathbf{j}_{s\omega} \cdot \mathbf{A}_\omega^\dagger - \rho_{s\omega} \phi_\omega^\dagger \right) \\ &= -\int d^3\mathbf{x} \frac{\mathbf{B}_\omega^\dagger \mathbf{B}_\omega}{\mu_0} - \sum_s \int d^3\mathbf{x} f_{s\omega} h_{s\omega}^\dagger. \end{aligned} \tag{6.1}$$

In linear studies, such a *dispersion relation* is sufficient to determine stability, accessed when solving for the roots $(\omega_r, \gamma)$ of the energylike relation.

When moving to the nonlinear frame, some additional difficulties arise.

- **Several eigenmodes can couple together.** Nonlinearities can couple multiple eigenfrequencies, and consequently, the complete electromagnetic Lagrangian should be written as a sum of several modes of various eigenfrequencies.

  This difficulty is real, but it does not prevent the use of energylike relations of the form $\mathcal{L}_\omega = 0$. Indeed, it is easy to see that the linearity of Maxwell equations and

of the Fourier transform, still gives a sense to the energylike relations 6.1, where the fields $\mathcal{F}_\omega$ are taken to be Fourier-like transforms of the nonlinear solution, $\mathcal{F}_\omega = (T/2\pi)\int_0^{2\pi/T} dt\mathcal{F}(t)\exp(i\omega t)$ with $T$ larger than any time period of interest. Making use of an energylike relation of the form 6.1,

$$\mathcal{L}_\omega \equiv \mathcal{L}(\omega) = 0 \tag{6.2}$$

is simply equivalent to the choice of one single oscillation frequency $\omega$ and it is valid nonlinearly, though now the nonlinear particle nonlinear responses need to be incorporated.

- **The energylike relation is in general a time dependent equation.** The nonlinear behavior of a "mode", cannot be reduced to a single frequency $\omega$. Starting for example from a linear eigenfrequency $\omega_0 = \omega_{r0} + \gamma_0$ ($\gamma_0 > 0$), a mode can reach saturation $\gamma = 0$, or its oscillation frequency can change. The shape of the eigenfunctions can also evolve. In other words, the energy relation 6.2 is in general of the form

$$\mathcal{L}(\omega_{r0} + \delta\omega_r(t) + i\gamma(t), t) = 0 \tag{6.3}$$

For example, if the mode structure is conserved, and there is a smallness parameter $\bar{\epsilon}$ such that $\delta\omega_r = O(\bar{\epsilon}\omega_{r0})$, $\mathcal{L} = \mathcal{L}_{(0)} + \mathcal{L}_{(1)}$ with $\mathcal{L}_{(1)} = O(\bar{\epsilon}\mathcal{L}_0)$, Eq. 6.3 can be expanded in the form

$$(\delta\omega_r + i\gamma)\partial_\omega\mathcal{L}_{(0)}(\omega_{r0}) = -\mathcal{L}_{(1)}(\omega_{r0}) \tag{6.4}$$

which can be seen as a time dependent energy equation on the mode real amplitude $\mathcal{A}$ if $\delta\omega_r = 0$,

$$\omega_{r0}\partial_\omega\mathcal{L}_{(0)}(\omega_{r0})\frac{d}{dt}\mathcal{A} = -\omega_{r0}\mathcal{L}_{(1)}(\omega_{r0}, \mathcal{A}). \tag{6.5}$$

Moreover, such an equation may need to be coupled to a time dependent equation for the nonlinear particle responses.

- **The system may not remain close to threshold, or close to an attractor.** In order to display the energy equation 6.5, we needed to assume that the system remained close to a given frequency point $\omega_{r0}$ (the threshold frequency for example, but it should also be possible to consider a nonlinear attractor as well). In particular, when $\omega_{r0}\partial_\omega\mathcal{L}$ is almost real, such an assumption is equivalent to say that the mode energy density is assumed constant for the studied process. However, such an expansion makes sense only if $|\gamma\partial_\omega\mathcal{L}|$ remains small, which may not be the case.

  Some numerical situations have been found where a restoring force constrained a system to remain close to the linear threshold, even for a strongly driven mode [125]. However, in some experiments, strong frequency sweeping was found, with $\delta\omega_r \sim \omega_{r0}$ (see Fig. 6.1), which does not seem to fit the framework. In particular, we may expect $\partial_\omega\mathcal{L}$ to be huge when *resonances* are included in the derivative.

A particular framework which avoids most of these difficulties is the **kinetic perturbative framework**, which is traditionally used for the study of the kinetic nonlinear saturation of gap modes (see section 2.2.4 and Refs. [55]).

In this framework and in analogy with our previous computation of the linear stability analysis, a well defined linear eigenmode with a real eigenfunction and a real frequency

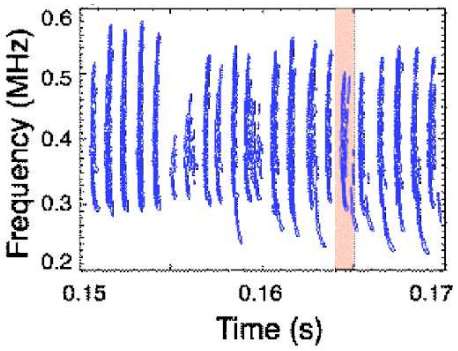


Figure 6.1: Frequency spectrum of sweeping modes measured in NSTX [126].

$\omega_{r0}$ exists, which is *perturbatively* damped and driven by wave-particle resonances. Nonlinearly, it is assumed that this linear structure is not modified, and in particular that the system remains close to the threshold linear eigenfrequency, $\delta\omega_r + i\gamma \ll \omega_{r0}$. In this case, an expansion of the form 6.4 is possible, where $\mathcal{L}_{(0)}$ contains the *linear* thermal response assumed unchanged, and $\mathcal{L}_{(1)}$ contains the damping and driving *resonant* processes, treated nonlinearly.

Moreover, when time decoupling is possible between the particle response and the wave response, as it is the case in the most basic (but most studied) version of *nonlinear trapping*, Eq. 6.4 does not even need to be expanded in the form of a time-dependent equation, or to be coupled with additional equations [55].

Such a framework is useful and can find some applicability, but it cannot catch MHD nonlinearities (see section 2.2.4) corresponding to the nonlinear modification of $\mathcal{L}_{(0)}$, strongly driven modes (EPMs) or experimental situations characterized by a strong frequency sweeping.

It is worth noting that some other approaches exist and/or could be developed: the use of a set of initial value time dependent equations [127, 63], the use of *conjugate problems* where resonances are internalized in order to avoid strong derivatives in Eq. 6.4 and make possible the use of expansions close to attractors [128], the use of alternate conservation laws, such as the conservation of potential vorticity [129] as an addition to energy conservation laws. It can indeed be expected that a single equation cannot cover all the degrees of freedom of the time evolution, in particular if an expansion of the form Eq. 6.4 is not possible.

In the following, and for this preliminary analysis of nonlinear theories, most ideas will refer to this limited kinetic perturbative framework. More precisely, our focus will be on the study of a scenario, where an energylike relation of the form

$$(\delta\omega_r + i\gamma)\ \omega_{r0}\partial_\omega \mathcal{L}_{(0)}(\omega_{r0}) = -\omega_{r0}\mathcal{L}_{i(1)} - \omega_{r0}\mathcal{L}_{h(1)} \tag{6.6}$$

is valid, where $\omega_{r0}\partial_\omega \mathcal{L}_{(0)} = \omega_{r0}\partial_{\omega_r}\mathrm{Re}\mathcal{L}_{(0)}$ is *real* and similar to the energy density defined in section 3.1.2 of a well defined linear eigenmode (MHD nonlinearities are neglected), $-\omega_{r0}\mathcal{L}_{i(1)}(\omega_{r0})$ and $-\omega_{r0}\mathcal{L}_{h(1)}(\omega_{r0})$ respectively refer to the perturbative contribution of the resonant thermal ions and hot ions.

This picture is the same as the one we developed for the linear analysis, where we simply calculated the imaginary part of the resonant contribution in section 5.2 (with the normalization 5.3) implied by the linear response of the particles. The aim is now to see how the situation is changed in the presence of a nonlinear response of the particles.

For simplicity, the results of the previous linear analysis will be referred to using simple notations

$$\begin{array}{rcl} \gamma_l & = & -\mathrm{Im}\left(\mathcal{L}_{i(1)}(\omega_{r0})\right)/\partial_{\omega_r}\mathrm{Re}\mathcal{L}_{(0)}(\omega_{r0}) > 0 \\ \gamma_d & = & +\mathrm{Im}\left(\mathcal{L}_{h(1)}(\omega_{r0})\right)/\partial_{\omega_r}\mathrm{Re}\mathcal{L}_{(0)}(\omega_{r0}) > 0 \end{array} \tag{6.7}$$

with the linear particle response included. Until now, our linear analysis simply consisted in determining the sign of $\gamma = \gamma_l - \gamma_d$.

## 6.2 Application of the nonlinear trapping theory to Beta Alfvén Eigenmodes and limits

Let us now focus on the nonlinear response of the resonating populations, in the light of the **nonlinear trapping theory**, mainly developed in Refs. [54], [130] and [55], which is currently the most used theory for the study of gap modes.

We start with a short review of it (in its most basic formulation), designed to enhance its validy limits and to set up some notation for the subsequent analysis.

### 6.2.1 The nonlinear trapping model

Let us consider a population of particles of distribution function $F$, and a perturbation which can be reduced to **one single resonance** in the particle action-angle space, that is to say to a hamiltonian of the form

$$H = H_{(0)}(\mathbf{J}) + h(\mathbf{J},t)\cos(\mathbf{n}\cdot\boldsymbol{\alpha} - \omega_{r0}t - \int dt\delta\omega_r(t)\ ) \tag{6.8}$$

where a nonlinear time evolution of the oscillation frequency $\delta\omega_r(t)$ is allowed.

Linearly, resonant particles belong to a surface defined by $\omega_{r0} = \mathbf{n}\cdot\boldsymbol{\Omega}_{(0)}(\mathbf{J}) \equiv \mathbf{n}\cdot\partial_{\mathbf{J}}H_{(0)}$. If, close to a point of the resonant curve $\mathbf{J}_R$, the Hamiltonian can be approximated by

$$H = H_{(0)}(\mathbf{J}_R) + \partial_{\mathbf{J}}H_{(0)}\cdot\delta\mathbf{J} + h(\mathbf{J}_R,t)\cos(\mathbf{n}\cdot\boldsymbol{\alpha} - \omega_{r0}t - \int dt\delta\omega_r), \text{with } \mathbf{J} = \mathbf{J}_0 + \delta\mathbf{J} \tag{6.9}$$

(the $\mathbf{J}$-dependence of $h$ needs to be low), major geometric difficulties can be locally overlooked. The dynamics is reduced to a 2D problem characterized by the variables

$$q = \mathbf{n}\cdot\boldsymbol{\alpha} - \omega_{r0}t - \int dt\ \delta\omega_r,\ \ p = \mathbf{n}\cdot\partial_{\mathbf{J}}H - \omega_{r0} - \delta\omega_r \approx \mathbf{n}\cdot\partial_{\mathbf{J}}H_{(0)}\cdot\delta\mathbf{J} - \delta\omega_r \tag{6.10}$$

which are easily seen to be conjugate variables for the Hamiltonian

$$\mathcal{H} = \frac{1}{2}p^2 - \mathsf{C}h(t)\cos q + \dot{\delta\omega}_r\ q, \tag{6.11}$$

with $\mathsf{C} = \mathbf{n}\cdot\partial_{\mathbf{J}}\boldsymbol{\Omega}_0(\mathbf{J}_R)\cdot\mathbf{n}$ the Hamiltonian curvature at resonance, in the $\mathbf{n}$-direction.

Physically, $q$ is obviously similar to an angle variable. Noticing that the variations of the action variables $\dot{\delta\mathbf{J}} = -h\sin(q)\mathbf{n}$ simply occur in one direction defined by $\mathbf{n}$ (in the action three dimensional phase-space) and could simply be described by a scalar $\delta J$ such that $\delta\mathbf{J} = \delta J\mathbf{n}$, the variable $p$ can be simply related to $\delta J$ from its definition in Eq. 6.10, $p = \mathsf{C}\delta J - \delta\omega_r$. Hence, $p$ can be seen as a measure along $\mathbf{n}$ in the action space.

In the absence of frequency sweeping $\dot{\delta\omega}_r = 0$ and for a slow time dependence of the perturbation amplitude ($h$ almost constant), Eq. 6.11 is the traditional Hamiltonian describing

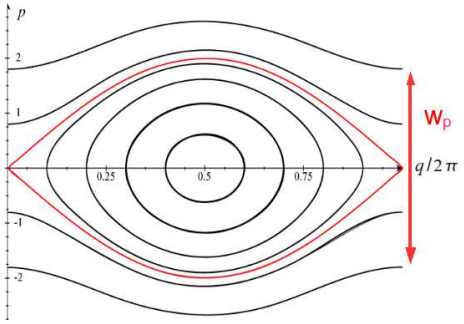


Figure 6.2: Equipotentials of the characteristic Hamiltonian of a pendulum (Eq. 6.11 without explicit time dependence)

the motion of a pendulum and leading to the creation of a **phase-space island**. Indeed, it is easy to see that under these conditions, particles are constrained to follow the energy equipotentials (the constant-$\mathcal{H}$ lines), represented in Fig. 6.2 for the Hamiltonian 6.11. This picture shows the creation of a $(q,p)$ phase-space island where some particles are trapped into the potential well created by the wave. Typical quantities describing this island can be derived from Eq. 6.11

$$\begin{array}{lrcl} \text{- the island width in the } p \text{ direction:} & w_p & = & 2\sqrt{Ch} \\ \text{- the bounce frequency of very trapped particles in the well:} & \omega_B & = & \sqrt{Ch} \end{array} \tag{6.12}$$

More generally, such a **nonlinear trapping** of the resonant particles inside the wave potential well makes sense if the typical bounce frequency of a particle inside such a well is large compared to the other typical frequencies of the problem: $\nu_{\text{eff}}$, the frequency of **diffusive processes** (collisions, turbulent diffusion...) which can decorrelate the particles from the wave dynamics, or the characteristic frequencies of the mode evolution. The latter processes include in particular the **evolution of the mode amplitude** related to $\dot{\omega_B}$ or the **rate of frequency sweeping**, related to $\dot{\delta\omega_r}$.

It is possible to be somehow more explicit, noticing that if the bounce motion is well decoupled from the other time scales, the quantity $\mathcal{J}(\mathcal{H},t) = (1/2\pi)\oint dq\, p(q,\mathcal{H},t)$, where the integral is taken along a bounce motion, is an *adiabatic invariant*, according to hamiltonian theory. This invariance of $\mathcal{J}$ can be seen as the condition to be in the nonlinear trapping regime. Calculating the time dependence of $\mathcal{J}$, it comes $\dot{\mathcal{J}} = \tau(\dot{\mathcal{H}} - \langle\dot{\mathcal{H}}\rangle)$, where $\tau = (1/2\pi)\oint dq/p$ and $\dot{\mathcal{H}} = q\ddot{\delta\omega} - (\dot{\omega_b^2})\cos q$. Hence, sufficient conditions to be in the trapping regime appear to be

$$\ddot{\delta\omega_r} \ll \omega_B^3\ , \qquad \dot{\omega_b} \ll \omega_B^2 \qquad \text{and} \qquad \nu_{\text{eff}} \ll \omega_B, \tag{6.13}$$

As a result of this trapping, the distribution function gets flat in the $p$ direction, which simply stands for the creation of a **phase-space coherent structure** (the island), as already mentionned and illustrated in Fig. 2.6. As such, resonant particles can no longer drive or damp the wave resonantly, unless some collisions destroy the coherent structure (the upper figure in Fig. 2.6), or the structure moves in phase-space, leading to the frequency sweeping (the lower figure in Fig. 2.6).

The nonlinear response of particles trapped into a potential well can be calculated from the full Boltzmann equation

$$\frac{dF}{dt} = \mathcal{Q} + \mathcal{C}\cdot F \tag{6.14}$$

where $\mathcal{Q}$ is again a source, and we choose to include $\mathcal{C}$ any background dissipative process which can break the island structure (not only collisions). Note that contrary to linear theories, where these dissipative effects are usually neglected ($\nu_{\text{eff}} \ll \gamma_L, \gamma_d \sim \omega_B$), nonlinear theories require their consideration, because nonlinear trapping can reduce driving and damping rates to the same order as dissipative processes.

Such a calculation has been done in Ref. [55] **for a driving resonant species, and introduced in a perturbative energylike relation of the form 6.6, where a fixed damping rate $\gamma_d$ was considered**, with the additional assumption that dissipative effects are negligible in the computation of the linear drive which is correct for

$$(\partial_p F_{(0)}/F_{(0)})^{-1} \gg \nu_{\text{eff}}, \tag{6.15}$$

following Ref. [54]. This calculation shows that the drive is modified nonlinearly and depends on both $\nu_{\text{eff}}$ and $\delta\omega_r$. **Different saturation regimes have been identified:**

- **A simple saturation at the given frequency** occurs when $\nu_{\text{eff}}$ is "large enough". Such saturation mechanisms are well known in plasma physics and result from a nonlinear reduction of the linear drive $\gamma_l$.

  The corresponding reduction factors have been calculated explicitely for different dissipative processes [54, 81]:

  | | | |
  |---|---|---|
  | $\rightarrow$ if $\mathcal{Q} + \mathcal{C} \cdot F$ | $= -\nu(F - F_{(0)})$ is a Krook operator, | $\nu_{\text{eff}} = \nu$ |
  | then | $\gamma_l$ is nonlinearly replaced by | $2.0\ \nu^* \gamma_l$ |
  | $\rightarrow$ if $\mathcal{Q} + \mathcal{C} \cdot F$ | $= -D_p \partial_{pp}(F - F_{(0)})$ is a diffusive operator, | $\nu_{\text{eff}} = 2D_p/w_p^2$ |
  | then | $\gamma_l$ is nonlinearly replaced by | $3.5\nu^* \gamma_l$ |

  where $\nu$ in the Krook operator is a collision frequency, whereas $D_p$ stands for a diffusion coefficient along the $p$ coordinate, and $\nu^* = \nu_{\text{eff}}/\omega_B \ll 1$ for nonlinear trapping theories to apply.

  Note that **the calculation of the limit $\nu^* \rightarrow 1$ is also tractable**, and it is a classical results of *neoclassical theory*. When $\nu^*$ becomes large, it can be shown that $\gamma_l$ is nonlinearly conserved. In other words, **the "reduction factor" is equal to 1.** [81]. In the following, we will refer to this limit as the **quasi-linear regime**, but this terminology should not be mixed with the quasilinear approximation used in turbulence studies, where the quasilinear regime refers a to regime where several islands overlap such that a stochastization of the particle trajectories is reached. Nevertheless, in analogy to the latter regime, "our" quasi-linear approximation assumes the existence of a **decorrelation process** which is faster than the trapping frequency ($\nu$ in this case, turbulent diffusion in the case of the the other regime).

- **A sweeping of coherent structure associated to a frequency sweeping** occurs at low $\nu_{\text{eff}}$ [55], with a characteristic time evolution $\propto \sqrt{t}$.

- **Intermediate oscillatory, chaotic, or excitation-relaxation regimes** have also been prediced and identified numerically [131, 130, 132].

Finally, the nonlinear trapping model displays several interesting behaviors, which are thought to reproduce several experimental observation of gap modes [22]. Nevertheless, it is useful to keep in mind some of its validity limits: the consideration of **one single resonance**, and the necessity for the **perturbation to be smoothly dependent on the equilibrium invariants** in Eq. 6.9, and finally the necessity of a **time scale separation between the kinetic nonlinear response of resonant particles and the wave time evolution** (Eqs. 6.13).

### 6.2.2 Application to Beta Alfvén Eigenmodes

Let us determine the relevant resonances and time scales involved in the dynamics of Beta Alfvén Eigenmodes, to determine the validity of the nonlinear trapping model.

In the following, we look at the case of energetic and thermal ions separately, neglecting in a first approximation their non-resonant response.

#### Resonance with energetic ions

*Linearly*, we know from the previous chapters that the resonant behavior of particles can be described by the resonant Lagrangian Eq. 5.2. For energetic ions, we already explained in section 5.1.2 that it makes sense to focus on one single resonance given by $(\mathsf{n}_1 = 0, \mathsf{n}_2 = 0, \mathsf{n}_3 = \mathsf{n})$. Keeping this single term only and recalling that $\mathcal{E}_\omega = 0$ in the MHD region where resonance with energetic ions is effective, the particle resonant response is seen to be the same as the one derived from the equivalent perturbed Hamiltonian

$$\tilde{h}_h = -\int \frac{d\alpha_1}{2\pi} \int \frac{d\alpha_2}{2\pi} \int \frac{d\alpha_3}{2\pi} \left( e_h \frac{\mathbf{v}_{gh} \cdot \nabla \psi_\omega}{-i\omega} \right) e^{-i\mathsf{n}_3 \alpha_3}. \tag{6.16}$$

With this single resonance considered, the problem is reduced to the form of Eq. 6.8.

*Nonlinearly*, we assume that Eq. 6.8 is still valid, such that the previous analysis can be applied. This implies in particular that we consider the linear structure of the wave to be conserved nonlinearly, or in other words that we neglect MHD nonlinearities. With this assumption and following the nonlinear trapping model described above, an island is formed in the 2D plane $(q = \mathsf{n}\alpha_3, p = \mathsf{n}\Omega_{h,d} - \omega_{r0} \approx \mathsf{C}_h e_h \delta\Psi)$, that is, approximately in the **radial direction**. Hence, the relevant frequencies associated with this behavior and a typical value of the resonance invariants $\mathbf{J}_R$,

$$\begin{aligned}
\omega_{Bh}^2 &= \mathsf{C}_h \tilde{h}_h(\mathbf{J}_R) \\
&\quad \text{with the curvature } \mathsf{C}_h = \mathsf{n}^2 \partial_{J_3} \Omega_{h,d}(\mathbf{J}_R) \sim \frac{\mathsf{n}^2 q}{e_h r B_0} \frac{1}{L_{Th}} \Omega_{h,d}(\mathbf{J}_R), \\
&\quad \text{and the perturbed Hamiltonian calculated in Appendix E.12} \\
&\quad \tilde{h}_h(\mathbf{J}_R) = e_h \psi_\omega^{\mathsf{m}}(\mathbf{J}_R). \\
\nu_h^{\text{eff}} &= \frac{1}{2} \frac{D_{ph}}{(w_{ph}/2)^2} = \frac{1}{2} \frac{D_{ph}}{\omega_{Bh}^2} \sim \frac{1}{2} \frac{D_0}{\omega_{Bh}^2} \frac{(\mathsf{n}\Omega_{h,d})^2}{L_{Th}^2}
\end{aligned} \tag{6.17}$$

with $D_0$ the **spatial diffusion** coefficient $(m^2 s^{-1})$, $L_{Th}$ a typical gradient of the equilibrium fast ion population.

#### Resonance with thermal ions

We can make a similar assessment for the thermal ions. In this case, several resonances can be of importance, and we kept the two resonances of the form $\omega = \pm v_\parallel / qR_0$ in the linear computation of Landau damping. The previous framework assumes these two resonances to be well separated in phase space, such that they can be considered one by one. Taking for example the resonance of the form $\omega = v_\parallel / qR_0$, or $(\mathsf{n}_1 = 0, \mathsf{n}_2 = \mathsf{m} + 1, \mathsf{n}_3 = \mathsf{n})$, the equivalent Lagrangian can be derived from Eq. E.20 of the appendices. If we choose to expand the perturbed hamiltonian around the point representing purely passing particles $(\mu = 0)$ and at the location where Landau damping is stronger, that is at the mode resonant surface, it comes

$$\tilde{h}_i(\mathbf{J}_R) = e \left( \frac{1}{2} \left( \frac{\omega q R_0}{v_{ti}} \right)^2 + \tau_e \right) \left( \frac{v_{ti}}{R_0 \omega} \right) \rho_i \partial_r \psi_\omega^{\mathsf{m}} \quad . \tag{6.18}$$

Let us calculate the Hamiltonian curvature $\mathsf{C}_i$ at this point. For passing particles and in the large aspect ratio limit, the equilibrium motion invariants 2.32 can be approximated by

$$\begin{array}{ll} \Omega_2 \approx \frac{v_\parallel}{qR_0}, & J_2 \approx e\Phi(\Psi), \\ \Omega_3 \approx \frac{v_\parallel}{R_0}, & J_3 = e\Psi + m_i R_0 v_\parallel = e\Psi(J_2) + m_i R_0 v_\parallel \ . \end{array} \tag{6.19}$$

The Hamiltonian curvature at this point follows

$$\mathsf{C}_i = \mathbf{n}\cdot\partial_{\mathbf{J}}(k_\parallel^{\mathsf{m}+1} v_\parallel) = \frac{(k_\parallel^{\mathsf{m}+1})^2}{m_i} - \frac{(\mathsf{m}+1)}{m_i q^2 R_0^2}\,\frac{\mathsf{m}+1}{r} sqR_0 \frac{\rho_i}{r}\frac{\omega q R_0}{v_{ti}} \approx \frac{1}{m_i q^2 R_0^2}\ , \tag{6.20}$$

where the different quantities need to be assessed at the resonant surface $r_s$, corresponding to the direction of the new canonical system of coordinates $(q, p = \mathsf{C}_i\delta J)$. More precisely, coming back to the *natural* space-velocity space, and making an expansion around the resonant point $\mathbf{J}_R$ using Eqs. 6.19, $\mathbf{J} = \mathbf{J}_R + \delta J\mathbf{n}$, we can relate the $\delta J$ variations to the variations of the more natural variables $\delta r$ and $\delta v_\parallel$

$$\frac{\delta r}{a} = -\frac{q}{r^2 eB_0}\delta(e\Psi) = -\frac{q}{r^2 eB_0}\left(-\frac{\mathsf{n}_2}{q(J_2)}\delta J\right) = \frac{\mathsf{m}+1}{r^2 eB_0}\,\delta J \tag{6.21}$$

$$\frac{\delta v_\parallel}{v_{ti}} = \frac{\delta(m_i R_0 v_\parallel)}{m_i R_0 v_{ti}} = \frac{1}{m_i R_0 v_{ti}}\left(\mathsf{n}_3 + \frac{\mathsf{n}_2}{q(J_2)}\right)\delta J = \frac{1}{m_i R_0 v_{ti}}\frac{1}{q}\delta J \tag{6.22}$$

It follows that the direction described by $p = C\delta J$ has components both in the *radial* and *velocity* directions. Nevertheless, at the typical macroscales involved, the **alignement along the velocity direction dominates**.

We can now display the characteristic frequencies involved. In velocity space, **collisions** are the relevant dissipative process. It comes

$$\omega_{Bi}^2 = \left(\frac{v_{ti}}{qR_0}\right)^2 \frac{h_i(\mathbf{J}_R)}{T_i}$$

$$\nu_i^{\text{eff}} = \frac{1}{2}\frac{D_{pi}}{(w_{pi}/2)^2} = \frac{1}{2}\frac{D_{pi}}{\omega_{Bi}^2} \sim \frac{1}{2}\nu_{ii}\frac{v_{ti}^2}{q^2R_0^2}\,\frac{1}{\omega_{Bi}^2}$$

with $\nu_{ii}$ is the ion-ion collision frequency.

### Numerical application

Let us assess these various frequencies for Tore-Supra relevant parameters for the type of shots described in chapter 5: $R_0 = 2.45$m, $R_0/L_{ph} = 30$, and the mode structure is assumed to verify $\xi \sim 1$mm (the MHD displacement), $\rho_i k_r \sim (\rho_i k_\theta)^{1/4}$ in the inertial region, $\omega_{r0}/2\pi \sim (v_{ti}/R_0)/2\pi \sim (v_{ti}/qR_0)/2\pi \sim 5.10^4$ Hz.

For the dissipative processes, we take a background spatial diffusion of $D_0 = 0.1\text{m}^2\text{s}^{-1}$ and a collision frequency $\nu_{ei} = 10Hz$. It comes

$$\text{For energetic ions: } \frac{2\pi}{\omega_{Bh}} \sim 2.10^{-4}s, \quad \nu_h^* = \frac{\nu_h^{\text{eff}}}{\omega_{Bh}} \sim 0.02 \tag{6.23}$$

$$\text{For thermal ions: } \frac{2\pi}{\omega_{Bi}} \sim 1.10^{-4}s, \quad \nu_i^* = \frac{\nu_i^{\text{eff}}}{\omega_{Bi}} \sim 0.3 \quad \text{if } \rho_i k_\theta \sim 0.01 \tag{6.24}$$

$$\frac{2\pi}{\omega_{Bi}} \sim 6.10^{-5}s, \quad \nu_i^* = \frac{\nu_i^{\text{eff}}}{\omega_{Bi}} \sim 0.02 \quad \text{if } \rho_i k_\theta \sim 0.001 \tag{6.25}$$

### 6.2.3 Validity analysis

From the previous paragraph, the consideration of **one single resonance** fully makes sense for the energetic ions, and it seems reasonable to separate the two resonances defined by $v_\parallel = \omega_{r0} q R_0$ and $v_\parallel = -\omega_{r0} q R_0$. Indeed, a breaking of the latter condition would mean that the thermal ion population is strongly modified by Landau damping, and we could expect the nonlinear eigenmode to have much stronger nonlinear features (not the long-lived stable frequency oscillations observed in Tore-Supra).

Moreover, the condition of **nonlinear trapping** seems valid for both the resonant energetic ions and the resonant thermal ions. First, $\nu_h^*, \nu_i^* \ll 1$. Secondly, the nonlinear time scale evolution which could possibly compete with the trapping frequencies $\omega_{Bi}$ and $\omega_{Bh}$ needs to be faster than $10^{-4}s$, and we did not observe such very fast time scale evolutions in our experiments.

These remarks seem to advocate for the use of the nonlinear trapping model, and it may be tempting to apply the results briefly outlined above. However some caution is necessary for the study of BAEs:

- The local expansion around $\mathbf{J}_R$ in Eq. 6.9 may be questionned, because it implies the disappearing of some geometry, and in particular the complete access to the mode radial structure.

  For energetic ions which resonate with the mode in the BAE MHD region (characterized by smooth radial gradients), this may not be an issue. For resonant thermal ions, which mainly resonate in the BAE inertial layer, the equivalent Hamiltonian is proportional to $\rho_i \partial_r \psi_\omega^{\mathsf{m}}$ (see Eq. 6.18) and strongly varies in the inertial region, to match the smoother MHD region. In particular, if a radial component of the perturbed hamiltonian needs to be kept, a coupling of several dimensions occurs: the problem can not be reduced to 2 dimensions only.

  Note that a response to this argument could be that a smoother structure can be expected for the mode in the nonlinear regime (either due to MHD nonlinearities or resonant flattening...) than the one described in chapter 4. Such argument may be relevant, but it does not allow a direct application of the above theory.

- We claimed the validity of nonlinear trapping based on the remark that Tore-Supra experiments did not display fast dynamics, such as fast sweeping.

  However, some other regimes could be possible where the nonlinear distortion of the energetic particle drive is so strong that sweeping occurs on time scales of the order of the bounce frequency, as claimed in Ref. [63].

- So far, the kinetic nonlinear saturation of Alfvén gap modes has been mainly studied using a fixed damping $\gamma_d$, such that saturation occurs due to the reduction of the kinetic resonant drive only. For BAEs, which are both *damped* and *driven* via resonant processes, it may be interesting to determine the effects of a simultaneous nonlinear evolution of drive and damping.

- Finally, it has to be noted that most of the current results concerning the nonlinear saturation of modes driven by fast particles, have been derived in the perturbative framework, described in 6.1. It is in particular true for the different saturation regimes outlined at the end of subsection 6.2.1, though some efforts are currently done to avoid this approximation [127].

This perturbative framework gives sense to the artificial separation between the main bulk of the thermal ions made in Eq. 6.6, and the assumed small group of resonant damping thermal ions (thought to be negligible for the mode linear structure). However, should the validity of this framework break, new regimes could be found and a strong impact on the BAE structure may be expected because of the possibility of resonance with thermal ions.

In the next two sections, we attempt to provide some response to the last two points.

## 6.3 Effects of a self-consistent nonlinear damping

### 6.3.1 Motivation: the possibility of subcritical behaviors

The most simple resonant saturation mechanism described by the nonlinear trapping theory with a fixed damping $\gamma_d$, relies on the idea that the linear drive is *nonlinearly* subject to a **reduction**:

$$\gamma_l \rightarrow c_0 \nu_l^* \gamma_l \qquad \text{with } c_0 \text{ a multiplying factor of order 1,} \tag{6.26}$$

where $\nu_l^* < 1$ is a decreasing function of the mode amplitude. We indicated in subsection 6.2.1 that $\nu_l^*$ could be calculated as a function of the driving species bounce frequency $\omega_{Bl}$ ($l$ is used here to refer to the driving species) which can be seen as a measure of the mode amplitude, $\omega_{Bl} = \sqrt{C_l h_l}$.

Hence, above the linear threshold $\gamma_l > \gamma_d$, saturation can occur for the amplitude $\omega_{Bl}$ verifying $c_0 \nu_l^*(\omega_{Bl})\gamma_l = \gamma_d$.

If damping is no longer taken fixed, but assumed to result from a resonant process as well, we may wonder if a similar reduction factor $\nu_d^*$ also applies for the damping, and if, in this case, saturation is still possible.

The existence of these nonlinear reduction factors rises in particular the question of the possibility of **subcritical modes**. Indeed, if $\nu_l^* > \nu_d^*$, one may question the existence of linearly stable modes $\gamma_l < \gamma_d$ which become unstable nonlinearly, ie: $\nu_l^* \gamma_l > \nu_d^* \gamma_d$, because of the nonlinear reduction of the damping rate.

If such subcritical modes exist and correspond to the explanation given above, they should be considered an issue for the stability of BAEs. Indeed, our rough computation of the reduction factors corresponding to ion Landau damping and hot ion drive (in subsection 6.2.2) returned

$$\nu_d^* = \nu_i^* \sim \nu_h^* = \nu_l^* \tag{6.27}$$

which suggests that subcritical behaviors could be relevant to experimental conditions for some particular range of parameters.

In the following, we verify the possibility of a subcritical activity using a simple electrostatic 2D numerical model, and compare the behavior of these modes with the idea of distinct reduction factors developed above. Our focus will be on the behavior of subcritical modes with a well defined frequency, characterized by a "simple saturation". Such modes will be referred to as **metastable modes**, and may be relevant to Tore-Supra experiments.

As will be obvious from the simulations to be presented, subcritical regimes characterized by a sweeping/chirping oscillation frequency also exist. They will be studied in a different PhD work.

### 6.3.2 Model

#### The Bump On Tail (BOT) problem and its analogy to the BAE problem

In order to get some insight into the simultaneous nonlinear evolution of two competing resonant phenomena, we make use of a simple variation of the traditional **electrostatic 2D Bump-on-Tail (BOT) problem** [50], **to which we add a self-consistent resonant damping**.

The 2D electrostatic BOT problem is a model for an electroneutral plasma, where an electron population characterized by an equilibrium small bump in velocity space (see the red curve in Fig. 6.3) is computed using the 2D Boltzmann equation, whereas the ion population is considered fixed. In such plasmas, waves oscillating at the **electron plasma frequency**

$$\omega_{pe} = \sqrt{n_e e^2/(m_e \epsilon_0)}, \tag{6.28}$$

the so-called Langmuir waves can develop, and the velocity bump can provide a linear resonant drive for them if resonance occurs in the positive slope of the bump. In order to model the competition of two resonant mechanisms, we take advantage of a similar model with a population presenting a bump on tail ($F_1$), and add a second species ($F_2$) to this picture, intended to present a negative slope at the localization of resonance in order to provide damping (the blue curve in Fig. 6.3). The idea is to substitute the BAE problem by a simpler 2D problem, with the correspondence

$$\begin{array}{lcl} \text{BAE} & \rightarrow & \text{Langmuir wave} \\ \text{Energetic particles} & \rightarrow & \text{Bump of the first population} \\ \text{Damping thermal ions} & \rightarrow & \text{Second populationBump of first population.} \end{array} \tag{6.29}$$

More precisely, we make use of two populations of particles of distribution functions $F_1$ and $F_2$ modelled using 2D Boltzmann equations with simple Krook collision operator, and related using Poisson equation for the computation of the electrostatic field:

$$\begin{array}{l} \partial_t F_1 + v\partial_x F_1 + (e_1 E/m_1)\ \partial_v F_1 = -\nu_1 (F_1 - F_{1(0)}), \\ \partial_t F_2 + v\partial_x F_2 + (e_2 E/m_2)\ \partial_v F_2 = -\nu_2 (F_2 - F_{2(0)}), \\ -\partial_x E = (1/\epsilon_0) \int dv\ [e_1 (F_1 - F_{1(0)}) + e_2 (F_2 - F_{2(0)})], \end{array} \tag{6.30}$$

and we assume the first population to present a bump $F_{1(0)}$.

Why is this reduced 2D problem relevant to the BAE problem? Under the approximation of the nonlinear trapping theory developed above, we know that the BAE model can be reduced to a 2D Boltzmann equation for each of the two resonant species involved. Next, their contribution to the wave can be taken into account using an energylike equation, which is nothing but an expression of Maxwell equation. Hence, the problem presented above makes sense for the BAEs as well (even if the two resonant processes at stake do not take place in the same phase-space direction), as long as no interaction between the two populations involved is needed outside of Maxwell equations (for example, collisions between the two populations). The Hamiltonian curvature, $\mathsf{C}_s = k^2/m_s$ in the electrostatic problem (for a wave number $k$ and a species $s$), simply needs to be replaced by the BAE relevant curvatures, and the Krook collision frequency by the relevant dissipative processes $\nu_{\text{eff}}$ given earlier in subsection 6.2.2.

A weaker feature of this model is that we chose to fully separate the damping mechanism from the bulk (in order to recover the traditional features of the fixed $\gamma_d$ model), whereas the thermal ions are the damping species in the case of BAEs. In a perturbative approach (where the resonant thermal ions are not assumed to contribute significantly to the wave structure itself) however, such a separation makes some sense.

### Numerical implementation

The model 6.30 was implemented using the **CALVi** plateform developed by the INRIA-Calvi Team, which gathers several pre-compiled Fortran routines behind a Python interface, designed to offer multiple schemes to solve the 2D Vlasov equation [133].

Simarly as in Ref. [132], we can notice that taking some reference quantities $n_0, T_0, e_0, m_0$ ($T_0$ a temperature of the order of the bulk plasma, $n_0$ a density of the order of the bulk density, $m_0 = m_1, e_0 = e_1$) and using the normalized variables

$$\begin{array}{lllllllllll} x & \to & (x/\lambda_{D0}) & , & t & \to & \omega_{p0}t & , & v & \to & v/V_0 \\ F_i & \to & (V_0/N_0)F_i & , & n_s & \to & n_s/N_0 & , & \omega_{ps} & \to & \omega_{ps}/\omega_{p0} \\ E & \to & \sqrt{\epsilon_0/(N_0T_0)}\,E & , & \nu_1 & \to & \nu_1/\omega_{p0} & & & & \end{array} \tag{6.31}$$

$$\text{with } \lambda_{D0} = \sqrt{\epsilon_0 T_0/(n_0 e_0^2)}, V_0 = \sqrt{T_0/m_0}, \omega_{p0} = \sqrt{n_0 e_0^2/(m_0\epsilon_0)} \tag{6.32}$$

(some reference Debye length, thermal velocity and plasma frequency),

the BOT problem can be rewritten with typical quantities of the order of 1. Such normalizations were used in the code and in the results displayed below.

Finally, the implemented model is the following

$$\partial_t F_1 + v\partial_x F_1 + E\partial_v F_1 = -\nu_1(F_1 - F_{1(0)}) \tag{6.33}$$

$$\partial_t F_2 + v\partial_x F_2 + \left[\frac{e_2}{e_1}\right]\left[\frac{m_1}{m_2}\right] E\partial_v F_2 = -\nu_2(F_2 - F_{2(0)}) \tag{6.34}$$

$$-\partial_x E = \int dv(F_1 - F_{1(0)}) + \frac{e_2}{e_1}\int dv(F_2 - F_{2(0)}) \tag{6.35}$$

with equilibrium distribution functions of the form

$$\text{with } F_{1(0)}(v) = \frac{n_\text{b}}{\sqrt{2\pi}v_{tb}}\exp\left[-\frac{1}{2}\left(\frac{v}{v_{tb}}\right)^2\right] + \frac{n_\text{l}}{\sqrt{2\pi}v_{tl}}\exp\left[-\frac{1}{2}\left(\frac{v-v_0}{v_{tl}}\right)^2\right] \tag{6.36}$$

$$F_{2(0)}(v) = \frac{n_d}{\sqrt{2\pi}v_{td}}\exp\left[-\frac{1}{2}\left(\frac{v}{v_{td}}\right)^2\right] \tag{6.37}$$

and the possibility to enforce an initial perturbation of the first species, of amplitude $\alpha$ and wave number $k$

$$F_1(x, v, t = 0) = F_{1(0)}(v)(1 + \alpha\cos(kx)). \tag{6.38}$$

Noticing that the problem could in fact be devided into three species, the bulk $b$, the driving species $l$ and the damping $d$ species, the alternate notation $\nu_b = \nu_l = \nu_1$, $\nu_d = \nu_2$ $e_d/e_l = e_2/e_1$, $m_d/m_l = m_2/m_1$, is used from now on.

### The adiabatic/perturbative approximation

In order to allow for some analytic comparisons of the simulated results with the ideas developed in subsection 6.3.1, a simple **perturbative approach** is used in the following, and the bulk plasma is taken to be fully **adiabatic** in order to avoid any ambiguity on the species responsible for the mode damping. More precisely, we take $n_b \gg n_l \sim n_d$, and $kv_{tb} \ll \omega_{pb}$, where $\omega_{pb}$ is the normalized plasma frequency of the bulk species. Such approximations are illustrated in Fig. 6.3 and allow for a non-ambiguous definition of the linear drive $\gamma_L$ and damping $\gamma_d$.

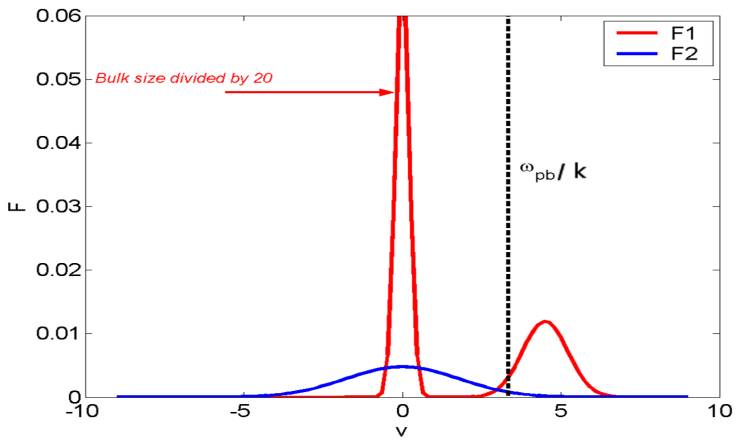


Figure 6.3: Shape of the equilibrium distribution functions, for typical parameters of the simulations. More precisely, the fixed parameters of q. 6.43 are used with $n_d = 0.03$.

As an addition, we consider limited dissipations $\nu_b = \nu_l \ll \omega_{bp}, (k\partial_v F_{l(0)}/F_{l(0)})^{-1}$ $\nu_d \ll (k\partial_v F_{d(0)}/F_{d(0)})^{-1}$.

The calculation of the particle linear responses from the linear expansion of Boltzmann equations 6.33, 6.34 for perturbation of frequency $\omega$ and wave number $k$, and their introduction in Poisson equation 6.35 is a tractable problem which returns the general dispersion relation

$$-k^2 = \sum_{s=b,l,d} \frac{\omega_{ps}^2}{v_{ts}^2} \left(1 + \frac{\omega + i\nu_s - \delta_{s=l}\ kv_0}{\sqrt{2}\ kv_{ts}}\right) Z\left(\frac{\omega + i\nu_s - \delta_{s=l} kv_0}{\sqrt{2}\ kv_{ts}}\right). \tag{6.39}$$

where $Z$ is the plasma dispersion function, also called the Fried Et Conte function and already defined before Eq. 5.11.

In general however, it is not possible to define independently the linear drive $\gamma_l$ and the linear damping $\gamma_d$, because the addition/removal of a non-perturbative species can significantly modify the oscillation frequency, and hence of the localization and rate of resonant energy transfers. In the perturbative adiabatic framework, this is possible. When the bulk density dominates, the dispersion relation is almost real. At the lower order, the adiabatic approximation $\omega \gg kv_{tb}$ associated to the limited dissipation returns:

$$\omega^2 = \omega_{pb}^2. \tag{6.40}$$

To the next order, the bump is clearly found to induce a drive, and the second species a damping. Assessing the first order modification of $\gamma$ implied by the introduction of these two species, it comes

$$\gamma_l = \frac{-1}{2}\frac{\omega_{pb}}{k^2}\left(\frac{\omega_{pl}^2}{v_{tl}^2}\right)\left(1 + \frac{\omega_{pb} - kv_0}{\sqrt{2}kv_{tl}}\right) \mathrm{Im}Z\left(\frac{\omega_{pb} - kv_0}{\sqrt{2}kv_{tl}}\right) \tag{6.41}$$

$$\gamma_d = \frac{-1}{2}\frac{\omega_{pb}}{k^2}\left(\frac{\omega_{pd}^2}{v_{td}^2}\right)\left(1 + \frac{\omega_{pb}}{\sqrt{2}kv_{td}}\right) \mathrm{Im}Z\left(\frac{\omega_{pb}}{\sqrt{2}kv_{td}}\right). \tag{6.42}$$

### Fixed and free parameters

The aim of the subsequent analysis is to study the stability of the BOT problem. For that purpose, several stability diagrams are possible. In order to recover the features of the

BOT problem with a fixed damping, we choose to vary parameters which are already present there and are known to be crucial for stability as well as for the determination of the relevant saturation regime [55]: **the collisionality of the first species** $\nu_1$ and **the damping rate** $\gamma_d \propto \omega_{pd}^2 \propto n_d$. An advantage of such stability diagrams is that they were already produced for the BOT with a fixed damping in Refs. [132, 134].

Consequently, in all the following simulations, we keep fixed:

$$\begin{array}{ll} \text{-the wave number,} & k = 0.3 \\ \text{-the equilibrium distribution function } F_{1(0)}, & n_b = 1.0, v_{tb} = 0.3, n_l = 0.03, \\ & v_{tl} = 1.0, v_0 = 4.5 \\ \text{-and some parameters of the damping species,} & v_{td} = 2.5, e_d/e_l = 1.0. \end{array} \tag{6.43}$$

Stability diagrams are ploted varying $\nu_b = \nu_l$ and $n_d \propto \gamma_d$, whereas the mass ratio $m_d/m_l$ and the collisionality of the damping species $\nu_d$, which are both involved in the nonlinear dynamics (as will be clear in Eq. 6.44), are changed from one stability diagram to another. Finally, to validate the metastable character of the found mode, the amplitude of the initial perturbation is also varied, and expressed in terms of $\omega_{Bb}$ in the whole description.

This independent variation of the collisionality, density, and mass may thought to be somehow artificial (in particular because these quantities are physically related). But it is justified recalling that the aim of this analysis is not to provide a better understanding of Langmuir waves, but to catch a piece of physics which may take place in different phase-space directions. In particular, $\nu$ is not simply intended to represent collisions, but any dissipative process.

### 6.3.3 Recovering the known saturation regimes of the perturbative nonlinear trapping model with a fixed damping

A first example of such type of diagram is given in Fig. 6.4 corresponding to $m_d/m_l = 2.0$, $\nu_d = 0.01$, $\omega_{Bb}(t = 0) = 0.1$. It has been represented along with the linear stability threshold, numerically derived from the numerical resolution of Eq. 6.39 using the root solver described in section 5.3.

In this picture, different regimes have been identified, also illustrated in Fig. 6.5.

- **Simple saturation regimes** correspond to field perturbations characterized by a well defined oscillation frequency, whose amplitude converges to a fixed value (see Fig. 6.5)
- **Damped modes** correspond to a decrease of the field amplitude, much below 10% of the initial amplitude.
- **Chaotic regimes** refer to behaviors characterized by some indetermination of the oscillation frequency and associated to bounces of the perturbed field amplitude (see Fig. 6.5). It includes in particular the existence frequency shifts, associated to the creation of phase-space structures (as in the spectrogram of Fig. 6.5) [55].
- **Intermediate regimes** which do not clearly fall into the previous categories have been distinguished. Most of them present an oscillatory behavior of the field amplitude, or an excitation-relaxation dynamics. Similar oscillations and excitation-relaxation phenomena have identified and explained in Refs. [131, 130].

Finally, the model presented here is found to reproduce the same regimes as those predicted in standard theories of nonlinear trapping with a fixed damping. The stability diagram presented in Fig. 6.4 reproduces the same qualitative features of the diagrams of

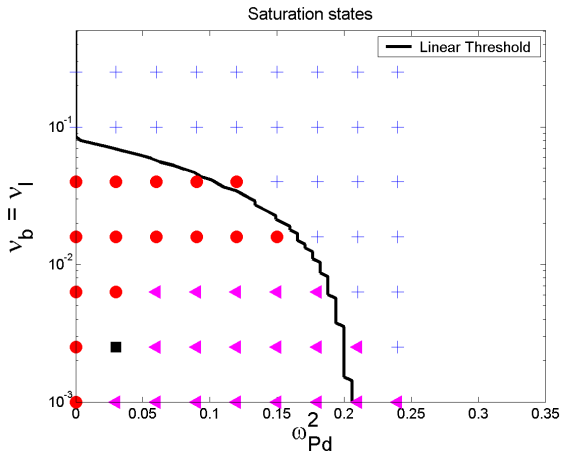


Figure 6.4: Stability diagram without metastability, obtained for the parameters $m_d/m_l = 2.0$, $\nu_d = 0.01$, $\omega_{Bb}(t = 0) = 0.1$. Four behaviors are distinguished: simple saturations (red dots), chaotic regimes (pink triangles), damped modes (blue crosses), and intermediate oscillatory behaviors (black squares).

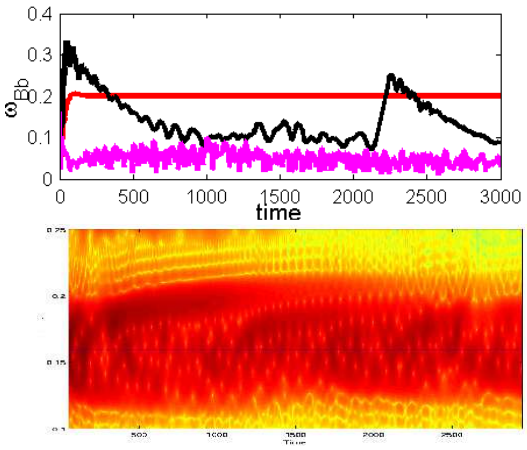


Figure 6.5: Some examples of nonlinear saturation regimes, extracted from the stability diagram Fig. 6.4. First, the field amplitude (expressed in terms of $\omega_{Bb}$) has been represented, corresponding to three different types of saturation regimes: simple saturation, chaotic behavior, or relaxation-excitation dynamics. Next, a spectrogram of the field signal is represented showing the existence of frequency sweeping at low collisionality.

Refs. [132, 134], where similar parameters have been used for species 1 (though not a fully adiabatic model in Ref. [132], and a collisionality which only applies to the bump in Ref. [134]).

From a stability point of view, modes (/pseudo modes) are mainly found inside the linear stability region, which seems to advocate for the validity of the linear analysis.

### 6.3.4 Metastability

The validity of the linear stability analysis breaks down when the characteristic parameters of the damping species are varied.

#### Existence of metastable modes

When the collisionality $\nu_d$ or the mass of the damping species $m_d/m_l$ are reduced, some modes appear outside of the linear stability regions, which can only live if the initial perturbation is large enough.

An example of such mode found for $m_d/m_l = 0.5$, $\nu_d = 0.005$, $\omega^2_{pd} = 0.21$, $\nu_b = \nu_l = 0.016$, is given in Fig. 6.6, where we represented the time evolution of its amplitude. The local-

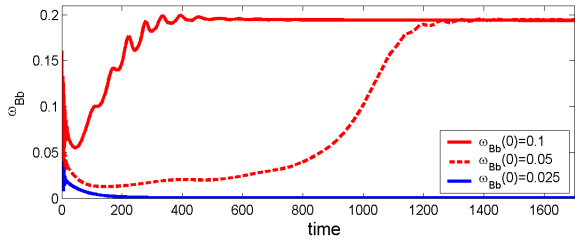


Figure 6.6: Time evolution of the amplitude of a metastable mode, for various initial conditions.

ization of this mode in a stability diagram is given in Fig. 6.7, and clearly shows that it is localized outside of the stability window. This idea is confirmed by Fig. 6.6. In this figure, the existence of the mode is seen to depend on the amplitude of the initial perturbation. In any cases, the amplitude presents an initial decreasing phase, which can be interpreted as a linear (stable) phase, and possibly grow in a later phase to reach a finite saturation level if the initial perturbation is large enough. This behavior indicates that the simulated mode is **metastable**.

The stability diagram corresponding to $m_d/m_l = 0.5$, $\nu_d = 0.005$, $\omega_{Bb}(t=0) = 0.1$, can be simulated and it is represented in Fig. 6.7. It shows the existence of several modes outside of the linear stability region. Again, when the initial perturbation amplitude is decreased,

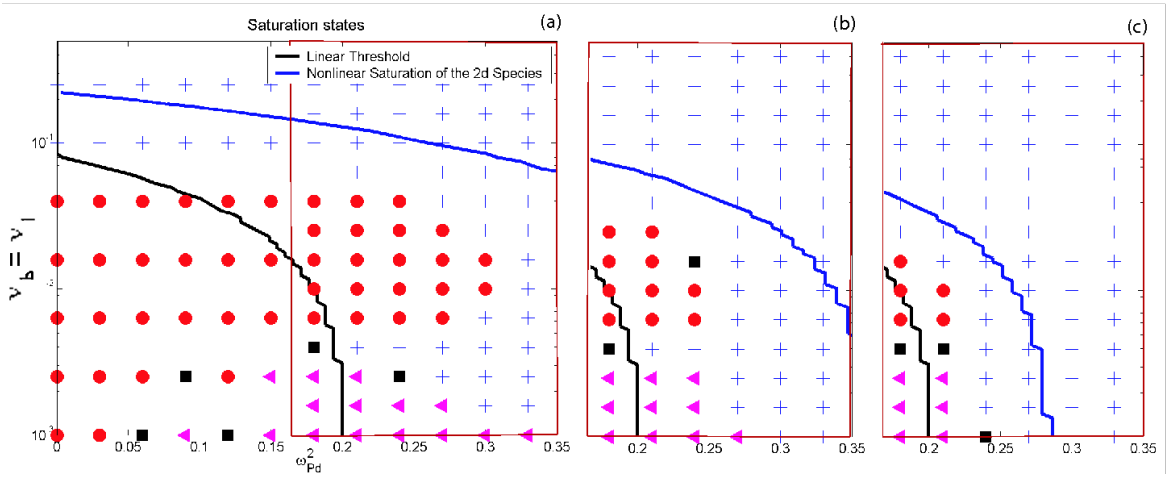


Figure 6.7: Stability diagrams corresponding to $m_d/m_l = 0.5$, $\nu_d = 0.005$, for various magnitudes of the initial perturbation: $\omega_{Bb}(t=0) = 0.1$ in Fig. (a), $\omega_{Bb}(t=0) = 0.05$ in Fig. (b), $\omega_{Bb}(t=0) = 0.025$ in Fig. (c).

these subcritical modes disappear.

More precisely, we plotted in Fig. 6.7, the curve $\omega_{Bd}(t) = -\gamma$ ($\gamma$ being the linear growth rate). If the simulated modes are metastable, a condition for their existence is that they reach the nonlinear regime. In particular, if our intuition of metastability developed in subsection 6.3.1 is correct, the damping species needs to reach the nonlinear regime to survive. A measure of the necessary time to reach the nonlinear regime is the bounce frequency $\omega_{Bd}$ (its inverse gives the necessary time for a particle trajectory to be significanlty modified by the wave). Hence, in the subcritical region (where $\gamma < 0$), the curve $\omega_{Bd}(t) = -\gamma$, gives some indication of the possibility for a mode to reach the nonlinear regime before being significanlty damped.

This curve somehow follows the boundary of the metastable region, and confirms the idea that the observed subcritical activity depends on the possibilty for the damping species to reach the nonlinear regime.

Note that the runs carried out in this analysis also clearly show the existence of subcritical chaotic behaviors. However, we will not be considering them in the following.

### Interpretation of metastability

Let us now determine if the observation of metastable modes is in agreement with the interpretation given in subsection 6.3.1, that is to say with the idea that it results from **different**

**nonlinear reduction factors**. In the following, the consequences of such an interpretation are drawn and compared with the results of 6 stability diagrams, obtained using an initial perturbation $\omega_{Bb} = 0.1$, and the 6 possible combinations of the damping species parameters: $\nu_d = 0.001, 0.005, 0.01$ and $m_d/m_l = 0.5, 2.0$.

The reduction factors $\nu_l^*$ and $\nu_d^*$ (or more precisely $2.0\nu_l^*$ and $2.0\nu_d^*$ ) can be easily calculated for the BOT problem, for which the curvature of the Hamiltonian is equal to $\mathsf{C}_s = k^2/m_s$ for a species $s$. Using $\omega_{Bb}$ as a reference amplitude, it comes

$$\nu_l^* = \frac{\nu_l}{\omega_{Bb}}, \qquad \nu_d^* = \frac{\nu_d}{\omega_{Bb}}\sqrt{\frac{m_d}{m_l}} = \frac{\nu_l}{\omega_{Bb}}\left(\frac{\nu_d}{\nu_l}\sqrt{\frac{m_d}{m_l}}\right). \tag{6.44}$$

In the framework of the nonlinear trapping theory, the role of the damping species collisionality (compared to $\nu_l$) and of the mass ratio $m_d/m_l$ which were both decreased when moving from Fig. 6.4 to Fig. 6.7 is clear: their drop leads to a smaller nonlinear reduction factor and agrees with the idea that metastability results from the nonlinear reduction of damping.

Using the perturbative framework summarized by Eq. 6.6 and the nonlinear trapping reduction, one could expect

$$\text{metastability for } \nu_l^*\gamma_l > \nu_d^*\gamma_d \qquad \text{and saturation for } \nu_l^*\gamma_l = \nu_d^*\gamma_d. \tag{6.45}$$

Unfortunately, because both sides of the latter equality are proportional to $1/\omega_{Bb}$, such a model does not lead to saturation. This is in contradiction with our simulations which clearly displayed well defined saturation levels, which could be reproduced under variations of the initial conditions (see for example the saturation levels of the two metastable modes in Fig. 6.6). This suggests that some corrections are needed.

The assessment of the reduction factors based on the simulated saturation levels for our 6 sets of parameters (and for both linearly unstable modes and metastable modes) returns $\nu_l^* \in [0, 0.25]$ and $\nu_d^* \in [0, 0.20]$. Two remarks follow.

- The computed values of $\nu_l^*, \nu_d^*$ show that the use of the nonlinear trapping model is legimate, but that some large $\nu^*$ effects play a role. In subsection 6.2, we indicated that for large $\nu^*$ (in particular for a negligible mode amplitude $\omega_{Bb} \to 0$), the resonant response almost remained linear (it is the *quasilinear response*, of "reduction factor" 1.0). Hence the idea to fit the two regimes to take into account some large-$\nu^*$ effects. This can be done making an inverse average of the multiplying factors involved in the nonlinear trapping and quasilinear regimes. In other words, a more reasonable reduction factor may be

$$\begin{array}{lll} \dfrac{2.0\nu^*}{1.0 + 2.0\nu*} & \to 2.0\nu^* & \text{for small } \nu^* \\ & \to 1.0 & \text{for a null amplitude of the mode} \end{array} \tag{6.46}$$

- In the energy balance Eq. 6.6, the contribution of the background dissipation was not considered, which is valid if the values of the driving and damping species exceed any lower background dissipation. Linearly, such an assumption can be reasonable ($\gamma_l = 0.12$ with our parameters), but this fully breaks down when moving to the nonlinear regime, where both the drive and damping are multiplied by their reduction factor $\nu^* \ll 1$.

  The effect of the bulk collisions on the energy balance Eq. 6.6 can be calculated in a simple way, noticing that they simply imply a frequency shit $\omega \to \omega + i\nu_b$ is the BOT

dispersion relation, compared to the non-collisional case. In other words, writing $\mathcal{L}_b$ the contribution of the bulk, it comes

$$\mathcal{L}_b(\omega) = \mathcal{L}_{(0)}(\omega - i\nu_b) = \partial_\omega \mathcal{L}_{(0)}(\omega_{r0})(\omega - i\nu_b - \omega_{r0}) = i\partial_\omega \mathcal{L}_{(0)}(\omega_{r0})(\gamma - \nu_b) \quad (6.47)$$

The background damping is simply given by the dissipation frequency $\nu_b$.

Finally the two previous remarks suggest a saturation for

$$\frac{2.0\nu_l}{\omega_{Bl} + 2.0\nu_l}\gamma_l = \frac{2.0\nu_d}{\omega_{Bd} + 2.0\nu_d}\gamma_d + \nu_b \qquad \text{or again,} \quad (6.48)$$

$$0.25{*}\nu_b\omega_{Bb}^2 - 0.5\left(\nu_l(-\nu_b + \gamma_l) + \nu_d\sqrt{m_d/m_l}(-\nu_b - \gamma_d)\right)\omega_{Bb} - \nu_l\nu_d(-\nu_b + \gamma_l - \gamma_d) = 0 \quad (6.49)$$

If this model is valid, the existence of saturated modes depends on the existence of positive roots for the mode amplitude $\omega_{Bb}$. The present equation is a second order equation, and we can notice that the product of its two roots is directly related to the condition for linear stability, whereas the sum of them is the same as the criterion given in Eq. 6.45 (modulo the corrections resulting from the introduction of bulk dissipation).

It follows that **linearly unstable modes can allways reach saturation**. The situation is different in the subcritical region of course. But **metastability is possible**. When solutions exists, **they are (both) positive if the generalized version of Eq. 6.45 is verified**

$$\nu_l(-\nu_b + \gamma_l) > \nu_d\sqrt{m_d/m_l}(-\nu_b - \gamma_d)) \quad (6.50)$$

In this case however, only one of the two roots is stable, as illustrated in Fig. 6.8, where we represented the nonlinear driving rate and the dissipation rate as a function of the mode amplitude. The latter stable roots are represented in Fig. 6.9 (when they exist).

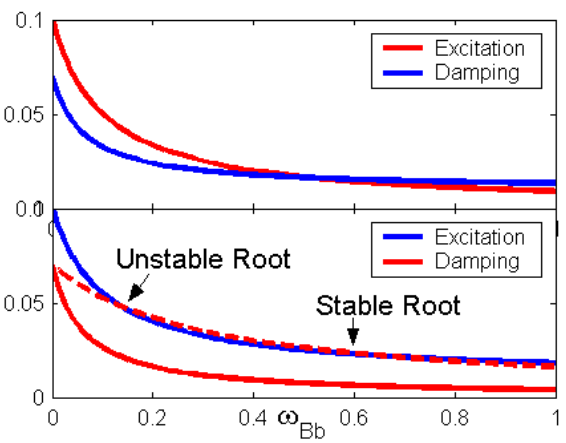


Figure 6.8: Illustration of the different situations offered by the proposed nonlinear model, which may lead to a saturation.

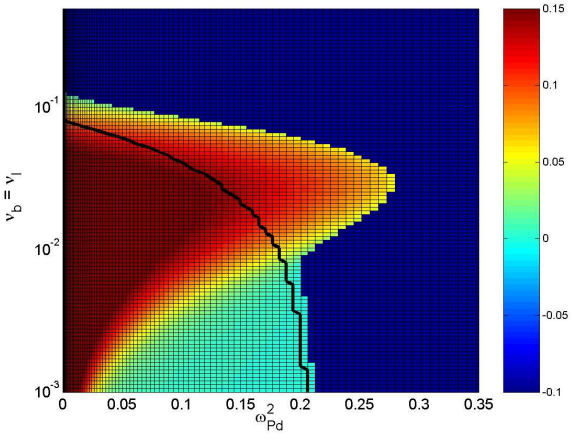


Figure 6.9: Stable saturation level predicted by the proposed nonlinear model, for the stability diagram of parameters $m_d/m_l = 0.5$, $\nu_d = 0.01$.

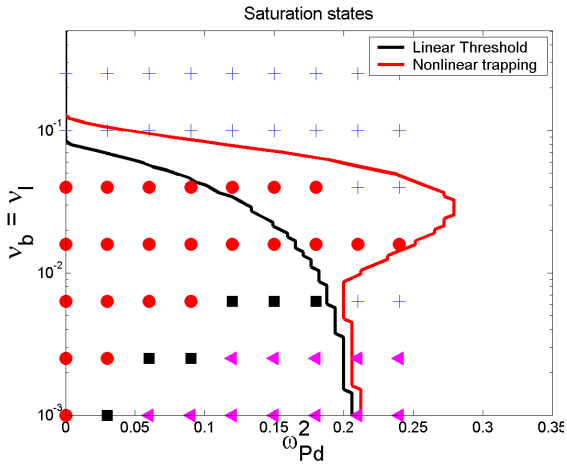


Figure 6.10: Stability diagram without metastability, obtained for the parameters $m_d/m_l = 0.5$, $\nu_d = 0.01$, $\omega_{Bb}(t=0) = 0.1$.

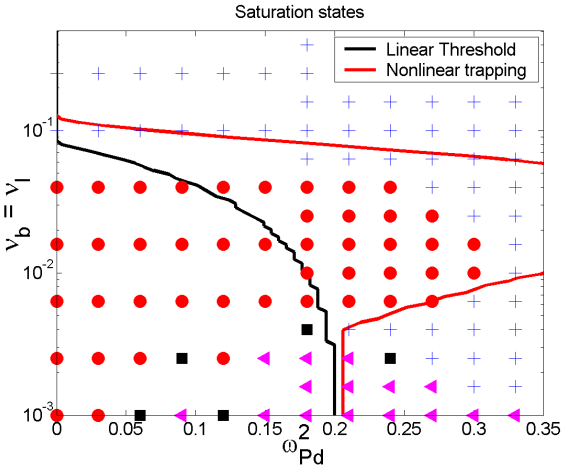


Figure 6.11: Stability diagram without metastability, obtained for the parameters $m_d/m_l = 0.5$, $\nu_d = 0.005$, $\omega_{Bb}(t=0) = 0.1$.

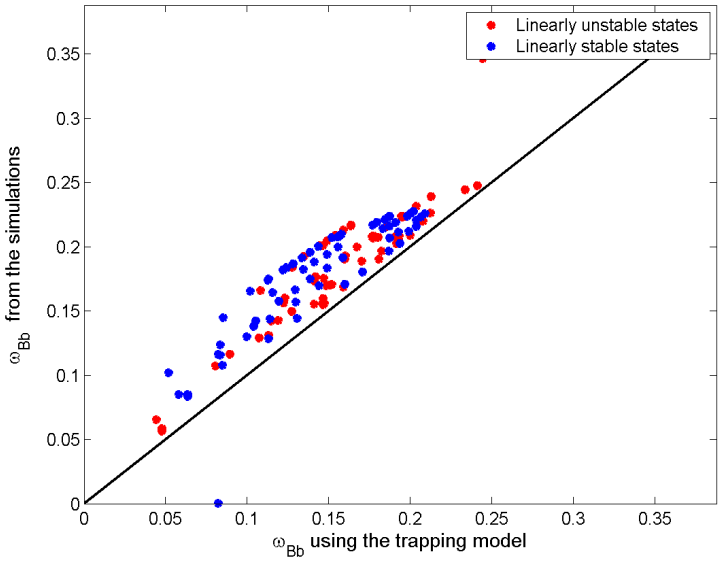


Figure 6.12: Simulated nonlinear saturation levels compared to prediction, for linearly unstable and metastable modes.

### Model verification

In the next three plots, the existence criteria (Figs. 6.10) and saturation levels (6.12 where our 6 sets of parameters are represented) derived from Eq. 6.49 are compared with the simulations.

A clear agreement appears, which confirms the possibility and relevance of metastability, due to kinetic nonlinear saturation. In particular, this study confirms that dissipative effects become particularly important in nonlinear regimes, even when they are negligible in a linear analysis.

Because of the order of magnitudes computed in subsection 6.2.2, metastability via kinetic resonant saturation should be seen as a serious candidate for the existence of subcritical

activity.

## 6.4 Breaking of the condition perturbative-adiabatic approach... towards a BAE relevant description

In this section, we simply want to make a few concluding comments on the perturbative-adiabatic approach, a lot used in past theories (which we also used in this thesis...), starting from a BAE relevant non-adiabatic run, with:

$$\begin{array}{ll} \text{A non-perturbative bump, with} & n_l = 0.15, v_{tl} = 1.0 \\ \text{A non adiabatic species - damping species, with} & m_d/m_l = 0.5, n_d = 1.0, \\ & v_{td} = 1.2 = \omega_{pd}/k, \nu_d = 0.01. \end{array} \tag{6.51}$$

and the initial condition $\omega_{Bd}(t = 0) = 0.14$. In particular, the bulk is not adiabatic $\omega_{pd}/kv_{td} = 2.7(\sim \sqrt{7/2+2})$.

In this figure, various cases corresponding to different values of the bump collisionality are represented. The time evolution of the mode amplitude is shown as well as the frequency spectrum for some of these cases, where the blue lines represent the frequency $\omega_{pb} = \omega_{pd}$.

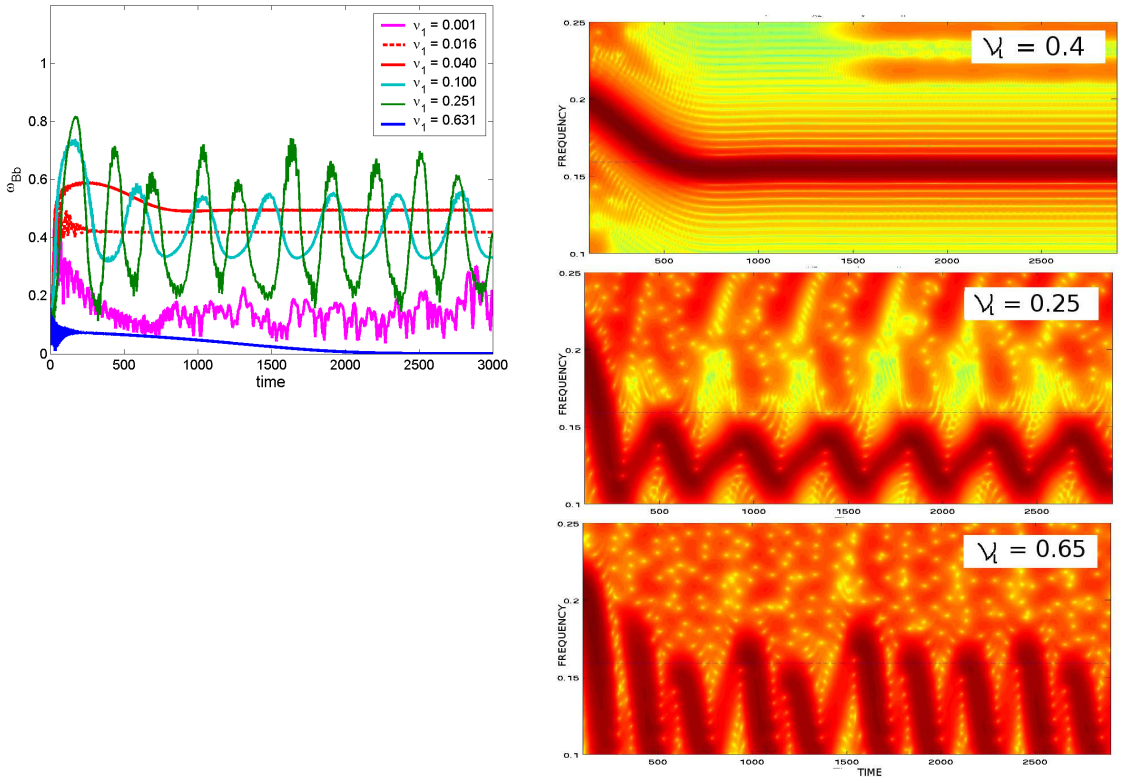


Figure 6.13: Some nonlinear states obtained from a non-adiabatic model for the bulk plasma, and for different values of the driving species collisionality.

What this set of figures shows is that moving to the non perturbative/non-adiabatic case may lead to very different saturation regimes, as the one described above, and traditionally considered in theory/experiment comparisons. The oscillatory regimes shown in these figures are different and topologically separated from the chirping or chaotic structures mentionned earlier. They seem to correspond to a cycle between two stable solutions.

A second point is that nonlinear saturation may not be such a smooth, stabilizing process, as suggested by the current the nonlinear trapping theory presented here. In this case, sweeping is clearly associated to a **growth**.

A lot remains to be understood by the author of the present manuscript. But our aim is definitely to go further in this direction. This was simply to finish with nice pictures...

## 6.5 Summary

*In this chapter, we analyzed some difficulties related to the nonlinear description of energetic particles with the attempt to catch their relevance for Beta Alfvén Eigenmodes, and we analyzed one particular problem in details: the possible existence of metastable modes due to resonant saturation.*

- *We found that the time scales involved in the modes observed in Tore-Supra were consistent with the approximations of the nonlinear trapping theory.*
- *We raised the question of a possible* **nonlinear modification of stability***, and suggested one process leading to metastable modes: the possibility for the driving and damping mechanisms at stake, to saturate at different levels, because kinetic resonant nonlinearities.*
- *We developed a 2-D model (based on pre-compiled routines), catching the kinetic features of the wave-particle interaction, to check the proposed idea of metastability.* **Simulations confirmed the proposed mechanism, both qualitatively and quantitatively***.*
- *Again, the analysis puts forward the necessity to avoid the perturbative treatment of energetic particles.*

# 7 Conclusion

One of the major scientific goals for ITER is to reach and explore the burning plasma regime, in which significant amounts of energy are generated by the DT fusion reactions. Such a regime is characterized by a large population of fusion-produced alpha particles, born with a largely suprathermal energy, 3.5 MeV. As a consequence of their interaction with the plasma, such energetic particles may not only be redistributed and lost, they can also endanger the whole plasma stability and impact on turbulence and plasma confinement properties.

In this thesis, we studied one type of interaction which can take place between energetic particles and the main plasma: **the destabilization of a meso-scale acoustic mode by energetic particles, the Beta Alfvén Eigenmode (BAE)**. For this, we made use of a framework which applies more generally to a large class of energetic particle phenomena, with an effort to keep the presentation general whenever the particular physics of BAEs was not involved.

The first part of the work was devoted to the building of the latter framework, a variational gyrokinetic framework, based on previous formulations [68]. The effort done here was to define the physical meaning of the instabilities such dispersion relation can display, offer a clean and compact formulation of the gyrokinetic equation relevant for both geometric and particle variables and appropriate for the modelling of resonant behaviors, and finally draw the link between well-established formulations used in this field: a traditional set of gyrokinetic equations used for the study of shear Alfvén waves, and the Magneto-HydroDynamic formalism. Finally, the applicability of such a variational framework to nonlinear kinetic regimes was assessed.

The second part was devoted to the characterization of BAEs, with two goals. A first goal was to determine the eigenmode properties which can be of interest in the destabilization of the mode. For this, we proposed a derivation of the BAE dispersion relation using a Fourier decomposition, and limited to a perturbative computation of transit effects, which could recover previous derivations, conducted in the so-called ballooning representation. We also calculated the BAE structure explicitely. A second goal was to distinguish BAEs from other modes belonging to the acoustic frequency range, and we showed in particular what were the similarities and differences between BAEs and the so-called Geodesic Acoustic Modes, in the light of our derivation. This analysis allowed us to identify Tore-Supra modes as BAEs.

Finally, we entered the core of the analysis in a third part, that is the problem of the destabilization of BAEs by a population of energetic particles. Such a problem can be seen as a competition between the mode thermal damping, called Landau damping, and the drive by energetic particles making necessary the determination of a threshold for BAE destabilization. We first started such a determination with a perturbative linear analysis designed to offer an intuitive understanding of the experimental tunable parameters at stake in the threshold, and we compared this analysis with experiments carried out in the Tore-Supra tokamak. The latter comparison displayed qualitative and quantitative agreement,

allowing to build some confidence in the mechanisms at stake in the BAE destabilization as well as the on the rough role of global macroscopic parameters involved. We could also provide some explanation for more detailed behaviors such as an obvious role of the shear in the destabilization. However, some caution is needed for the latter interpretations because of two aspects: the use of a perturbative approach and the apparition of a set of phenomena which cannot fit our framework, such as the frequency upshift of the BAE frequency during the course of a sawtooth period or the harder observations of BAEs at low magnetic field.

Among other interpretations, the mismatch between linear theory and experiments could be associated with a nonlinear modification of stability. In the thesis, we proposed one scenario, appropriate for BAEs, which makes possible the existence of metastable modes and we verified it numerically.

Though it can provide some intuitive, tractable understanding of the physics at stake, the most questionable feature of the thesis is the use of the perturbative approach.

In the near future, we would like to improve the linear model used in the thesis to include diamagnetic effects [124] as well as a non-perturbative treatment of Landau damping based on Ref. [41], to make a test of the relative role of each component for Tore-Supra parameters, and provide some explanations for the shift between the BAE basic formula and the experiments.

Another point which needs to be addressed, is the reason for the stable frequency behavior of BAEs in Tore-Supra, compared to other tokamak devices characterized by frequency sweeping [95], which is not fully clarified at the moment. Following the nonlinear sweeping model predicted in Ref. [55], phase-space structures associated frequency chirping occurs for negligible dissipative phenomena, and the Tore-Supra shots we conducted are indeed highly collisional. However, there may exist other situations leading to frequency sweeping. Some more analysis needs to be made for this issue.

Finally, the investigation of a nonlinear modification of stability displayed interesting and conclusive results, which could be relevant in tokamak conditions. Again, a non-pertubative treatment may be more realistic and could lead not only to a nonlinear modification of the amplitude of the driving and damping mechanisms at stake, but also to a strong modification of the mode structure itself. Also, such nonlinear effects need an experimental investigation.

On a broader scale, we can note that recent research in the field of energetic particles has definitely fallen into nonlinear studies, which are necessary for the computation of energetic particle losses. It may be important to fit in a consistant picture the different regimes considered for the nonlinear evolution: the so-called MHD nonlinearities and kinetic resonant nonlinearities, low scale and large scale chirping regimes possibly associated to a wave growth, and to add some effects of geometry, which are often overlooked.

Ideally, such studies should go in the direction of a control of the unwanted phenomena related to fast particles.

# Publications & Orals

**Publications**

• C. Nguyen, X. Garbet and A.-I. Smolyakov. Variational derivation of the dispersion relation of kinetic coherent modes in the acoustic frequency range in tokamaks, *Physics of Plasmas, 15, 1*, 2008.
• C. Nguyen, X. Garbet, R. Sabot, L.-G. Eriksson, M. Goniche, P. Maget, V. Basiuk, J. Decker, D. Elbèze, G. T. A. Huysmans, A. Macor, J.-L. Ségui and M. Schneider. Excitation of Beta Alfvén Eigenmodes in Tore-Supra, *Plasma Physics and Controlled Fusion, 51, 095002*, 2009.
• C. Nguyen, X. Garbet, V. Grandgirard and M. Lesur. On the possibility of a nonlinear modification of the stability of fast particle driven modes, *To be submitted*, 2009.
• A.-I. Smolyakov, C. Nguyen and X. Garbet. Kinetic theory of electromagnetic geodesic acoustic modes, *Plasma Physics Controlled Fusion, 50, 115008*, 2008.
• A.-I. Smolyakov, C. Nguyen and X. Garbet. Electromagnetic effects on Geodesic Acoustic Modes And Beta Alfvén Eigenmodes, *Submitted to Nuclear Fusion*, 2009.
• A. Macor, M. Goniche, J.-F. Artaud, J. Decker, D. Elbèze, X. Garbet, G. Giruzzi, G. T. Hoang, P. Maget, D. Mazon, D. Molina, C. Nguyen, Y. Peysson, R. Sabot and J.-L. Ségui. Redistribution of Suprathermal Electrons due to Fishbone Frequency Jumps, *Physical Review Letters, 102, 155005*, 2009.
• R. Sabot, A. Macor, C. Nguyen, J. Decker, D. Elbeze, L.-G. Eriksson, X. Garbet, M. Goniche, G. T. A. Huysmans, Y. Ladroit, P. Maget and J.-L. Ségui. Observation of acoustic and sub-acoustic fast particles driven modes in Tore-Supra, *Nuclear Fusion, 49, 085033*, 2009.
• X. Garbet, G. Dif-Pradalier, C. Nguyen, Y. Sarazin, V. Grandgirard and P. Ghendrih. Neoclassical equilibrium in gyrokinetic simulations, *Physics of Plasmas, 16, 062503*, 2009.

**Orals**

• American Transport Task Force workshop (Denver, 2008).
• IAEA Technical Meeting on Energetic Particles (Kiev, 2009).
• Invited to European Fusion Theory Conference (Riga, 2009).
• Invited to European Physical Society (Dublin, 2010).

# Bibliography


[1] T. H. Rider. *Fundamental Limitations on Plasma Fusion Systems Not in Thermodynamical Equilibrium*. PhD thesis, MIT, 1995.

[2] T. R. Jarboe. Review of spheromak research. *Plasma Physics and Controlled Fusion*, 36:945–990, June 1994.

[3] J. F. Lyon, G. Grieger, F. Rau, A. Iiyoshi, A. P. Navarro, L. M. Kovrizhnykh, O. S. Pavlichenko, and S. M. Hamberger. Stellerators. *Nuclear Fusion*, 30:1695–1715, 1990.

[4] H. H. Duong, W. W. Heidbrink, E. J. Strait, T. W. Petrie, R. Lee, R. A. Moyer, and J. G. Watkins. Loss of energetic beam ions during TAE instabilities. *Nuclear Fusion*, 33:749–765, May 1993.

[5] R. B. White, E. Fredrickson, D. Darrow, M. Zarnstorff, R. Wilson, S. Zweben, K. Hill, Y. Chen, and G. Fu. Toroidal Alfvén eigenmode-induced ripple trapping. *Physics of Plasmas*, 2:2871–2873, August 1995.

[6] C. Angioni, A. G. Peeters, and G. V. Pereverzev. Gyrokinetic simulation of alpha particle transport and consequences on iter transport modelling. 13th EU-US TTF Workshop and 1st EFDA Transport Topical Group meeting, 2008.

[7] D. R. Nicholson. *Introduction to Plasma Theory*. John Wiley and Sons, 1983.

[8] R. D. Hazeltine and J. D. Meiss. *Plasma Confinement*. Addison-Wesley Publishing Company, Redwood City, 2007.

[9] D. Biskamp. *Nonlinear Magnetohydrodynamics*. Cambridge University Press, 1997.

[10] A. J. Brizard and T. S. Hahm. Foundations of nonlinear gyrokinetic theory. *Review of Modern Physics*, 79:421–468, April 2007.

[11] H. Goldstein, C. P. Poole, and J. L. Safko. *Classical Mechanics*. Addison Wesley, 3rd edition, 2001.

[12] R. G. Littlejohn. Variational principles of guiding center motion. *Journal of Plasma Physics*, 29:111–125, 1983.

[13] R. B. White. *The theory of Toroidally Confined Plasmas*. World Scientific Publishing Company; 2 Revised edition, 2006.

[14] A. N. Kaufman. Quasilinear Diffusion of an Axisymmetric Toroidal Plasma. *Physics of Fluids*, 15:1063–1069, June 1972.

[15] X. Garbet. Instabilités, turbulence et transport dans un plasma magnétisé.

[16] F. Zonca, P. Buratti, A. Cardinali, L. Chen, J.-Q. Dong, Y.-X. Long, A. V. Milovanov, F. Romanelli, P. Smeulders, L. Wang, Z.-T. Wang, C. Castaldo, R. Cesario, E. Giovannozzi, M. Marinucci, and V. Pericoli Ridolfini. Electron fishbones: theory and experimental evidence. *Nuclear Fusion*, 47:1588–1597, November 2007.

[17] A. Hasegawa and L. Chen. Plasma Heating by Alfvén-Wave Phase Mixing. *Physical Review Letters*, 32:454–456, March 1974.

[18] G. Vlad, F. Zonca, and S. Briguglio. Dynamics of Alfvén waves in tokamaks. *Nuovo Cimento Rivista Serie*, 22:1–97, July 1999.

[19] A. Hasegawa and L. Chen. Kinetic processes in plasma heating by resonant mode conversion of Alfven wave. *Physics of Fluids*, 19:1924–1934, 1976.

[20] J. Vaclavik and K. Appert. Theory of plasma heating by low frequency waves: magnetic pumping and Alfvén resonance heating. *Nuclear Fusion*, 31:1945–1997, 1991.

[21] H. Grad. Plasmas. *Physics Today*, 22(12):34–36, December 1969.

[22] W. W. Heidbrink. Basic physics of Alfvén instabilities driven by energetic particles in toroidally confined plasmas. *Physics of Plasmas*, 15(5):055501–+, May 2008.

[23] K. Appert, R. Gruber, F. Troyon, and J. Vaclavik. Excitation of global eigenmodes of the Alfven wave in Tokamaks. *Plasma Physics*, 24:1147–1159, September 1982.

[24] K. Appert, J. Vaclavik, and L. Villard. Spectrum of low-frequency, nonaxisymmetric oscillations in a cold, current-carrying plasma column. *Physics of Fluids*, 27:432–437, February 1984.

[25] K. Appert, G. A. Collins, F. Hofmann, R. Keller, A. Lietti, J. B. Lister, A. Pochelon, and L. Villard. Observations of toroidal coupling for low-n Alfvén modes in the TCA tokamak. *Physical Review Letters*, 54:1671–1674, April 1985.

[26] H. L. Berk, D. N. Borba, B. N. Breizman, S. D. Pinches, and S. E. Sharapov. Theoretical Interpretation of Alfvén Cascades in Tokamaks with Nonmonotonic q Profiles. *Physical Review Letters*, 87(18):185002–+, October 2001.

[27] B. N. Breizman, H. L. Berk, M. S. Pekker, S. D. Pinches, and S. E. Sharapov. Theory of Alfvén eigenmodes in shear reversed plasmas. *Physics of Plasmas*, 10:3649–3660, September 2003.

[28] C. E. Kieras and J. A. Tataronis. The shear Alfvén continuous spectrum of axisymmetric toroidal equilibria in the large aspect ratio limit. *Journal of Plasma Physics*, 28:395–+, 1982.

[29] C. Z. Cheng and M. S. Chance. Low-n shear alfvén spectra in axisymmetric toroidal plasmas. *Physics of Fluids*, 29(11):3695–3701, 1986.

[30] H. L. Berk, J. W. Vandam, Z. Guo, and D. M. Lindberg. *Continuum damping of low-n toroidicity-induced shear Alfven eigenmodes*. September 1991.

[31] L. Chen and F. Zonca. Theory of Alfvén waves and energetic particle physics in burning plasmas. *Nuclear Fusion*, 47:727–+, October 2007.

[32] M Goniche, G. T. A. Huysmans, F. Turco, P. Maget, J. L. Segui, J. F. Artaud, G. Giruzzi, F. Imbeaux, P. Lotte, D. Mazon, and D. Molina. Identification of fast particle triggered modes by means of correlation electron cyclotron emission on Tore-Supra. *Fusion Science and Technology*, 53(1):88–96, 2008.

[33] S. M. Mahajan. Spectrum of Alfvén waves, a brief review. *Physica Scripta Volume T*, 55:160–+, 1994.

[34] C. Z. Cheng, L. Chen, and M. S. Chance. High-n ideal and resistive shear Alfvén waves in tokamaks. *Annals of Physics*, 161:21–47, April 1985.

[35] L. Chen. Theory of magnetohydrodynamic instabilities excited by energetic particles in tokamaks. *Physics of Plasmas*, 1:1519–1522, 1994.

[36] F. Zonca and L. Chen. Resonant damping of toroidicity-induced shear-Alfvén eigenmodes in tokamaks. *Physical Review Letters*, 68:592–595, February 1992.

[37] G.-Y. Fu. Energetic-Particle-Induced Geodesic Acoustic Mode. *Physical Review Letters*, 101(18):185002–+, October 2008.

[38] F. Zonca, L. Chen, and R. A. Santoro. Kinetic theory of low-frequency Alfvén modes in tokamaks. *Plasma Physics and Controlled Fusion*, 38:2011–2028, 1996.

[39] R. Betti and J. P. Freidberg. Stability of Alfvén gap modes in burning plasmas. *Physics of Fluids B*, 4:1465–1474, June 1992.

[40] P. Lauber. *Linear Gyrokinetic Description of Fast Particle Effects on the MHD Stability in Tokamaks*. PhD thesis, Technische Universität München, 2003.

[41] F. Zonca, L. Chen, R. A. Santoro, and J. Q. Dong. LETTER TO THE EDITOR: Existence of discrete modes in an unstable shear Alfvén continuous spectrum . *Plasma Physics and Controlled Fusion*, 40:2009–2021, 1998.

[42] I. Chavdarovski and F. Zonca. Effects of trapped particle dynamics on the structures of low-frequency shear Alfvén continuous spectrum. *to be published in Plasma Physics and Controlled Fusion*, 2009.

[43] M. N. Rosenbluth, S. T. Tsai, J. W. van Dam, and M. G. Engquist. Energetic Particle Stabilization of Ballooning Modes in Tokamaks. *Physical Review Letters*, 51:1967–1970, November 1983.

[44] F. Porcelli. Fast particle stabilisation. *Plasma Physics and Controlled Fusion*, 33:1601–1620, November 1991.

[45] R. B. White, M. N. Bussac, and F. Romanelli. High-$\beta$, sawtooth-free tokamak operation using energetic trapped particles. *Physical Review Letters*, 62(5):539–542, Jan 1989.

[46] L. Chen, R. B. White, and M. N. Rosenbluth. Excitation of Internal Kink Modes by Trapped Energetic Beam Ions. *Physical Review Letters*, 52:1122–1125, 1984.

[47] H. Biglari and L. Chen. Unified theory of resonant excitation of kinetic ballooning modes by energetic ions and alpha particles in tokamaks. *Physical Review Letters*, 67:3681–3684, December 1991.

[48] F. Zonca and L. Chen. The general fishbone-like dispersion relation: a unified description for shear Alfvén Mode excitations. *Proceedings of the 34th EPS Conference on Plasma Physics, Warsaw, Poland*, 2007.

[49] H. L. Berk, C. J. Boswell, D. Borba, A. C. A. Figueiredo, T. Johnson, M. F. F. Nave, S. D. Pinches, S. E. Sharapov, and J. EFDA contributors. Explanation of the JET n = 0 chirping mode. *Nuclear Fusion*, 46:888–+, October 2006.

[50] T. O'Neil. Collisionless Damping of Nonlinear Plasma Oscillations. *Physics of Fluids*, 8:2255–2262, December 1965.

[51] G. Y. Fu and C. Z. Cheng. Excitation of high-n toroidicity-induced shear Alfvén eigenmodes by energetic particles and fusion alpha particles in tokamaks. *Physics of Fluids B*, 4:3722–3734, November 1992.

[52] F. Zonca, F. Romanelli, G. Vlad, and C. Kar. Nonlinear Saturation of Toroidal Alfvén Eigenmodes. *Physical Review Letters*, 74:698–701, January 1995.

[53] A. Ödblom, B. N. Breizman, S. E. Sharapov, T. C. Hender, and V. P. Pastukhov. Nonlinear magnetohydrodynamical effects in precessional fishbone oscillations. *Physics of Plasmas*, 9:155–166, January 2002.

[54] H. L. Berk and B. N. Breizman. Saturation of a single mode driven by an energetic injected beam. III. Alfvén wave problem. *Physics of Fluids B*, 2:2246–2252, September 1990.

[55] H. L. Berk, B. N. Breizman, J. Candy, M. Pekker, and N. V. Petviashvili. Spontaneous hole-clump pair creation. *Physics of Plasmas*, 6:3102–3113, August 1999.

[56] S.D. Pinches, V.G. Kiptily, S.E. Sharapov, D.S. Darrow, L.-G. Eriksson, H.-U. Fahrbach, M. Garcia-Munoz, M. Reich, E. Strumberger, A. Werner, the ASDEX Upgrade Team, and JET-EFDA Contributors. Observation and modelling of fast ion loss in jet and asdex upgrade. *Nuclear Fusion*, 46(10):S904–S910, 2006.

[57] C. T. Hsu and D. J. Sigmar. Alpha-particle losses from toroidicity-induced Alfvén eigenmodes. Part I: Phase-space topology of energetic particle orbits in tokamak plasma. *Physics of Fluids B*, 4:1492–1505, June 1992.

[58] S. E. Sharapov, B. Alper, D. Borba, L.-G. Eriksson, A. Fasoli, R. D. Gill, A. Gondhalekar, C. Gormezano, R. F. Heeter, G. T. A. Huysmans, J. Jacquinot, A. A. Korotkov, P. Lamalle, M. J. Mantsinen, D. C. McDonald, F. G. Rimini, D. F. H. Start, D. Testa, P. R. Thomas, and JET Team. Energetic particle physics in JET. *Nuclear Fusion*, 40:1363–1381, July 2000.

[59] D. J. Sigmar, C. T. Hsu, R. White, and C. Z. Cheng. Alpha-particle losses from toroidicity-induced Alfvén eigenmodes. Part II: Monte Carlo simulations and anomalous alpha-loss processes. *Physics of Fluids B*, 4:1506–1516, June 1992.

[60] J. Candy, D. Borba, H. L. Berk, G. T. A. Huysmans, and W. Kerner. Nonlinear interaction of fast particles with Alfvén waves in toroidal plasmas. *Physics of Plasmas*, 4:2597–2611, July 1997.

[61] H. L. Berk, B. N. Breizman, and M. Pekker. Numerical simulation of bump-on-tail instability with source and sink. *Physics of Plasmas*, 2:3007–3016, August 1995.

[62] F. Zonca, S. Briguglio, L. Chen, G. Fogaccia, and G. Vlad. Transition from weak to strong energetic ion transport in burning plasmas. *Nuclear Fusion*, 45(6):477–484, 2005.

[63] F. Zonca, P. Buratti, A. Cardinali, L. Chen, J. Q. Dong, Y. X. Long, A. V. Milovanov, F. Romanelli, P. Smeulders, L. Wang, Z. T. Wang, C. Castaldo, R. Cesario, E. Giovannozzi, M. Marinucci, and V. Pericoli Ridolfini. Electron fishbones: Theory and experimental evidence, 2007.

[64] E. Mazzucato. Microwave reflectometry for magnetically confined plasmas. *Review of Scientific Instruments*, 69:2201–2217, June 1998.

[65] V. Basiuk, J. F. Artaud, F. Imbeaux, X. Litaudon, A. Bécoulet, L.-G. Eriksson, G. T. Hoang, G. Huysmans, D. Mazon, D. Moreau, and Y. Peysson. Simulations of steady-state scenarios for Tore Supra using the CRONOS code. *Nuclear Fusion*, 43:822–830, September 2003.

[66] L.-G. Eriksson, T. Hellsten, and U. Willen. Comparison of time dependent simulations with experiments in ion cyclotron heated plasmas. *Nuclear Fusion*, 33:1037–1048, July 1993.

[67] F. Troyon, R. Gruber, H. Saurenmann, S. Semenzato, and S. Succi. MHD-Limits to Plasma Confinement. *Plasma Physics and Controlled Fusion*, 26:209–215, January 1984.

[68] D. Edery, X. Garbet, J.-P. Roubin, and A. Samain. Variational formalism for kinetic-MHD instabilities in tokamaks . *Plasma Physics and Controlled Fusion*, 34:1089–1112, 1992.

[69] H. L. Berk and D. Pfirsch. Relation of wave energy and momentum with the plasma dispersion relation in an inhomogeneous plasma. *Physics of Fluids*, 31:1532–1543, June 1988.

[70] A. Brizard. Hermitian structure for linearized ideal MHD equations with equilibrium flows. *Physics Letters A*, 168:357–362, September 1992.

[71] A. Brizard. On the relation between pseudo-Hermiticity and dissipation. *Physics Letters A*, 187:382–390, May 1994.

[72] C. N. Lashmore-Davies. Two-stream instability, wave energy, and the energy principle. *Physics of Plasmas*, 14(9):092101–+, September 2007.

[73] A. Hasegawa. Theory of Longitudinal Plasma Instabilities. *Physical Review*, 169:204–214, May 1968.

[74] C. N. Lashmore-Davies. Negative energy waves. *Journal of Plasma Physics*, 71:101–109, April 2005.

[75] S.-T. Tsai and L. Chen. Theory of kinetic ballooning modes excited by energetic particles in tokamaks. *Physics of Fluids B*, 5:3284–3290, 1993.

[76] B. N. Breizman, M. S. Pekker, and S. E. Sharapov. Plasma pressure effect on Alfvén cascade eigenmodes. *Physics of Plasmas*, 12(11):112506–+, November 2005.

[77] F. Zonca, L. Chen, J. Q. Dong, and R. A. Santoro. Existence of ion temperature gradient driven shear Alfvén instabilities in tokamaks. *Physics of Plasmas*, 6:1917–1924, 1999.

[78] P. J. Catto, W. M. Tang, and D. E. Baldwin. Generalized gyrokinetics. *Plasma Physics*, 23:639–650, July 1981.

[79] E. A. Frieman and L. Chen. Nonlinear gyrokinetic equations for low-frequency electromagnetic waves in general plasma equilibria. *Physics of Fluids*, 25:502–508, March 1982.

[80] T. M. Antonsen and B. Lane. Kinetic equations for low frequency instabilities in inhomogeneous plasmas. *Physics of Fluids*, 23:1205–1214, 1980.

[81] X. Garbet, G. Dif-Pradalier, C. Nguyen, P. Angelino, Y. Sarazin, V. Grandgirard, P. Ghendrih, and A. Samain. A minimal collision operator for implementing neo-classical transport in gyrokinetic simulations. *to be published in Physics of Plasmas*, 2009.

[82] T. S. Hahm. Nonlinear gyrokinetic equations for tokamak microturbulence. *Physics of Fluids*, 31:2670–2673, September 1988.

[83] L. Chen and A. Hasegawa. Kinetic theory of geomagnetic pulsations. I - Internal excitations by energetic particles. *Journal of Geophysical Research*, 96:1503–1512, 1991.

[84] M. S. Chu, J. M. Greene, L. L. Lao, A. D. Turnbull, and M. S. Chance. A numerical study of the high-n shear Alfvén spectrum gap and the high-n gap mode. *Physics of Fluids B*, 4:3713–3721, 1992.

[85] N. N. Gorelenkov, H. L. Berk, E. Fredrickson, S. E. Sharapov, and Jet Efda Contributors. Predictions and observations of low-shear beta-induced shear Alfvén acoustic eigenmodes in toroidal plasmas. *Physics Letters A*, 370:70–77, 2007.

[86] G. T. A. Huysmans, W. Kerner, D. Borba, H. A. Holties, and J. P. Goedbloed. Modeling the excitation of global Alfvén modes by an external antenna in the Joint European Torus (JET). *Physics of Plasmas*, 2:1605–1613, 1995.

[87] V. S. Udintsev, M. Goniche, G. Giruzzi, G. T. A. Huysmans, F. Imbeaux, P. Maget, X. Garbet, R. Sabot, J. L. Ségui, F. Turco, T. P. Goodman, D. Molina, H. Weisen, and the Tore Supra team. LETTER TO THE EDITOR: Studies of high frequency hot ion instabilities by means of correlation ECE on Tore Supra. *Plasma Physics and Controlled Fusion*, 48:L33–L44, 2006.

[88] R. Sabot, F. Clairet, and the Tore Supra Team. Recent results on turbulence and MHD activity achieved by reflectometry. *Plasma Physics and Controlled Fusion*, 48:B421–B432, 2006.

[89] A. D. Turnbull, E. J. Strait, W. W. Heidbrink, M. S. Chu, H. H. Duong, J. M. Greene, L. L. Lao, T. S. Taylor, and S. J. Thompson. Global Alfvén modes: Theory and experiment. *Physics of Fluids B*, 5:2546–2553, 1993.

[90] W. W. Heidbrink, E. J. Strait, M. S. Chu, and A. D. Turnbull. Observation of beta-induced Alfvén eigenmodes in the DIII-D tokamak. *Physical Review Letters*, 71:855–858, 1993.

[91] Buratti P. Observation of high-frequency waves during strong tearing mode activity in FTU plasmas without fast ions. *Nuclear Fusion*, 45:1446–1450, 2005.

[92] S. V. Annibaldi, F. Zonca, and P. Buratti. Excitation of beta-induced Alfvén eigenmodes in the presence of a magnetic island. *Plasma Physics and Controlled Fusion*, 49:475–483, 2007.

[93] 0. Zimmerman and et al. Proc 32nd EPS Conf. on Plasma Physics and Controlled Fusion (Tarragona, Spain) P4-059, 2005.

[94] F. Nabais, D. Borba, M. Mantsinen, M. F. F. Nave, S. E. Sharapov, and Joint European Torus-European Fusion Development Agreement (JET-EFDA) contributors. Fishbones in joint european torus plasmas with high ion-cyclotron-resonance-heated fast ions energy content. *Physics of Plasmas*, 12(10):102509, 2005.

[95] F. Zonca, L. Chen, A. Botrugno, P. Buratti, A. Cardinali, R. Cesario, V. Pericoli Ridolfini, and JET-EFDA contributors. High-frequency fishbones at JET: theoretical interpretation of experimental observations. *Nuclear Fusion*, 49:085009, 2009.

[96] K. Hallatschek and D. Biskamp. Transport Control by Coherent Zonal Flows in the Core/Edge Transitional Regime. *Physical Review Letters*, 86:1223–1226, 2001.

[97] N. Miyato, Y. Kishimoto, and J. Li. Global structure of zonal flow and electromagnetic ion temperature gradient driven turbulence in tokamak plasmas. *Physics of Plasmas*, 11:5557–5564, December 2004.

[98] B. D. Scott. Energetics of the interaction between electromagnetic ExB turbulence and zonal flows. *New Journal of Physics*, 7:92–+, March 2005.

[99] K. Itoh, K. Hallatschek, and S.-I. Itoh. Excitation of geodesic acoustic mode in toroidal plasmas. *Plasma Physics and Controlled Fusion*, 47:451–458, March 2005.

[100] V. Naulin, A. Kendl, O. E. Garcia, A. H. Nielsen, and J. J. Rasmussen. Shear flow generation and energetics in electromagnetic turbulence. *Physics of Plasmas*, 12(5):052515–+, May 2005.

[101] H. Sugama and T.-H. Watanabe. Collisionless damping of zonal flows in helical systems. *Physics of Plasmas*, 13(1):012501–+, January 2006.

[102] P. Angelino, A. Bottino, R. Hatzky, S. Jolliet, O. Sauter, T. M. Tran, and L. Villard. Effects of plasma current on nonlinear interactions of ITG turbulence, zonal flows and geodesic acoustic modes. *Plasma Physics and Controlled Fusion*, 48:557–571, May 2006.

[103] G. R. McKee, R. J. Fonck, M. Jakubowski, K. H. Burrell, K. Hallatschek, R. A. Moyer, and D. L. Rudakov. Experimental characterization of coherent, radially-sheared zonal flows in the DIII-D tokamak. *Physics of Plasmas*, 10(1712), 2003.

[104] Y. Hamada, A. Nishizawa, T. Ido, T. Watari, M. Kojima, Y. Kawasumi, K. Narihara, K. Toi, and JIPPT-IIU Group. Zonal flows in the geodesic acoustic mode frequency range in the JIPP T-IIU tokamak plasmas. *Nuclear Fusion*, 45:81–88, February 2005.

[105] T. Ido, Y. Miura, K. Kamiya, Y. Hamada, K. Hoshino, A. Fujisawa, K. Itoh, S.-I. Itoh, A. Nishizawa, H. Ogawa, Y. Kusama, and JFT-2M group. Geodesic acoustic-mode in JFT-2M tokamak plasmas. *Plasma Physics and Controlled Fusion*, 48:41–+, April 2006.

[106] A. V. Melnikov et al. *Plasma Physics and Controlled Fusion*, 48:S87–S110, 2006.

[107] G. D. Conway, B. Scott, J. Schirmer, M. Reich, A. Kendl, and the ASDEX Upgrade Team. Direct measurement of zonal flows and geodesic acoustic mode oscillations in ASDEX Upgrade using Doppler reflectometry. *Plasma Physics and Controlled Fusion*, 47:1165–1185, August 2005.

[108] M. G. Shats, H. Xia, and M. Yokoyama. Mean E $\times$ B flows and GAM-like oscillations in the H-1 heliac. *Plasma Physics and Controlled Fusion*, 48:17–+, April 2006.

[109] C. J. Boswell, H. L. Berk, D. N. Borba, T. Johnson, S. D. Pinches, and S. E. Sharapov. Observation and explanation of the JET n=0 chirping mode. *Physics Letters A*, 358:154–158, October 2006.

[110] N. N. Gorelenkov, M. A. van Zeeland, H. L. Berk, N. A. Crocker, D. Darrow, E. Fredrickson, G.-Y. Fu, W. W. Heidbrink, J. Menard, and R. Nazikian. Beta-induced Alfvén-acoustic eigenmodes in National Spherical Torus Experiment and DIII-D driven by beam ions. *Physics of Plasmas*, 16(5):056107–+, May 2009.

[111] R. Nazikian, H. L. Berk, R. V. Budny, K. H. Burrell, E. J. Doyle, R. J. Fonck, N. N. Gorelenkov, C. Holcomb, G. J. Kramer, R. J. Jayakumar, R. J. La Haye, G. R. McKee, M. A. Makowski, W. A. Peebles, T. L. Rhodes, W. M. Solomon, E. J. Strait, M. A. Vanzeeland, and L. Zeng. Multitude of Core-Localized Shear Alfvén Waves in a High-Temperature Fusion Plasma. *Physical Review Letters*, 96(10):105006–+, March 2006.

[112] C. Nguyen, X. Garbet, R. Sabot, L.-G. Eriksson, M. Goniche, P. Maget, V. Basiuk, J. Decker, D. Elbèze, G. T. A. Huysmans, A. Macor, J.-L. Ségui, and M. Schneider. Excitation of Beta Alfvén Eigenmodes in Tore-Supra. *Plasma Physics and Controlled Fusion*, 51:095002, 2009.

[113] F. Zonca and L. Chen. Radial structures and nonlinear excitation of geodesic acoustic modes. *Europhysics Letters*, 83:35001–+, August 2008.

[114] A. I. Smolyakov, C. Nguyen, and X. Garbet. Kinetic theory of electromagnetic geodesic acoustic modes. *Plasma Physics and Controlled Fusion*, 50:115008, 2008.

[115] R. Fitzpatrick. Stability of coupled tearing and twisting modes in tokamaks. *Physics Plasmas*, 1:3308–3336, October 1994.

[116] F. Pegoraro and T. J. Schep. Theory of resistive modes in the ballooning representation. *Plasma Physics and Controlled Fusion*, 28:647–667, April 1986.

[117] A. I. Smolyakov, C. Nguyen, and X. Garbet. Electromagnetic effects on geodesic acoustic and beta-induced Alfvén; eigenmodes. *Submitted to Nuclear Fusion*, 2009.

[118] R. Sabot, A. Macor, C. Nguyen, J. Decker, D. Elbèze, L. G. Eriksson, X. Garbet, M. Goniche, G. T. A. Huysmans, P. Maget, and J. L. Ségui. Observation of acoustic and subacoustic fast particles driven modes in Tore-Supra. *Nuclear Fusion*, 49(8):085033–+, August 2009.

[119] R. Nazikian, G. Y. Fu, M. E. Austin, H. L. Berk, R. V. Budny, N. N. Gorelenkov, W. W. Heidbrink, C. T. Holcomb, G. J. Kramer, G. R. McKee, M. A. Makowski, W. M. Solomon, M. Shafer, E. J. Strait, and M. A. V. Zeeland. Intense Geodesic Acousticlike Modes Driven by Suprathermal Ions in a Tokamak Plasma. *Physical Review Letters*, 101(18):185001–+, October 2008.

[120] W. Kerner, D. Borba, G. T. A. Huysmans, F. Porcelli, S. Poedts, J. P. Goedbloed, and R. Betti. Stability of global Alfven waves (TAE, EAE) in JET tritium discharges. *Plasma Physics and Controlled Fusion*, 36:911–923, May 1994.

[121] M. N. Bussac, R. Pellat, D. Edery, and J. L. Soule. Internal kink modes in toroidal plasmas with circular cross sections. *Physical Review Letters*, 35:1638–1641, December 1975.

[122] http://www.matpack.de/.

[123] B. Davies. Locating the Zeros of an Analytic Function. *Journal of Computational Physics*, 66:36–+, September 1986.

[124] P. Lauber, M. Brüdgam, S. Günter, M. Curran, M. García Munoz, V. Igochine, M. Maraschek, K. Sassenberg, and Asdex-Upgrade Team. Fast particle driven modes in asdex upgrade. IAEA Technical Meeting on energetic particles, Kiev, 2009.

[125] R. G. L. Vann, H. L. Berk, and A. R. Soto-Chavez. Strongly Driven Frequency-Sweeping Events in Plasmas. *Physical Review Letters*, 99(2):025003–+, July 2007.

[126] E. Fredrickson, N. N. Gorelenkov, and H.L. Berk. Proceedings of the APS, 2006.

[127] B. N. Breizman. Nonlinear travelling waves in energetic particle phase space. IAEA Technical Meeting on energetic particles, Kiev, 2009.

[128] A. Brizard. Eulerian action principles for linearized reduced dynamical equations. *Physics of Plasmas*, 1:2460–2472, August 1994.

[129] P. H. Diamond. Conservation of potential vorticity. Festival de Théorie, Aix-en-Provence, 2009.

[130] H. L. Berk, B. N. Breizman, and N. V. Petviashvili. Spontaneous hole-clump pair creation in weakly unstable plasmas [Physics Letters A 234 (1997) 213]. *Physics Letters A*, 238:408–408, February 1998.

[131] H. L. Berk, B. N. Breizman, and H. Ye. Scenarios for the nonlinear evolution of alpha-particle-induced Alfvén wave instability. *Physical Review Letters*, 68:3563–3566, June 1992.

[132] R. G. L. Vann. *Characterisation of fully nonlinear Berk-Breizman phenomenology.* PhD thesis, University of Warwick, 2003.

[133] http://www-math.u-strasbg.fr/calvi/?lang=en.

[134] M. Lesur, Y. Idomura, and X. Garbet. Fully nonlinear features of the energetic beam-driven instability. *Physics of Plasmas*, 16:9, September 2009.

[135] J. W. Connor, R. J. Hastie, and J. B. Taylor. Shear, periodicity, and plasma ballooning modes. *Physical Review Letters*, 40:396–399, February 1978.

# A

# Notions of Hamiltonian mechanics

We recall in this section some fundamentals of hamiltonian mechanics necessary for our subsequent derivation of the gyrokinetic equation. Those are largely described in the review paper by Brizard et al.[10].

## A.1 Hamilton's equations in general coordinates

The motion of a single charged particle in an electromagnetic field can be described using the differential one-form particle Lagrangian:

$$\hat{\underline{\Gamma}}(\mathbf{x},\mathbf{p}) = \mathbf{p}\cdot\mathsf{d}\mathbf{x} - \hat{H}\mathsf{d}t \tag{A.1}$$

where $(\mathbf{x},\mathbf{p}) = (\mathbf{x}, m\mathbf{v}+e\mathbf{A})$ are the particle canonical coordinates in 6 dimensional phase-space, $\hat{H}$ is the electromagnetic hamiltonian $\hat{H} = |\mathbf{p}-eA|^2/2m+e\phi$, and $\mathsf{d}$ denotes an exterior derivative. (Contrary to Brizard et al.[10], we simply use the usual 6 dimensional phase-space, more practical for our subsequent derivations.) More generally, we can use an arbitrary 6 dimensional phase-space system of indepedent coordinates $\mathbf{Z} = (Z^a)_{a=1...6}$ associated with a Lagrangian of the form $\underline{\Gamma}(\mathbf{Z},t) = \mathbf{\Gamma}(\mathbf{Z},t)\cdot\mathsf{d}\mathbf{Z} - H(\mathbf{Z},t)\mathsf{d}t$ verifying $\underline{\Gamma}(\mathbf{Z},t) = \hat{\underline{\Gamma}}(\mathbf{x},\mathbf{p}) + \mathsf{d}S$, with S a scalar field depending on phase space coordinates and time.

**Hamilton's principle** asserts that the dynamically allowed paths in a time interval $[t_1,t_2]$ with given initial and final conditions are stationary points of the action integral $\mathcal{A} = \int_{t_1}^{t_2}\underline{\Gamma}$ for the class of phase space paths, ie $\delta\mathcal{A}=0$, where :

$$\delta\mathcal{A} = \delta\int_{t_1}^{t_2}\left(\mathbf{\Gamma}\cdot\frac{d\mathbf{Z}}{dt} - H\right)dt = \int_{t_1}^{t_2}\left(\frac{\partial\Gamma_b}{\partial Z^a}\cdot\frac{dZ^b}{dt}\delta Z^a + \Gamma_a\frac{d\delta Z^a}{dt} - \frac{\partial H}{\partial Z^a}\delta Z^a\right)dt \tag{A.2}$$

Integrating Eq. A.2 by parts and using the invariance of the initial and final conditions ($\delta Z^a = 0$ at the end points), we get:

$$\delta\mathcal{A} = \int_{t_1}^{t_2}\left(\omega_{ab}\frac{dZ^b}{dt} - \frac{\partial\Gamma_a}{\partial t} - \frac{\partial H}{\partial Z^a}\right)\delta Z^a \tag{A.3}$$

where the $\omega_{ab}$'s are defined as:

$$\omega_{ab} = \frac{\partial\Gamma_b}{\partial Z^a} - \frac{\partial\Gamma_a}{\partial Z^b}\ , \quad a,b = 1...6 \tag{A.4}$$

and correspond to the matrix coefficients of the two-form $\omega = \mathsf{d}\left(\mathbf{\Gamma}(\mathbf{Z},t)\cdot\mathsf{d}\mathbf{Z}\right)$. And finally, $\delta\mathcal{A}=0$ returns [12]:

$$\omega_{ab}\frac{dZ^b}{dt} = \frac{\partial H}{\partial Z^a} + \frac{\partial\Gamma_a}{\partial t} \tag{A.5}$$

For regular Lagrangian systems, $\omega$ is invertible with inverse $J \equiv \omega^{-1}$, and equations A.5 can be rewritten in the following form, known as Hamilton's equations:

$$\frac{dZ^a}{dt} = J^{ab}\left(\frac{\partial H}{\partial Z^b} + \frac{\partial \Gamma_b}{\partial t}\right) = [Z^a, H] + [Z^a, Z^b]\frac{\partial \Gamma_b}{\partial t} \tag{A.6}$$

where Poisson brackets are defined by the relations:

$$[f, g] = \frac{\partial f}{\partial Z^a}[Z^a, Z^b]\frac{\partial g}{\partial Z^b} \tag{A.7}$$

$$[Z^a, Z^b] = J^{ab}(\mathbf{Z}) \tag{A.8}$$

## A.2 Hamiltonian formulation of the Vlasov equation

Based on an averaging of the individual particles behaviors, the Vlasov equation suggests a description of the collective behavior of a dense set of charged particles, which states that the full time derivative of the particles phase-space distribution function $F$ cancels. Its Hamiltonian formulation reads:

$$\frac{dF}{dt} = \frac{\partial F}{\partial t} + \frac{\partial F}{\partial Z^a}\frac{dZ^a}{dt} = \frac{\partial F}{\partial t} - [H, F] - \frac{\partial \mathbf{\Gamma}}{\partial t} \cdot [\mathbf{Z}, F] \tag{A.9}$$

## A.3 Coordinate Transformations

Coordinate transformations are appropriate means to simplify the six dimensional Vlasov equation. Gyrokinetic theory in particular, is based on their use.

Let's consider a time-dependent coordinate transformation $\mathbf{Z}$ to $\bar{\mathbf{Z}} = \bar{\mathbf{Z}}(\mathbf{Z}, t)$. Under such a coordinate transformation, both the expressions of the phase-space distribution function and of the particle Lagrangian are modified. Of course, the new distribution function $\bar{F}$ has to verify $\bar{F}(\bar{Z}, t) = F(Z, t)$ to describe the same population of particles. As for the particle Lagrangian, one more degree of freedom is offered by the variational form of Hamilton's principle, and the physics of the charged particle motion is simply conserved if the new Lagrangian verifies a gauge transformation [12], ie: $\bar{\underline{\Gamma}}(\bar{\mathbf{Z}}, t) = \underline{\Gamma}(\mathbf{Z}, t) + \mathsf{d}S$ with S a scalar field depending on phase space coordinates and time. This latter condition relates the hamiltonians and the so-called symplectic components of the Lagrangian $\mathbf{\Gamma} = (\Gamma_a)_{a=1...6}$ of the two coordinate systems, and it shows the conservation of Poisson brackets in a coordinate transformation. Indeed, $\bar{\mathbf{\Gamma}} \cdot \mathsf{d}\bar{\mathbf{Z}} - \bar{H}\mathsf{d}t = \mathbf{\Gamma} \cdot \mathsf{d}\mathbf{Z} - H\mathsf{d}t + \mathsf{d}G$ implies:

$$\bar{\Gamma}_a(\bar{\mathbf{Z}}, t) = \Gamma_b(\mathbf{Z}, t)\frac{\partial Z_b}{\partial \bar{Z}_a} + \frac{\partial G}{\partial \bar{Z}_a} \tag{A.10}$$

$$\bar{H}(\bar{\mathbf{Z}}, t) = H(\mathbf{Z}, t) + \Gamma_a\frac{\partial Z_a}{\partial t} + \frac{\partial G}{\partial t} \tag{A.11}$$

and hence:

$$\bar{\omega}_{ab} = \frac{\partial \bar{\Gamma}_b}{\partial \bar{Z}^a} - \frac{\partial \bar{\Gamma}_a}{\partial \bar{Z}^b} = \frac{\partial Z_c}{\partial \bar{Z}^a}\left(\frac{\partial \Gamma_d}{\partial Z^c} - \frac{\partial \Gamma_c}{\partial Z^d}\right)\frac{\partial Z_d}{\partial \bar{Z}^b} = \frac{\partial Z_c}{\partial \bar{Z}^a}\omega_{cd}\frac{\partial Z_d}{\partial \bar{Z}^b} \tag{A.12}$$

which can be inverted to yield:

$$\bar{[}f, g\bar{]} = \frac{\partial f}{\partial \bar{Z}^a}\bar{J}^{ab}\frac{\partial g}{\partial \bar{Z}^b} = \frac{\partial f}{\partial \bar{Z}^a}\frac{\partial \bar{Z}^a}{\partial Z_c}J^{cd}\frac{\partial \bar{Z}^b}{\partial Z_d}\frac{\partial g}{\partial \bar{Z}^b} = [f, g], \quad \text{for any} f \text{ and } g \tag{A.13}$$

For perturbative treatments ot the Vlasov equation, a particular class of coordinate transformations is used, the class of Lie near-identity transformations, defined as:

$$\mathcal{T}_\delta : \mathbf{Z} \longrightarrow \bar{\mathbf{Z}} = \exp\left(\sum_1^\infty \mathbf{G}_n \cdot \mathsf{d}\right)\mathbf{Z} \tag{A.14}$$

where the $\mathbf{G}_n(\mathbf{Z},t)$'s, or generator vector fields of the transformation, verify $\mathbf{G}_n = O(\delta^n)$, and $\delta << 1$ is a dimensionless ordering parameter. Under such a transformation, the conservation of the *values* taken by a given scalar function f, ie : $\bar{f}(\bar{\mathbf{Z}},t) = f(\mathbf{Z},t)$, or by a given 1-form $\underline{\Gamma}$, ie $\bar{\underline{\Gamma}}(\bar{\mathbf{Z}},t) = \underline{\Gamma}(\mathbf{Z},t)$, fully defines the new functions $\bar{f}$ and $\bar{\underline{\Gamma}}$ which can be expressed using a so-called *push-forward* operator $\mathsf{T}_\delta^{-1}$ (the inverse operator of the so-called *pull-back* operator $\mathsf{T}_\delta$): $\mathsf{T}_\delta^{-1}$: $f \longrightarrow \bar{f}$, $\mathsf{T}_\delta^{-1}$: $\underline{\Gamma} \longrightarrow \bar{\underline{\Gamma}}$. For near-identity transformations, Lie-transform perturbation theory shows that [10]:

$$\mathsf{T}_\delta^{\pm 1} = \exp\left(\pm\sum_1^\infty \mathcal{L}_n\right) \tag{A.15}$$

where $\mathcal{L}_n$ is a Lie derivative:

$$\mathcal{L}_n f \equiv \mathbf{G}_n \cdot \mathsf{d}f = G_n^a \frac{\partial f}{\partial Z^a} \quad \text{for a scalar function } f \tag{A.16}$$

$$\mathcal{L}_n \underline{\Gamma} \equiv \mathbf{G}_n \cdot \mathsf{d}\underline{\Gamma} + \mathsf{d}(\mathbf{G}_n \cdot \underline{\Gamma}) = \left[G_n^a\left(\frac{\partial \underline{\Gamma}_b}{\partial Z_a} - \frac{\partial \underline{\Gamma}_a}{\partial Z_b}\right) + \frac{\partial\, G_n^a \underline{\Gamma}_a}{\partial Z_b}\right]\mathsf{d}Z^b \quad \text{for a 1-form } \underline{\Gamma} \tag{A.17}$$

Note that in the latter equation Eq. A.17, we simply wrote : $\underline{\Gamma} = \underline{\Gamma}_a \mathsf{d}Z^a$ (without separating the symplectic components $\mathbf{\Gamma} \cdot \mathsf{d}\mathbf{Z}$ and the hamiltonian part $-H\mathsf{d}t$). Hence, $a$ and $b$ should be taken from 1 to 7 to describe the 7-dimensional space: $(Z_{a=1\ldots6}, Z_7 = t)$. This equation makes sense if we use: $G_n^7 = 0$, $\underline{\Gamma}_7 = -H, \underline{\Gamma}_{a=1\ldots6} = \Gamma_{a=1\ldots6}$.
Identity A.15 simply results from the development of the expressions $\bar{f}(\bar{\mathbf{Z}},t) = f(\mathbf{Z},t)$ and $\bar{\underline{\Gamma}}(\bar{\mathbf{Z}},t) = \underline{\Gamma}(\mathbf{Z},t)$. To the first order in $\delta$ (of interest to us in this paper), it is easily shown:

$$\bar{f}(\bar{\mathbf{Z}},t) = f(\bar{\mathbf{Z}} - \mathbf{G}_1, t) = f(\bar{\mathbf{Z}}) - \mathbf{G}_1 \cdot \nabla f = f(\bar{\mathbf{Z}}) - \mathbf{G}_1 \cdot \mathsf{d}f \tag{A.18}$$

$$\bar{\underline{\Gamma}}(\bar{\mathbf{Z}},t) = \underline{\Gamma}(\bar{\mathbf{Z}} - \mathbf{G}_1, t)\mathsf{d}(\bar{\mathbf{Z}} - \mathbf{G}_1) = \underline{\Gamma}(\bar{\mathbf{Z}}) - \left(G_1^a \frac{\partial \underline{\Gamma}_b}{\partial Z_a} + \underline{\Gamma}_a \frac{\partial G_1^a}{\partial Z_b}\right)\mathsf{d}Z^b \tag{A.19}$$

Let's now see the benefit of such a transformation for perturbative analysis. Assume a first order perturbation of an initial state $\underline{\Gamma} = \underline{\Gamma}_0 + \underline{\Gamma}_1$ ($\underline{\Gamma}_1 = O(\delta)$). Such a perturbation modifies the charged particle equations of motion, and may have an impact on both the Poisson bracket structure given by $\omega = \omega_0 + \omega_1$, and the Hamiltonian $H = H_0 + H_1$. Hence, it may be desirable to use a near-identity coordinate transformation to simplify the new equations of motion. As explained before, the transformed Lagrangian has to verify $\bar{\underline{\Gamma}}(\bar{\mathbf{Z}},t) = \underline{\Gamma}(\mathbf{Z},t) + \mathsf{d}S$, or $\bar{\Gamma} = \mathsf{T}_\delta^{-1}\Gamma + \mathsf{d}S$. If we apply identity Eq. A.15 and separate the hamiltonian part of the Lagrangian (so that $\mathbf{Z}$ now lives in the 6 dimensional phase-space), the first order order of this equality reads:

$$\bar{\mathbf{\Gamma}}_\mathbf{1} \cdot \mathsf{d}\mathbf{Z} - \bar{H}_1 \mathsf{d}t = \mathbf{\Gamma}_1 \cdot \mathsf{d}\mathbf{Z} - H_1 \mathsf{d}t - \mathbf{G}_1 \cdot \omega_0 + \left(\mathbf{G}_1 \cdot \mathsf{d}H_0 + \mathbf{G}_1 \cdot \frac{\partial \Gamma_0}{\partial t}\right)\mathsf{d}t + \mathsf{d}S_1 \tag{A.20}$$

where we included in $S_1$ both the first order of $S$ and the field $\mathbf{G}_1 \cdot \underline{\Gamma}$ resulting from the application of the Lie derivative Eq. A.17. The components of this equation may be separated to give:

$$G_1^a = [S_1, Z^a]_0 + (\Gamma_{1b} - \bar{\Gamma}_{1b})J_0^{ba} \tag{A.21}$$

and:

$$\begin{aligned}\bar{H}_1 &= H_1 - \mathbf{G}_1 \cdot \mathtt{d}H_0 - \mathbf{G}_1 \cdot \frac{\partial \Gamma_0}{\partial t} - \frac{\partial S_1}{\partial t} \\ &= H_1 - [S_1, H_0] - [S_1, \mathbf{Z}] \cdot \frac{\partial \mathbf{\Gamma}}{\partial t} - (\Gamma_1^a - \bar{\Gamma}_1^a) \left( [Z^a, H_0] + [Z^a, \mathbf{Z}] \cdot \frac{\partial \mathbf{\Gamma}}{\partial t} \right) - \frac{\partial S_1}{\partial t} \\ &= H_1 - (\mathbf{\Gamma}_1 - \bar{\mathbf{\Gamma}}_1) \cdot \frac{d_0 \mathbf{Z}}{dt} - \frac{d_0 S_1}{dt} \end{aligned} \tag{A.22}$$

where $d_0/dt$ is the full time derivative along the unperturbed particle trajectory. Then, two degrees of freedom clearly appear in the transformation: the choice of $\mathbf{G}_1$ and the choice of $S_1$, which allow to fix both the new Poisson bracket structure derived from $\bar{\Gamma}_1$ using Eq. A.21, and the new Hamiltonian $\bar{H}_1$ using Eq. A.22.

In modern Gyrokinetic theory, near-identity transformations are used to simplify the Poisson bracket structure and to remove the fast gyromotion of the particle from the new Hamiltonian. Hence, a new particle trajectory or "gyrocenter" trajectory, which is independent from the fast gyromotion, is determined, whereas the complexity of the fast gyromotion gets fully included in the coordinate transformation itself.

# B

# Charged particle motion

## B.1 Derivation of action-angle variables

We derive in the following section the system of action-angle variables used in the thesis, starting from the guiding-center coordinates defined in Ref. [12]. For this, we will make a large use of the Hamiltonian formulas recalled in Eq. 2.24, and use similar procedure and arguments as can be found in Refs. [13, 14].

We start from the the guiding-center Lagrangian given by Littlejohn [12] presented in the thesis core 2.26,

$$\underline{\Gamma}_{\rm gc}(\mathbf{Z}) = (e\mathbf{A}_{(0)}(\mathbf{X}) + mv_\parallel \mathbf{b}_{(0)})\cdot \mathsf{d}\mathbf{X} + \frac{m}{e}\mu \mathsf{d}\gamma - \left(\frac{1}{2}mv_\parallel^2 + \mu B_{(0)}(\mathbf{X}) + e\phi_{(0)}(\mathbf{X})\right)\mathsf{d}t \quad \text{(B.1)}$$

To make use of the configuration todoidal and poloidal periodicities, it is appropriate to write the fields using their covariant representation. Noticing from Eq. 2.2 that $\mathbf{B}_{(0)} = \nabla\Psi\times\nabla\varphi + \nabla\Phi\times\nabla\theta$, it directly comes a convenient choice for the vector potential $\mathbf{A}_{(0)}$

$$\mathbf{A}_{(0)} = \Psi\nabla\varphi + \Phi\nabla\theta. \quad \text{(B.2)}$$

Next, we use Eq. 2.7 to write the magnetic field covariant representation

$$\mathbf{B}_{(0)} = B_\Psi\nabla\Psi + B_\theta\nabla\theta + I(\Psi)\nabla\varphi. \quad \text{(B.3)}$$

The Lagrangian becomes

$$\underline{\Gamma}_{\rm gc}(\mathbf{Z}) = \left(\frac{mv_\parallel}{B_{(0)}}B_\theta + e\Phi\right)\mathsf{d}\theta + \left(e\Psi + \frac{mv_\parallel}{B_{(0)}}I\right)\mathsf{d}\varphi + \frac{m}{e}\mu\mathsf{d}\gamma + \frac{mv_\parallel}{B_{(0)}}B_\Psi \mathsf{d}\Psi - H_{\rm gc}\mathsf{d}t \quad \text{(B.4)}$$

In order to display a canonical system of variables, we need to remove one coordinate. Noticing that a change of coordinate $\mathbf{X}\to\mathbf{X}+\mathbf{X}'$ leads to additional terms in the Lagrangian $\underline{\Gamma}\to\underline{\Gamma} + \mathbf{A}_{(0)}\cdot\mathsf{d}\mathbf{X}' + (mv_\parallel/B_{(0)})\mathbf{B}_{(0)}\cdot\mathsf{d}\mathbf{X}'$ the $\Psi$-dependence is found to disappear with

$$\begin{aligned} &\text{- the second order in } \rho^* \text{ change of coordinates:} && \mathsf{d}\mathbf{X}' = -\tfrac{B_\Psi}{B_{(0)}^2}\mathbf{B}_{(0)}\mathsf{d}\Psi \\ &\text{- a choice of a Gauge for } \mathbf{A}_{(0)} \text{such that:} && \mathbf{A}_{(0)}\cdot\mathbf{B}_{(0)} = 0 \end{aligned} \quad \text{(B.5)}$$

Finally the Lagrangian is expressed in a system of canonical coordinates $(\gamma,\theta,\varphi,P_\gamma,P_\theta,P_\varphi)$

$$\underline{\Gamma} = P_\theta\mathsf{d}\theta + P_\varphi\mathsf{d}\varphi + \frac{m}{e}\mu\mathsf{d}\gamma - H_{(0)}\mathsf{d}t, \quad \text{(B.6)}$$

with

$$P_\gamma = \frac{m}{e}\mu \quad \text{(B.7)}$$

$$P_\theta = \frac{mv_\parallel}{B_{(0)}}B_\theta + e\Phi \quad \text{(B.8)}$$

$$P_\varphi = e\Psi + \frac{mv_\parallel}{B_{(0)}}I(\Psi). \quad \text{(B.9)}$$

Here, $P_\gamma$ is directly associated to the traditional adiabatic invariant $\mu$, and $P_\varphi, \dot{P}_\varphi = \partial_\varphi H_{(0)}$ is clearly an exact motion invariant associated with axisymmetry (at equilibrium). A priori, $P_\theta$ has no reason to be an invariant and we need additional work to display a set of action-angle variables. Noticing that $H_{(0)}(\theta, P_\gamma, P_\theta, P_\varphi)$, where $H_{(0)}$ is an invariant at equilibrium, we can rewrite $P_\theta = P_\theta(\theta, H_{(0)}, P_\gamma, P_\varphi)$, and we can cancel the $\theta$-dependence using a $\theta$-averaging, at constant invariants, ie: along a particle trajectory. For this, we define

$$J_2 = \oint \frac{d\theta}{2\pi} P_\theta(\theta, H_{(0)}, P_\gamma, P_\varphi) \tag{B.10}$$

which is an invariant by definition.

Let us now show that $J_2$ can be used as invariant in a set of action-angle variables. The clean way to proceed is to use a coordinate transformation, as described in Eq. 2.24. We make the transformation $(\gamma, \theta, \varphi, P_\gamma, P_\theta, P_\varphi) \rightarrow (\alpha_1, \alpha_2, \alpha_3, J_1, J_2, J_3)$, using the following transformation generating function

$$G(\gamma, \theta, \varphi, J_1, J_2, J_3) = \gamma J_1 + \varphi J_3 + \int_0^\theta d\theta' P_\theta(\theta', J_1, J_2, J_3). \tag{B.11}$$

Such generating function implies the following requirements for the new coordinates

$$P_\gamma = \partial_\gamma G = J_1; \quad P_\theta = \partial_\theta G = P_\theta; \quad P_\varphi = \partial_\varphi G = J_3 \tag{B.12}$$

$$\boldsymbol{\alpha} = \partial_{\mathbf{J}} G = (\gamma, 0, \varphi) + \int_0^\theta d\theta' \; \partial_{\mathbf{J}} P_\theta(\theta', J_1, J_2, J_3). \tag{B.13}$$

Hence, we obtain a set of canonical variables characterized by three motion invariants, $J_1$, $J_2$ and $J_3$.

We can be more explicit and derive the physical meaning of the associated angles using Eq. B.13. For this, let us define the bounce frequency,

$$\frac{1}{\Omega_b} = \oint \frac{d\theta}{2\pi} \frac{1}{\dot{\theta}} = \oint \frac{d\theta}{2\pi} \frac{\partial P_\theta}{\partial H_{(0)}}|_{J_1, J_3}. \tag{B.14}$$

The derivation of Eq. B.10 according to $J_2$ with the definition $\Omega_2 = \partial_{J_2|J_1,J_3} H_{(0)}$ directly shows that $\Omega_2 = \Omega_b$, and it follows from B.13 that

$$\alpha_2 = \Omega_b \int_0^\theta \frac{d\theta'}{\dot{\theta}'} \qquad\qquad \alpha_3 = \varphi + \hat{\varphi} \tag{B.15}$$

where $\oint \hat{\varphi} = 0$

$$\Omega_3 = \Omega_b \oint \frac{d\theta}{2\pi} \frac{1}{\dot{\theta}} \; \Omega_3 = \Omega_b \left\{ \oint \frac{d\theta}{2\pi} \frac{1}{\dot{\theta}} \; \dot{\varphi} + \partial_{J_3} \oint \frac{d\theta}{2\pi} P_\theta(\theta, J_1, J_2, J_3) \right\} = \Omega_b \oint \frac{d\theta}{2\pi} \frac{1}{\dot{\theta}} \; \dot{\varphi} \tag{B.16}$$

$(\alpha_2, \Omega_2)$ and $(\alpha_3, \Omega_3)$ are clearly found to be associated respectively with the bounce and toroidal drift motion of particles.

$\sim$ *Approximate calculation of the bounce and drift motion* $\sim$
Let us be a little bit more explicit on the bounce and drift motion involved, using our knowledge of the equilibrium particles drifts [1]. We know from subsection 2.1.2 that the motion of a charged particle in the tokamak geometry can be divided into a parallel and lower order drift motion $\mathbf{v} = v_\parallel \mathbf{b} + \mathbf{v}_g$, such that

$$\dot{\Psi} = \mathbf{v}_g \cdot \nabla\Psi \tag{B.17}$$
$$\dot{\theta} = v_\parallel \mathbf{b} \cdot \nabla\theta + \mathbf{v}_g \cdot \nabla\theta \tag{B.18}$$
$$\dot{\varphi} = v_\parallel q\mathbf{b} \cdot \nabla\theta + \mathbf{v}_g \cdot \nabla\varphi \tag{B.19}$$

At the lower order, $\dot{\theta}$ is dominated by the parallel velocity and the bounce frequency can be rewritten

$$\Omega_2^{-1} = \oint \frac{d\theta}{2\pi} \frac{1}{\mathbf{b} \cdot \nabla\theta \; v_\parallel}. \tag{B.20}$$

The drift motion remains relevant in the drift frequency. Indeed, noticing

$$\begin{aligned} \dot{\varphi} - q(\bar{\Psi})\dot{\theta} &= \frac{v_\parallel}{B_{(0)}}(q(\Psi) - q(\bar{\Psi}))\mathbf{B}_{(0)} \cdot \nabla\theta + \mathbf{v}_g \cdot \nabla(\varphi - q(\bar{\Psi})\theta) \\ &\approx q'\delta\Psi\dot{\theta} + \mathbf{v}_g \cdot \nabla(\varphi - q(\bar{\Psi})\theta) \end{aligned}$$

it comes

$$\Omega_3 = \Omega_b \oint \frac{d\theta}{2\pi} \frac{1}{\dot{\theta}} \dot{\varphi} = \Omega_b \oint \frac{d\theta}{2\pi} \frac{1}{\dot{\theta}} \left( -q'\dot{\Psi}\theta + \mathbf{v}_g \cdot \nabla(\varphi - q(\bar{\Psi})\theta) \right) + q(\bar{\Psi})\Omega_b \oint \frac{d\theta}{2\pi} \tag{B.21}$$

where the last term in Eq. B.21 cancels for trapped particles in the small radial drift approximation, such that the particle drift is the main contribution in $\Omega_3$. In this study, the particle radial drift has been neglected and the last term of Eq. B.21 was consequenlty rewritten $q(\bar{\Psi})\Omega_b\delta_{passing}$ in Eq. 2.33.

## B.2 Expressions of the equilibrium characteristic frequencies for some well defined geometries

### Circular geometry

We now derive the expression of the normalized bounce and drift frequencies, such that

$$\Omega_2 = \Omega_b = \pm\frac{1}{qR_0}\sqrt{\frac{2\mathsf{E}}{m}}\bar{\Omega}_b, \quad \Omega_3 = \Omega_d + \delta_{\text{passing}}q(r)\Omega_b = \frac{q(r)}{r}\frac{E}{eB_0R_0}\bar{\Omega}_d + \delta_{\text{passing}}q(r)\Omega_b \tag{B.22}$$

in a simple circular equilibrium, without Grad-Shafranov shift and in the large aspect ratio.

In such a geometry, $\mathbf{b} \cdot \nabla\theta \approx 1/qR$. It directly comes

$$\bar{\Omega}_b = \left( \oint \frac{d\theta}{2\pi} \frac{1}{\sqrt{1 - \lambda(1 + \epsilon\cos\theta)}} \right)^{-1} \tag{B.23}$$

[1] Note that these drift should normally be accessed directly from the action-angle formulation, but that such a formulation of the drifts is much less tractable.

with $\lambda = \mu B_0/\mathsf{E}, \epsilon = r/R_0$. Using $\kappa^2 = 2\epsilon\lambda/[1-(1-\epsilon)\lambda]$, and keeping only first order effects in $\epsilon$, it follows

$$\bar{\Omega}_b^{-1} = \sqrt{\frac{2\epsilon + (1-\epsilon)\kappa^2}{2\epsilon}} \oint \frac{d\theta}{2\pi} \frac{1}{\sqrt{1-\kappa^2\sin^2(\theta/2)}} \tag{B.24}$$

where we recall that by convention, we take for passing particles ($\kappa < 1$), $\oint = \int_0^{2\pi}$, and for trapped particles ($\kappa > 1$), $\oint = \int_{-\theta_0}^{\theta_0}$.

Using the change of variable $\sin u = \kappa \sin(\theta/2)$ for the trapped particles $\theta \in [-\theta_0, \theta_0]$, the normalized bounce frequency is given explicitely by the formulas

$$\bar{\Omega}_b^{-1} = \sqrt{\frac{2\epsilon + (1-\epsilon)\kappa^2}{2\epsilon}} \frac{2}{\pi} \begin{cases} \mathbb{K}(\kappa) & \text{for circulating particles} \\ (1/\kappa)\mathbb{K}(1/\kappa) & \text{for trapped particles} \end{cases} . \tag{B.25}$$

where $\mathbb{K}(\kappa)$ is the firs elliptic integral of the first kind, $\mathbb{K}(\kappa) = \int_0^{\pi/2} \sqrt{1+\kappa^2 cos\theta}^{\,-1} d\theta$, for $\kappa < 1$.

Similarly,

$$\bar{\Omega}_d = \bar{\Omega}_b \oint \frac{d\theta}{2\pi} \frac{(2-\lambda B)(\cos\theta + s\theta\sin\theta)}{\sqrt{1-\lambda(1+\epsilon\cos\theta)}} , \tag{B.26}$$

returns

$$\bar{\Omega}_d = \bar{\Omega}_b \frac{\kappa^2}{\sqrt{2\epsilon+(1-\epsilon)\kappa^2}} \frac{1}{\sqrt{2\epsilon}} \oint \frac{d\theta}{2\pi} \frac{\cos\theta + s\theta\sin\theta}{\sqrt{1-\kappa^2\sin^2(\theta/2)}} \tag{B.27}$$

$$= \frac{\kappa^2}{2\epsilon+(1-\epsilon)\kappa^2} \begin{cases} 1 + \frac{2}{\kappa^2}(\frac{\mathbb{E}}{\mathbb{K}} - 1) + \frac{4s}{\kappa^2}\frac{\mathbb{E}}{\mathbb{K}} & \text{for circulating particles} \\ 2\frac{\mathbb{E}(1/\kappa)}{\mathbb{K}(1/\kappa)} - 1 + 4s\left[\frac{\mathbb{E}(1/\kappa)}{\mathbb{K}(1/\kappa)} - \left(\frac{1}{\kappa^2} - 1\right)\right] & \text{for trapped particles} \end{cases} \tag{B.28}$$

where $\mathbb{E}$ is the elliptic integral of the second kind, $\mathbb{E} = \int_0^{\pi/2} \sqrt{1+\kappa^2 cos\theta}\; d\theta$.

### Circular geometry with shift

For the analysis performed in the thesis, we made use of slightly more general expressions of the bounce and drift frequencies, which we found in Ref. [16] and include the existence of a Grad-Shafranov shift, characterized by $\alpha = -q^2 R_0 \partial_r \beta$.

$$\bar{\Omega}_b^{-1} = \sqrt{\frac{2\epsilon + (1-\epsilon)\kappa^2}{2\epsilon}} \frac{2}{\pi} \begin{cases} \mathbb{K}(\kappa) & \text{for circulating particles} \\ (1/\kappa)\mathbb{K}(1/\kappa) & \text{for trapped particles} \end{cases}$$

$$\bar{\Omega}_d = \frac{\kappa^2}{2\epsilon+(1-\epsilon^2)\kappa^2} \begin{cases} 1 + \frac{2}{\kappa^2}(\frac{\mathbb{E}}{\mathbb{K}} - 1) - \frac{4\alpha}{2\kappa^2}\left(2(1-\frac{1}{\kappa^2}) - (1-\frac{2}{\kappa^2})\frac{\mathbb{E}}{\mathbb{K}}\right) - \frac{\alpha}{2q^2} \\ +\frac{4s}{\kappa^2}\left(\frac{\mathbb{E}}{\mathbb{K}} - \frac{\pi}{2\mathbb{K}}\sqrt{1-\kappa^2}\right) \text{ for circulating particles} \\ 2\frac{\mathbb{E}}{\mathbb{K}} - 1 + 4s\left[\frac{\mathbb{E}}{\mathbb{K}} + \left(\frac{1}{\kappa^2} - 1\right)\right] - \frac{\alpha}{2q^2} \\ -\frac{4\alpha}{3}\left[1 - \frac{1}{\kappa^2} + (\frac{2}{\kappa^2} - 1)\frac{\mathbb{E}}{\mathbb{K}})\right] \text{ for trapped particles} \end{cases} \tag{B.29}$$

# C

# Field orderings in the BAE inertial layer

We derive in this appendix the orderings claimed in Eq. 4.11, starting from the expressions of electroneutrality and vorticity derived from the Lagrangian in the acoustic frequency range

$$-\left(1+\frac{1}{\tau_e}\right)\mathcal{E}_\omega+(1-\Gamma_0)\psi_\omega=-\left\langle\left(\frac{-i\omega}{-i\omega+v_\parallel\nabla_\parallel+\mathbf{v}_{gi}\cdot\nabla}\right)J_0^2\left(\frac{\mathbf{v}_{gi}\cdot\nabla}{-i\omega}\psi_\omega+\mathcal{E}_\omega\right)\right\rangle \tag{C.1}$$

$$\begin{aligned}-\frac{v_A^2}{\omega^2}\nabla_\parallel(\rho_i^2\nabla_\perp^2)\nabla_\parallel\psi_\omega+(1-\Gamma_0)(\psi_\omega-\mathcal{E}_\omega)-\left\langle\left(\frac{\mathbf{v}_{gi}\cdot\nabla}{-i\omega}\right)(1-J_0^2)\right\rangle\psi_\omega\\ =+\left\langle\left(\frac{\mathbf{v}_{gi}\cdot\nabla}{-i\omega}\right)\left(\frac{-i\omega}{-i\omega+v_\parallel\nabla_\parallel+\mathbf{v}_{gs}\cdot\nabla}\right)J_0^2\left(\frac{\mathbf{v}_{gi}\cdot\nabla}{-i\omega}\psi_\omega+\mathcal{E}_\omega\right)\right\rangle\end{aligned} \tag{C.2}$$

In a cylidrical equilibrium, the curvature verifies $\mathbf{b}_{(0)}\times\kappa=-\frac{\mathbf{1}}{\mathbf{R_0}}\left[\sin(\theta)\,\mathbf{e_r}+\cos(\theta)\,\mathbf{e}_\theta\right]$ and implies a coupling of poloidal components via the $\mathbf{v}_{gi}\cdot\nabla$ operator such that for any poloidal number $\mathsf{m}'$,

$$(\mathbf{v}_{gi}\cdot\nabla\psi_\omega)^{\mathsf{m}'}=i\sum_{\epsilon=\pm1}\omega_{gi,\epsilon}\psi_\omega^{\mathsf{m}'+\epsilon} \tag{C.3}$$

where $\omega_{gi,\epsilon}$ is an operator defined as $\omega_{gi,\epsilon}=\frac{1}{2}v_{gi}(+i\epsilon k_r+\frac{\mathsf{m}'+\epsilon}{r})\approx i\epsilon\frac{v_{gi}k_r}{2}\equiv+i\epsilon\omega_{di}$. $ik_r$ stands for the $\partial_r$ operator and $v_{gi}=\frac{-1}{eB_{(0)}R}\left(m_iv_\parallel^2+\mu_iB_{(0)}\right)$.

We make the expansion of the resonance operator: $(-i\omega)(-i\omega+v_\parallel\nabla_\parallel+\mathbf{v}_{gi}\cdot\nabla)^{-1}=1-\frac{v_\parallel\nabla_\parallel}{-i\omega}-\frac{\mathbf{v}_{gi}\cdot\nabla}{-i\omega}+O((k_\perp\rho_i)^2)$, and assume $\psi^{\mathsf{m}+1}=-\psi^{\mathsf{m}-1}$, $\psi^{\mathsf{m}+2}=\psi^{\mathsf{m}-2}$ $\mathcal{E}^{\mathsf{m}+1}=-\mathcal{E}^{\mathsf{m}-1}$, $\mathcal{E}^{\mathsf{m}+2}=\mathcal{E}^{\mathsf{m}-2}$. If follows from electroneutrality, expanded to the leading order in the different harmonics, that

$$\begin{aligned}\frac{1}{\tau_e}\mathcal{E}_\omega^{\mathsf{m}}&=\left\langle\frac{-i\omega_{di}}{\omega}\right\rangle(\psi_\omega^{\mathsf{m}+1}-\psi_\omega^{\mathsf{m}-1})+\left(1-\Gamma_0-2\left\langle\left(\frac{\omega_{di}}{\omega}\right)^2\right\rangle\right)\psi_\omega^{\mathsf{m}}\\&\quad+\left\langle\left(\frac{\omega_{di}}{\omega}\right)^2\right\rangle(\psi_\omega^{\mathsf{m}+2}+\psi_\omega^{\mathsf{m}-2})\\&\quad+O\left((\rho_ik_\perp)\psi_\omega^{\mathsf{m}+1},(\rho_ik_\perp)^2\psi_\omega^{\mathsf{m}+2},(\rho_ik_\perp)^{-2}\Lambda^2\psi_\omega^{\mathsf{m}},(\rho_ik_\perp)^3\psi_\omega^{\mathsf{m}}\right)\\\frac{1}{\tau_e}\mathcal{E}_\omega^{\mathsf{m}+1}&=\left\langle-i\frac{\omega_{di}}{\omega}\right\rangle(\psi_\omega^{\mathsf{m}+2}-\psi_\omega^{\mathsf{m}})=O\left((\rho_ik_\perp)\psi_\omega^{\mathsf{m}}\right)\\\frac{1}{\tau_e}\mathcal{E}_\omega^{m+2}&=\left\langle-i\frac{\omega_{di}}{\omega}\right\rangle(-\psi_\omega^{\mathsf{m}+1})+\left(1-\Gamma_0-2\left\langle\left(\frac{\omega_{di}}{\omega}\right)^2\right\rangle\right)\psi_\omega^{\mathsf{m}+2}-\left\langle\left(\frac{\omega_{di}}{\omega}\right)^2\right\rangle(\psi_\omega^{\mathsf{m}+2}+\psi_\omega^{\mathsf{m}})\\&=O\left((\rho_ik_\perp)\psi_\omega^{\mathsf{m}+1},(\rho_ik_\perp)^2\psi_\omega^{\mathsf{m}}\right)\end{aligned} \tag{C.4}$$

where $\Lambda^2 = (\omega^2/\omega_{BAE}^2)(1-\omega^2/\omega_{BAE}^2)$, $\omega_{BAE}^2 = (v_{ti}/R_0)^2(7/2+2\tau_e)$ (the last expression of Eq. 4.2 is recovered). Next, noticing that for the sidebands $qRk_\parallel^{\mathsf{m}+l} = l + qRk_\parallel^{\mathsf{m}} \sim 1$, for $l = 1$ or 2, vorticity yields

$$\frac{(\rho_i k_\perp)^2}{\beta}\psi_\omega^{\mathsf{m}+\mathsf{l}} \sim (1-\Gamma_0)\mathcal{E}_\omega^{\mathsf{m}+\mathsf{l}} + \left\langle \frac{i\omega_{di}}{\omega} \right\rangle (\mathcal{E}_\omega^{\mathsf{m}+1} - \mathcal{E}_\omega^{\mathsf{m}-1}), \text{for } l = 1,2 \tag{C.5}$$

From Eq. (C.5), it appears that $\psi^{\mathsf{m}+1/\mathsf{m}+2} = O((\rho_i k_\perp)^4 \psi^{\mathsf{m}})$, and we can combine this result with the previous equations to show: $\mathcal{E}_\omega^{\mathsf{m}} = O((\rho_i k_\perp)^{-2}\Lambda^2\psi_\omega^{\mathsf{m}})$, $\mathcal{E}_\omega^{\mathsf{m}+1} = O((\rho_i k_\perp)\psi_\omega^{\mathsf{m}})$ and $\mathcal{E}_\omega^{\mathsf{m}+2} = O((\rho_i k_\perp)^2\psi_\omega^{\mathsf{m}})$. With the assumption of closeness to the BAE gap edge relevant to the consideration of fourth order terms Eq. 4.8, the main poloidal component appears to be negligible, $\mathcal{E}_\omega^m = O((\rho_i k_\perp)^5 \psi_\omega^m)$.

# D

# Ballooning representation

Once one has chosen a toroidal field number $\mathsf{n}$, the calculation of a perturbation structure is reduced to a 2D problem, ie: the determination of the perturbation radial and poloidal dependences. The ballooning representation [135] makes use of the anisotropy of tokamak instabilities $k_\perp \gg k_\parallel$, which is especially true for high-$\mathsf{n}$ modes, to reduce the problem to one dimension only. It is based on an expansion with $1/\mathsf{n}$ as a small parameter.

The starting point is a coordinate transformation from the traditional geometric variables $(\theta, \varphi)$ to the coordinates

$$\alpha = \varphi - q(r)\theta \qquad \text{standing for a flux surface perpendicular coordinate} \tag{D.1}$$

$$\vartheta \in [-\infty, +\infty] \qquad \text{a field align coordinate.} \tag{D.2}$$

where $\vartheta = \theta$ in $[0, 2\pi]$.

In the ballooning representation, a field is represented in the form

$$\delta\phi(r,\theta,\phi,t) \quad \rightarrow \quad \hat{\phi}_\omega(r,\vartheta)\exp\left\{i\mathsf{n}\left(\varphi - q(r)(\vartheta-\vartheta_k)\right) - i\omega t\right\} \tag{D.3}$$

where $\vartheta_k = -(i/2\pi n q')\partial_{r|\eta,\alpha}$.

Such a representation can be obtained following the procedure

$$\phi_\omega = \sum_{\mathsf{m}} e^{i\mathsf{m}\theta + i\mathsf{n}\varphi}\phi_\omega^{\mathsf{m}}(r) = \sum_{\mathsf{m}} e^{i\mathsf{n}\alpha}e^{iqR_0k_\parallel^{\mathsf{m}}\theta}\phi_\omega(r,\mathsf{m}) \tag{D.4}$$

$$= \sum_{\mathsf{m}} e^{i\mathsf{n}\alpha}e^{iqR_0k_\parallel^{\mathsf{m}}\theta}\int_{-\infty}^{+\infty} d\vartheta e^{-qR_0k_\parallel^{\mathsf{m}}\vartheta}\hat{\phi}_\omega(r,\vartheta) \tag{D.5}$$

where the Fourier transform of $\phi(r,\mathsf{m})$ seen as a continuous function of $\mathsf{m}$ has been taken.

At the lower order of the ballooning expansion, the $r$-dependence of $\hat{\phi}$ can be neglected, whereas $\vartheta_k$ can be seen as a pure parameter (It is implicit in the lower order equations). Three consequences follow

- The problem is reduced to a 1D problem in $\vartheta$, for $\hat{\phi}(\vartheta)$.
- From Eq. D.5, and using the expansion $qR_0k_\parallel^{\mathsf{m}} = k_\theta s x$, $\hat{\phi}(\vartheta)$ is found to the Fourier transform of the radius dependent function $\phi_{\omega\mathsf{m}}(x/k_\theta s)$.
- The transformed equations can be accessed from the mode structure equation in $(r,\theta)$ space, making the following substitutions:

$$\nabla_\parallel \rightarrow \frac{1}{qR_0}\partial_\vartheta \tag{D.6}$$

$$\text{ou plus general: } B/2\pi J \tag{D.7}$$

$$\partial_r \rightarrow -i\mathsf{n}q'(\vartheta - \vartheta_k) \tag{D.8}$$

$$\partial_\theta \rightarrow -i\mathsf{n}q \tag{D.9}$$

# E

# Some details on the derivation of the fishbone-like dispersion relation

In this Appendix, we give some details on the calculation of the integrals which appear in the fihsbone-like dispersion relation.

## E.1 Volume elements

To compute the integrals of the fishbone dispersion relation, it is useful to express the traditional canonical variables $(\mathbf{x}, \mathbf{p})$ as a function of the equilibrium invariants chosen for this analysis: $r$, $\mathsf{E}$ and $\lambda = \mu B_0/\mathsf{E}$. It comes

$$\begin{aligned} d\mathbf{\Gamma} = d^3\mathbf{x}d^3\mathbf{p} &= (R_0 d\varphi r d\theta dr)\left(2\pi m_s^2\sqrt{\frac{2\mathsf{E}}{m_s}}d\mathsf{E}\; d\left(\frac{v_\parallel}{v}\right)\right) \\ &= 2\sqrt{2}\;\pi\; m_s^{3/2}(R_0 d\varphi r dr)\sqrt{\mathsf{E}}d\mathsf{E}\sum_\pm \frac{b_{(0)}(r,\theta)d\lambda}{2\sqrt{1-\lambda b_{(0)}(r,\theta)}}. \end{aligned} \tag{E.1}$$

Noticing that volume elements are conserved when moving from one canonical set of coordinate, the same result can be recovered from the action-angle variables,

$$\begin{aligned} d\mathbf{\Gamma} = \sum_\pm d^3\boldsymbol{\alpha} d^3\mathbf{J} &= \sum_\pm d^3\boldsymbol{\alpha}\left(\frac{m_s}{e_s}d\mu\right)\left(\frac{d\mathsf{E}}{\Omega_b}\right)(e_s d\Psi) \\ &= \sum_\pm d^3\boldsymbol{\alpha}\; m_s^{3/2}\frac{1}{B_0}d\lambda(\sqrt{\frac{\mathsf{E}}{2}}d\mathsf{E})\int\frac{d\theta}{2\pi}\frac{1}{\mathbf{b}_{(0)}\cdot\nabla\theta}\frac{1}{\sqrt{1-\lambda b_{(0)}(r,\theta)}}\left(\frac{B_0}{q}rdr\right). \end{aligned} \tag{E.2}$$

Note however that the two calculations are useful in general.

## E.2 Energetic particle term

### E.2.1 Normalization of the anisotropic Maxwellian

Assume we have a distribution function of the form,

$$F_h = \tilde{n}(r)f_\lambda(\lambda)e^{-\mathsf{E}/T_h(r)}. \tag{E.3}$$

For consistency, $T_h$ needs to have the dimensions of an energy and can be understood as a temperature. Let us link $\tilde{n}$ to the more traditional density of the hot population $n_h$.

By definition $n = \int d^3\mathbf{p}F_h$, such that the average density corresponding to the radius r,

$n(r)$, is

$$\begin{aligned} n(r) &= \int \frac{d\theta}{2\pi} d^3\mathbf{p}\ F_h = \sqrt{2}\pi m_s^{3/2}\tilde{n}(r) \int d\lambda \int \frac{d\theta}{2\pi} \frac{b_{(0)}(r,\theta)}{\sqrt{1-\lambda b_{(0)}(r,\theta)}} \\ &= \sqrt{2}\pi m_s^{3/2}\tilde{n}(r) \int \sqrt{\mathsf{E}} d\mathsf{E} e^{-\mathsf{E}/T_h(r)} \sum_{\pm} \int d\lambda f_\lambda(\lambda) \int \frac{d\theta}{2\pi} \frac{b_{(0)}(r,\theta)d\lambda}{\sqrt{1-\lambda b_{(0)}(r,\theta)}} \ . \end{aligned} \tag{E.4}$$

$n(r)$ can be interpreted as the average density in the radial shell, when the approximation of very thin banana is made.

Finally, the correct normalization for $F_h$ is given by

$$\tilde{n}(r) = \frac{n_h(r)}{(2\pi m_h T_h)^{3/2}} \frac{2}{< \bar{\Omega}_b(\lambda, r) >_\lambda} \ . \tag{E.5}$$

### E.2.2 Projection onto the action-angle basis

The main difficulty for the computation of resonances is the necessity to make the projection of the fields, naturally expressed in the *geometric variables*, onto the *particle coordinates*, the action-angle variables. This projection can *a priori* lead to an infinite number of components in the action-angle space.

For the resonant excitation of BAEs, it is explained in subsection 5.1.2 that one main component was relevant for resonance: the resonance with trapped particles for the triplet $(\mathsf{n}_1, \mathsf{n}_2, \mathsf{n}_3) = (0, 0, \mathsf{n})$.

So we need to to compute

$$-\tilde{h} = e_h \int \frac{d\alpha_1}{2\pi} \int \frac{d\alpha_2}{2\pi} \int \frac{d\alpha_3}{2\pi} \left( \frac{\mathbf{v}_{gh} \cdot \nabla \psi_\omega}{-i\omega} + \mathcal{E}_\omega \right) e^{-i\mathsf{n}_3 \alpha_3} \tag{E.6}$$

for the fast trapped particles, with the additional assumption that the hot particles simply interact with the mode in the MHD-like region where $\mathcal{E}_\omega = 0$ (This is argued in subsection 5.1.2).

In the following, we simply use the main poloidal component $\psi_\omega = \psi_\omega^{\mathsf{m}} \exp(i\mathsf{m}\theta + i\mathsf{n}\varphi)$, which is dominant for our derivation of the BAE structure. For strong perpendicular gradients compared to parallel gradients, the results of the ballooning representation can be used, and return an integrand of the form

$$\mathbf{v}_{gh} \cdot \nabla \psi_\omega = -v_{gh} \left( \sin\theta \partial_r + \frac{\cos\theta}{r} \partial_\theta \right) \psi_\omega \tag{E.7}$$

$$= -ik_\theta v_{gh} \left( s(\theta - \theta_d) \sin\theta + \frac{\cos\theta}{r} \right) \psi_\omega^{\mathsf{m}}(r) e^{i\mathsf{n}(\varphi - q\theta - \alpha_3)} e^{iqR_0 k_\parallel^{\mathsf{m}} \theta}. \tag{E.8}$$

We may now make the projection onto the action-angle variables. For this, we need to be able to express the angle variables as a function of the geometric variables $(\theta, \varphi)$. It is possible to choose a description such that $\alpha_2$ simply depends on $\theta$, and the $\varphi$-dependence is fully included in $\alpha_3$. More precisely, we can write

$$\varphi = \alpha_3 + \hat{\alpha} + q(\bar{\Psi})\hat{\theta} \tag{E.9}$$

$$\theta = \delta_{\text{passing}} \alpha_2 + \hat{\theta} \tag{E.10}$$

It follows that $i\mathsf{n}(\varphi - q\theta - \alpha_3) = i\mathsf{n}\hat{\alpha}$.

To compute the integrals, we now make a few assumptions.

- For the gyroaverage, we simply choose $J_0(k_\perp \rho_\perp) = 1$ in the MHD region, and $J_0(k_\perp \rho_\perp) = 0$ in the inertia region.
- For the $\alpha_2$ integrand, we neglect the $\theta$-dependence of $\hat{\alpha}$ and $\hat{\theta}$, which makes some sense for sufficiently trapped particles.

  Moreover, we use closeness to the resonant (in agreement with the ballooning representation), such that $qR_0k_\parallel = 0$.

  Finally, we do not take into account the banana width of the particle (assumption of thin bananas), such that no $\theta$ dependence does not appear $\psi^{\mathsf{m}}(r)$. This is meaningful in the MHD region where radial gradients are smooth, such that the radial drift is less important.
- The later integration is the easiest because of the cancellation of the $\varphi$ dependence in the integrand.

From the definition of the drift frequency ($\Omega_3 = \Omega_d$ for the trapped particles), where we take $\mathbf{v}_{gh} \cdot \nabla\varphi = 0$ ($\mathbf{B}_{(0)}$ almost in the $\varphi$ direction), it finally comes

$$-\tilde{h} = J_0(\rho_{h\perp}k_\perp)e_h \frac{\mathsf{m}}{q}\frac{\Omega_{h,d}}{\omega}\psi^{\mathsf{m}}_\omega(r) \tag{E.11}$$

where the $\theta_d$ dependence disappeared with parity.

$\tilde{h}$ can be understood as a modified Hamiltonian. In particular, where resonance with the particles occurs,

$$\mathsf{m}/q = -\mathsf{n}, \qquad \mathsf{n}\Omega_{h3} = \omega, \qquad \tilde{h} = e_h\psi^{\mathsf{m}}_\omega. \tag{E.12}$$

### E.2.3 Complete form the energetic particle term used in the thesis

In this subsection, we simply make more explicit the derivation of Eq. 5.11 and give some details on the distribution function used in our analysis of the BAE linear stability.

We start from Eq. 5.8 and assume the fast ion population to be a anisotropic Maxwellian of the form $F_h = \tilde{n}_h(r) f_\lambda(\lambda) \exp(-E/T_h(r)\ )$ where $f_\lambda$ is chosen to be a peaked function

$$f_\lambda = \delta(\lambda - \lambda_0) \text{ or } f_\lambda = \frac{1}{\sqrt{\pi}\Delta\lambda}\exp\left(-(\lambda-\lambda_0)^2/\Delta\lambda^2\right) \tag{E.13}$$

$$\tilde{n}(r) = \frac{n_h(r)}{(2\pi m_h T_h)^{3/2}}\frac{2}{<\bar{\Omega}_b(\lambda, r)>_\lambda} \tag{E.14}$$

with the notation $<...>_\lambda = \int_0^{1+r/R} d\lambda f_\lambda$. It directly comes

$$\delta\hat{W}_k = \sqrt{\pi}(q(r_s)^2\mathsf{m})\int_0^a \frac{1}{r_s^2} r dr |\bar{\xi}|^2 \beta_h \int_{1-r/R}^{1+r/R} d\lambda \frac{\bar{\Omega}_b\bar{\Omega}_d^2}{<\bar{\Omega}_b>_\lambda} \times$$
$$\int_0^{+\infty} \frac{dE}{E - E_{res}}\left(\frac{E}{T_h}\right)^{5/2} e^{-E/T_h}\left\{-\frac{E_{res}}{T_h}f_\lambda - \frac{E_{res}}{T_h}\frac{T_h}{E}\lambda f'_\lambda - \frac{1}{\bar{\Omega}_d}\frac{R\partial_r F_h}{F_h}f_\lambda\right\}. \tag{E.15}$$

The two first terms are related to the energy gradient (the traditional Maxwellian term and the anistropy induced energy gradient [109]) and the last one to the radial gradient. More precisely,

$$\frac{\partial_r F_h}{F_h} = \frac{\partial_r n_h}{n_h} - \frac{\partial_r <\bar{\Omega}_b>}{<\bar{\Omega}_b>} + \left(\frac{E}{T_h} - \frac{3}{2}\right)\frac{\partial_r T_h}{T_h}. \tag{E.16}$$

Hence,

$$\begin{aligned}\delta\hat{W}_k &= \pi(q(r_s)^2\mathsf{m})\int_0^a \frac{1}{r_s^2} r dr |\bar{\xi}|^2 \beta_h \int_{1-r/R}^{1+r/R} d\lambda \frac{\bar{\Omega}_b \bar{\Omega}_d^2}{<\bar{\Omega}_b>_\lambda} \times \\ &\left\{ -\frac{E_{res}}{T_h} Z_5 f_\lambda - \frac{E_{res}}{T_h} Z_3 \lambda f'_\lambda \right. \\ &\left. -\frac{1}{\bar{\Omega}_d}\left[\frac{R\partial_r n_h}{n_h} Z_5 - \frac{R\partial_r <\bar{\Omega}_b>}{<\bar{\Omega}_b>} Z_5 + \frac{R\partial_r T_h}{T_h}\left(Z_7 - \frac{3}{2}Z_5\right)\right] f_\lambda \right\} \end{aligned} \tag{E.17}$$

with $Z_p = Z_p(y_0)$ such that $y_0^2 = E_{res}/T_h$, and Z, such that $Z(y_0) = y_0 Z_{-1}(y_0)$, is the Fried et Conte or plasma dispersion function,

$$\sqrt{\pi} Z_p(y_0) = \int_{-\infty}^{+\infty} dy y^{p+1} \exp(-y^2)/(y^2 - y_0^2), Z_3(y_0) = \frac{1}{2} + y_0^2 + y_0^3 Z(y_0), \tag{E.18}$$

$$Z_5(y_0) = \frac{3}{4} + \frac{y_0^2}{2} + y_0^4 + y_0^5 Z(y_0), Z_7(y_0) = \frac{15}{8} + \frac{3}{4}y_0^2 + \frac{y_0^4}{2} + y_0^6 + y_0^7 Z(y_0). \tag{E.19}$$

## E.3 Details for the computation of inertia

In this Appendix subsection, $\psi_\omega$ and $\mathcal{E}_\omega$ refer to the full electromagnetic fields including all poloidal components, and each poloidal component is clearly indicated by its wave numbers (n,m'), whereas the main mode poloidal mode number is m.

Passing thermal ions are expected to resonate with BAEs, which leads to Landau damping. To calculate the value of the energy transfer, we compute the imaginary part of Eq. 5.2, considered for thermal ions ($s = i$). For passing particles, resonances are of the form $\mathsf{n}_2\Omega_{i,2} + \mathsf{n}_3\Omega_{i,3} \approx (v_\parallel/qR)(\mathsf{m}' + \mathsf{n}q) = k_\parallel^{\mathsf{m}',\mathsf{n}} v_\parallel$, for any poloidal component $(\mathsf{n}_2, \mathsf{n}_3) = (\mathsf{m}', \mathsf{n})$. Hence close to the BAE inertial region, resonances are expected to involve the mode sidebands characterized by the poloidal mode numbers $\mathsf{m}' = \mathsf{m} \pm 1$ (where m now stands for the main poloidal component mode number) and to be of the form $k_\parallel^{\mathsf{m}\pm1,\mathsf{n}} \approx \pm 1/qR$.

From Eqs. 4.16, we know the fields involved. Eq. 5.2 (or equivalent resonant Hamiltonian) reads

$$\left(\frac{\mathbf{v}_{gi}\cdot\nabla\psi_\omega}{-i\omega} + \mathcal{E}_\omega\right)_{(\mathsf{m}+1,\mathsf{n})} = \frac{1}{2}\frac{v_{gi}}{\omega}\partial_r\psi_\omega^{\mathsf{m}} - \frac{T_e}{T_i}\left(\frac{v_{ti}}{R\omega}\right)\rho_i\partial_r\psi_\omega^{\mathsf{m}} \tag{E.20}$$

to the lower order, with $v_{gi} = -(m_i v_\parallel^2 + \mu B)/eBR$, $v_{ti} = \sqrt{T_i/m_i}$ the ion thermal velocity. Hence, noticing that for thermal ions, diamagnetic effects may be neglected ($\mathsf{n}\Omega_{*i}/\omega \ll 1$), the imaginary part of the thermal ion resonant contribution becomes

$$\begin{aligned}\mathrm{Im}\left(\mathcal{L}_{i\omega}^{res}\right) &= \mathrm{Im}\left(-\int d^3\mathbf{x}\frac{ne^2}{T_i}\left(\rho_i\partial_r\psi_\omega^{\mathsf{m}}\right)^2\left(\frac{v_{ti}}{R\omega}\right)^2 \times \right. \\ &\left. \sum_{\epsilon=\pm1}\int d^3\mathbf{p}\frac{F_i}{n}\frac{\omega}{\omega + \epsilon v_\parallel/qR}\left(\frac{1}{2}\left(\frac{v_\parallel}{v_{ti}}\right)^2 + \frac{1}{4}\left(\frac{v_\perp}{v_{ti}}\right)^2 + \frac{T_e}{T_i}\right)^2\right) \end{aligned} \tag{E.21}$$

$$\begin{aligned} &= \int d^3\mathbf{x}\frac{ne^2}{T_i}(\rho_i\partial_r\psi_\omega^{\mathsf{m}})^2\frac{\sqrt{\pi}}{2\sqrt{2}}\, q\left(\frac{v_{ti}}{R\omega}\right)\exp\left(-\frac{1}{2}\left(\frac{qR\omega}{v_{ti}}\right)^2\right)\times \\ &\left[2 + 2\left(\left(\frac{qR\omega}{v_{ti}}\right)^2 + 2\frac{T_e}{T_i}\right) + \left(\left(\frac{qR\omega}{v_{ti}}\right)^2 + 2\frac{T_e}{T_i}\right)^2\right]. \end{aligned} \tag{E.22}$$